University of Alberta

Rho-Kinase-Mediated Diphosphorylation of Myosin Regulatory Light Chain
is a Unique Biochemical Mechanism
in Human Uterine Myocytes

by

Hector Noel Aguilar

A thesis submitted to the Faculty of Graduate Studies and Research
in partial fulfillment of the requirements for the degree of

Doctor of Philosophy

Department of Physiology

Fall 2011
Edmonton, Alberta

Dedication

Dedico este trabajo a mi mamá.

No puedo agradecerle suficiente por lo que usted ha hecho por mí.

La amo mucho.

Abstract

Rationale: Smooth muscle (SM) contraction results from activation of the cellular contractile machinery by phosphorylation of myosin regulatory light chain (RLC) at S19 (pRLC) by RLC kinase (MLCK). Subsequent phosphorylation at T18 yields diphosphorylated-RLC (ppRLC), which has been shown to enhance the myosin ATPase activity, and therefore might have implications for the ability of the muscle to generate tension. In uterine myocytes, the extent of diphosphorylation is greater than that observed in vascular myocytes. In preliminary experiments using cultured human uterine smooth muscle cells (hUSMC), we observed that rho-kinase (ROK) inhibition caused a marked reduction in ppRLC, but surprisingly, not pRLC. Therefore we pursued a quantitative comparison in ROK-mediated phosphorylation of RLC in hUSMC and human vascular myocytes (hVSMC).

Objectives: 1) to develop and validate quantitative methods for assessment of phosphorylated RLC, and 2) to apply these methods in studies comparing ROK-mediated phosphorylation of RLC in hUSMC and hVSMC.

Findings: We have developed and validated two assays for quantitative measurements of phosphorylated RLC using phospho-specific antibodies: 1) a high-throughput in-cell western assay, and 2) western blotting-based quantification of RLC-phospho-states after separation with phos-tag SDS-PAGE. These techniques revealed that hUSMC differ from hVSMC in their primary phosphorylation responses to stimulation. hUSMC respond to oxytocin with increased pRLC and ppRLC, whereas hVSMC respond to endothelin-1 with increased pRLC only. In hUSMC, only ppRLC was sensitive to ROK inhibition using a pharmacologic inhibitor, and this occurred at

approximately 100-fold lower concentration of ROK inhibitor than that required to achieve an equivalent reduction of pRLC in hVSMC.

Conclusions: In hUSMC, ROK phosphorylates RLC at T18 downstream of MLCK-mediated phosphorylation at S19. This sequential phosphorylation of RLC forms ppRLC. This role of ROK activity appears unique to hUSMC and is a fundamental difference from hVSMC. These findings suggest the possibility of a uterine-specific therapeutic avenue for prevention or arrest of preterm labor achieved by targeting ROK to reduce ppRLC levels in hUSMC. Our data also suggest that ROK inhibition might avoid the prohibitive side effects of currently used agents for preterm labour, of which the most common and serious is hypotension that results from unwanted vascular relaxation.

Acknowledgements

I would like to thank the research nurses at the Royal Alexandra Hospital in Edmonton, Alberta, for their help in tissue collection. I would also like to thank the members of my lab, our technician Barbara Zielnik and MSc. student Curtis Tracey for their help in preparing cell cultures and completing these studies. I am also grateful to the Canadian Institutes of Health Research and Alberta Innovates-Health Solutions for their financial support during the course of my graduate studies. I would also like to thank my good friend Dr. R. Magnus Friis for sharing and discussing ideas and approaches that helped me complete this work. Most importantly I would like to express my gratitude to my PhD supervisor, Dr. B.F. Mitchell, for the many hours and days he contributed to in the form of review, active discussion, and guidance for the content of this thesis. I cannot thank you enough for your enthusiasm toward my project, even during the lengthy initial incubation period when it seemed all our efforts went unrewarded!

Table of Contents

List of Tables

List of Figures

Table 1: Abbreviations

Abbreviation	*Meaning*
$[Ca^{2+}]_i$	Intracellular Concentration of Ca^{2+}
^0C	Degrees Celsius
0pRLC	Phospho-state corresponding to non-phosphorylated RLC
1pRLC	Phospho-state corresponding to monophosphorylated RLC irrespective of phospho-site modified
2pRLC	Phospho-state corresponding to diphosphorylated RLC irrespective of phospho-site modified
3pRLC	Phospho-state corresponding to triphosphorylated RLC irrespective of phospho-site modified
4-α-PMA	Negative control for PMA
Ab	Antibody (Abs, antibodies)
ANOVA	Analysis of Variance
ATP	Adenosine Triphosphate
C-terminal	Carboxy terminal
C3 transferase	Cell permeable rhoA inhibitor
CalA	CalyculinA, PP1 (and PP2A) inhibitor – effectively an MLCP inhibitor
Calp	Calpeptin, rhoA activator
CaM	Calmodulin
cAMP	Cyclic Adenosine Monophosphate
CPI-17	Protein-kinase C-potentiated Myosin Phosphatase Inhibitor of 17 kDa (i.e. PPP1R14A)
CV	Coefficient of variation
DAG	Diacylglycerol
DMEM	Dulbecco's modified eagles medium
DMF	Dimethylformamide
DMSO	Dimethylsulfoxide
DNA	Deoxyribonucleic Acid
EDTA	Ethylenediaminetetraacetic Acid
ELC	Essential Light Chain (17 kDa)
ELISA	Enzyme-Linked Immunosorbant Assay
ET-1	Endothelin-1
FBS	Fetal Bovine Serum
g	Acceleration due to Earth's gravity
g	Grams
g-H	See 'Glycyl-H-1152'
G-protein	GTP-Binding Protein
GAP	GTPase Activating Protein
GAPDH	Glyceraldehyde-3-phosphate dehydrogenase
GDI	Guanine Nucleotide Dissociation Inhibitor
GDP	Guanosine Diphosphate
GEF	Guanine Nucleotide Exchange Factor
Glycyl-H-1152	ATP-competitive cell-permeable inhibitor of ROK I/II
GPCR	G-protein Coupled Receptor
GTP	Guanosine Triphosphate
hUSMC	Human uterine smooth muscle cell (uterine myocyte)
hVSMC	Human vascular smooth muscle cell
ICW	In-cell-western
IF	Immunofluorescence
ILK	Integrin Linked Kinase

Abbreviation	*Meaning*
kDa	Kilodalton
L	Liters
Lipofectamine	Refers specifically to Lipofectamine RNAiMAX reagent (see section 8.4.2.5)
M	Moles*L^{-1}
mA	milliamperes
MII	Myosin II
min	Minutes
ML7	MLCK inhibitor
MLCK	RLC Kinase
MLCP	RLC Phosphatase
MMAb	Mouse monoclonal Ab
mRNA	Messenger Ribonucleic Acid
MYPT1	Myosin Binding Subunit (i.e. MYPT1) of MLCP
N-terminal	Amino terminal
NIR	Near-Infrared
OBB	Odyssey Blocking Buffer
OT	Oxytocin
P value	Probability (of incorrectly rejecting the null hypothesis)
p19RLC	Phosphoisotype of RLC modified at S19 (normally reflects the sum of pRLC and ppRLC)
p1RLC	Phosphoisotype of RLC modified at S1
p696	Phosphorylated MYPT1 at T696
p853	Phosphorylated MYPT1 at T853
PBS	Phosphate Buffered Saline
PBS-T	PBS containing Tween-20
Phos-tag	Phosphate-binding tag (retards phospho-protein mobility when used with SDS-PAGE)
PIP_2	Phosphatidyl Inositol 4,5-Bisphosphate
PKA	Protein Kinase A
PKC	Protein Kinase C
PLC	Phospholipase C
PMA	phorbol-12-myristate-13-acetate, PKC activator (phorbol ester)
PP	Protein Phosphatase
PP1c	Protein Phosphatase 1c (catalytic subunit of MLCP)
ppRLC	Diphosphorylated RLC (T18/S19 simultaneously)
pRLC	Monophosphorylated RLC at S19 only
PTB	Preterm Birth
PTL	Preterm Labour
R-P	Rhodamine-Phalloidin
Rho-15	Putative ROK I-specific inhibitor (in contrast to SR-3677 and g-H)
RLC	Myosin Regulatory Light Chain (20 kDa)
RNA	Ribonucleic Acid
ROKI	Rho-kinase I (i.e. ROKβ)
ROKII	Rho-kinase II (i.e. ROKα)
RPAb	Rabbit polyclonal Ab
SD	Standard Deviation
SDS-PAGE	Sodium Dodecyl Sulphate Polyacrylamide Gel Electrophoresis
SEM	Standard Error of the Mean
siRNA	Small interfering RNA
SM	Smooth Muscle
SMC	Smooth Muscle Cell
SR3677	Putative ROK II-specific inhibitor (in contrast to Rho-15 and g-H)

Abbreviation	*Meaning*
TAT-rhoA	Recombinant fusion protein of wild type rhoA fused with a viral protein transduction peptide from human immunodeficiency virus (see appendix 8.5)
tRLC	'total' RLC (i.e. an Ab without phosphospecificity, therefore detects all phosphoisotypes of RLC)
V	Volts/Voltage
W7	Cell-permeable calmodulin antagonist
WB	Western Blotting
WT	Wild type
Y-27632	ATP-competitive cell-permeable inhibitor of ROK I/II

Table 2: Antibody Information

Antibody Target	*Phospho-Specificity*	*Abbreviation*	*Supplier*	*Catalog Number*	*Clonality (RPAb or MMAb)*	*Dilution (WB/ICW)*	*Notes*
GAPDH	None	GAPDH	Santa Cruz		MMAb	1:2000/1:500	
MYPT1	None	MYPT1	BD Biosciences	# 612164	MMAb	1:500/1:500	Excellent readout in ICW for siRNA knockdown optimization (see Appendix 8.4).
Phospho-S1-RLC	Phospho-Ser1	p1RLC	ECM Biosciences	MP3461	RPAb	1:2000/1:2000	
Phospho-S19-RLC	Phospho-Ser19	p19RLC (total phosphorylation at S19)	Cell Signaling	#3671	RPAb	1:200/1:200	
Phospho-S19-RLC	Phospho-Ser19 (obstructed by Phospho-T18)	pRLC (monophosphorylation of RLC)	Cell Signaling	#3675	MMAb	1:2000/1:1000	
Phospho-T18/S19-RLC	Phospho-Thr18 and Phospho-Ser19 simultaneously	ppRLC (diphosphorylation of RLC)	Cell Signaling	#3674	RPAb	1:500/1:500	
Phospho-T696-MYPT1	Phospho-Thr696	p696	Millipore/Upstate	#ABS45	RPAb	1:1000/---	Suitability for ICW uncertain – both WB and ICW demonstrated no change with OT stimulation.
Phospho-T853-MYPT1	Phospho-Thr853	p853	Cell Signaling	#4563	RPAb	1:500/---	Suitability for ICW questionable – WB showed clear changes (see Chapter 5), but no changes on ICW.

Antibody Target	*Phospho-Specificity*	*Abbreviation*	*Supplier*	*Catalog Number*	*Clonality (RPAb or MMAb)*	*Dilution (WB/ICW)*	*Notes*
rhoA	None	rhoA	BD Biosciences	#610990	MMAb	1:200/1:200	
RLC (C-terminus)	None	tRLC	LifeSpan BioSciences	LS-C81207	RPAb	1:1000/---	
RLC (N-terminus)	None		Cell Signaling	#3672	RPAb		Used this Ab for data in Ch. 3. However, the signal was inferior to that of the tRLC Ab aimed at the C-terminus on WB, therefore the C-terminal RLC Ab was used for all data in Ch. 4 and 5.
ROKII	None	ROKII	BD Biosciences	#610623	MMAb	1:500/---	Suitability for ICW uncertain. Could not measure reduced protein levels after siRNA treatment, but knockdown protocol requires further optimization (see Appendix 8.4).
α-actin	None	α-actin	Santa Cruz	sc-56499	MMAb	1:4000/---	

Table 3: Mathematical Prefixes

Number	Prefix	Symbol
10^{3}	kilo-	k
10^{-1}	deci-	d
10^{-2}	centi-	c
10^{-3}	milli-	m
10^{-6}	micro-	μ
10^{-9}	nano-	n
10^{-12}	pico-	p
10^{-15}	femto-	f
10^{-18}	atto-	a

Table 4: Amino Acid Abbreviations

Amino Acid	Abbreviation	Single Letter Code
Alanine	Ala	A
Arginine	Arg	R
Asparagine	Asn	N
Aspartic Acid	Asp	D
Cysteine	Cys	C
Glutamic Acid	Glu	E
Glutamine	Gln	Q
Glycine	Gly	G
Histidine	His	H
Isoleucine	Ile	I
Leucine	Leu	L
Lysine	Lys	K
Methionine	Met	M
Phenylalanine	Phe	F
Proline	Pro	P
Serine	Ser	S
Threonine	Thr	T
Tryptophan	Trp	W
Tyrosine	Tyr	Y
Valine	Val	V

Chapter 1

Introduction and Rationale

1 Introduction and Rationale

1.1 Overview

Preterm delivery complicates greater than 8% of births in Canada. Approximately 10% of these preterm babies will die or suffer lifelong significant disabilities related to their preterm birth (PTB). The emotional costs to the family and the financial costs to health care system are enormous. Currently, no reliable method exists for predicting preterm labour (PTL). However, even in the presence of reliable predictors, there currently exists no effective method of treatment to reduce uterine contractility to permit the pregnancy to be carried until full term. Therefore, this work is aimed at our improving our understanding the biochemical mechanisms that control contractility of the human uterus. The overarching aim is to determine a therapeutically exploitable biochemical mechanism to prevent the premature delivery of the fetus.

The pivotal event that controls contractions in smooth muscle (SM) is the phosphorylation of myosin regulatory light chain (RLC), which causes activation of the myocyte contractile apparatus. The intracellular level of phosphorylated RLC is regulated by two basic processes: phosphorylation of RLC and dephosphorylation of phosphorylated RLC. RLC is primarily phosphorylated at S19 by RLC kinase (MLCK) to form phospho-S19-RLC (pRLC), and dephosphorylated at the same site by RLC phosphatase (MLCP). However, pRLC can be further phosphorylated at T18 to form diphospho-RLC (ppRLC), which enhances the myosin ATPase activity that powers the contraction. Our studies strongly suggest that, in contrast to human vascular SM, human uterine SM is uniquely dependent on the synthesis of ppRLC for a significant proportion of the tension generated by the uterine muscle layer (myometrium). In addition, the synthesis of ppRLC is strongly dependent on the activity of rhoA-associated kinase (ROK). Thus, targeting of ROK using pharmacological agents might specifically reduce uterine contractility while avoiding side effects associated with other SM beds. By extension, ROK inhibition might be a clinically useful method of preventing or arresting PTL for the prevention of PTB.

The remainder of this chapter is devoted to providing the background and rationale for the experiments proposed in chapter 2, and an effort was made to discuss only the pertinent information. However, we have authored a more thorough review of the

biochemical mechanisms underlying uterine contractility,(1) which provided much of the content for this section and offers a significant amount of additional detail to some of the concepts presented here. This review article is appended in section 8.1.

1.2 Preterm Birth

PTB is defined as birth occurring at less than 37 weeks of gestation, in comparison to a normal length gestation lasting between 38-40 weeks after conception. PTBs account for between 5-15% of all births and result in 75% of neonatal mortality, and 50% of all neonatal health problems.(2, 3) In Canada, PTB occurs in more than 8% of pregnant women and is associated with the great majority of infant death and chronic disability arising from birth.(4) The sequelae include cerebral palsy, mental retardation, blindness, other major sensori-motor disabilities, learning disorders and a variety of other conditions that restrict full achievement of genetic potential. While it can be argued that, in general terms, medical management of PTB has improved,(5, 6) its incidence is rising.(3, 7, 8) Further, while advances in neonatal care have conferred increased survival rates among preterm infants, in the long term, they may suffer from a variety of conditions due to their relative immaturity.(9-18) Many of these problems persist into school age and adolescence and complicate child development, cognition, and hinder affected individuals in achieving their full potential. In addition, the treatment of preterm infants is accompanied by high costs to society. In the short term, these are in the form of spending on expensive medical care for the neonate, and in the long term, in the form of providing special care and programs during school age. In addition to developmental difficulties early in life, it has been proposed that preterm infants may be predisposed to adult morbidities such as cardiovascular disease and non-insulin dependent diabetes mellitus.(3) If true, then the economic and social burden of PTB is further compounded as preterm babies progress to adulthood.

There are several recognized causes of PTL.(19) In a significant number of cases, immediate obstetrical intervention is required due to maternal or fetal infection or evidence of fetal compromise. However, 50-60% of all PTL falls in the ‘idiopathic’ category with an apparently healthy fetus.(3) In these cases, there is no identifiable cause, and no contraindication for prolonging pregnancy to enable the fetus to achieve full maturation. In

these idiopathic cases, successful preventive strategies could have very beneficial effects for the babies and their families.

1.3 Tocolysis

The available treatments for PTL, termed 'tocolytics', are aimed to prevent or arrest unwanted uterine activity. These drugs fall into various categories, including β-adrenergic agonists, calcium channel blockers, cyclo-oxygenase (COX) inhibitors, oxytocin (OT) receptor antagonists, magnesium sulfate, and nitric oxide (NO) donors.(20-22) Subsequent sections will review in detail the relevant physiological and biochemical mechanisms being exploited by several of these agents. But at this time it is worth briefly mentioning their diverse mechanisms of action. NO donors and β-adrenergic agents likely function by activating cyclic-nucleotide-dependent kinases that actively inhibit the contractile machinery and cause SM relaxation. In contrast, calcium channel blockers act by decreasing the amount of calcium ions (Ca^{2+}) available to activate the contractile machinery, and OT receptor antagonists act by interfering with binding and subsequent activation of plasma membrane receptor by OT, which is a powerful uterine stimulant. Similarly, COX inhibitors act by preventing stimulation of the muscle tissue, but this effect is achieved by reducing the production of prostaglandins, which are thought to contribute to uterine stimulation at the time of parturition. The mechanism of action of magnesium sulfate is unknown, but might be similar to that of the calcium channel blockers.

A recent systematic review (23) of β-adrenergic agents ('β-sympathomimetics', e.g. ritodrine, salbutamol, terbutaline) showed that these drugs were effective at decreasing the number of births within 48 hrs of treatment initiation compared to placebo, but do not achieve a significant reduction relative to placebo within 7 days of initiation. Importantly, there was no demonstrated benefit on neonatal or perinatal mortality. The review also showed that these drugs are often significantly associated with termination of treatment due to unwanted side effects, such as chest pain, dyspnea, maternal or fetal tachycardia, palpitations, and others. The reviewers concluded that there was no support for use of any specific agent among the available β-adrenergic drugs. Importantly, despite the prolongation of pregnancy achieved within 48 hrs of initiation of treatment, there was no evidence that this delay in the timing of birth significantly improved neonatal outcomes.

Similarly, a recent meta-analysis of the available data on the calcium channel blocker nifedipine evaluated the efficacy of this treatment for acute tocolysis and maintenance therapy for prevention of PTL.(24) This work showed that there are no differences in rate of delivery within 48 hrs in patients treated prior to 37 weeks of gestation when comparing nifedipine to β-adrenergic drugs or to magnesium sulfate, but that nifedipine showed a benefit over β-adrenergic drugs within 7 days of initiation of treatment in patients before 34 weeks of pregnancy. Maintenance therapy with nifedipine was determined to be no better than placebo at prolonging gestation or improving neonatal outcomes. However, nifedipine was less likely to be discontinued due to adverse maternal side effects compared to β-adrenergic drugs.

A review of the available trial data for magnesium sulfate determined that this agent was ineffective at delaying birth or preventing PTB, and as such the reviewers concluded that this agent cannot be recommended for clinical use.(25) In contrast, a review of cyclo-oxygenase (COX) inhibitors showed that the non-selective inhibitor indomethacin performed better than placebo and all other tocolytics in terms of reducing the number of births prior to 37 weeks gestation, and did so with fewer side effects to the mother compared to β-adrenergic drugs. Despite these apparent benefits, on the basis of relatively limited evidence for COX inhibitors, the reviewers could not advise the use of COX inhibitors in treatment and prevent of PTL.(26) Importantly, and mirroring the previous conclusions for other tocolytics, there was no evidence of improved outcomes for neonates with use of indomethacin. Similar evaluations of the efficacy of NO donors, primarily nitroglycerine, also concluded that there was insufficient evidence to demonstrate benefit over placebo or no treatment in terms of gestational prolongation, despite a slight suggestion of improved side-effects profile relative to other agents.(27)

One of the primary drawbacks to the drugs described above is their relative non-specificity for any SM bed. Previous work in rats and women indicated that the number of OT receptors expressed in uterine myocytes increases as parturition approaches.(28, 29) Therefore, in an attempt to more specifically target the myometrium, OT receptor antagonists were developed.(30, 31) A multi-center trial evaluating the efficacy of the first such OT receptor antagonist, atosiban, showed prolongation of pregnancy for up to 7 days

when treatment began at gestational age ≥ 28 weeks, and this occurred with low rates of side effects to the mother, and no significant difference in infant morbidity and mortality compared to the placebo group. The authors suggested that their observations supported a role for use of atosiban to treat PTL.(32) A subsequent systematic review evaluating continuous administration of atosiban as maintenance therapy to prevent recurrence of PTL did not show clinically significant benefits.(33) Atosiban has been approved for use in Europe where it is the first line agent in several countries,(20, 21) due to fewer cardiovascular side effects occurring with its use compared to nifedipine or ritodrine.(22) Atosiban has not been approved for use in the USA or Canada. A second OT receptor antagonist, barusiban, was developed to improve selectivity for the intended target, since atosiban was known to bind vasopressin receptors.(34) Though barusiban was well tolerated by patients, there was no significant pregnancy prolongation within 48 hrs of treatment initiation compared to placebo,(35) perhaps suggesting that the contribution of an effect at the vasopressin receptors needs to be evaluated as well.

As described, when they are effective, these agents can prolong pregnancy by 48 hrs and in some cases 7 days.(24, 36-38). This window of time enables administration of antenatal steroids to maximize lung maturation. Interestingly, administration of antenatal corticosteroids has been shown to reduce the risk of neonatal death and respiratory distress syndrome and other neonatal morbidities. A review of evidence for the use of antenatal corticosteroids for this purpose supported the use of a single course of steroids in women at risk of PTB, and suggested that a single course of corticosteroids should be used routinely in preterm deliveries.(39, 40) However, in spite of this rationale, review of tocolytic trials has not provided any suggestion that tocolytic therapy will increase the chance of completing a course of antenatal corticosteroids.(32, 41-43)

1.4 The Uterus and Contractile Activity

The uterus is a hollow organ with a well-differentiated lining layer (endometrium), a thick muscular coat (myometrium) and a serosal outer layer. Uterine contractions occur throughout the menstrual cycle in the non-pregnant state and throughout gestation. There are four important parameters that change under various physiological or pathophysiological conditions: frequency, amplitude, duration and direction of propagation.

Over the past two decades, considerable information regarding myometrial function in non-pregnant women has been obtained from the use of open-tipped pressure catheter recordings or from three-dimensional ultrasound or magnetic resonance imaging (MRI). Several reviews have described these changes and their potential clinical significance.(44-47) Contractile activity in the non-pregnant uterus appears to be fundamentally different than in the pregnant organ. The contractions observed during the menstrual cycle have been termed 'endometrial waves'.(48) Using a variety of imaging techniques, these contractions appear to involve only the sub-endometrial layer of the myometrium. These observations have led to a new concept of uterine anatomy that encompasses two distinct zones of the myometrium (Figure 1-1).

In non-primate species, the myometrium consists of two distinct layers – an outer longitudinal layer and an inner circular layer. However, in the human, the myometrial substructure is not so well defined.(49) The outer longitudinal layer is much less distinct and the major thickness of the myometrium is composed of intertwined muscle bundles that frequently surround abundant vascular channels. This histological arrangement might be of vital hemostatic importance following delivery of the hemochorial placenta that is characteristic of primates. Perhaps of particular interest to the physiology of the myometrium in the non-pregnant state, the inner (subendometrial) portion of the myometrium has been the focus of compelling research over the past three decades (reviewed in 47).

Previous work using MRI demonstrated a distinct tissue layer occupying the inner one-third of the myometrium.(50) During the reproductive years, this 'junctional' or 'sub-endometrial' layer appears anatomically distinct from the outer, denser myometrium but this distinctiveness is blurred in pre-pubertal and post-menopausal years. Some evidence supports the view that this junctional layer is also embryologically and functionally distinct from the outer myometrium.(51) It is suggested that the inner, junctional myometrium, which is composed of short muscle bundles arranged in a predominantly circular pattern, is derived from the paramesonephric (Mullerian) ducts of the female embryo but the outer, more predominant myometrium originates from non-Mullerian tissue. The junctional myometrium is rich in estrogen and progesterone receptors that are regulated throughout the menstrual cycle.(51) In contrast, there appears to be no such cyclic changes in sex

steroid receptor expression in the thick outer layer of the myometrium, which contains predominantly long muscle fibers arranged longitudinally and is the major contractile tissue during parturition and abortion.

Regardless of the presence or absence of physiologically distinct myometrial zones, uterine contractions are dependent on the individual contractile activity of the cellular elements, the uterine myocyte (human uterine smooth muscle cell; hUSMC). The remainder of this section will describe the molecular mechanisms that are likely to be involved in this activity. Most myometrial research has focused on changes that occur during pregnancy and in particular, those that might be related to the occurrence of PTL (for review see 52).

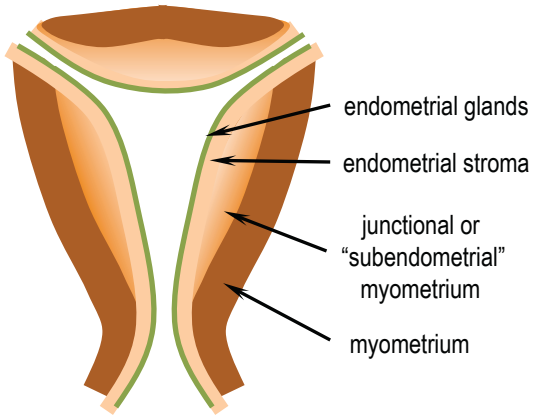

Figure 1-1. Concept of the Sub-Endometrial Layer of Myometrium.

This thinner, innermost layer of muscle fibers, which are arranged predominantly in a circular configuration around the uterine cavity, is suggested to be of different embryological origin with physiological properties distinct from the more prominent outer layer. The circular sub-endometrial layer may facilitate the changing vectors of 'endometrial waves' that might play important roles in common reproductive disorders. The outer layer is likely to be more important in more intense uterine activity including abortion or parturition.

1.5 Smooth Muscle Contractile Apparatus

SM cells (SMCs) are relatively small and densely packed with myofilaments and associated dense bodies that occupy 80-90% of the cell volume and constitute the contractile machinery (see Figure 1-2 and excellent reviews 53-55). The primary and most thoroughly studied constituents of these structures are actin and myosin.

1.5.1 Actin

As in all muscle tissue, the predominant proteins expressed in uterine SM are actin and myosin. In skeletal or striated muscle, there is approximately three-fold more myosin than actin. Conversely, SM has more actin than myosin on a molar basis by a factor ranging from 2 - 10.(53) In uterine SM, there is approximately six-fold more actin than myosin.(56) In SMCs, there are two major pools of filamentous actin. The thin filaments that form part of the contractile machinery are predominantly composed of α- and γ-actin.(57) These filaments ultimately slide along the myosin thick filaments to shorten the cell during a contraction (Figure 1-2). Another pool of actin (mainly β-actin) constitutes an important structural protein of the cytoskeleton just below the plasma membrane. Although not a part of the classical contractile machinery, this actin polymerizes in the presence of a contractile stimulant and, by strengthening the plasma membrane, might play an integral role in development of the mechanical tension generated.(55)

According to the current concept of uterine SM contractile activity, muscle shortening occurs when the thin filaments exert tension along the longitudinal direction of the cell through their intracellular attachments called ‘dense bodies’. Dense bodies serve as anchors from which the thin filaments can exert force to bring the polar cell membranes towards each other resulting in cell shortening. Interestingly, dense bodies also are associated with β-actin, which is the type found in the cytoskeleton, suggesting that dense bodies might integrate the functions of the contractile machinery and the cytoskeleton during contraction. In comparison, dense bands are associated with the plasma membrane, and tether the cytoskeleton to the actin filaments, which thus play an important role in transmitting the forces from the contractile units toward the plasma membrane to bring about cell shortening. The dense bands form rib-like structures around the circumference of the cell.

1.5.2 Myosin

The term 'myosin' encompasses a large superfamily of genes that share the ability to bind to actin and possess ATPase enzyme activity. The 'myosin motor' of human muscle tissue (Figure 1-2) is predominantly of the class myosin II (MII, for review, see 58). In SM, MII is a hexamer molecule composed of two heavy chains (MHC), and two pairs of myosin light chains. The MII hexamer consists of three regions. The tail domain is made up of the C-terminal ends of the MHCs, which are intertwined in an α-helical rod and form the major constituents of the thick filaments of SMCs. The *head* domain is composed of the globular N-terminal end of the MHCs that protrudes laterally from the filament. The head constitutes the 'motor domain' that contains the actin-binding region as well as the ATP hydrolysis site that provides the energy required for force production. The intermediate *neck* domain is the region creating the angle between the head and tail. This hinge-like lever arm is the site of non-covalent binding of the RLCs – one from each pair binds to each MHC.

There are two pairs of myosin light chains. The regulatory light chain (RLC) has a molecular mass of 20 kDa and the essential light chain (ELC) has a molecular mass of 17 kDa. In vascular and uterine SM, RLC plays a pivotal role in regulating muscle contraction.(59, 60) Its role will be discussed extensively in the following sections. The ELC is called the essential light chain and its exact function is unclear. However, ELC might contribute to the structural stability of the myosin head along with RLC and might also play a role in the regulation of contraction through physical interactions with actin that are dependent on the particular ELC isoform expressed in a given tissue.(61) The head and neck domains, along with the light chains, that lean outward from the thick filaments are called *cross-bridges* to reflect their function as the parts of the myosin macromolecule that interact with the actin filaments during contractile activity.

In SM, there is a single gene that codes for the dominant MHC. However, there are splice variants of this gene that result in 4 distinct SM MHC isoforms.(58, 62, 63) In uterine SM, the SM MHC isoforms expressed as a result of the actions steroid hormones might contribute to the physiological role of the myometrium.(64) In addition, SM might contain non-muscle (NM) MHC that can arise from multiple genes.(58, 65) To add further complexity, two variants of ELC ($ELC_{a/b}$) also exist, as a result of alternate splicing at the ELC gene. In contrast, different genes encode the two RLC isoforms, one coding for RLC

that will associate with SM MHC and the other a distinct protein that associates only with NM MHC.(58, 65-67) Literally hundreds of permutations of 4 light and 2 heavy chains are possible if we allow complete promiscuity amongst all splicing possibilities and combinations of NM and SM MHCs, though it is unlikely that more than a few such combinations are actually used or permitted within a specific SM bed. Despite varying expression ratios of the multiple MHC/RLC/ELC splice variants, a high level of functional specificity can be achieved.(58, 68) Thus, the possibility for fine-tuning of the contractile machinery exists. In this regard, differences in expression of various MII isoforms have been demonstrated to occur in different regions of the same organ.(69) Thus, regional differences in isoform expression could produce slightly different contractility profiles, which might influence the vector of propagation of forces. Clearly, much more research is required to clarify the physiological roles that might be fulfilled for each SM tissue by this heterogeneity of expression and isoform association amongst MII constituents.

Once the contraction has occurred, the cross bridge attachments need to be released in order that the muscle can relax. Though less is known about this phenomenon, it appears to be related to dephosphorylation of RLC. In some situations, the dephosphorylated RLC is very slow to allow detachment of the actin from the myosin cross bridge, resulting in a prolonged contraction. This has been referred to as a 'latch-bridge'.(70) This phenomenon might be of great value especially for tonically active SM beds as it would allow them to maintain basal tone through holding in an isometric state without a great energy cost.

Phosphorylation of S19 on RLC (pRLC) causes a conformational change that increases the angle in the neck domain of the MHC, thus mobilizing the cross-bridges and causing the actin thin filament to slide along the myosin thick filament. Upon MII activation, the myosin and actin filaments move by ~10 nm relative to each other in what is referred to as the 'power stroke'. Through an unknown mechanism, pRLC also activates the ATPase activity of the myosin head region to provide the energy to fuel the contraction. Subsequent phosphorylation of T18 on RLC to generate ppRLC might further increase the ATPase activity of MII.(71-73) However, pRLC has been the primary entity of interest in studies of regulation of SM contractile activity. This phosphorylation reaction is mediated by the

enzyme MLCK, which is predominantly regulated by the intracellular concentration of free calcium ion ($[Ca^{2+}]_i$). These mechanisms are the focus of section 0.

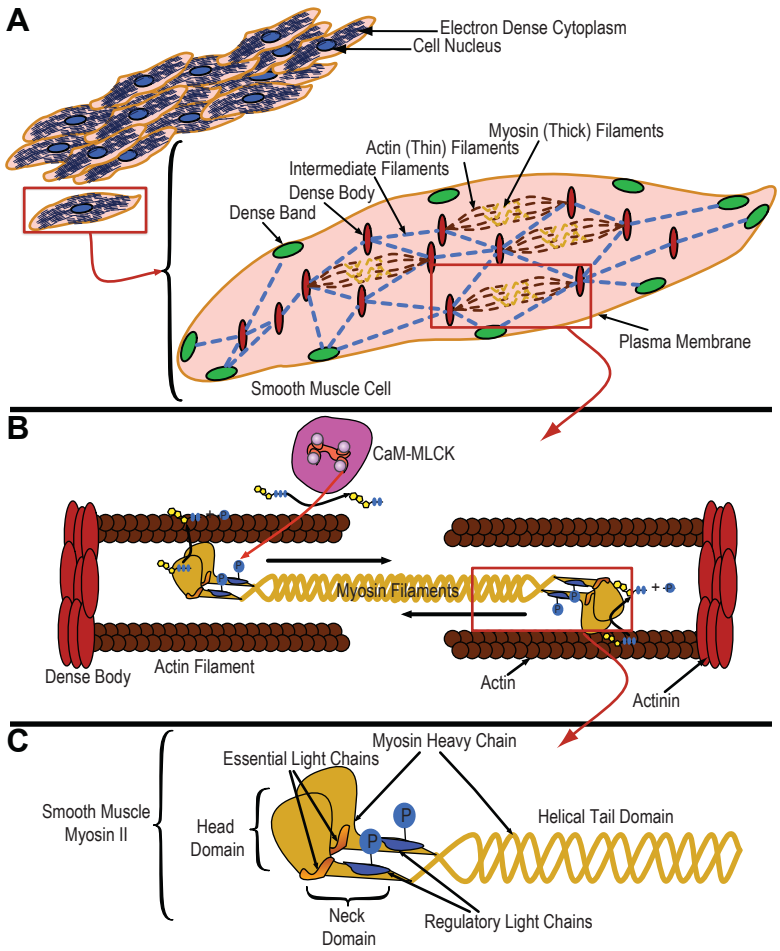

Figure 1-2. Smooth Muscle Contractile Machinery.

A. The smooth muscle cell (SMC) cytoplasm is densely packed with elements of the contractile machinery (thick and thin filaments), and other structural components (dense bodies, dense bands, intermediate filaments). The network formed by the combination of these elements results in force transduction along the longitudinal axis of the cell and cell shortening. **B.** The contractile elements are composed of myosin thick filaments and actin thin filaments anchored to dense bodies. The movement of thin filaments caused by phosphorylation of RLC and subsequent ATP hydrolysis of the myosin II ATPase decreases the distance between anchor points. **C.** Myosin II is a hexamer composed of two heavy chains, two essential light chains, and two regulatory light chains. Phosphorylation of the two regulatory light chains causes formation of a cross bridge between actin and myosin filaments and also creates in a change in the angle of the neck region of MII, which causes motion of the actin thin filaments resulting in shortening of the cell.

1.6 Excitation-Contraction Coupling

Uterine SM has a phasic pattern of contractile activity – maintenance of a resting tone with discrete, intermittent contractions of varying frequency, amplitude and duration. As noted earlier, the state of contractility is regulated predominantly by $[Ca^{2+}]_i$. From a functional point of view, the regulation of $[Ca^{2+}]_i$ can be considered in three phases: maintenance of basal concentrations, which play a role in resting tone of the SM; the marked increase in $[Ca^{2+}]_i$ that occurs with contractile agonist stimulation and results from firing of an action potential; and the restoration of $[Ca^{2+}]_i$ to resting state following stimulation (Figure 1-3). In general, these processes are controlled by inter-related ion channel and pump mechanisms. We will focus here on the mechanisms that regulate the firing of an action potential in uterine myocytes.

1.6.1 Myocyte Stimulation and Calcium Entry

As in all excitable tissues, in SM, the action potential is embodied by membrane depolarization. Agonist stimulation of G-protein coupled receptors (GPCRs) causes activation of receptor operated Ca^{2+} channels (ROC), which subsequently causes entry of extracellular Ca^{2+} through the opening of voltage-dependent Ca^{2+} channels (VDC) in the plasma membrane. These events in turn causes a dramatic rise in $[Ca^{2+}]_i$ and contraction to occur.(74) At the plasma membrane level, the predominant Ca^{2+} channels in the uterine myocyte are the L-type Ca^{2+} channels, which are ubiquitous, large conductance, VDCs.(75) When the uterine myocyte membrane potential is depolarized to approximately -40 mV, the L-type VDC opens to allow a massive influx of Ca^{2+}.(76) Further, activation of GPCRs in the myocyte plasma membrane result in activation of a trimeric G-proteins containing a $G_{\alpha q}$ or $G_{\alpha 11}$ subunit (Figure 1-3).(77) Activation of this subunit in the uterine myocyte stimulates membrane phospholipase C_β (PLC_β) to hydrolyze phosphatidylinositol bisphosphate (PIP_2) into inositol-trisphosphate (IP_3) and diacylglycerol (DAG), which serve as second messengers.(78-80) IP_3 interacts with a specific receptor (IP_3R) at the level of the sarcoplasmic reticulum (SR) causing release of Ca^{2+} from its intracellular storage site and a subsequent rise in $[Ca^{2+}]_i$.(81-83) Though single action potentials are sufficient to induce the propagation of an electrical wave of activity in the myometrium, multiple coordinated depolarizations are necessary for forceful and sustained contractions. (84)

The liberation of Ca^{2+} from intracellular stores along with the influx of Ca^{2+} from the extracellular space serve to activate the biochemical pathways which lead to actin-myosin cross-bridging and force development in the presence of ATP.

Ca^{2+} removal post-contraction is essential to induce relaxation of the SM and to replenish the SR for the next contractile stimulus (Figure 1-3). This is achieved by a variety of mechanisms, including the closure of plasma membrane Ca^{2+} channels and simultaneous extrusion of Ca^{2+} from the cytosolic compartment into the extracellular space and into intracellular stores via plasma membrane Ca^{2+} ATPase (PMCA) and the SR/ER Ca^{2+} ATPase (SERCA), respectively. These dynamic changes in intracellular Ca^{2+} serve to regulate the activity of MLCK as described below.

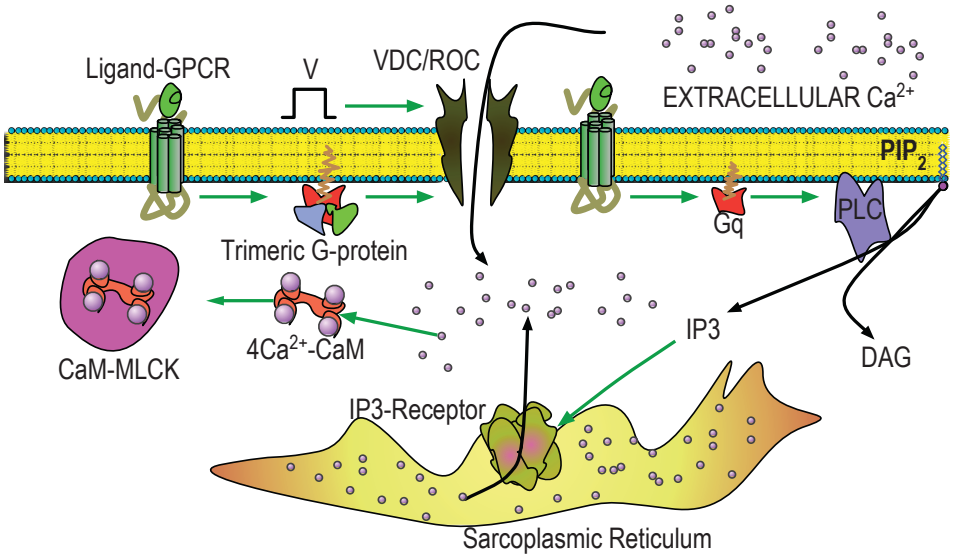

Figure 1-3. Excitation-Contraction Coupling in Smooth Muscle.

Agonist activation of G-protein coupled receptors (GPCRs) results in opening of receptor-operated (ROC) and voltage-dependent (VDC) plasma membrane Ca^{2+} channels. In parallel, the G-protein $G_{\alpha q}$ stimulates phospholipase C (PLC) to cleave phosphatidyl-inositol-bisphosphate (PIP_2) into diacylglycerol (DAG) and inositol-trisphosphate (IP_3), the latter of which activates a receptor at the level of the sarcoplasmic reticulum (SR) to induce Ca^{2+} release from internal stores. These events result in a rise in the internal level of Ca^{2+}, and ultimately activation of myosin light chain kinase (MLCK) through the intermediary activation of calmodulin (CaM). Green, red, and black lines depict activation, inhibition, and ion movement, respectively.

1.6.2 Myosin Light Chain Kinase

The events discussed above ultimately yield a marked increase in $[Ca^{2+}]_i$, which is the necessary trigger for activation of calmodulin (CaM), a Ca^{2+}-dependent cytosolic protein which binds four Ca^{2+} ions (Figure 1-3).(85) The $4Ca^{2+}$-CaM complex activates the key enzyme MLCK and causes an immediate and marked increase in phosphorylation of RLC, which activates the contractile machinery.(86) There are three isoforms of MLCK (smooth (smMLCK), skeletal (skMLCK), and cardiac (cMLCK)).(87) The remainder of this work will deal only with smMLCK ('MLCK' hereafter). The $4Ca^{2+}$-CaM complex assumes a conformation that allows activation of MLCK and markedly enhances the enzyme activity toward S19 of RLC to generate pRLC.(86, 88) This phosphorylation event is permissive on actin-myosin cross-bridging,(89-91) which might facilitate thick myofilament formation and further enhances the myosin ATPase activity *in vitro*.(92) Furthermore, in SM almost the entire pool of RLC might be phosphorylated within a few seconds during a maximal stimulus by virtue of the rapid kinetics of MLCK.(87, 93, 94)

MLCK is a ubiquitously expressed enzyme encoded by a single gene. There are two isoforms (220 kDa, 130 kDa) arising through use of alternate promoters.(95) The larger of these two MLCK isoforms is differentially expressed in embryonic tissues as compared to adult tissues and is also called 'NM' or 'endothelial' MLCK. This might indicate a different functional role for MLCK activity in the embryo as compared to adult tissues. The 130 kDa MLCK achieves its highest levels of expression in SM. In both rat and human myometrium, inhibition of MLCK using wortmannin (primarily a PI3K inhibitor) and ML9 (more specific for MLCK than wortmannin) entirely abolished contractions that were induced using OT or depolarization with KCl.(96) These findings indicate that there is no alternative pathway for contraction in uterine SM, and that phosphorylation of RLC by MLCK is both necessary and sufficient for contraction to occur. This is in contrast to the contractile mechanism of skeletal muscle, which depends on Ca^{2+} availability and requires proteins such as troponin C to undergo a conformational change so as to permit actomyosin complex formation.(97) MLCK contains several phosphorylation target-sites for PKA, PKC and other kinases. PKA-mediated phosphorylation of S512 of MLCK lies in the C-terminal portion of the CaM binding domain.(98-101) PKC can also phosphorylate S512.(57, 102) This event impairs the ability of CaM to activate MLCK, and has been

shown to decrease uterine contractile activity.(101) These mechanisms of inhibition of MLCK likely mediate a portion of the relaxant effects of the β-adrenergic agents mentioned in section 1.3. It is possible that some physiological antagonism for MLCK activation can be achieved by PKA or PKC, which might be useful to reduce myocyte activation during pregnancy.

The role of CaM is not limited to the activation of MLCK. In fact there is evidence that CaM might be involved in regulating membrane channels and Ca^{2+}-ATPases that serve to limit the transient rise in $[Ca^{2+}]_i$ and therefore aid in resetting the system for the next contraction. Note that the events of Ca^{2+} influx and contraction are separated temporally. The activation of MLCK by CaM and movement from the cytosol toward the contractile apparatus might be the rate-limiting steps of contraction (103) in terms of the speed of response of the smooth muscle cell (SMC).

1.7 Mechanisms of Calcium Sensitization

As mentioned previously, SM contraction is dependent on the state of phosphorylation of RLC, which is primarily regulated by Ca^{2+}-CaM. However, the concentration of $[Ca^{2+}]_i$ does not always parallel the intracellular concentration of pRLC and/or the degree of contractile activation. In some situations, particularly after stimulation with an agonist such as OT, a given rise in $[Ca^{2+}]_i$ will cause a larger-than-expected force of contraction. This phenomenon is known as 'Ca^{2+} sensitization' (CS).(104-106) The advent of Ca^{2+}-responsive fluorophores enabled the demonstration that the ratio of force output to Ca^{2+}-entry induced by SM agonists was not always constant.(107) Further, these agonists were capable of inducing larger amplitude forces compared to depolarizing stimuli such as high K^+ solutions.(106, 107) At the biochemical level, pRLC concentrations reflect an enzymatic balance between the activities of MLCK and RLC phosphatase (MLCP). Thus, either elevation in MLCK activity or inhibition of MLCP activity could produce the observed force enhancement. Subsequent experiments demonstrated that inhibition of MLCP is the major mechanism controlling CS.(108, 109) Abundant evidence is accumulating to demonstrate that a pathway is activated following stimulation of GPCRs to inhibit MLCP and thus potentiate the pRLC generated from the simultaneous activation of MLCK. This pathway involves the small GTPase rhoA and its effector, rhoA-associated kinase (ROK) (Figure 1-4). In SMCs, rhoA-ROK activation might be mediated by trimeric

G-proteins.(110, 111) ROK phosphorylation of the subcellular targeting subunit (MYPT1) of MLCP interferes with the ability of the catalytic subunit (PP1c) to act on pRLC, thereby preventing dephosphorylation.

1.7.1 RhoA and its Associated Kinase

RhoA is a small monomeric G-protein and a member of the rho subfamily of the Ras superfamily of monomeric GTPases. Human rhoA is a 193 amino acid protein of ~22 kDa.(112) RhoA follows activation and deactivation cycle like other G-proteins, which are dependent on the opposing activities of GTPase Activating Proteins (GAPs) and Guanine Nucleotide Exchange Factors (GEFs). GEFs are 'enablers' of G-protein activation as they promote the exchange of GDP for GTP, and in doing so encourage interaction between the G-protein and its downstream effectors.(113) Conversely, GAPs serve to terminate the transduced signal at the level of the G-protein promoting hydrolysis of the γ-phosphate of the bound GTP. This is achieved by enhancing the intrinsic GTPase activity of the G-protein. GAPs are necessary in order to serve as molecular 'off' switches because the rate of hydrolysis intrinsic to rhoA and other G-proteins is relatively slow.(114)

RhoA is activated by GPCRs linked through $G\alpha_{12/13}$,(115) and its activity is inducible in uterine and other SMs.(116-118) For activation, rhoA translocates to the plasma membrane by virtue of a C-terminal post-translational modification in the form of a prenyl (lipid) moiety.(119-121) The prenylation step is crucial to rhoA function in several ways. First, it confers the ability of proteins undergoing this modification to associate with biological membranes; rhoA is therefore capable of translocation to the plasma membrane where it can interact with GPCRs upon activation.(119, 120) This translocation event has been demonstrated to occur the myometrium.(121) In addition, the prenyl group confers the ability to interact with the plasma membrane and also with its corresponding GEFs.

In its inactive state, rhoA is sequestered in the cytosol by rho-guanine nucleotide dissociation inhibitor (rhoGDI). RhoGDI contains a hydrophobic pocket that surrounds the prenyl moiety on the C-terminus of rhoA and prevents its association with the plasma membrane and with the activating GEFs.(122-124) RhoGDI also diminishes the intrinsic GTPase activity of rhoA as well as the activating capacity of GAPs.(124, 125) RhoA can be inhibited by cyclic adenosine monophosphate (cAMP)- or cyclic guanosine monophosphate (cGMP)-induced phosphorylation at S188 mainly by enhancing

sequestration by rhoGDI.(126-128) RhoA was implicated as a mediator in the process of CS by experiments demonstrating that this phenomenon was diminished using a specific inhibitor of rhoA and that the molecular mechanism downstream of rhoA involved MLCP inhibition.(108, 129, 130)

ROK, a serine/threonine kinase(131, 132) is one of the main signal transduction effectors of rhoA. There are two isoforms (ROK-1 and ROK-2) arising from separate genes and both are expressed in human and rat myometrium,(133-136) but pregnancy-related increases in expression have only been reported for rats.(137) ROK is recruited to the plasma membrane of responsive cells upon rhoA translocation.(132, 138-140) The activation of ROK appears to involve trans-autophosphorylation and dimerization.(141, 142) As mentioned, ROK can inactivate MLCP by phosphorylation of MYPT1 (see the following section).(108, 143) An ATP-competitive cell-permeable inhibitor of ROK (Y-27632) diminishes spontaneous and agonist-stimulated myometrial contractility *in vitro*.(144-146) Further, agonist stimulation of uterine myocytes in culture promotes rhoA and ROK recruitment to the plasma membrane (Figure 1-4) suggesting that these proteins play a role in agonist-induced contractions.(116, 121) In addition to its effects on MLCP, ROK can also directly phosphorylate RLC on S19 *in vitro* leading to enhancement in myosin ATPase activity.(136, 147) The physiological relevance of this event has been questioned given that GTP-γ-S induced activation of rhoA did not increase the level of pRLC nor contraction to any significant extent *in vivo* using rabbit tracheal or guinea-pig ileal SM in the absence of Ca^{2+},(63, 148, 149) suggesting that MLCK remains a compulsory element in phosphorylation of S19 of RLC.

1.7.2 Myosin Light Chain Phosphatase (MLCP)

This key enzyme has been the subject of many recent reviews.(150-154) The MLCP holoenzyme is a serine/threonine phosphatase that consists of three subunits. The catalytic subunit of 38 kDa is a member of the type 1 protein phosphatase family (PP1c).(155) As with other members of this phosphatase family, it has broad substrate specificity and therefore the activity of the holoenzyme is determined mainly by the substrate targeting subunit, MYPT1. There are many endogenous peptide inhibitors of the PP1c catalytic subunit but the physiological significance of these with respect to the holoenzyme is unclear.(156)

MYPT1 (also known as the 'myosin binding subunit' (157)) is highly expressed in SM and has several isoforms resulting from splice variants of a single gene.(153, 158-161) This subunit associates with PP1c through a binding motif in its N-terminal region.(162) Its major function is to bind pRLC and provide access to the catalytic subunit for removal of the phosphate moiety. Phosphorylation of MYPT1 is an important mechanism of regulation of MLCP activity. MYPT1 has two major phosphorylation sites (T696, T853 in human sequence) that are targets for ROK.(157) Phosphorylation of T696 causes marked inhibition of PP1c activity, either by interacting with the catalytic site or by causing a conformational change.(152, 163) Phosphorylation of T853 disrupts the pRLC-binding motif and thus reduces the ability of MLCP to associate with its target (Figure 1-4). Phosphorylation of either of these sites has also been shown to disrupt the ability of MYPT1 to target PP1c to a particular subcellular location.(108, 143, 152, 164, 165) It is not clear which of these sites is the predominant mediator of ROK-induced inhibition in uterine myocytes.

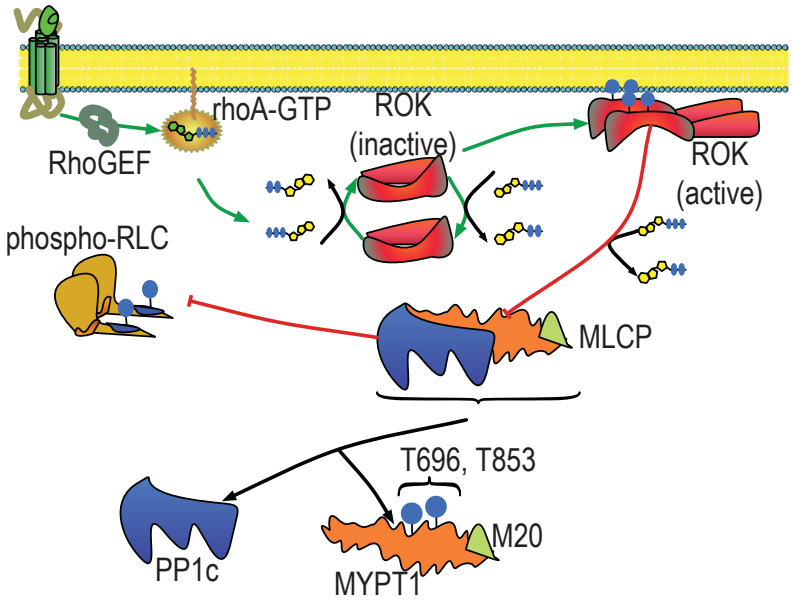

Figure 1-4. RhoA and Rho-Kinase Signaling Pathway.

Activation of GPCRs leads to recruitment of rhoA to the plasma membrane after exchange of GDP for GTP facilitated by a specific rho-guanine nucleotide exchange factor (GEF). Rho-associated kinase (ROK) is activated by rhoA in a mechanism proposed to involve trans-phosphorylation and oligomerization. ROK phosphorylates the myosin targeting subunit (MYPT1) of MLCP at two potential sites (T696, T853) thus promoting dissociation of the holoenzyme and preventing the dephosphorylation of RLC by the phosphatase subunit (PP1c) through interrupted targeting. Green and red lines depict activation and inhibition events, respectively.

If they are physiologically relevant, the biochemical determinants mediating CS are likely opposed by mechanisms working to decrease the sensitivity of SM to Ca^{2+}.This concept is termed 'Ca^{2+}-desensitization' (CD). CD might be dependent on cyclic nucleotides and might depend on the expression of a specific isoform of MYPT1,(166-168) and potentially increase MLCP activity as part of CD and SM relaxation. For example, protein kinase G (PKG) phosphorylates S695 of MYPT1 which causes relaxation, probably by interfering with phosphorylation of T696.(167) Further, phosphorylation by protein kinase C (PKC) of an undetermined residue in the N-terminal portion of MYPT1 reduced its affinity for PP1c and hence the activity of MLCP.(169) MYPT1 also can be phosphorylated by a host of other kinases but their physiological roles are uncertain. The variety of phosphorylation targets available on MYPT1 indicates that this protein might be a key convergence point for many signaling pathways involved in contractility modulation. The physiological relevance of CD remains elusive. However, implementation of such a mechanism in tissues such as the human myometrium would aid in ensuring a long period of dormancy during gestation and therefore its potential physiological relevance is worthy of investigation.

The third subunit of MLCP is a small peptide of approximately 20 kDa termed sm-M20.(170) Though it might bind RLC, this does not affect the rate of phosphatase activity.(152) Its role is unknown.

1.7.3 RhoA and ROK in Uterine Smooth Muscle

This signaling pathway is becoming increasingly recognized as a potential functional mechanism for the regulation of uterine contractility. Most of the studies have been focused on the uterus during gestation but these same mechanisms might be equally applicable in the non-pregnant state. The mRNAs for rhoA, ROK-1 and ROK-2 are present in the non-gravid uterus and increase during pregnancy.(133, 144, 171-173)

Further evidence supporting a physiological role for rhoA-ROK is provided by the presence of antagonism to this system during the quiescent phase of pregnancy. The rnd family of proteins (rnd1-3) consists of monomeric G-proteins with preferential affinity for GTP compared to GDP and with low GTPase activity. By diminishing the availability of GTP, they can interfere with rhoA-ROK interactions resulting in CD.(174) Protein levels of

rnd2 and rnd3 are increased in human myometrium during pregnancy compared to tissues from non-pregnant women.(175) Conversely, when assessing mRNA levels using semi-quantitative techniques, pregnant rats had increased concentrations of all 3 rnd isoforms whereas, in human myometrium, the rnd2 and rnd3 mRNAs were increased.(171, 175) Though this area requires further study, the data are compatible with a role for rnd proteins regulating myometrial activity in pregnancy, presumably by affecting rhoA-ROK.

Various uterotonins have been evaluated for their ability to induce rhoA-ROK activity. This mechanism appears to be an important component of the potent contractile effects of OT on the human myometrium.(176) Further, OT-stimulated contractions of human myometrium obtained at term elective cesarean section are inhibited by the ROK inhibitor Y-27632 independently of the change in $[Ca^{2+}]_i$.(177) In addition, ROK inhibition impedes tension development and promotes relaxation without altering the level of $[Ca^{2+}]_i$ in spontaneous and agonist-stimulated contraction.(134, 135, 145, 149, 177, 178) Similar observations were made in rat muscle strips stimulated with carbachol.(179) Finally, rhoA and ROK translocate to the plasma membrane in freshly isolated myometrial cells stimulated with uterine agonists, indicating rhoA-ROK activation.(116) Taken together, these data argue for a role for rhoA-ROK in regulating the contractility of the myometrium of different species and inducible by physiologically relevant stimuli.

On the other hand, there are some data that question the role of ROK in OT-induced contractions in human myometrium obtained at term elective cesarean section. Y-27632 caused no significant attenuation of force in spontaneous contractions induced by a physiological concentration (10 nM) of OT. However, when the muscle strips were pre-exposed to KCl, then treated with a higher concentration of OT (100 nM) that is more likely to produce a tetanic contraction, there was a significant suppressive effect of the ROK inhibitor.(145) This suggests that the ROK pathway is more important in promoting force enhancement during tonic rather than phasic contractions. Clearly, further studies are necessary to determine the importance of these pathways in basal or stimulated uterine myocyte contractile function.

Prostaglandin $F_{2\alpha}$ ($PGF_{2\alpha}$) has also been implicated in the induction of rhoA-ROK activity in human,(178) avian,(180) and in murine tissues with the accompanying formation of GTP-rhoA.(181) Upon $PGF_{2\alpha}$ stimulation of human myometrial strips, peak $[Ca^{2+}]_i$

remains unchanged, but peak force of spontaneous contractions is significantly increased.(178)

1.8 Therapeutic Approaches to Regulation of Uterine Contractile Activity

The tocolytic drugs described in section 1.3 are largely directed towards limiting the contractile stimuli or the pathways that lead to contractile activation in the uterus, rather than directly interfering with the contractile machinery. Hence, the duration of the effects (and side-effects) of treatment might actually be longer than the duration of the decreased uterine contractility. Even with the great volume of research information concerning uterine contractility in late gestation, most attempts to prevent or inhibit uterine contractions have had little, if any beneficial effect and have resulted in common and serious side effects.(43) Thus, there is a great need to develop new and successful strategies for tocolysis. The simplest strategy would be to administer a drug that specifically reduces uterine contractility and minimizes off-target effects, particularly in the cardiovascular system. At present, there are many well-characterized inhibitors of many of the pathways described above which have not already been used as tocolytics.

For example, direct pharmacological antagonists of CaM and MLCK have been thoroughly studied *in vitro* and demonstrated the expected reduction in pRLC levels. The energy supply could be disrupted using myosin ATPase inhibitors to reduce the rate of active cross bridge cycling. RhoA or ROK could be manipulated using well-studied agents that inhibit activity of this pathway. The concerns with all of these agents relate to their likely non-specificity for uterine SM and, as has been learned from their use in pregnancy, the resulting potential for significant side effects. Considering the centrality of many of these protein targets in mediating SM contractility in all muscle beds, it might be difficult to develop pharmacological tools with therapeutic efficacy for uterine disorders without significant advances in drug targeting technologies.

Another strategy would be to improve our specific understanding of the molecular physiology of uterine SM to identify a suitable uterine-specific target. As described above, rhoA or ROK might be important therapeutic targets for regulation of uterine activity. However, despite the large volume of literature demonstrating the relationships between agonist stimulation and rhoA-ROK activation, there is little information regarding the

physiological role of this mechanism in the human uterus. To date, most of our understanding of the workings of uterine SM has been extrapolated from studies performed in a variety of non-human animals, and in non-uterine SMs. Relatively few studies have focused on uterine SM from any species, and only a fraction of these studies have used human uterine SM.

The data presented in the following chapters aim to reduce this knowledge gap, by focusing on human uterine SM, and further, to determine whether there exists the possibility to exploit a biochemical mechanism at work in uterine myocytes that is not involved, or plays a lesser role, in the contractility of other SMs. These biochemical differences must be reflected at the level of phosphorylation of RLC since it is the final common pathway to myometrial force production. Thus, while it is probable that any one of a variety of pathophysiological processes might precipitate PTL, they must all act by increasing phosphorylation of RLC. Therefore, tocolytics acting at this fundamental level of myocyte function might be more successful in treating PTL of varied origins.

Chapter 2

Hypotheses, Objectives and Experimental Aims

2 Hypotheses, Objectives and Experimental Aims

From the preceding discussion, it is evident that we require an improved understanding of the regulation of myometrial contractility. Uterine stimulants act through GPCRs linked to several intracellular cascades responsible for inducing myometrial contractions. In particular we were interested in evaluating the contribution of rhoA-ROK downstream of GPCR activation by physiologically relevant stimuli to determine if interference with this signaling system might be suitable and specific for reducing unwanted uterine activity. Our interest in rhoA-ROK emerged from evidence suggesting rhoA-ROK plays a role in myometrial SM contractility.(182) The precise intracellular role and physiological relevance of rhoA-ROK with regards to uterine function remain undiscovered. The myometrium is a phasically contracting SM, whereas many of the SMs in which rhoA-ROK has been studied thus far are tonically active.(183) We were interested in the possibility that this pathway serves a different purpose, or at least behaves in a different manner, in SMs with different contractile profiles. Elucidation of such a difference might indicate a novel strategy for tocolysis, or provide a feasible alternative strategy for improving efficacy or reducing the occurrence of unwanted side-effects in comparison to tocolytic therapies currently available.

Ultimately, myocyte activation, irrespective of stimulus and intervening signaling systems, results in increased phosphorylation of RLC. Thus, we aimed to determine the role of rhoA and ROK in the phosphorylation of RLC in cultured human uterine myocytes (hUSMC) as a biochemical indication of the mechanisms that might be at work in intact myometrium. A major aspect of this work also involved a direct comparison of biochemical parameters between hUSMC and vascular myocytes (hVSMC).

2.1.1 Primary Hypotheses

The **primary hypotheses investigated** in this work were:

A. Diphosphorylation (T18/S19) of RLC is mediated by ROK in hUSMC.

B. Diphosphorylation (T18/S19) of RLC is a unique feature of hUSMC that differentiates them from hVSMC.

These hypotheses were conceived and tested secondary to development and validation of two complementary technologies for rapid and quantitative assessment of phosphorylated RLC in cultured hUSMC using phospho-specific Abs. These techniques are the in-cell western assay, and quantification of phospho-states corresponding to RLC by western immunoblotting after phos-tag SDS-PAGE.

2.1.2 Development of the In-Cell Western Assay for High-Throughput Quantification of Phosphorylated RLC

Specifically, **the objectives of this work were:**

A. Provide a technical evaluation of in-cell westerns (ICWs) using near-infrared fluorescence-based western immunoblots (WBs) as a reference standard.

B. Evaluate the relative ability of ICWs and WBs measure phosphorylation of RLC in response to a physiological stimulus in hUSMC.

The corresponding **experimental aims designed to achieve these objectives were:**

A. Assess and compare the linearity, specificity and precision of signals measurable by ICW and WB.

B. Evaluate and compare results obtained from ICW and WB assessments with regard to concentration- and time-dependency of physiological phosphorylation events.

These data are presented in chapter 3. An additional goal of this work was to determine the suitability of ICW as a technique that may be substituted for WB in signaling studies, particularly for high-throughput experimental protocols involving concentration-response measurements to a variety of pharmacologic agents.

2.1.3 Development of Western-Based Assay for Quantification of RLC Phospho-States

In similar terms, **the objectives of this work were:**

A. Develop a method for quantification of phospho-state distribution data, in general terms and specifically for measurements of RLC in hUSMC.

B. Evaluate and validate this method under various treatment conditions likely to result in altered phosphorylation of RLC in hUSMC.

C. Evaluate whether the reported changes in phosphorylation of RLC result from activity at T18 and S19 alone, or whether they might be explained by activity at distinct phosphorylation sites.

The **experimental aims designed to achieve these objectives were:**

A. Detect and quantify multiple phospho-states corresponding to RLC using WB after a variant of SDS-PAGE capable of separating proteins on the basis of phosphorylation stoichiometry.

B. Quantify changes in the phospho-state distribution of RLC in hUSMC challenged with a muscle stimulant (oxytocin), or activators and inhibitors of the rhoA-ROK system (calpeptin and glycyl-H1152 (g-H), respectively).

C. Induce phosphorylation of RLC in hUSMC at sites other than T18 or S19 using an activator of PKC and determine whether novel phospho-states can be detected.

These data are presented in chapter 4.

2.1.4 Comparison of Rho-Kinase-Mediated Phosphorylation of RLC in Human Uterine and Vascular Myocytes

The development of these two techniques, and in particular, the quantification of phospho-states of RLC strongly suggested a necessity to differentiate and quantify mono- (S19, pRLC) and di-phosphorylated (T18/S19, ppRLC) RLC in hUSMC, resulting in our primary hypotheses. We addressed these hypotheses specifically with the following objectives and experimental aims:

The **primary objectives of this work were:**

A. Compare the sensitivity of phosphorylation of RLC in resting hUSMC and hVSMC challenged with a ROK inhibitor.

B. Determine the predominant phosphorylation changes in RLC associated with agonist stimulation in hUSMC and hVSMC.

C. Assess the effect of ROK inhibition on the predominant phosphorylation changes in RLC associated with stimulation of hUSMC and hVSMC.

In addition, **the secondary objectives were:**

A. Determine whether the predominant phosphorylation changes in RLC observed in hUSMC are properties of specific agonists, or general features of myocyte activation.

B. Assess the relative contribution of MLCK and ROK in mediating changes in phosphorylation of RLC in stimulated hUSMC.

C. Evaluate the role of ROK-mediated inhibition of MLCP in resting and agonist-induced phosphorylation of RLC in hUSMC.

To achieve these primary and secondary objectives, the **experimental aims were:**

A. Determine the changes in the phospho-states for RLC in stimulated hUSMC in the presence or absence of MLCK or ROK inhibitors (ML7 or g-H).

B. Measure resting concentrations of pRLC and ppRLC in hUSMC and hVSMC challenged with increasing concentrations of a ROK inhibitor (g-H).

C. Measure stimulated concentrations of pRLC and ppRLC in hUSMC and hVSMC challenged with OT or endothelin-1 (ET-1).

D. Measure concentrations of pRLC and ppRLC in stimulated hUSMC and hVSMC in the presence and absence of a ROK inhibitor (g-H).

E. Measure concentrations of pRLC and ppRLC in stimulated hUSMC in the presence and absence of an MLCK inhibitor (ML7).

F. Measure concentrations of pRLC and ppRLC in response to increasing concentrations of an MLCP inhibitor (calyculin A), in combination with g-H or OT.

G. Measure phosphorylation of MYPT1 in resting or stimulated hUSMC treated with g-H.

These data are presented in chapter 5.

Chapter 3
Primary Methodology 1

Quantification of Rapid Myosin Regulatory Light Chain Phosphorylation Using High-Throughput In-Cell Western Assays: Comparison to Western Immunoblots.

Abstract

Background: Quantification of phospho-proteins is crucial when studying cellular signaling pathways. Western immunoblotting (WB) is commonly used for the measurement of relative levels of signaling intermediates in experimental samples. However, WB is in general a labor-intensive and low-throughput technique. Because of variability in protein yield and phospho-signal preservation during protein harvesting, and potential loss of antigen during protein transfer, WB provides only semi-quantitative data. By comparison, the 'in-cell western' (ICW) technique has high-throughput capacity and requires less extensive sample preparation. Thus, we compared the ICW technique to WB for measuring phosphorylated myosin regulatory light chain (p19RLC) in primary cultures of uterine myocytes to assess their relative specificity, sensitivity, precision, and quantification of biologically relevant responses.

Methodology/Principal Findings: ICWs are cell-based microplate assays for quantification of protein targets in their cellular context. ICWs utilize a two-channel infrared (IR) scanner (Odyssey®) to quantify signals arising from near-infrared (NIR) fluorophores conjugated to secondary antibodies. One channel is dedicated to measuring the protein of interest and the second is used for data normalization of the signal in each well of the microplate. Using uterine myocytes, we assessed oxytocin (OT)-stimulated RLC phosphorylation measured by ICW and WB, both using NIR fluorescence. ICW and WB data were comparable regarding signal linearity, signal specificity, and time course of phosphorylation response to OT.

Conclusion/Significance: ICW and WB yield comparable biological data. The advantages of ICW over WB are its high-throughput capacity, improved precision, and reduced sample preparation requirements. ICW might provide better sensitivity and precision with low-quantity samples or for protocols requiring large numbers of samples. These features make the ICW technique an excellent tool for the study of phosphorylation endpoints. However, the drawbacks of ICW include the need for a cell culture format and the lack of utility where protein purification, protein concentration or stoichiometric analyses are required.

The contents of this chapter have been adapted from reference 184.

In chapters 3 to 5, the technical validations of two techniques are presented independently of the primary experiments that constitute the novel contribution of this thesis to the scientific literature. Though applied here specifically to the quantitative assessment of phosphorylated RLC, these technologies were developed in a general way so that they may be applied to other biochemical measurements of interest. Therefore, all three chapters contain specific introductory, materials and methods, results, and discussion sections.

At this time it is critical to clarify some of the terminology to be used in the following chapters. Specifically, in these studies we differentiate between monophosphorylated (S19) and diphosphorylated (T18/S19) RLC, and denote these phosphoisotypes as pRLC and ppRLC, respectively. In addition, data regarding 'total' phosphorylation at S19 (the sum of pRLC and ppRLC, denoted as p19RLC)) are provided. These forms of phospho-RLC were quantified by the methods described in chapters 3 and 4, using antibodies (Abs) that cross-react specifically with pRLC, ppRLC, or p19RLC. The specificity of these Abs is demonstrated in Figure 3-2 and the primary implications and consequences of their cross-reactivity are discussed in chapter 4. We then exploit these cross-reactivity differences to obtain much of the data in chapter 5.

3 Quantification of Rapid Myosin Regulatory Light Chain Phosphorylation Using High-Throughput In-Cell Western Assays: Comparison to Western Immunoblots.

3.1 Introduction

Western immunoblotting (WB) is widely utilized to study relative levels of signaling intermediates including a variety of phosphoproteins. The increasing availability of Abs for specific phosphoproteins has enhanced the popularity of this relatively inexpensive technique. Recently, there has been increasing use of near-infrared (NIR) fluorophore–conjugated Abs for the WB technique. Compared to chemiluminescent antigen detection, NIR fluorophores extend the linear range of detection and potentially improve WB sensitivity.(185, 186) These two properties improve quantification of highly abundant or relatively scarce proteins in cell lysates. Currently available NIR scanners (Odyssey®) for this purpose have two separate channels. This enables simultaneous detection of two different proteins, providing that the primary Abs are raised in different species and that the species-specific secondary Abs are labeled with different fluorophores. This segregation of signals is particularly useful in phosphorylation studies since it facilitates normalization of the phosphoprotein signal to that of the total protein. However, WB continues to be a low-throughput, labor-intensive technique. An additional consideration for the assessment of phosphoproteins is the potential for excessive variability particularly during protein transfer from the gel to the membrane, which might diminish the precision of the assay.(187, 188)

The in-cell western (ICW) technique is a cell-based assay for the measurement of proteins in their cellular context. ICWs utilize 96-well or 384-well microplates into which adherent or non-adherent cells can be plated and analyzed using the Odyssey® scanner. This methodology requires the segregation of signals derived from the protein of interest and a normalization signal (reference protein (actin, glyceraldehyde-3-phosphate-dehydrogenase (GAPDH), etc.), or total cell content) into one of the two detection channels. ICWs eliminate the need for protein harvesting, lysate preparation, electrophoretic separation and electrophoretic transfer steps. However, due to the absence of a protein separation step, ICWs require that primary Abs be highly specific for the proteins of interest in the context of microscopy. Currently, only a few reports contain data

produced by ICWs, and none of these include thorough validations of the ICW technique beyond evaluating antibody (Ab) specificity using WB.(189-193)

T**he objectives of the this chapter were:**

A. Provide a technical evaluation of in-cell westerns (ICWs) using near-infrared fluorescence-based western immunoblots (WBs) as a reference standard.

B. Evaluate the relative ability of ICWs and WBs measure phosphorylation of RLC in response to a physiological stimulus in hUSMC.

The corresponding **experimental aims designed to achieve these objectives were:**

A. Assess and compare the linearity, specificity and precision of signals measurable by ICW and WB.

B. Evaluate and compare results obtained from ICW and WB assessments with regard to concentration- and time-dependency of physiological phosphorylation events.

An additional goal of the work in this chapter was to determine the suitability of ICW as a technique that may be substituted for WB in signaling studies, particularly for high-throughput experimental protocols involving concentration-response measurements to a variety of pharmacologic agents.

3.2 Materials and Methods

3.2.1 Primary hUSMC Cultures

The protocol to obtain biopsies from the lower segment of the uterus at the time of cesarean section was reviewed and approved by the Human Ethics Review Board of the University of Alberta and the Ethics Review Board of Capital Health, the provider of health services in the region. A research nurse at the Royal Alexandra Hospital in Edmonton obtained informed and written consent from each patient. Myometrial biopsies were obtained from the lower segment of the uterus from non-labouring patients at term (37 – 40 weeks) gestation during elective caesarean section. Biopsies were cut into small pieces with ethanol-sterilized tools in a sterile cell culture hood, then incubated in filter sterilized (0.22 μm) Hanks Balanced salt solution (HBSS, Gibco, (Invitrogen, Carlsbad, CA)) containing 1% antimycotic/antibiotic (Gibco; 10,000 U/mL of penicillin, 10,000 μg/mL of streptomycin, 25 μg/mL of amphotericin B), 2 mg/mL collagenase (Sigma-Aldrich, St. Louis, MO), and 200 ng/mL DNase I (Roche, Laval, QC) in a 50 mL conical tube (Corning) in a total volume of 10 mL of the prepared HBSS. These tubes were incubated for 1 hr at 37^0C with shaking. After 1h, the debris was allowed to settle and the supernatant (containing fibroblasts) was discarded. The remaining tissue was incubated in another 10 mL of prepared HBSS at 37^0C while shaking, for 4 hrs to overnight (O/N). The dispersed cell mixture was filtered through a 100 μm cell strainer, centrifuged at 2000x*g* for 5 min, and washed twice with sterile phosphate buffered saline (PBS). Isolated hUSMC were grown in Dulbecco's modified Eagle's medium (DMEM, Gibco) supplemented with 10% fetal bovine serum (FBS, Gibco) and 1% antimycotic/antibiotic (Gibco) at 37^0C in humidified 5% CO_2/95% air. Cell cultures were grown to 80-100% confluence in a single well of a 6-well plate post-isolation from tissue biopsies, then in T25 and T75 flasks (Ultident, St. Laurent, QC). Incubation at 37^0C with trypsin (0.05%, Gibco) was used to free cells from the substrate. An excess of culturing medium was used to quench the trypsinization reaction. Cells were monodispersed by vigorous pipetting, counted using a hemocytometer and then plated at the desired cell density onto sterile black-walled 96 well (Greiner Bio-One, Monroe, NC) microplates for ICW, in sterile 6-well plates (Corning, Lowell, MA) for WB, or on 8-chamber slides (VWR Int., USA) for fluorescence microscopy experiments.

3.2.2 Pharmacological Agents

Prior to experiments, the cells were washed once with pre-warmed DMEM containing no additives, and then placed into the incubator in DMEM without additives for 2-4 hrs. All stimulants, pharmacological agents, and drug diluents (DMSO) were diluted in DMEM without additives to the final concentration prior to experiments. OT (1 mM, ddH_2O), ML-7 (MLCK inhibitor (5 mM, DMSO), W7 (calmodulin antagonist (50 mM, DMSO)), edelfosine (phospholipase C inhibitor (5 mM, 100% EtOH)), and nifedipine (calcium channel blocker (50 mM, DMSO)) were all acquired from Calbiochem.

3.2.3 Total Protein Extraction

For WB, total cellular protein was extracted by two methods. Method 1: cells were washed after treatment with ice-cold PBS followed by addition of ice-cold lysis buffer containing 50 mM Tris-HCl pH 8.0, 137 mM NaCl, 5 mM EDTA, 0.1% Triton X-100, 1 mM PMSF, 1X protease inhibitor cocktail (Sigma-Aldrich, Final concentrations: 1.04 mM ASBSF, 0.8 μM Aprotinin, 21 μM Leupeptin, 36 μM Bestatin, 15 μM Pepstatin A, 14 μM E-64), and 1X phosphatase inhibitor cocktail (PhoSTOP, Roche) for detection of phosphoproteins. Cells were freed from the substrate using a cell scraper and collected into wet-ice-cooled microfuge tubes, then snap frozen in liquid nitrogen and stored at -80^{0}C for later use. Protein concentrations were determined by combining 1 part sample to 99 parts Precision Red™ advanced protein measurement reagent (ADV02, Cytoskeleton, Denver, CO, USA) according to the manufacturer's instructions. Method 2: after treatment, cells were lysed in an acetone solution containing 10% trichloroacetate (TCA) 10 mM dithiothreitol (DTT), and protease inhibitors as indicated above. This solution was pre-cooled in a dry-ice methanol bath before addition to the culture plate. Cells were immediately scraped from the substrate as above, and then collected into wet-ice-cooled microfuge tubes. These tubes were centrifuged at 18,000x*g* for 30 min at 4^{0}C, the supernatant was removed, and the pellet was resuspended by vortexing in acetone containing 10 mM DTT, and allowed to sit O/N. The next day, tubes were centrifuged at 18,000x*g* for 15 min at 4^{0}C. The washing solution was removed and the pellets were allowed to air-dry for 20-30 min. The dried pellets were resuspended in 60 μL of 1X SDS-PAGE loading buffer (see below) and incubated at 65^{0}C for 10 min before storage or loading 17.5 μL from each onto SDS-PAGE minigels.

3.2.4 SDS-PAGE and Protein Transfer

Total protein was prepared for electrophoresis by adding 5X loading buffer (Final concentrations: 10% glycerol, 3% SDS w/v, 85 mM Tris HCl pH 6.8, 85 mM dithiothreitol, 0.1% bromophenol blue) and boiling for 10 minutes. Approximately 25 μg/lane of protein was loaded onto 15% or 18% Tris-Glycine-SDS minigels, or alternatively, onto 12% gels with or without 30 μM phos-tag (194) reagent (NARD Institute, Ltd., www.phos-tag.com) combined with 60 μM $MnCl_2$ to demonstrate shifts in mobility for phosphoproteins. SDS-PAGE was carried out in 1X SDS running buffer (10X Tris-Glycine-SDS buffer, BioRad, Hercules, CA, USA) using a constant current of 15 mA for the stacking (4.2% acrylamide, pH 6.8) gel and then a constant 25-30 mA for the separating (15% or 18% acrylamide, pH 8.8) gel in a Mini-PROTEAN 3 electrophoresis apparatus (BioRad), according to the Laemmli method.(195) Precision Plus Protein all blue standard (2.5 μL/lane, BioRad) was loaded on each gel for visualization in the 700-channel of the Odyssey® imager. The gel was transferred to nitrocellulose (Li-COR, Biosciences, Lincoln, NE, USA) at 4^0C in a Mini-Trans-Blot cell (BioRad) apparatus using a buffer containing 20% MeOH and 1X Tris-Glycine (10X Tris-Glycine, Li-COR) for 1.5 hrs at 100 V. Gels containing phos-tag and $MnCl_2$ were incubated at room temperature (R/T) for 15-20 min in transfer buffer of the same composition supplemented with 2 mM EDTA to chelate and remove Mn^{2+} ions, then allowed to equilibrate in transfer buffer without EDTA for an additional 15-20 min prior to transfer.

3.2.5 Western Immunoblotting

After transfer, membranes were rinsed briefly in PBS. Nitrocellulose membranes were placed into Odyssey® blocking buffer (OBB, Li-COR) diluted 1:1 with PBS immediately and blocked for 1 hr at R/T. Primary Abs were diluted in OBB combined 1:1 with PBS, containing 0.1% Tween-20, and incubated O/N at 4^0C. The final Ab concentrations used were 1:1000 for GAPDH (mouse MAb, Santa Cruz), 1:500 for RLC (Rabbit PAb, Cell Signaling), 1:200 for p19RLC (rabbit PAb, Cell Signaling), and 1:200 for ppRLC (diphospho T18 S19, rabbit PAb, Santa Cruz). After primary Ab incubations, membranes were washed 3X (10 min each) with PBS containing 0.1% Tween-20 (PBS-T) at R/T on a bench top shaker. Secondary Abs conjugated to IRDye 800CW (Li-COR) or Alexa Fluor 680 (Molecular Probes, Invitrogen) were diluted to 1:20,000 in OBB combined

1:1 with PBS, containing 0.1% Tween-20 and 0.01% SDS. Membranes were incubated with secondary Ab solutions for 1.5 hrs at R/T and in the dark on a bench top shaker. After secondary Ab incubations, the membranes were washed 3X (10 min each) with PBS-T at R/T on a bench top shaker in the dark, then briefly rinsed in PBS before scanning. Membranes were scanned and analyzed using an Odyssey® IR scanner using Odyssey® imaging software 3.0. Scan settings were medium or high image quality, 169 μm resolution, intensity 3.0-5.0 for both channels with no offset. Ab signals were analyzed as integrated intensities of regions defined around the bands of interest in either channel.

3.2.6 In-Cell Westerns

A detailed technical protocol for this technique is presented in appendix 8.2. hUSMC were plated in sterile black-walled 96 (half-area) (Greiner Bio-One, Monroe, NC) plates at the desired density then placed at R/T for 30-60 minutes before transfer to the incubator to reduce excessive settling at the well edges.(196) The plates were incubated O/N at 37^0C as indicated above. Prior to treatment, all wells were washed with DMEM, and incubated in DMEM for 2-4 hrs before beginning the experiments. Cell treatments were dispensed with a calibrated digital multichannel pipette with a repeater function to ensure accuracy in treatment timing. After treatment, cells were fixed immediately by adding concentrated formalin to a final concentration of 3.7% formaldehyde and incubating at R/T for 10 minutes. After fixation, the plates were washed with PBS then permeabilized by washing 3X (10 min each) on a bench top shaker with PBS containing 0.1% Triton-X-100, and then rinsed once with PBS. Cells were blocked using 20 μL/well OBB for 1 hr at R/T. Primary Abs were prepared as for WB and the plates were incubated O/N at 4^0C using 20 μL/well. The final Ab concentrations used were 1:500 for GAPDH (mouse MAb, Santa Cruz) and 1:200 for p19RLC (Rabbit PAb, Cell Signaling). After primary Ab incubations, plates were washed 3X (10 min each) with 100 μL/well PBS-T at R/T on a bench top shaker. Secondary Abs were prepared as for WB with a few modifications: IRDye 800CW conjugates of Goat-anti-rabbit-IgG (Li-COR), goat-anti-mouse-IgG (Li-COR) were used at 1:1000 dilution for detection of Ab targets in the 800-channel (green pseudocolor). 800-channel Ab signals were normalized to the 700-channel (red pseudocolor) signals derived from Alexa-Fluor 680 conjugated goat-anti-mouse-IgG secondary at 1:1000 (Molecular Probes, Invitrogen), or DRAQ5 (Biostatus Ltd., Leicestershire, UK) combined with

Sapphire700 (Li-COR) at 1:10,000 and 1:1000 respectively. Plates were incubated with 20 μL/well secondary Ab solutions for 90 min at R/T in the dark. Background control wells were prepared by omitting primary Abs, DRAQ5 and Sapphire700 (i.e. secondary only). After secondary Ab incubations, plates were washed 3X (10 min each) with PBS-T at R/T on a bench top shaker in the dark, and then filled with 50 μL/well PBS to reduce surface disturbances when scanning. Plates were scanned and analyzed using an Odyssey® IR scanner using Odyssey® imaging software 3.0. Scan settings were medium or high image quality, 169 μm resolution, intensity 5.0 for the 700-channel, and 7.0 for the 800-channel with an offset of 4.0 mm. For signal quantification, Ab signals were analyzed as the average 800-channel integrated intensities from duplicate wells normalized to the 700-channel signal integrated intensity to correct for well-to-well variations in cell number. Results are expressed as percent relative responses (means ± standard errors of the mean) compared to vehicle-treated controls.

3.2.7 Microscopy

8-chamber sterile culture slides (BD Falcon) were seeded, cultured, treated, fixed, and prepared for fluorescence or brightfield microscopy exactly as culture plates for ICWs, with the exception of utilizing a lower dilution of primary Abs (1:50 RLC (Rabbit PAb, Cell Signaling), 1:50 p19RLC (Rabbit PAb, Cell Signaling), 1:200 GAPDH) and DyLight 488-conjugated goat-anti-rabbit-IgG (Cell Signaling) and goat-anti-mouse-IgG (Cell Signaling) Abs at a dilution of 1:100. After secondary Ab application, cells were rinsed 3X in PBS-T and then incubated with 50 nM rhodamine-phalloidin (Cytoskeleton, Denver, CO, USA) for 10 min at R/T to reveal F-actin fiber distribution. Slides were rinsed 3X in PBS then mounted in VECTASHIELD (Vector Laboratories, Burlington, ON, Canada) mounting medium containing DAPI to detect nuclei. Slides were allowed to rest for 60 min in the dark and stored at 4^0C if necessary before visualizing under an Olympus IX81 fluorescent microscope (Carson Scientific Imaging Group; Ontario, Canada) using Slidebook 2D, 3D Timelapse Imaging Software (Intelligent Imaging Innovations Inc.; CO, U.S.A.).

3.2.8 Statistical Analysis

The results were expressed using means (± S.E.M.). Statistical analysis was performed using one-way ANOVA to compare the means of 3 or more groups at a time in

OT-induced phosphorylation of RLC time course studies. Two-way ANOVA was used to determine if pharmacological inhibitors had an effect on the OT-induced phosphorylation of RLC. A P-value of 0.05 was used to establish statistical significance.

3.3 Results

3.3.1 Signal Linearity and Specificity for WB and ICW

We assessed the linearity of both phosphorylated (p19RLC) and non-phosphorylated (GAPDH, total RLC (tRLC)) protein signals via WBs prepared using 2-fold serial dilutions of hUSMC lysates starting at 50 μg total protein/lane. Preliminary experiments measuring GAPDH reached a lower limit of 0.19 μg protein/lane and showed that WB could not discriminate between protein loads ≤1.6 μg/lane. Therefore 1.6 μg/lane was selected as the lowest load for subsequent experiments. The data from representative membranes for signals from GAPDH, p19RLC and tRLC ranging from 50 to 1.6 μg/lane are shown in Figure 3-1. Though all three proteins may be quantified above 50 μg protein/lane (lane 1) in our experience, loading Tris-Glycine minigels with greater protein loads may decrease band resolution. The high correlation coefficients over this range for GAPDH, tRLC, and p19RLC (0.97, 0.99, 0.97, respectively) support the conclusion that this technique can detect changes in specific protein concentrations. Even when the analysis is restricted to protein applications less than ≤ 12.5 μg/lane (Figure 3-1 inset), the correlation coefficients remain high for GAPDH (0.87) tRLC (0.98) and p19RLC (0.96).

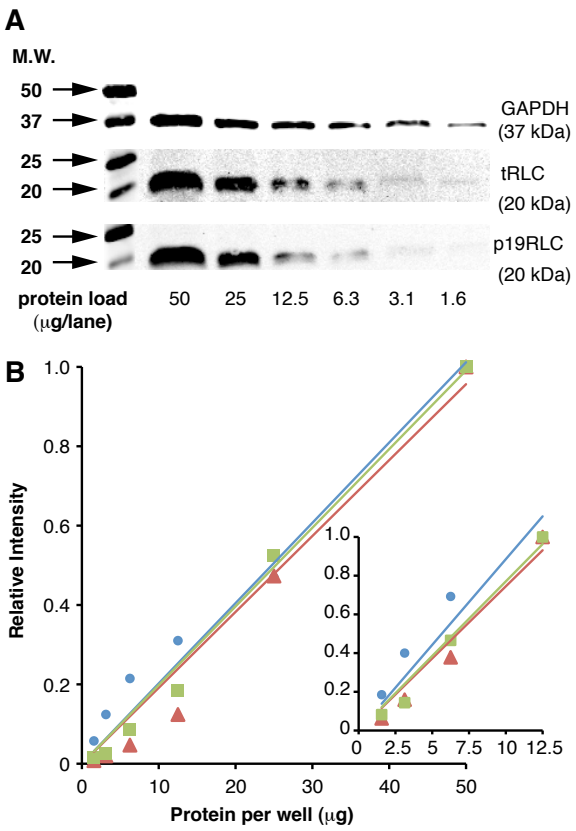

Figure 3-1. Signal Linearity Using WB.

A. Tris-Glycine-SDS gels were loaded with total hUSMC lysate (2-fold dilutions from 50 μg to 1.6 μg). GAPDH, tRLC, and phospho-(S19)-RLC (p19RLC) were detectable with 1.6 μg total protein/lane. **B.** Quantification of bands shown in panel A. Normalized values are expressed as a fraction of the band intensity measured at 50 μg/lane. Fit of a linear model through the origin showed excellent correlation for all three proteins (GAPDH: ●; RLC: ■; p19RLC: ▲). The inset graph illustrates the correlation coefficient when only the lanes with ≤ 12.5 μg protein are analyzed. Molecular weight markers (MW) are shown at the left.

The specificity of the Abs was assessed in Figure 3-2. The full length WB demonstrates the expected prominent bands relative to the molecular weight (MW) marker for each of the proteins. Though bands of different sizes are detectable at several other positions, their relative intensities compared to the predominant bands are considered quantitatively insignificant (<5% signal relative to the band of interest). Introduction of 30 μM phos-tag into the polyacrylamide matrix markedly enhances separation of phosphorylated proteins by retarding their movement.(194) Our data (Figure 3-2) demonstrate that the rabbit polyclonal (RPAb) anti-p19RLC Ab recognizes only the phosphorylated (mono- and di-) RLC species, in contrast to the anti-tRLC Ab, which

reveals the unphosphorylated form as well as the mono- and diphospho-RLC (ppRLC). For reference, the anti-ppRLC Ab identifies only the uppermost band in these last three panels, which corresponds to ppRLC. These results confirm those in a previous study and indicate the highly specific nature of these Abs.(197) Figure 3-2C also demonstrates the specificity of a mouse monoclonal (MMAb) Ab that is directed toward phospho-S19-RLC, but only detects mono-phosphorylated RLC (pRLC). The difference in cross-reactivity likely results from obstruction of the MMAb by phosphorylation of the adjacent T18. As will become clear in chapter 5, this key difference in reactivity enabled us to differentiate between mono- and diphosphorylation of RLC.

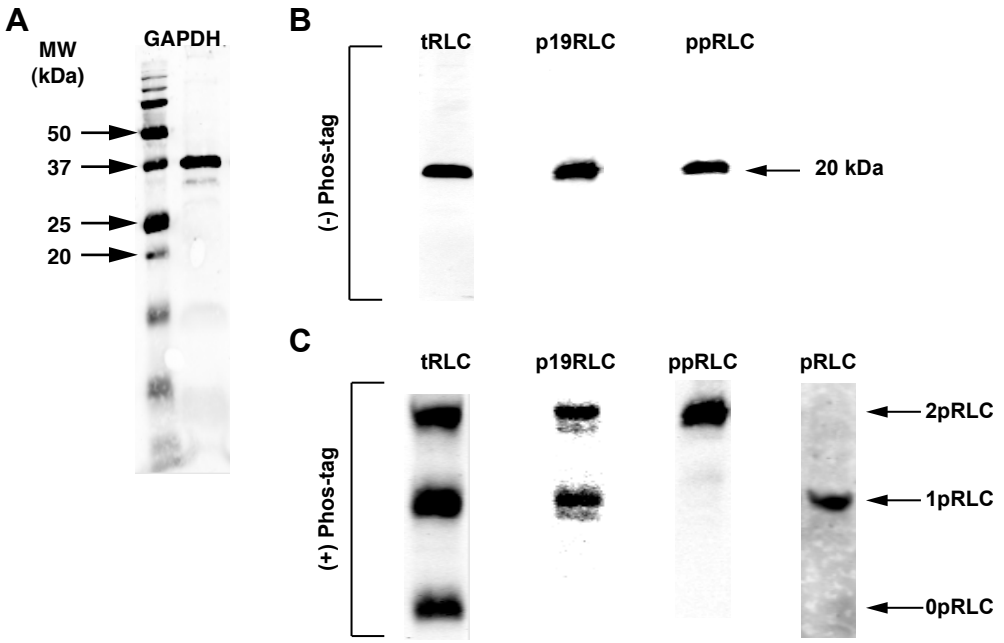

Figure 3-2. Antibody Specificity Using WB.

A. Full length WB with single lanes loaded with 25 μg of protein/lane demonstrating the signal specificity of the ant-GAPDH Ab. **B.** WB performed as in panel A demonstrating specificity of Abs toward total-RLC (tRLC), p19RLC, and ppRLC. **C.** WB of hUSMC lysates separated by phos-tag (30 μM) SDS-PAGE, to promote mobility shifts in phosphorylated proteins. Probing for tRLC reveals 3 bands corresponding to unphosphorylated (0pRLC), mono-phosphorylated (1pRLC), and diphosphorylated (2pRLC) RLC. The rabbit polyclonal (RPAb) anti-p19RLC Ab reacts with 1pRLC and 2pRLC and fails to recognize the unphosphorylated species. The anti-ppRLC Ab recognizes primarily 2pRLC. The mouse monoclonal (MMAb) Ab toward pRLC recognizes only the 1pRLC band. MW (Molecular weight).

We assessed the linearity between signal intensity and cell number for ICWs using the Ab to p19RLC, and two normalization references (Figure 3-3). The first normalization reference used an Ab toward GAPDH. The second utilized a combination of two cell dyes (DRAQ5)(198) and Sapphire700, referred to as 'cell dyes' in this chapter) that provide an estimate of the cell content of the well and is detected in a separate channel of the IR scanner. hUSMC were seeded into 96-well plates (15 mm^2/well) from 750 cells/well through to 15,000 cells/well, resulting in adherent monolayers corresponding to cell densities of 0, 50, 100, 200, 300, 400, 500, 600, 700, 800, 900, and 1000 cells/mm^2. Signals for GAPDH, p19RLC, and cell dyes were detectable above background readings (empty wells) down to 750 cells/well. It was apparent that the relationship between well numbers and concentrations of p19RLC and GAPDH was plateauing at cell numbers beyond 10,500/well (700 cells/mm^2). Using only the wells with equal to or less than cell density 700 cells/mm^2 (inset), the correlation coefficients to a linear model for both GAPDH (0.99) and p19RLC (0.96) were very high, supporting the conclusion that this assay has precision to measure changes in protein concentrations with optimal performance using 1,000 – 10,500 cells/well, which corresponds to 0.3 to 4 μg protein/well, based on average lysate yields for this cell type. Further, these data suggest that ICWs exhibit improved sensitivity compared to WB as we reliably measured GAPDH in ICWs below the lower limit of signal discrimination (1.6 μg/lane) by WB.

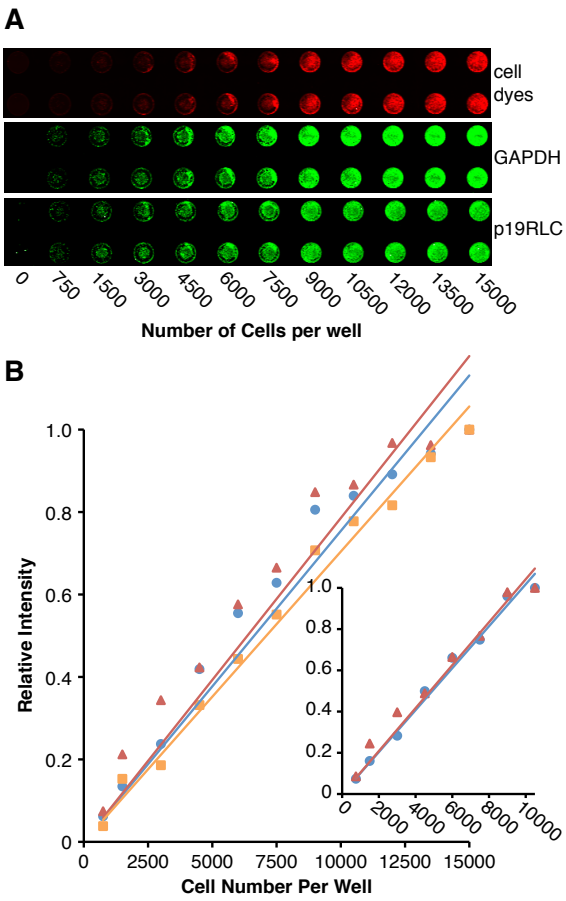

Figure 3-3. Signal Linearity With the ICW Assay.

A. 96-well microplates were loaded with an increasing number of cells/well. Signals from anti-GAPDH and anti-p19RLC Abs appear as green fluorophores. Signals from cell dyes (cell number normalization) appear as red fluorophores. **B.** Quantification of signals shown in panel A. Normalized values are expressed as a fraction of the signal intensity of the wells containing 15,000 cells for GAPDH (●), p19RLC (▲). The signal from the cell dyes also is shown (■). The GAPDH and p19RLC signals appear to plateau at the higher cell densities so the line of best fit has been calculated and illustrated by expressing the normalized values as a fraction of the intensity of the wells containing 10,500 cells (inset) for GAPDH (●), and p19RLC (▲).

To evaluate Ab signal specificity for GAPDH, tRLC and p19RLC in the ICW, we visualized the signals using immunofluorescence microscopy (Figure 3-4). Slides for microscopy were prepared identically to ICW plates (see methods) to ensure that the microscopic visualizations were directly comparable to ICW measurements. The only difference in protocols was the use of secondary Abs conjugated to Alexa-Fluor 488 for primary Ab detection for microscopy. Each slide was also stained with rhodamine-phalloidin to demonstrate filamentous actin (F-actin). In the absence of primary Abs, there is no appreciable signal (Figure 3-4A panels i and ii). Using the Ab to GAPDH, there is diffuse cytosolic staining, in marked contrast to the filamentous appearance of F-actin (Figure 3-4A panels iii and iv). For tRLC (Figure 3-4A panels v and vi) the staining pattern is similar to F-actin (and in contrast to GAPDH), in keeping with the molecular co-localization of these elements of the contractile apparatus. There is no appreciable signal after pre-adsorption of the p19RLC Ab with a specific blocking peptide containing phospho-S19 of RLC either in the resting state (Figure 3-4B panels i and ii) or after stimulation with 100 nM OT (panels iii and iv). Similarly, in our preliminary ICWs, the signal from resting and stimulated cells was reduced to background levels when the Ab toward p19RLC was preadsorbed with the same blocking peptide. In the absence of the blocking peptide, there is only a faint signal in resting cells (Figure 3-4B panels v and vi) but this signal is rapidly inducible (20-second stimulation) in response to OT. The subcellular distribution for p19RLC is identical to that of tRLC and F-actin (panels Avi, Bvii).

Figure 3-4. Antibody Specificity Using the ICW Assay.

In each pair of micrographs, the left panel illustrates filamentous actin (F-actin) stained with rhodamine-phalloidin (red). The corresponding right panels are immunofluorescence micrographs stained with Abs conjugated to Alexa-Fluor 488 (green). Nuclei are stained with DAPI (blue) in all panels. Images are shown at 400X and 200X magnification in panels A and B, respectively. White bars represent 25 and 50 microns, respectively. **A.** Demonstration of GAPDH and tRLC. Panels i and ii. The actin fibers stain in a filamentous pattern typical of uterine smooth muscle. There is no detectable signal with omission of the primary Abs. Panels iii and iv. The GAPDH staining shows a diffuse cytosolic pattern in contrast to the fibrillar pattern of actin. Panels v and vi. TRLC has a similar staining pattern to actin. **B.** Demonstration of p19RLC. Panels i –iv. There is no detectable background fluorescence when the Ab has been preadsorbed with blocking peptide (BP) containing phospho-S19 of RLC, either in the resting state (panel ii) or with stimulation using 100 nM OT (20 sec stimulus, panel iv). Only a small amount of p19RLC is detectable in the resting myocyte (panel vi) but this is markedly increased upon stimulation with OT (100 nM, 20 sec: panel viii).

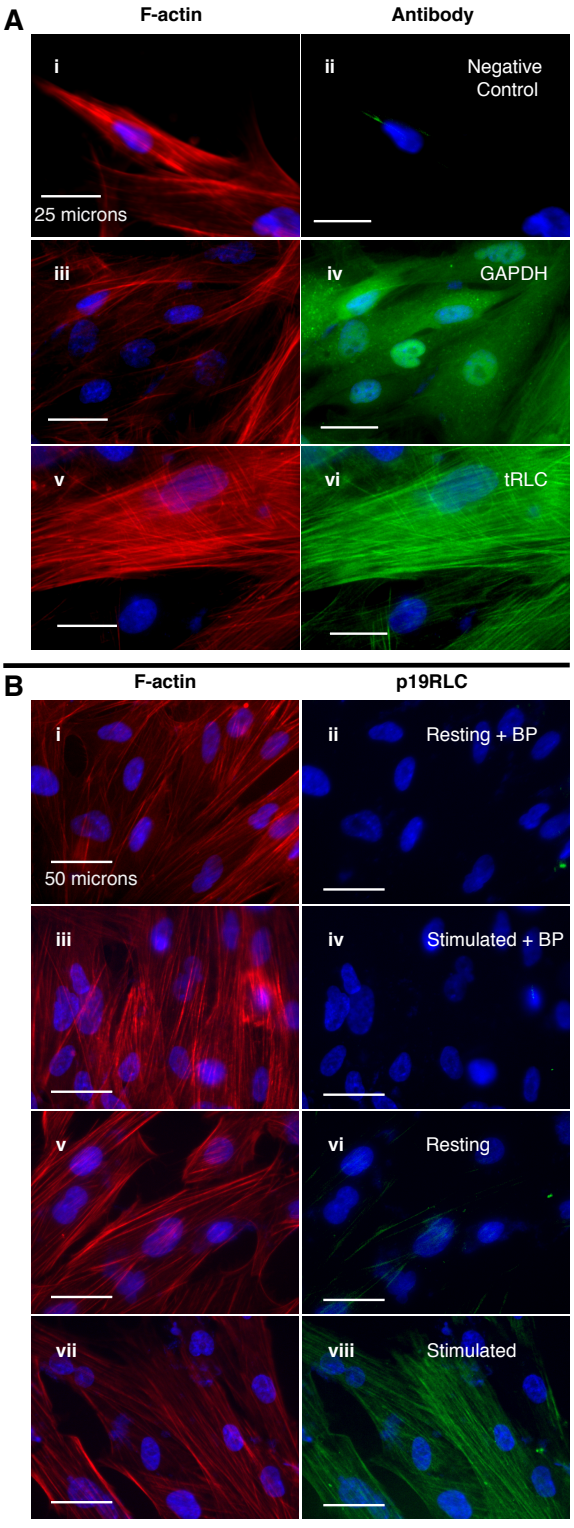

3.3.2 Assay Precision for WB and ICW

To assess assay precision, we studied the intra-assay and inter-assay variability of each technique for GAPDH and p19RLC. We also evaluated the variability of normalization of p19RLC to GAPDH and compared this to normalization using the cell dye markers in the ICW technique. For WB, two SDS-PAGE mini-gels were loaded with 13 replicates of 20 μg of protein/lane from the same lysate. The resultant blots (Figure 3-5A) were prepared simultaneously from the same electrophoresis and transfer tanks. By using secondary Abs with distinct fluorophores, both proteins were assessed on each blot. The intra-assay variability in signal intensity across the lanes for GAPDH and p19RLC is presented in Figure 3-5B. The intra-assay coefficients of variation (CV) for GAPDH and p19RLC were 0.21 and 0.20 in blot 1, respectively, and 0.16 and for both proteins in blot 2. Blot 1 particularly emphasizes that the pattern of signal variation across the lanes was not similar for the two proteins. Hence, when the ratio of one protein to the other was calculated, the CV (0.27: Figure 3-5B ratio) was magnified. To determine the intra-assay CV for the ICW technique, 30 wells in each of two plates were prepared simultaneously and probed for p19RLC or GAPDH. The CV for signals obtained for p19RLC (Plate 1), and GAPDH (Plate 2) were 0.10 and 0.07. The CV for the cell dye estimate of cell content for plates 1 and 2 were 0.05 and 0.15, respectively. When the concentrations of p19RLC or GAPDH were normalized to the cell dyes, the CV varied from 0.08 to 0.16. In summary, the intra-assay CVs for measurement of p19RLC and GAPDH alone are comparable between ICW and WB but the ICW technique may have a slight advantage regarding the precision of the normalized data.

The inter-assay CVs were calculated from repeated measurement of the same samples at different times using different blots for WB or on several different plates for ICW. The inter-assay CV with the ICW technique was 0.08 for p19RLC and 0.15 for the ratio of p19RLC to the cell dyes. For the WB technique, the inter-assay CV was 0.16 for p19RLC and 0.25 for the ratio p19RLC to GAPDH.

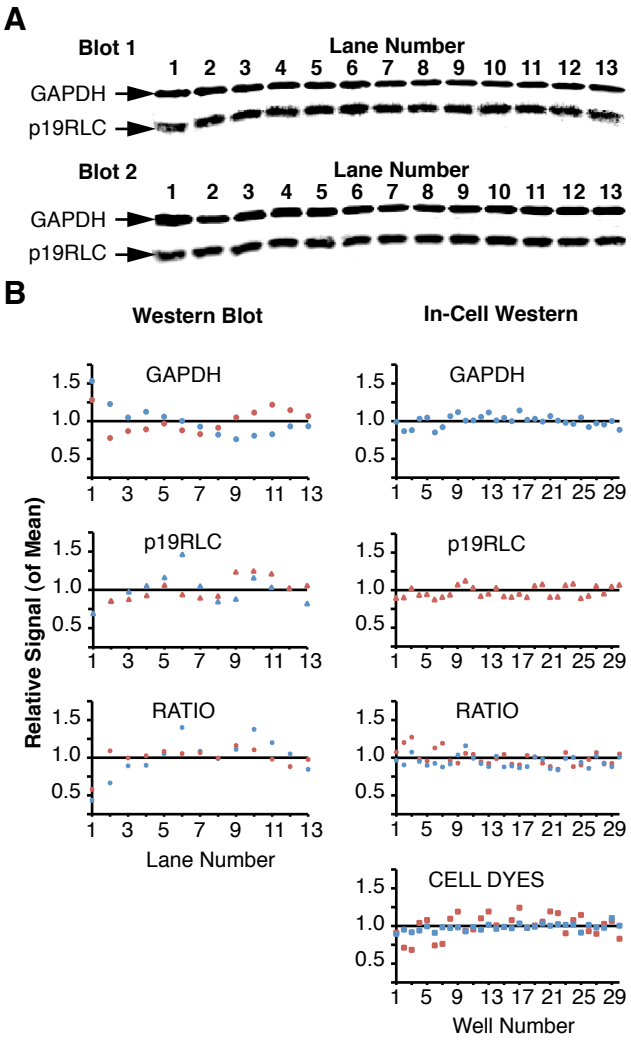

Figure 3-5. Assessment of Intra-Assay Variability in WBs and ICW Assays.

A. WB membranes showing GAPDH and p19RLC levels in 13 replicate samples in two WB. **B.** In the panels on the left are the individual band intensities from WBs in A expressed as a fold-signal intensity relative to the mean of the thirteen samples in each of the two blots. The data from blot 1 are shown in blue and from blot 2 in red. The data are provided for GAPDH and p19RLC individually and for the ratio GAPDH/p19RLC. In the panels on the right are the intensities of the signals from wells distributed across ICW plates plotted as fold-signal intensity relative to the mean values for each of two plates (plate one in blue and plate 2 in red). The data are provided individually for GAPDH, p19RLC, and in the lowermost panel for the cell dyes used in data normalization. The ratios of GAPDH and p19RLC to the cell dyes are also shown in red and blue, respectively.

3.3.3 Measurement of Phosphorylation of RLC in Response to a Physiological Stimulus

ICWs were used to measure the effects of cell density, time course and concentration-responses for OT–induced increase in p19RLC. Subsequent experiments were aimed at determining the optimal cell density and time course for OT-induced

p19RLC formation. Stimulation with increasing concentrations and incubation times of OT for cell densities of 500, 550, 600, and 650 cells/mm^2 demonstrated that the largest amplitude concentration-dependent rise in p19RLC inducible by OT is achieved at a cell density of 600 cells/mm^2 after treatment for 20 seconds (Figure 3-6). At a density of 650 cells/mm^2 and at time points beyond 20 seconds for all densities tested, the response to OT was diminished.

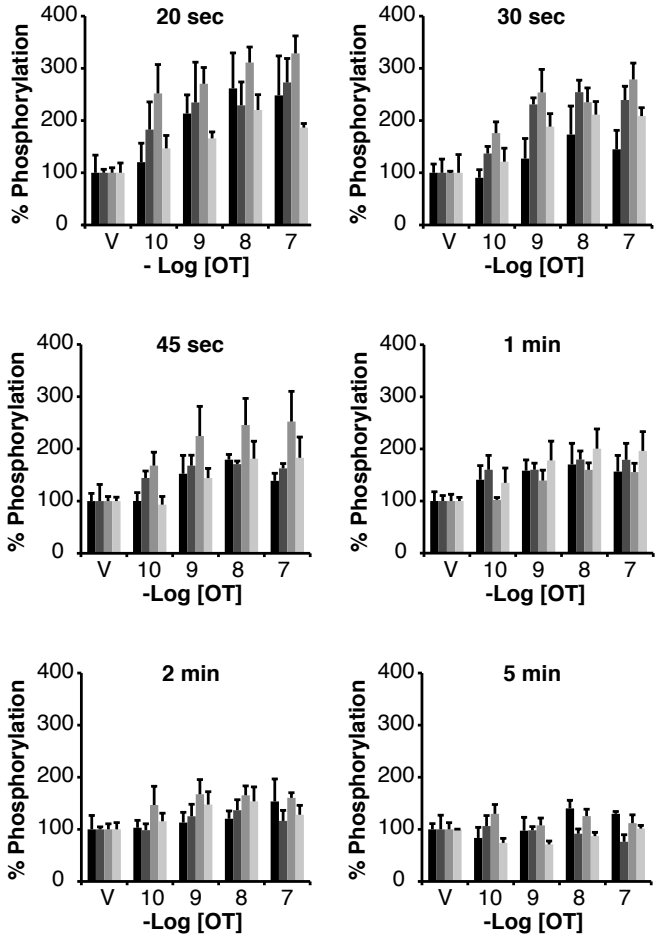

Figure 3-6. Cell Density Optimization for the ICW Assay.

hUSMC were seeded at densities of 500 (darkest histogram in each grouping), 550, 600 and 650 (lightest histogram in each grouping) cells/mm^2. Cells were treated with increasing concentrations of OT (10^{-10} to 10^{-7} M) for 20, 30, 45 or 60 seconds or 2 or 5 minutes (n=4 at each time point at each concentration of OT). Concentrations of p19RLC were measured using the ICW assay.

We next determined the time course of the concentration-response relationships of OT stimulation of hUSMC (at 600 cells/mm^2) with respect to p19RLC concentrations by

WB and ICW under identical conditions (Figure 3-7). Using the ICW technique, a brisk response is measurable as early as 20 seconds after stimulation, then decays significantly by 1 min and returns to baseline levels by 5 min (Figure 3-7A). Qualitatively, the responses obtained by WB were similar with increases in p19RLC formation acutely (<1 min) and decay of p19RLC beyond 1 min. However, there were differences between the techniques with respect to quantitative data. In the first WB experiments, wet-ice cooled PBS and a lysis buffer containing phosphatase and protease inhibitors (see methods) was used to extract the protein. The maximal response to OT was measured at 171 ± 26% of vehicle control values (Figure 3-7B) compared to the 329 ± 37% using the ICW technique (Figure 3-7A). Since the PBS/lysis buffer is a rather mild extraction technique, we repeated the experiments using the more stringent dry-ice-cooled TCA/Acetone/DTT extraction method. This enhanced the maximal response to OT to 321 ± 20% (Figure 3-7C) but the variability about the measurements appeared greater than with the ICW technique. In summary, the ICW and WB techniques yielded similar patterns of biological data with a suggestion that the ICW might have superior precision.

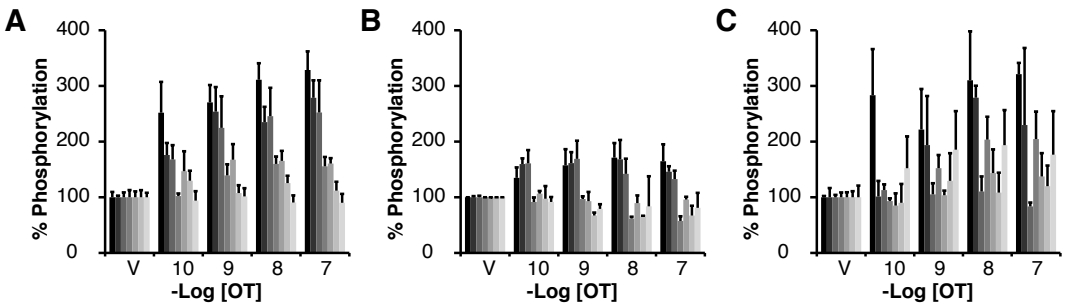

Figure 3-7. Comparison Between WB and ICW for Cell Responses to OT.

A. Quantification of p19RLC by ICW, using the cell dyes as a normalization reference. **B** and **C.** Quantification of p19RLC by WB using GAPDH as a normalization reference. In panel B, the protein was extracted under mild (cold PBS/Lysis Buffer) conditions. In panel C, protein extraction was performed using the more stringent (TCA/Acetone/DTT) conditions. In all panels, the normalized data are expressed as a percentage of the vehicle (V) controls. For all experiments, hUSMC were plated at a density of 600 cells/mm^2 and treated with vehicle or increasing concentrations of OT (10^{-10} to 10^{-7} M). The time course varied from 20 sec (darkest histogram in each grouping) through 30, 45 and 60 sec or 2, 5 or 10 minutes (lightest histogram in each grouping).

3.3.4 Physiological Validation of Phosphorylation of RLC Measured by In-Cell Western Assays

To reinforce the physiological validity of the responses measured by ICW, we performed experiments in the presence or absence of pharmacological inhibitors known to perturb the biochemical pathways mediating phosphorylation of RLC. hUSMC were seeded at 600 cells/mm^2 and stimulated with OT (100 pM to 100 nM, 20 sec). Inhibition of MLCK (ML7, 50 μM), calmodulin (CaM) antagonism (W7, 50 μM), inhibition of phosphatidyl-inositol-specific phospholipase C (PLC) (edelfosine, 20 μM), and inhibition of plasma membrane calcium (Ca^{2+})-channels (nifedipine, 20 μM) significantly attenuated the OT-induced rise in p19RLC, as assessed by two-way ANOVA ($p < 0.01$, Figure 3-8). These results indicate that the phosphorylation of RLC measured by ICW behaves as expected in accordance with current knowledge of the biochemical pathways mediating physiological p19RLC responses in SMC.(87, 199)

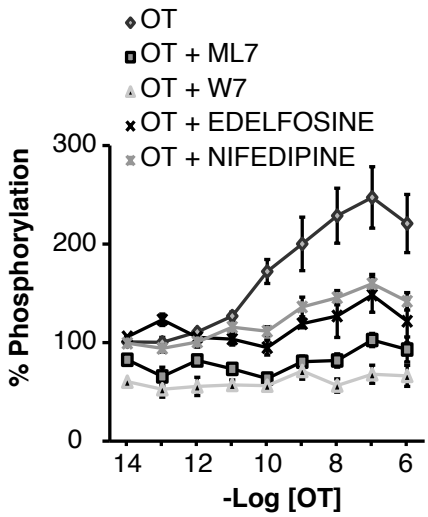

Figure 3-8. Assessment Using the ICW Technique of Pharmacological Manipulation of p19RLC.

hUSMC were seeded in microplate wells at 600 cells/mm^2 and treated with OT (from 10^{-14} to 10^{-6} M) for 20 sec in the presence or absence of 15-minute pre-incubation with specific pharmacological agents (n=7 separate cultures). The normalized data are expressed as a percentage of the vehicle controls. As expected, the cells demonstrated a brisk response to OT that was diminished in the presence of an inhibitor of MLCK (ML-7, 50 μM), CaM (W7, 50 μM), phosphatidyl inositol-PLC (Edelfosine, 20 μM), and L-type Ca^{2+} channels (Nifedipine, 20 μM). Relative p19RLC levels (normalized to cell content) are expressed as a percentage of vehicle control. All of the pharmacological agents significantly ($p<0.01$) attenuated the concentration-dependent p19RLC increase induced by OT as determined by two-way ANOVA.

3.4 Discussion

Protein phosphorylation is the most commonly studied post-translational modification due to its central role in regulating cellular physiology. Phosphoprotein levels are dynamically regulated in response to a plethora of biological stimuli mediated by the opposing activities of protein kinases and phosphatases.(200) These enzymes encode external and internal signals through the complement of phosphoproteins that are produced in the cell interior. Using experimental manipulations rooted in knowledge of signaling pathways, scientists can decipher the role of phosphorylated intermediates in cellular responses provided they are quantifiable. The increasing commercial availability of phosphoprotein-specific Abs has enhanced the use of WB as a standard method for this purpose. However, the WB technique is a relatively labor-intensive assay best suited for experimental approaches that require low-throughput measurements. To enhance the speed and throughput of sample processing while remaining within the paradigm of using phospho-specific Abs for detection and quantification, we looked to the ICW assay.

3.4.1 Technical Aspects of Phospho-Protein Quantification by ICW

Our data demonstrate that the ICW technique provides signal linearity and specificity at least equal to WB. The ICW technique also provides biological response amplitudes similar to those attainable by the very robust protein collection method using dry-ice cooled TCA/Acetone/DTT, demonstrating that formalin fixation is also a useful and robust method for phosphoprotein signal preservation. Phospho-RLC has similarly been preserved and quantified reliably after cell fixation in other reports.(201) The ICW and WB techniques are qualitatively similar in terms of the concentration range of measurable stimulation (100 pM to 100 nM) and the time course for the rise and decay of the p19RLC. Both techniques were capable of measuring p19RLC formation as early as 20 seconds post-stimulus. This rapid induction of p19RLC agrees with other OT-response data in the literature.(56, 202) The diminished responses measured by WB using the relatively mild cold PBS/cold lysis buffer method could result from phospho-signal loss during cell lysis and harvesting, since the time necessary to complete these steps exceeds the optimal treatment length (20 sec) for a maximal response in contrast to the nearly instantaneous quenching achievable by TCA/Acetone/DTT and formalin fixation. Because we have

prepared both WBs and ICWs with identical blocking and Ab incubation solutions, it is unlikely that the diminished phospho-signal measured from cold PBS/cold lysis buffer samples by WB is explained by residual phosphatase activity present in the incubation buffers.(203)

The WB technique is considered by many to be a 'semi-quantitative' assay because of the relative lack of precision of the measurements. Variability may arise from the protein extraction method employed or from application of the protein to the gel. Perhaps most problematic is the transfer of the separated proteins to the blotting membrane. Uneven distribution of proteins across blotting membranes may occur since protein movement out of the polyacrylamide gel matrix occurs at unequal rates and to different extents as influenced by protein MW and solubility in the transfer buffer.(187, 188, 204-206) In particular, transfer conditions optimized for smaller proteins may not be efficient for larger proteins, and vice-versa.(187, 207) In addition, the choice of membrane, blocking and Ab solutions, and wash buffers may influence the amounts of protein retained on the membranes before Ab probing.(208, 209) These factors introduce considerable inter-assay variability, limiting the precision of the technique and ultimately complicate protein quantification via WB.

The potentially improved precision of ICW compared to WBs might be attributable to minimizing sample handling through elimination of protein extraction, electrophoresis, and protein transfer steps. Use of a calibrated digital multichannel pipette further reduces assay variability by allowing rapid treatment and quenching of many samples nearly simultaneously. In addition, the ability to take duplicate or higher number replicate measurements may further enhance precision. Though replicate measurements are feasible in the setting of WB, this is an uncommon, but perhaps advisable, practice.(210) Further, our data demonstrate that WBs may have significant lane-to-lane variability in protein transfer evidenced by inconsistencies in protein signals within and between membranes. This variability is inconsistent between two protein signals (p19RLC, GAPDH) measured on the same membrane, and therefore has the potential to magnify the variability when one protein signal is normalized to that of another protein. By comparison,

with the ICW technique, the normalization of a protein to the cell content of the well using a combination of cell dyes appeared to give more precise normalization data (Figure 3-7).

In our evaluation of acute phosphorylation responses, data normalization was straightforward since protein levels were constant. However, where experiments concern longer treatment courses, it may be prudent to avoid data normalization to that of a reference protein and instead opt to use the cell dyes to avoid inaccurate interpretation of results due to changing reference protein levels. The potential for wavering levels of reference proteins has prompted others to suggest alternatives for data normalization in WBs.(210)

In the absence of purified antigen, it is impossible to obtain valid assessments of the sensitivity of assays such as WB or ICW. However, our data suggest that the ICW technique yields a precise measure of antigens down to 0.3 μg protein/well. As noted in Figure 3-3B, there is a high correlation with the linear plot down to 0.3 μg protein/well for all three proteins. This is in contrast to WB where the lower limit of signal discrimination for band intensities for GAPDH was 1.6 μg protein/lane. As GAPDH was the most intense signal measurable in our WB experiments, it is unlikely that p19RLC or tRLC would be quantifiable below this protein load.

3.4.2 Validation of Antibody Specificity

As with WB, specificity of the Ab is of paramount importance in the ICW technique. It has been suggested that the Abs proposed for evaluation of protein antigens in fixed cells should be tested for signal intensity and specificity by WB.(211) Reliance on WB for evaluation of Ab specificity (or rather, the level of non-specificity) for what is essentially a microscopy application in ICW, presupposes that the proteome is represented identically in both techniques. However, antigen preparation is achieved using different methods for WB (reduction and linearization with DTT or 2-mercaptoethanol, and SDS) and microscopy (organic denaturation and fixation by cross-linkages). Therefore, the complement of cellular antigens is presented to the Ab in a different configuration. Hence, validation of Ab specificity for ICW using WB may prove most useful where the Ab recognizes a continuous epitope that is fully unmasked during fixation. Whether the Ab will interact with epitopes in partially denatured proteins cannot be addressed by this approach. Logically then, WB

data are less appropriate for validation of Abs raised against discontinuous epitopes encompassing amino acid residues in close proximity on the surface of a protein but separated in space in the linear amino acid sequence. This may be a more significant consideration for Abs raised against short peptides (both mono- and polyclonal), in contrast to those (polyclonals) raised against various parts of the immunizing protein.(207, 212)

One potentially less significant consideration here is that the proteome is unlikely to be represented in its entirety on a WB membrane since the gel polyacrylamide content (gel percentage) is selected so as to optimize resolution of the protein of interest from other cellular proteins. This may result in exclusion of low MW proteins on the resultant WB if a low percentage gel is used, and may under-represent the complement of large MW proteins if a high gel percentage is selected due to their restricted mobility out of the gel during protein transfer. Thus, if one insists on WB validation of ICW Abs, it may be useful to employ gradient gels to resolve a large MW range for this purpose. In any case, it is important to demonstrate that the Ab will detect the protein of interest using microscopic techniques with appropriate negative controls to rule out non-specific signals. This is particularly crucial since ICWs lack the ability to separate protein signals in space as is done in WBs via SDS-PAGE.

3.4.3 Advantages of ICW

The biggest advantages of the ICW assay compared to WB are the diminished preparation time and resource utilization as well as the potential for development of high-throughput assays with the capability to scan multiple microplates simultaneously. The relatively small amount of cellular material in each well allows rapid quenching of treatments and preservation of the cell-interior by simple addition of fixing solution. This more uniform and exact termination of experimental treatments likely provides more precise information regarding dynamic reactions that occur in rapid time courses, exemplified by many phosphorylation reactions.

A principal prerequisite for performing ICWs is the availability of a culture method allowing for an even distribution of cells across the well surface. Cell cultures used for ICW can be adherent or non-adherent. However, if they are adherent, the cells must grow as a

monolayer in culture, and, if non-adherent, must be prepared so they lie in a monolayer at the time of scanning. This will ensure a uniform signal from the well surface. In our studies, which used freshly seeded hUSMC, there was an optimal density of cells for a response to a physiological stimulus. The plateauing of p19RLC and GAPDH signals at higher cell densities in our linearity assessment was unlikely to be due to exceeding the capabilities of the IR scanner, but rather to cell overcrowding, for two reasons. First, there were no saturated pixels in the well signals. Second, in the time course assessment we detected higher signal intensities for p19RLC at 600 cells/mm^2 in stimulated myocytes than those obtained by simply plating a higher density of cells. It is likely that the optimal density for a biological response is dependent on the cell type used, as well as other conditions, and this parameter should be assessed whenever a new cell type is studied.

Our data also demonstrate the validity of the ICW technique to monitor physiological events in a dynamic system. Phosphorylation of RLC at S19 results from influx of Ca^{2+} ions into the myocyte cytosol whether derived from the extracellular space through plasma membrane channels, or from intracellular stores whose release is triggered by the generation of inositol-trisphosphate by PLC. This Ca^{2+} influx results in activation of MLCK by the intermediary Ca^{2+} binding protein, CaM.(87, 199) We have demonstrated that pharmacological manipulation of Ca^{2+} flux, CaM activity or MLCK itself has the predicted effects on concentrations of p19RLC.

3.4.4 Limitations of ICW

Clearly, there are significant limitations to the usefulness of the ICW technique. Its application is restricted to the study of proteins in cell cultures for which a specific Ab is available. It is not suitable for study of phosphoproteins or other proteins from whole tissues or in experimental situations where freshly isolated tissues are required for simultaneous measurement of physiological and biochemical endpoints. ICWs are also restricted to the study of proteins present in high enough levels to be detectable from the cellular material in a single well, as it is not possible to concentrate low-abundance proteins. In contrast, WBs can be preceded by a protein-concentrating or protein-purifying technique such as immunoprecipitation. Another disadvantage of ICWs is that they do not allow determination of the stoichiometry of phosphorylation, such as can be obtained using

urea/glycerol PAGE (213) or via phos-tag SDS-PAGE ((194) and chapter 4). Further, unless one has access to an infrared microscope, ICWs do not permit routine identification of the proteins yielding the measured signal, which is verified in each WB membrane using the MW marker. Lastly, whereas WBs are routinely used to analyze samples that have been frozen in storage, ICWs are unlikely to be useful in the same way since ice crystals formed during freezing may damage the integrity of the cellular structures necessary to obtain reliable data by this method. Therefore, in our experience, ICWs should be used to analyze microplates that have been stored only briefly at 4^0C. We have not formally addressed the length of time that protein phosphorylation is preserved in ICWs, and for this reason we proceeded with the preparation of microplates immediately after cell fixation. Our general observations are that some phospho-antigens are stable over several days (perhaps weeks) after fixation and storage at 4^0C in PBS, but others decay more rapidly. Thus the window of time for plate development must be determined empirically for each phosphoprotein.

3.4.5 Conclusions

In conclusion, we have provided validation of the use of the ICW technique to assess rapid phosphorylation events in hUSMC. It is likely that this technique is equally applicable to many other cell types to assess many other physiological reactions. We have demonstrated that there may be advantages of the ICW to conventional WB techniques with respect to sensitivity and precision and, depending on the proper validation of the Ab, the two techniques are of similar specificity. The major advantage of the ICW assay over WB is the relative ease of preparation of the samples and the potential for high-throughput data production. The increased relative cost of ICWs due to the need for lower dilutions of some Abs is offset by the much higher throughput capacity in addition to other savings in reagents by elimination of several preparative steps from the WB protocol. Our data demonstrate that the technical capabilities of ICWs meet or exceed the standard set by NIR fluorescent WBs. Considering the technical aspects of the two procedures, we conclude that the benefits of ICWs are generalizable irrespective of the protein target of interest.

Chapter 4
Primary Methodology 2

Phos-tag-Based Analysis of Myosin Regulatory Light Chain Phosphorylation in Human Uterine Myocytes.

Abstract

Background: The 'phosphate-binding tag' (phos-tag) reagent enables separation of phospho-proteins during SDS-PAGE by impeding migration proportional to their phosphorylation stoichiometry. Western blotting can then be used to detect and quantify the bands corresponding to the phospho-states of a target protein. We present a method for quantification of data regarding phospho-states derived from phos-tag SDS-PAGE. The method incorporates corrections for lane-to-lane loading variability and for the effects of drug vehicles thus enabling the comparison of multiple treatments by using the untreated cellular set-point as a reference. This method is exemplified by quantifying the phosphorylation of myosin regulatory light chain (RLC) in cultured human uterine myocytes.

Methodology/Principal Findings: We have evaluated and validated the concept that, when using an antibody (Ab) against the total-protein, the sum of all phosphorylation states in a single lane represents a 'closed system' since all possible phospho-states and phosphoisotypes are detected. Using this approach, we demonstrate that oxytocin (OT) and calpeptin (Calp) induce RLC kinase (MLCK)- and rho-kinase (ROK)-dependent enhancements in phosphorylation of RLC at T18 and S19. Treatment of myocytes with a phorbol ester (PMA) induced phosphorylation of S1-RLC, which caused a mobility shift in the phos-tag matrices distinct from phosphorylation at S19.

Conclusion/Significance: We have presented a method for analysis of phospho-state data that facilitates quantitative comparison to a reference control without the use of a traditional 'loading' or 'reference' standard. This analysis is useful for assessing effects of putative agonists and antagonists where all phospho-states are represented in control and experimental samples. We also demonstrated that phosphorylation of RLC at S1 is inducible in intact uterine myocytes, though the signal in the resting samples was not sufficiently abundant to allow quantification by the approach used here.

A portion of this chapter was adapted from reference 214.

4 Phos-tag-Based Analysis of Myosin Regulatory Light Chain Phosphorylation in Human Uterine Myocytes.

4.1 Introduction

As discussed in the previous chapter, the cellular responses mediated by protein phosphorylation are vast in number and function,(215) and therefore a variety of biochemical techniques has been developed to study this important cell signaling modality.(216) Among these, western immunoblotting (WB) is the most widely utilized for the routine measurement of phospho-proteins in experimental samples after 1-dimensional SDS-PAGE. The power and utility of this technique has recently been strengthened by the development of a dinuclear metal complex 'phosphate-binding tag' (phos-tag) that can be incorporated into the polyacrylamide gel matrix prior to SDS-PAGE.(194, 217) This modification of traditional SDS-PAGE, promotes a physical separation of phospho-proteins proportional to the phosphorylation stoichiometry. Thus a single protein might separate into multiple bands, each corresponding to a different phospho-state (forms of a protein containing the same number of phospho-modifications).

In traditional phospho-protein analyses by WB, the signal derived from a phospho-specific antibody (Ab) toward the target protein is normalized to a reference protein, or to the 'total' ('bulk') target protein using an Ab that does not discriminate between phosphorylated and non-phosphorylated forms. This type of analysis is normally limited to measuring changes at a single phospho-site per assay. In contrast, Mn^{2+}-phos-tag SDS-PAGE permits the study of the effects of experimental treatments on the target protein across its various phospho-states by probing replica membrane with an anti-total-target protein Ab and enables the study of protein phosphorylation in the absence of phospho-protein-specific Abs. Where phospho-protein-specific Abs are available, the technique yields information regarding the distribution of specific phosphoisotypes (i.e. identical phosphorylation sites) across various phospho-states (i.e. equivalent phosphorylation stoichiometries). As such, this technique permits identification of the phospho-states corresponding to specific phosphoisotypes. A previous report using Mn^{2+}-phos-tag SDS-PAGE to assess phosphorylation of RLC demonstrated the enhanced sensitivity of the technique.(197) Others have focused principally on discovery of novel phospho-states, or

quantifications of single phospho-states or phosphoisotypes.(218-220) We have used this methodology to validate the phospho-specificity of Abs directed toward RLC in lysates derived from primary cultures of human uterine myocytes.(184) Here we quantified the changes in the phospho-states of RLC, by employing a method that does not rely on a 'loading control' protein, and produces vehicle-corrected data that are expressed relative to the untreated distribution to enable a direct comparison between drugs with different vehicles.

As an exemplary model, we have measured the phospho-state distribution of RLC in hUSMC lysates under various experimental conditions. As mentioned previously, pRLC is associated with activation of the myosin heavy chain ATPase, which provides energy for the power stroke. However, ppRLC causes enhanced activation of the myosin ATPase.(71, 221) This potentially important distinction between mono- (pRLC) and di-phosphorylated (ppRLC) proteins exemplifies the utility of a relatively simple approach to assess phospho-state changes following experimental perturbations.

A potential complication in this phospho-RLC analysis is that a single phospho-state could contain more than one phosphoisotype. Similarly, one phospho-site might appear in more than one phospho-state.(73, 222, 223)

Therefore, **the objectives of this chapter were:**

A. Develop a method for quantification of phospho-state distribution data, in general terms and specifically for measurements of RLC in hUSMC.

B. Evaluate and validate this method under various treatment conditions likely to result in altered phosphorylation of RLC in hUSMC.

C. Evaluate whether the reported changes in phosphorylation of RLC result from activity at T18 and S19 alone, or whether they might be explained by activity at distinct phosphorylation sites.

The **experimental aims designed to achieve these objectives were:**

A. Detect and quantify multiple phospho-states corresponding to RLC using WB after a variant of SDS-PAGE capable of separating proteins on the basis of phosphorylation stoichiometry.

B. Quantify changes in the phospho-state distribution of RLC in hUSMC challenged with OT, or activators and inhibitors of the rhoA-ROK system (calpeptin and g-H, respectively).

C. Induce phosphorylation of RLC in hUSMC at sites other than T18 or S19 using an activator of PKC and determine whether novel phospho-states can be detected.

The scheme for data analyses provided in this chapter represents a novel method for evaluating phosphorylation reactions that might yield significant insight into the integration of cellular signals at the level of the target protein.

4.2 Materials and Methods

4.2.1 Primary hUSMC Cultures

This methodology has been detailed previously (see 3.2.1).

4.2.2 Pharmacological Agents

OT (1 mM, sterile ddH_2O), glycyl-H-1152 (g-H, 5 mM, DMSO), ML7 (5 mM, DMSO), and phorbol-12-myristate-13-acetate (PMA, 10 mM, DMSO) were obtained from Calbiochem (EMD Chemicals, Gibbstown, NJ, USA). 4-α-PMA (10 mM, DMSO) was purchased from Santa Cruz Biotechnology Inc. (Santa Cruz, CA, USA). Calpeptin (Calp, 400 mU/μL, DMF) and the cell permeable rhoA inhibitor (C3 transferase, 1 mg/mL, H_2O) were purchased from Cytoskeleton, Inc. (Denver, CO, USA). Calyculin A (200 μM, DMSO) was purchased from Cell Signaling (Beverly, MA, USA). hUSMC were treated for 20 sec with OT, 30 min with g-H, ML7, PMA, 4-α-PMA, or Calyculin A, and 15 min with Calp, as determined by optimization experiments.

4.2.3 Traditional and Phos-Tag SDS-PAGE

This methodology has been detailed previously (see 3.2.4). Electrophoresis was carried out by standard methods, in 15% acrylamide gels. In addition, two methods of phos-tag (NARD Institute, Ltd., www.phos-tag.com) SDS-PAGE were performed. The first method is described in 3.2.4 and in 194. The second method of phos-tag SDS-PAGE is detailed in 224. In this case, we used 40 μM Zn^{2+}-phos-tag in 8% acrylamide gels and performed electrophoresis in the modified buffer set indicated in 224. After electrophoresis, the divalent cations were removed from both types of phos-tag gels by incubation with transfer buffer containing 2 mM EDTA for 15 min. The gel contents were transferred to nitrocellulose for 1.5 hrs at 100 V by standard methods.

4.2.4 Western Immunoblotting

This methodology has been detailed previously (see 3.2.5). The final primary Ab dilutions used here were: C-terminal tRLC 1:1000 (LS-C81207, Rabbit PAb, LifeSpan BioSciences), p19RLC 1:200 (#3671, Rabbit, PAb, Cell Signaling), ppRLC 1:500 (#3674, Rabbit, PAb, Cell Signaling), p1RLC 1:2000 (MP3461, Rabbit, PAb, ECM Biosciences), rhoA 1:200 (#610990, Mouse, MAb, BD Biosci.), and α-actin 1:4000 (sc-56499, Mouse, MAb, Santa-Cruz).

4.2.5 In-Cell Westerns

This method was described in detail previously (see 3.2.6). The final antibody dilutions were: pRLC 1:1000 (#3675, Mouse MAb, Cell Signaling), ppRLC 1:500 (#3674, Rabbit PAb, Cell Signaling), p1RLC 1:2000 (MP3461, Rabbit PAb, ECM Biosciences).

4.2.6 Measurement of RhoA Activity by G-LISA

Relative rhoA activity was estimated by a commercially available ELISA-based assay ('G-LISA™', BK-124, Cytoskeleton Inc.) according to the manufacturers' specifications. This assay estimates the cellular content of GTP-bound ('active') rhoA through a colorimetric reaction that is quantified by measuring the optical density (A_{490nm}) on a microplate reader. Briefly, hUSMC were treated with 0.5 mU/mL Calp for 15 min, and then harvested by lysis in ice-cold buffer (provided). An aliquot of these samples was retained for protein content estimation by ADV02 reagent (Cytoskeleton, Inc.), and the rest was flash frozen in $N_2(l)$, and stored at -80^{0}C until needed. The frozen samples were thawed and prepared for the assay as specified. Approximately 25-30 μg total protein was used per well, and each sample was assayed in duplicate. The measured optical density measured at 490 nm was expressed relative to vehicle control. The absorbance data were corrected for variations in protein loading by quantifying total-rhoA content on WBs performed immediately following the rhoA activity assay. Preliminary experiments comparing hUSMC lysates to purified, constitutively active rhoA (G14V) positive controls demonstrated that our measurements were within the linear range of the assay.

4.2.7 Statistical Analysis

All results were expressed using means (±S.E.M.). Statistical analysis of Calp activation data was performed using one-way ANOVA followed by a post-hoc Tukey test.

4.3 Results and Discussion

4.3.1 Detection of Phosphorylation of RLC in hUSMC Lysates

Several studies have shown that three distinct phospho-states of RLC are detectable in SM preparations.(73, 197, 222, 223, 225-229) These three phosphoisotypes most likely correspond to unphosphorylated, mono-phosphorylated (S19), and diphosphorylated (T18/S19) RLC. To ensure preservation of phospho-modifications during cell lysis, we harvested total cellular proteins by trichloroacetate precipitation (see 3.2.3). As shown in the previous chapter, after traditional SDS-PAGE separation for lysates, Abs directed toward the C-terminus of total-RLC (tRLC, no phospho-specificity), p19RLC, and ppRLC recognize only a single band of 20 kDa on WB replica membranes (Figure 3-2B). In contrast, when hUSMC protein lysates are separated by Mn^{2+}-phos-tag SDS-PAGE these three Abs yield distinct banding patterns. The tRLC Ab (Figure 3-2C) produces three distinct bands in lysates from unstimulated hUSMC. These data do not provide information regarding the phosphoisotypes contained within each band. Thus, we have chosen '0pRLC', '1pRLC', and '2pRLC' as the terminology to emphasize phosphorylation stoichiometry irrespective of the phosphoisotypes represented.

The p19RLC Ab detects two phospho-RLC phospho-states and does not detect the 0pRLC state. For clarity, we have used '$0pRLC^{T}$', '$1pRLC^{T}$', and '$2pRLC^{T}$' to denote measurements obtained by the tRLC Ab, and the notation '$1pRLC^{19}$' and '$2pRLC^{19}$' for those reported by the p19RLC Ab. To verify that the upper of these three bands corresponds to 2pRLC, we probed a replica membrane with an anti-ppRLC Ab (Figure 3-2C).

4.3.2 Rationale and Experimental Approach for Parallel Quantification of RLC Phospho-States

In order to quantify these three phospho-states across various treatment groups, we have considered that the bands in each lane detected by the tRLC Ab represent a 'closed system', such that an enhancement of one of the three phospho-states must be reflected by an equivalent diminution of one (or both) of the others, and vice versa. Use of

this ‘closed system’ concept has several advantages that will be discussed in a later section that will address its validation.

To demonstrate quantifiable changes in the phospho-state distribution of RLC, we treated primary cultures of hUSMC with pharmacological agents likely to alter to alter phosphorylation of RLC. RhoA and ROK are known to regulate uterine contractility.(106-109, 182) Specifically, rhoA-ROK activation reduces MLCP activity, and therefore increases intracellular phospho-RLC concentrations. To manipulate this pathway pharmacologically, cells were treated with glycyl-H-1152 (g-H, rho-kinase inhibitor) and calpeptin (Calp, rhoA activator). We also treated uterine myocytes with OT.

Calp has been shown to specifically activate rhoA in fibroblasts cultures, possibly by influencing a protein tyrosine-phosphatase upstream of rhoA.(230, 231) To confirm that Calp increases rhoA activation in hUSMC, we quantified the GTP-bound ‘active’ rhoA in myocytes treated with Calp. Figure 4-1A confirms that Calp (0.5 mU/mL, 15 min) induces rhoA activation (2.43 ± 0.43 fold of vehicle, n=2) in cultured hUSMC. Further, we evaluated whether rhoA activation by Calp was associated with increased phosphorylation of RLC by the ICW technique. Figure 4-1B shows that Calp strongly induces ppRLC in comparison to pRLC. The Calp-induced enhancement in ppRLC can be attenuated by using a rhoA inhibitor (C3 transferase), again confirming that Calp activates rhoA. The cell-permeable ROK inhibitor g-H (1 μM, 30 min) was selected due to its high potency and selectivity for its target relative to other commercially available pharmacological inhibitors.(232-234) We have previously demonstrated the optimal time course and concentrations for OT in this experimental system.(184)

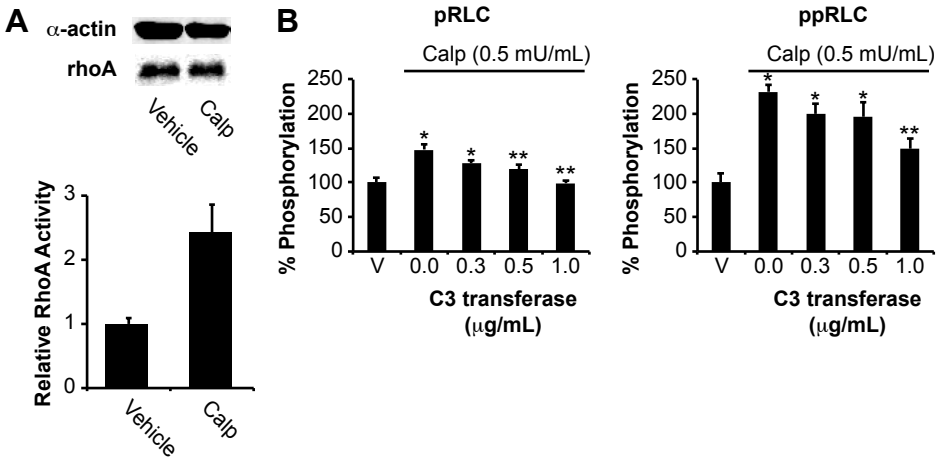

Figure 4-1. Validation of Increased RhoA Activity and Phosphorylation of RLC by Calpeptin.

A. Estimation of GTP-bound 'active' rhoA in hUSMC treated with Calp or vehicle (DMF) for 15 min (n=2). RhoA content was quantified relative to α-actin loading control, and used to correct rhoA activity data. Error bars represent standard deviations. **B.** Quantification of pRLC and ppRLC in hUSMC treated with Calp (0.5 mU/mL) and with increasing concentrations of a cell-permeable rhoA inhibitor (C3 transferase) by ICW (n=4). * and ** indicate significant differences from vehicle or Calp alone (second histogram), respectively. $p < 0.05$ in all cases as determined by one-way ANOVA followed by Tukey test. Error bars correspond to SEMs.

4.3.3 Quantification of Phospho-State Distributions

This analysis has two primary goals: 1) isolating the effect of the treatment of interest from any vehicle-induced change in the phospho-state distribution, and 2) facilitating comparisons across treatments by expressing them relative to a common reference point (untreated distribution). Figure 4-2A shows representative WBs obtained for the treatment groups described. Distribution data were obtained by expressing the signal integrated intensity at each band position as a fraction of their sum total (e.g. [signal $0pRLC^T$] / ([signal $0pRLC^T$] + [signal $1pRLC^T$] + [signal $2pRLC^T$]), etc.), and averaging these proportions for n=5-8 samples. This 'sum method' amounts to performing an alternate method of 'in-lane' normalization, in place of that commonly achieved by using a loading control. We propose that this 'in-lane normalization' method has several advantages that are discussed in a subsequent section. Note that the WBs have been intensified for all figures so that all three bands are visible, where possible. This is achieved by restricting the upper and lower boundaries of pixel intensity that are shown by the quantification software. The quantitative estimates of band intensity are completely independent of these manipulations. The blots presented here did not exhibit pixel

saturation, and therefore have not exceeded the upper limit of the scanner in detecting higher protein loads. Figure 4-2B demonstrates the raw phospho-RLC proportional distributions measured by this Ab. In the untreated distribution (n=12), approximately 47 ± 4% of the RLC pool is represented by $0pRLC^T$, 36 ± 2% by $1pRLC^T$, and 16 ± 3% by $2pRLC^T$.

Next, we corrected for the effects of the vehicles by subtracting the vehicle-induced changes from those of the corresponding treatments. The net treatment-induced changes are presented in Figure 4-2C and these data were used to calculate the effect of each treatment relative to the untreated distribution in Figure 4-2D. This provides a common reference and enables comparisons across treatments (for numerical data, see Table 5). Relative to the untreated distribution, g-H (n=5) promotes significant reduction in phospho-RLC, as evidenced by an enhancement in the proportion of $0pRLC^T$ to 86 ± 2 from 47 ± 4% in untreated samples, whereas $1pRLC^T$ and $2pRLC^T$ fell to 7 ± 2% and 6 ± 2% respectively. Calp (n=8) treatment causes a specific increase in $2pRLC^T$ from 16 ± 3% to 38 ± 8%, in agreement with the increase in ppRLC shown in Figure 4-1. This enhancement in $2pRLC^T$ is accompanied by a corresponding reduction in 0pRLC from 47 ± 4% to 29 ± 6%, but no change in $1pRLC^T$ (from 36 ± 2% to 34 ± 4%). These findings suggest that activation of rhoA, and presumably ROK, is associated with a specific increase in the intracellular concentrations of ppRLC. OT appears to enhance both $1pRLC^T$ and $2pRLC^T$, perhaps favouring the former (final proportions of 54 ± 11% and 36 ± 10%, respectively).

The data shown in Figure 4-2C illustrate that significant quantitative differences might result from the omission of a vehicle correction step. In particular for OT, the $2pRLC^T$ state appears to be strongly induced by the vehicle, and most likely results from the mechanical stimulation of cells by pipetting the treatment solution. The short duration of treatment (20 sec) prevents this stimulatory effect from returning to basal levels. Importantly, the OT vehicle does not reduce $0pRLC^T$ as OT does (Figure 4-2B and C). Thus, ignoring the effect of the OT vehicle underestimates the true extent of phosphorylation of RLC induced by OT.

In summary, these data are normalized in three successive ways: 1) in-lane normalized to correct for variations in protein loading and signal intensity, 2) vehicle normalized to ascertain that the measured effect can be attributed to the drug or treatment of interest, and 3) normalized to the untreated distribution to permit comparisons across treatments.

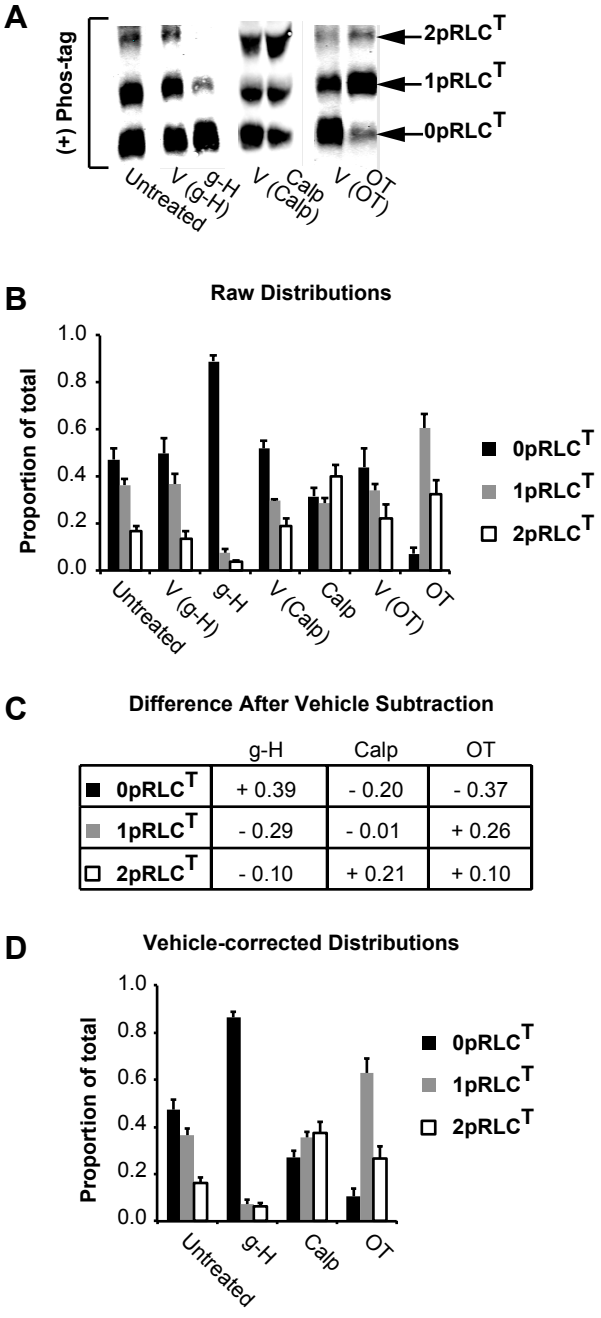

Figure 4-2. Quantification of RLC Phospho-State Distribution.

Panels A-D correspond to WB data derived using an Ab directed toward the C-terminus of RLC. **A.** Representative WBs demonstrating RLC phospho-states separated by Mn^{2+}-phos-tag SDS-PAGE. hUSMC were lysed and total protein was harvested after the following treatments: untreated, or treated with g-H, Calp, OT, or with their corresponding vehicles. **B.** Quantification of bands identified in panel A (untreated; n=12, g-H; n=5, Calp; n=8, OT; n=7). The signals derived from $0pRLC^T$, $1pRLC^T$, and $2pRLC^T$ are expressed as the proportion of their sum total within each lane. **C.** Absolute magnitude of the difference in each phospho-state caused by the treatments in comparison to the corresponding vehicle ('+' indicates enhancement relative to vehicle, '-' indicates diminution relative to vehicle). **D.** Vehicle-corrected distribution data obtained by combining the data in panel C to the untreated group distribution. g-H (glycyl-H-1152); ROK inhibitor (1 μM). Calp (0.5 mU/mL). OT (100 nM). All data are shown as means ± SEMs. The corresponding numerical data are compiled in Table 5.

4.3.4 Validation of the 'Closed-System' Concept

The method for data normalization of a closed system described above has several advantages over normalization to an in-lane loading control. Specifically, the use of a traditional loading control might not be feasible in Mn^{2+}-phos-tag acrylamide gels for several reasons. First, the physical separation of phospho-states along the vertical dimension of the gels increases the likelihood that the loading control protein overlaps with a band corresponding to the protein of interest. Second, if it is phosphorylated, the loading control protein might dissociate into two or more bands and might complicate identification and quantification of loading control and the protein of interest on the same blot. Despite these potential problems, to validate the 'closed system' concept we performed a traditional loading control quantification of the phospho-states detected by the tRLC Ab using SM α-actin as our in-lane reference.

Figure 4-3A demonstrates that the α-actin signal remains localized to a single position after traditional and Mn^{2+}-phos-tag SDS-PAGE separation without any evidence of phosphorylation under our experimental conditions. Though we were fortunate to have chosen α-actin, finding a loading control protein that does not suffer from at lease one of the above-mentioned problems might prove difficult. If a single-channel detection method is used, WB quantification might be unfeasible. Where dual-channel detection is used for segregating the loading control and target protein signals, the primary-Ab-secondary-Ab-fluorophore combinations must be of high specificity (see Figure 4-6). If used appropriately, the 'closed system' method for data quantification proposed here circumvents all of these difficulties by eliminating the need for measuring a loading control protein.

For this validation, the signals for $0pRLC^T$, $1pRLC^T$, and $2pRLC^T$ in the vehicle and treatment lanes were normalized individually to the in-lane α-actin signal, without expressing them as the proportions of the sum-total of signals as was performed to obtain Figure 4-2B. The α-actin-normalized fold-changes relative to vehicle are shown in Figure 4-3C. Qualitatively, these data are in agreement with those in Figure 4-2D. ROK inhibition with g-H promotes an increase in $0pRLC^T$ relative to $1pRLC^T$ and $2pRLC^T$. RhoA activation with Calp causes a large increase in $2pRLC^T$. OT treatment causes an enhancement of both $1pRLC^T$ and $2pRLC^T$ that is reflected as a dramatic reduction in $0pRLC^T$.

To provide a direct quantitative comparison between the Figure 4-3C and the in-lane sum method above, we computed the fold changes in the proportion of $0pRLC^T$, $1pRLC^T$, and $2pRLC^T$ in the treatment groups relative to their proportions in the vehicle groups. Both methods show that g-H treatment causes an increase in $0pRLC^T$ (sum method: 1.79 ± 0.05, α-actin: 2.28 ± 0.69 fold of vehicle), and a reduction in $1pRLC^T$ (sum method: 0.20 ± 0.05, α-actin: 0.27 ± 0.05) and $2pRLC^T$ (sum method: 0.26 ± 0.07, α-actin: 0.28 ± 0.09). Calp causes increased $2pRLC^T$ (sum method: 2.13 ± 0.40, α-actin: 1.99 ± 0.06). OT causes virtually complete phosphorylation of the pool of RLC, as evidenced by near abolition of $0pRLC^T$ (sum method: 0.16 ± 0.02, α-actin: 0.09 ± 0.03) and an increase in $1pRLC^T$ (sum method: 2.13 ± 0.40, α-actin: 1.95 ± 0.55) and $2pRLC^T$ (sum method: 1.47 ± 0.18, α-actin: 1.74 ± 0.82). The remarkable agreement between these α-actin normalized data and those in Figure 4-2D for these measurements demonstrate that the in-lane normalizations performed for the data in Figure 4-2 provide similar information to traditional loading controls.

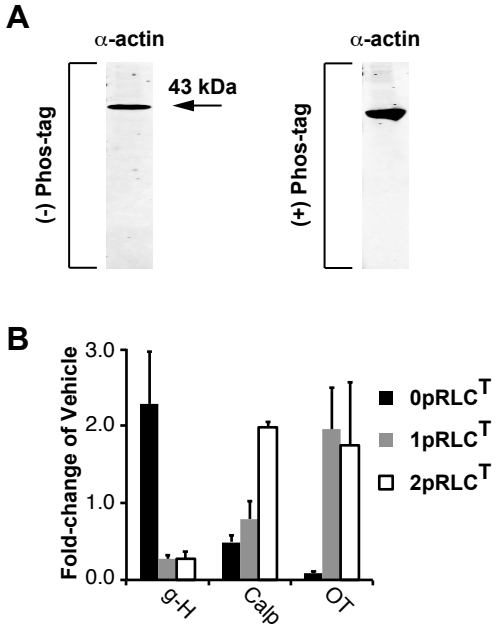

Figure 4-3. Validation of Phospho-State Data Quantification Using a Loading Control.

A. WB for α-actin after traditional and Mn^{2+}-phos-tag SDS-PAGE separation of proteins in lysates from uterine myocytes. In both blots, the anti-α-actin Ab recognizes only a single band. **B.** Each band in panel B was first normalized for α-actin, then corrected for the vehicle. The data are shown as fold-changes relative to vehicle for g-H (1 μM), Calp (0.5 mU/mL), OT (100 nM). All data are shown as means ± SEMs (n=4 in all groups).

4.3.5 Analysis of p19RLC Phosphoisotype Distribution

We next focused attention on the phosphoisotype composition of each of the phospho-states following Mn^{2+}-phos-tag separation. As demonstrated in Figure 3-2, we validated the specificity of two anti-phospho-S19-RLC Abs by WB after Mn^{2+}-phos-tag SDS-PAGE separation. These Abs were derived from mice (monoclonal – 'pRLC (MMAb)'), or rabbits (polyclonal – 'p19RLC (RPAb)'). The pRLC (MMAb) was unable to detect the 2pRLC band present in blots probed with the tRLC Ab and the p19RLC (RPAb). The most likely explanation for this finding is obstructed binding of the Ab in the presence of phospho-T18-RLC. Still, this Ab was useful for quantifying pRLC specifically, as was demonstrated in Figure 4-1 and as will be shown in chapter 5. Anti-total-protein Abs might also suffer from obstructed binding. Here, we selected the tRLC Ab on the basis of published evidence suggesting phosphorylation of RLC at sites concentrated in the first 20 amino acids of the N-terminal region in an attempt to avoid such interference.(73, 222, 223) To analyze changes in 1pRLC and 2pRLC containing phospho-S19-RLC, we used the p19RLC (RPAb) in our subsequent experiments for this chapter.

One important distinction between the data provided by the p19RLC and the tRLC Abs is that the p19RLC data does not represent a closed system, since it is unable to provide information about 0pRLC or about phospho-states that do not include phospho-S19. Therefore, the use of p19RLC Ab in this setting cannot assess quantitative changes in phospho-states, but can provide information about whether the proportions of phosphoisotypes (containing phospho-S19-RLC) within each phospho-state have changed. In Figure 4-4C, the y-axis corresponds to the proportion of the in-lane signal that is made up by $1pRLC^{19}$ or $2pRLC^{19}$ relative to their sum (i.e. [signal $1pRLC^{19}$] / ([signal $1pRLC^{19}$] + [signal $2pRLC^{19}$]), etc.). For numerical data, see Table 6.

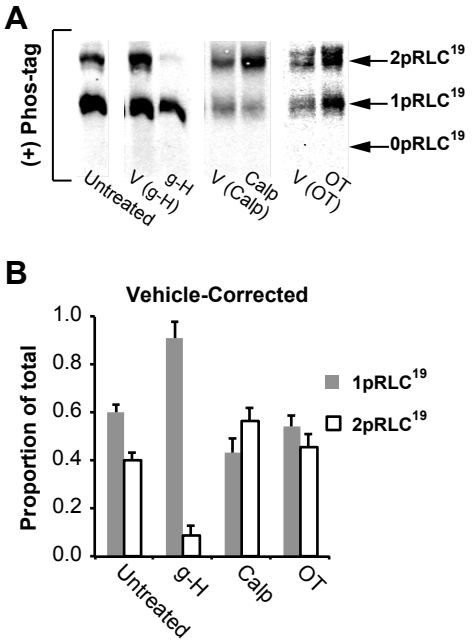

Figure 4-4. Demonstration of Phospho-S19-RLC Phosphoisotype Distribution in hUSMC.

A. hUSMC were lysed and total protein was harvested after the following treatments: untreated, or treated with g-H , Calp, OT, or with their corresponding vehicles. **B.** Vehicle-corrected distribution data for 1pRLC^{19} and 2pRLC^{19} obtained by normalizing the data in panel A to the untreated group distribution. g-H (1 μM, n=5). Calp (0.5 mU/mL, n=10). OT (100 nM, n=10). All data are shown as means ± SEMs. The corresponding numerical data are compiled in Table 6.

In the untreated group, the relative proportions of 1pRLC^{19} and 2pRLC^{19} are 60 ± 3% and 40 ± 3%, respectively. g-H treatment causes a shift in these proportions to 91 ± 7% and 9 ± 4%, suggesting that ROK inhibition causes specific loss of 2pRLC containing phospho-S19-RLC. However, the data provided earlier in Figure 4-2D clarify that both 1pRLC and 2pRLC are markedly reduced with g-H. In contrast, Calp changes the weighting of 1pRLC^{19} and 2pRLC^{19} to 43 ± 6% and 57 ± 5%, respectively, reflecting the specific enhancement in 2pRLC seen in Figures 4-1B and 4-2D. The corresponding values for OT are 54 ± 4% and 46 ± 5% indicating that OT induces both 1pRLC^{19} and 2pRLC^{19} to a similar extent, even if the total cellular content of 1pRLC is larger, as evidenced by the data in Figure 4-2D.

4.3.6 Phosphorylation of Serine-1 of RLC Is Inducible by Phorbol Esters

In addition to S19- and T18/S19-modified phosphoisotypes for RLC, other phospho-sites located at both the N- and C-termini of RLC have been discovered *in vitro*.(73, 222, 223) These findings give rise to the possibility of phospho-states greater than 2pRLC.(235) However, the data presented here thus far, and other published evidence suggest that only three phospho-states exist (refs (184, 197, 225, 226, 236) and Figure 3-2 and 4-2). Previous biochemical evidence from turkey gizzard SM suggested that protein kinase C (PKC) was capable of phosphorylating S1, S2, or T9 of RLC.(73, 237-239) Furthermore, phosphorylation of the PKC target sites prevented subsequent MLCK phosphorylation of RLC at S19, and vice versa. In addition, they demonstrated a reduction in the actin-activated myosin ATPase activity upon phosphorylation of RLC by PKC. Thus, PKC-mediated phosphorylation of RLC might impact myocyte function. To assess whether these changes occurred in hUSMC, we studied the effects of phorbol-12-myristate-13-acetate (PMA), a PKC activator, on the phospho-state distribution of RLC. Surprisingly, we identified additional phospho-states for RLC that correspond to phosphorylation sites distinct from T18 or S19.

Figure 4-5A demonstrates the separation of lysates treated with PMA (1 μM, 30 min) by Mn^{2+}-phos-tag SDS-PAGE. We noted the appearance of three bands at positions slightly above those we previously identified as 0pRLC, 1pRLC and 2pRLC, such that the tRLC Ab cross-reacted with six distinct bands. We hypothesized that these unidentified bands might correspond to phosphoisotypes of RLC that exhibit altered mobility in the Mn^{2+}-phos-tag matrix. As such these bands might represent 1pRLC, 2pRLC, and 3pRLC corresponding to phosphoisotypes modified at a site other than T18 or S19. However, without knowledge of the specific phosphoisotypes corresponding to these intermediate bands, the quantitative information provided by the preceding analysis is difficult to interpret. Thus, instead we turned our attention to identifying a candidate phosphorylation site that might account for these additional phosphoisotypes.

We used an Ab directed toward phospho-S1-RLC (p1RLC) to determine if phosphorylation at S1 was inducible by PMA. Figure 4-5B shows WB data that confirms

the induction of p1RLC with PMA, and is not affected by additional OT stimulation. We used the ICW assay to demonstrate (Figure 4-5C) that PMA induction of p1RLC is concentration-dependent, suggesting activation of intracellular signalling systems. Further, to distinguish between specific and nonspecific effects due to detergent-like properties of phorbol esters, we selected 4-α-PMA as negative control since this agent is ineffective at activating PKCs.(240) As shown in Figure 4-5C, treatment with 4-α-PMA did not result in increased concentrations of p1RLC, confirming the specificity of the PMA treatment.

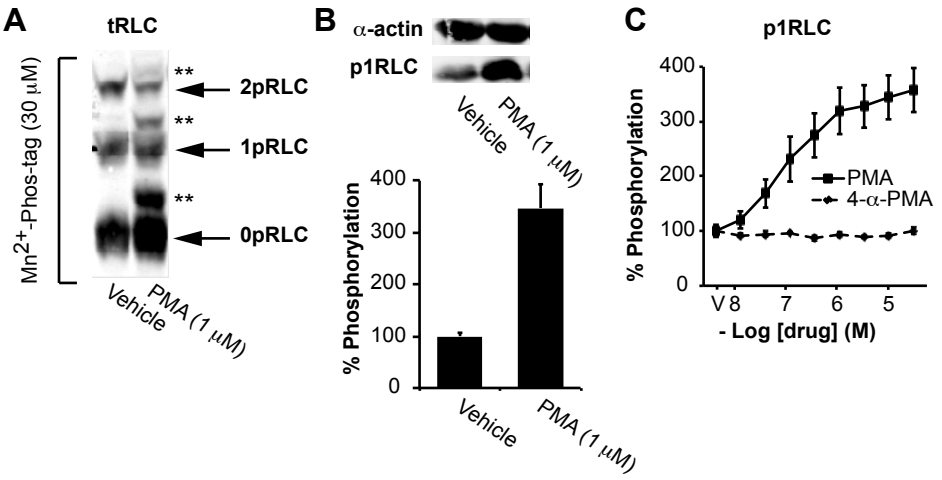

Figure 4-5. PMA Induces Phosphorylation of RLC At S1 and Alters Mobility of Phospho-RLC During Phos-Tag SDS-PAGE.

A. WBs produced by Mn^{2+}-phos-tag separation of lysates from hUSMC treated with PMA (1 μM) or vehicle. The membranes were probed with an Ab directed against the C- terminus of total-RLC (tRLC). 0pRLC, 1pRLC, and 2pRLC correspond to non-, mono-, and di-phosphorylated RLC. The bands labeled with ** exhibit unexpected mobility in the Mn^{2+}-phos-tag acrylamide matrix. **B.** Traditional WBs demonstrating phosphorylation of RLC at S1 (p1RLC) in hUSMC treated with PMA. **C.** Quantification of p1RLC concentrations in hUSMC treated with PMA and 4-α-PMA (negative control) by the ICW method. In **B** and **C**, the data represent 4 independent experiments and are presented as means ± SEM. PMA; phorbol ester.

Thus far, we have focused on the alkaline Mn^{2+}-phos-tag method. Subsequent attempts to improve resolution of the unidentified bands from 0pRLC, 1pRLC and 2pRLC by Mn^{2+}-phos-tag were inconsistent. Recently, an improved method of separation using Zn^{2+} instead of Mn^{2+} ions in the phos-tag matrix and an alternate buffer set for electrophoresis was developed.(224) We used this advanced Zn^{2+}-phos-tag method to study the PMA-induced changes in the RLC phospho-states. In order to detect as many phospho-states as possible, we studied the effects of PMA and of the protein phosphatase

1 and 2A inhibitor, calyculin A (CalA).(241) To elucidate the phosphoisotypes contained within each phospho-state, we used the MMAb directed toward p19RLC since it is detected independently using a secondary Ab directed toward murine primary Ab, whereas the tRLC and p1RLC (both RPAbs) are detected using a secondary Ab directed toward rabbit polyclonal Abs. Figure 4-6A demonstrates that the tRLC Ab recognizes more than 3 bands in the presence of PMA, whereas phosphatase inhibition with CalA enhances 1pRLC and 2pRLC, but does not create any additional phospho-states. When hUSMC are challenged with both PMA and CalA, a band corresponding to a 3pRLC state can be discerned, and most likely corresponds to RLC phosphorylated at S1, T18, and S19. Figure 4-6B shows that the intermediate bands produced by PMA with or without CalA contain p1RLC, and suggests that phosphoisotypes of RLC containing phospho-S1 move more rapidly through the phos-tag matrices than those containing phospho-S19 with equivalent phosphate stoichiometries. They also suggest that there exists a 3pRLC state corresponding to phospho-S1/T18/S19-RLC that is inducible with PMA treatment. Thus, it appears that S1, T18, and T19 can exist simultaneously, rather than in mutual exclusivity to one another. However, we cannot exclude the possibility that sites other than S1, T18, and S19 have been induced by PMA, in the absence of other phospho-site-specific Abs. To clarify this possibility, future studies might benefit from the use of phos-tag SDS-PAGE in combination with other techniques such as mass spectrometry.(242)

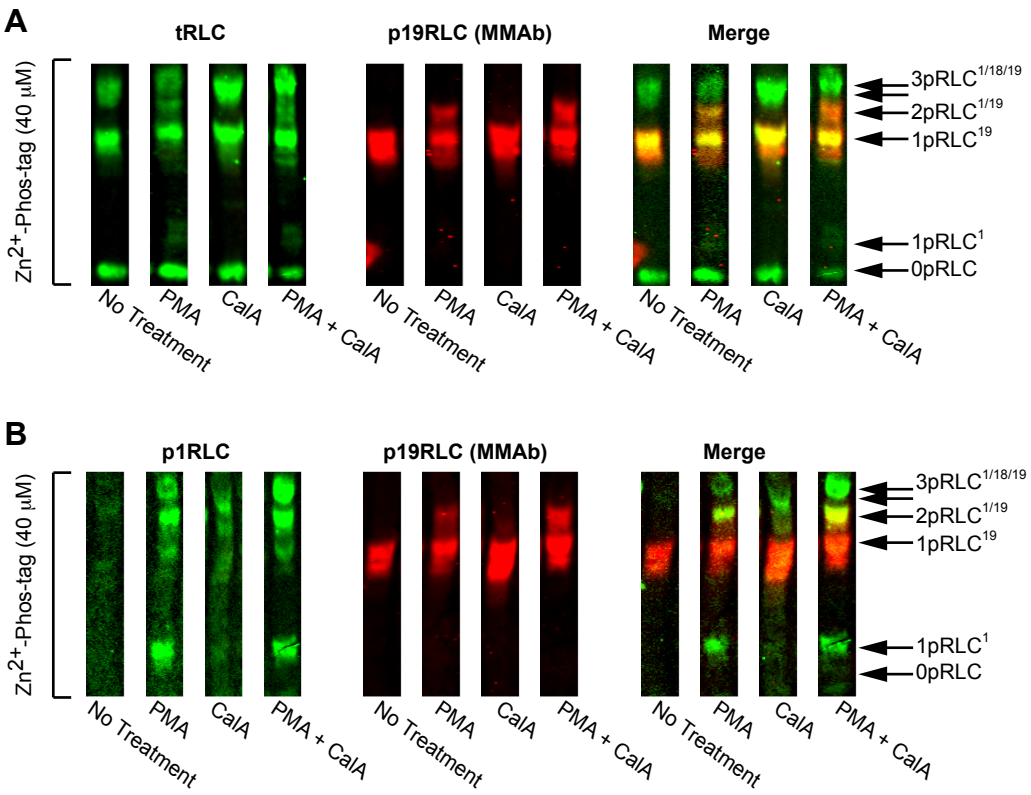

Figure 4-6. Advanced Phos-Tag Analysis of Phosphorylated RLC in PMA-Treated hUSMC.

A and **B.** WBs produced by Zn^{2+}-phos-tag (40 μM) separation of lysates from untreated samples, or samples treated with PMA (1 μM), CalA (20 nM), or with both. In both A and B, the red signal corresponds to a mouse monoclonal Ab (MMAb) targeting p19RLC that is detected independently of the green signals (tRLC in panel A, and p1RLC in panel B). A yellow signal indicates overlap of the individual green and red signals. 0pRLC, 1pRLC, 2pRLC and 3pRLC denote non-, mono-, di-, and tri-phosphorylated RLC. The superscripts denote the position of the phospho-modification: 1: S1, 18: T18, 19: S19. The unlabeled arrow below $3pRLC^{1/18/19}$ corresponds to $2pRLC^{18/19}$ that is particularly prominent in lysates treated with CalA alone. PMA; phorbol ester. CalA; calyculin A (PP1 and PP2 phosphatase inhibitor).

4.3.7 Physiological Relevance of RLC Phospho-State Distribution Measurements

In the present work, we treated three phospho-states of RLC as a closed system based on strong evidence that other states are unlikely to exist physiologically. This rationale is in agreement with our data (Figure 3-2, 4-2-4-4) and with studies performed in rat uteri demonstrating the three phospho-states for RLC (0pRLC, 1pRLC, and 2pRLC) as determined by two-dimensional analyses.(227, 229) Our results also agree with kinetic data regarding MLCK activity suggesting the potential for phosphorylation of nearly the whole pool of RLC during a physiological stimulus.(229) In particular, OT was shown to

induce phosphorylation in approximately 80% of the pool of RLC molecules available in rat uterus (229) compared to >90% phosphorylation in our data. In contrast, it appears that a much smaller portion of the RLC pool is phosphorylated at rest in vascular SM.(197) Further, in OT-stimulated uterine myocytes from rats it appears that ppRLC is quantitatively more prominent than pRLC.(228) Our data suggest that hUSMC might respond similarly to OT with respect to mono- and ppRLC at S19. This validated methodology can be used to explore potentially significant differences between experimental conditions, and is likely also applicable to studying tissue differences. This type of information could be of key importance in the design of pharmacological agents that will have specificity for a single tissue or a specific physiological situation.

In our early experiments, we assumed that all phosphoisotypes with equivalent phosphate stoichiometries comigrate in the phos-tag acrylamide matrix. However, the data in Figures 4-5 and 4-6 suggest this assumption is incorrect. Under some experimental conditions, some phosphoisotypes might exist that do not conform to these migration characteristics. We demonstrated that phosphoisotypes corresponding to phospho-S1-RLC exhibit altered mobility in the phos-tag matrix in comparison to phospho-S19-RLC. The explanation for this behaviour is unclear, though it is interesting that the unexpected migration occurred for phosphoisotypes with a phosphate groups conjugated to the extreme N-terminus of the amino acid backbone. These results might suggest that the phos-tag-Mn^{2+} is less effective at retarding phosphorylated proteins at the protein termini, or that phosphorylation of S1 of RLC changes the conformation of the protein such that the phos-tag-Mn^{2+} complex is unable to interact effectively with the phospho-S1 moeity. It is also possible that phosphorylation of S1 of RLC prevents complete linearization of the protein even under the reducing conditions of SDS-PAGE, thereby enabling more rapid migration than expected. Whatever the reason, this relatively rapid migration might facilitate further biochemical characterization of phosphoisotypes containing phospho-S1.

Some *in vitro* data suggest that PKC-mediated phosphorylation of RLC results in reduced myosin ATPase activity and impaired S19 phosphorylation by MLCK.(73, 222, 223, 238, 243) However, subsequent experiments using an *in vitro* motility assay for myosins isolated from various sources demonstrated that PKC phosphorylation of RLC

could not induce movement of myosin beads along actin cables on its own, and also did not alter the rate of movement of the myosin beads after MLCK-mediated phosphorylation of RLC.(244) However, the majority of available data regarding PKC actions on RLC are often irreconcilable regarding the specific site(s) of action and subsequent physiological relevance. The inconsistencies might stem from differences in model species and experimental approaches. Whatever the source of variability, the translational utility of PKC-mediated phosphorylation of RLC for therapeutic use in humans remains unclear. The p1RLC phosphoisotypes inducible by PMA (Figure 4-6) appear to make up only a small proportion of the total-RLC signal present. Co-incubation of PMA with CalA appears to improve the incorporation of p1RLC into a greater proportion of the RLC pool, but it is unclear whether these pharmacological manipulations are of any physiological significance. Still, it is interesting that p1RLC is inducible in intact myocytes, suggesting the presence of an intact signalling system aimed at phosphorylating a poorly characterized phospho-site on RLC. In the interest of uncovering novel therapeutic strategies for reducing SM contractility, this finding warrants further study.

Chapter 5
Primary Results

Rho-Kinase-Mediated Diphosphorylation of Myosin Regulatory Light Chains is a Unique Event in Uterine Myocytes.

Abstract

Rationale: Smooth muscle (SM) contraction results from phosphorylation of myosin regulatory light chain (RLC) at S19 (pRLC) by RLC kinase (MLCK). Subsequent phosphorylation at T18 yields diphosphorylated-RLC (ppRLC). In cultured uterine myocytes (hUSMC), rho-kinase (ROK) inhibition caused a marked reduction in resting and stimulated ppRLC. ROK inhibition attenuated tension developed by a variety of SMs.

Objectives: 1) to determine the role and mechanisms for ROK in mediating the OT-stimulated enhancement in ppRLC in hUSMC, and 2) to evaluate the uniqueness of such a mechanism in hUSMC.

Findings: hUSMC differ from vascular myocytes (hVSMC) in their phosphorylation responses to stimulation. hUSMC respond to OT by synthesizing pRLC and ppRLC, whereas hVSMC respond to endothelin-1 by synthesizing only pRLC. Inhibition of RLC phosphatase (MLCP) with calyculin A caused a marked enhancement in ppRLC, and a reduction in pRLC in stimulated hUSMC.

Conclusions: In hUSMC, ROK phosphorylates RLC at T18 downstream of MLCK-mediated phosphorylation at S19. This sequential phosphorylation of RLC forms ppRLC. This role of ROK activity appears unique to hUSMC and is a fundamental difference from hVSMC. These findings suggest uterine-specific therapeutic avenues for prevention or arrest of preterm labor.

The data presented in this chapter are adapted from reference 214 and from a manuscript currently under review.

5 Rho-Kinase-Mediated Diphosphorylation of Myosin Regulatory Light Chains is a Unique Event in Uterine Myocytes.

5.1 Introduction

The development of the technologies in chapters 3 and 4 provided the tools necessary to address our overall objective, which is to determine a suitable pharmacological target to prevent or treat PTL. Our approach is to discern such a target on the basis of demonstrated efficacy in reducing intracellular concentrations of phosphorylated RLC.

During the development of methods of advanced western analyses (chapter 4), we noted that treatment of hUSMC with g-H caused a marked reduction in ppRLC and that OT a significant increase in ppRLC. In light of evidence demonstrating that inhibition of ROK causes significant reduction in contractile activity,(134, 135, 144, 145, 177, 178) we formulated the following hypotheses, objectives and experimental aims:

The **primary hypotheses investigated** in this chapter were:

A. Diphosphorylation (T18/S19) of RLC is mediated by ROK in hUSMC.

B. Diphosphorylation (T18/S19) of RLC is a unique feature of hUSMC that differentiates them from hVSMC.

The **primary objectives of the work in this chapter were:**

A. Compare the sensitivity of phosphorylation of RLC in resting hUSMC and hVSMC challenged with a ROK inhibitor.

B. Determine the predominant phosphorylation changes in RLC associated with agonist stimulation in hUSMC and hVSMC.

C. Assess the effect of ROK inhibition on the predominant phosphorylation changes in RLC associated with stimulation of hUSMC and hVSMC.

In addition, **the secondary objectives were:**

A. Determine whether the predominant phosphorylation changes in RLC observed in hUSMC are properties of specific agonists, or general features of myocyte activation.

B. Assess the relative contribution of MLCK and ROK in mediating changes in phosphorylation of RLC in stimulated hUSMC.

C. Evaluate the role of ROK-mediated inhibition of MLCP in resting and agonist-induced phosphorylation of RLC in hUSMC.

The corresponding **experimental aims were:**

A. Determine the changes in the phospho-states for RLC in stimulated hUSMC in the presence or absence of MLCK or ROK inhibitors (ML7 or g-H).

B. Measure resting concentrations of pRLC and ppRLC in hUSMC and hVSMC challenged with increasing concentrations of a ROK inhibitor (g-H).

C. Measure stimulated concentrations of pRLC and ppRLC in hUSMC and hVSMC challenged with OT or endothelin-1 (ET-1).

D. Measure concentrations of pRLC and ppRLC in stimulated hUSMC and hVSMC in the presence and absence of a ROK inhibitor (g-H).

E. Measure concentrations of pRLC and ppRLC in stimulated hUSMC in the presence and absence of an MLCK inhibitor (ML7).

F. Measure concentrations of pRLC and ppRLC in response to increasing concentrations of an MLCP inhibitor (calyculin A), in combination with g-H or OT.

G. Measure phosphorylation of MYPT1 in resting or stimulated hUSMC treated with g-H.

5.2 Materials and Methods

5.2.1 Pharmacological Agents

OT (1 mM, ddH_2O), ET-1 (200 μM, 5% acetic acid), glycyl-H-1152 (5 mM, DMSO), ML7 (5 mM, DMF), endothall (10 mM, ddH_2O), and cantharidic acid (10 mM, DMSO) were acquired from Calbiochem (EMD Chemicals Inc., Gibbstown, USA). Calyculin A (200 μM, DMSO) was purchased from Cell Signaling (Beverly, USA). Calpeptin (400 mU/μL, DMF), and the rhoA G-LISA assay were acquired from Cytoskeleton, Inc. (Denver, USA). Rho-15 (5 mM, DMSO) and SR3677 (5 mM, DMSO) were obtained from SYNkinase (SYNthesis Med Chem, Melbourne).

5.2.2 Primary hUSMC Cultures

This methodology has been detailed previously (see 3.2.1).

5.2.3 Primary Human Coronary Artery Smooth Muscle Cell Cultures

The hVSMC (purified coronary artery myocytes - ATCC PCS-100-021) were purchased from American Type Culture Collection (ATCC, Manassas VA, USA) and cultured in Vascular Cell Basal Medium (ATCC PCS-100-030) supplemented with Vascular Smooth Muscle Cell Growth Kit (ATCC PCS-100-042). For all experiments, hVSMC were seeded in this supplemented growth medium O/N, but were washed and prepared for experiments in a manner identical to that described for hUSMC. The hVSMC experiments were performed 3 times (passage numbers 2-5) in quadruplicate to ensure reproducibility. The means of these experiments are reported.

5.2.4 Western Immunoblotting

This methodology has been detailed in sections 3.2.3 to 3.2.5. The final primary Ab dilutions were: total-RLC 1:2000 (LS-C81207, LifeSpan BioSciences), pRLC 1:2000 (#3675, Cell Signaling), ppRLC 1:500 (#3674, Cell Signaling), total-phospho-S19-RLC 1:200 (cross reacts with pRLC and ppRLC, #3671, Cell Signaling), ROKII 1:500 (#610623, BD Bio), phospho-T696-MYPT1 (#ABS45, Millipore), phospho-T853-MYPT1 (#4563, Cell Signaling), rhoA 1:200 (#610990, Mouse, MAb, BD Biosci.), and α-actin 1:4000 (sc-56499, Mouse, MAb, Santa-Cruz). Secondary Abs conjugated to IRDye 800CW (Li-COR) or Alexa Fluor 680 (Molecular Probes, Invitrogen) were utilized at 1:20,000.

5.2.5 In-Cell Westerns

This methodology is detailed in section 3.2.6. The final primary Ab dilutions were: pRLC 1:1000 (#3675, Cell Signaling), ppRLC 1:500 (#3674, Cell Signaling), total-phospho-S19-RLC 1:200 (cross reacts with pRLC and ppRLC, #3671, Cell Signaling). Secondary Abs were conjugated to IRDye 800CW (Li-COR). Ab signals were normalized to signals from DRAQ5 (Biostatus Ltd., Leicestershire, UK) combined with Sapphire700 (Li-COR) at 1:10,000 and 1:1000, respectively.

5.2.6 Measurement of RhoA Activity by G-LISA

This methodology is detailed in section 4.2.6. The hUSMC were treated with OT (100 nM) 20 sec, and then harvested by lysis in ice-cold buffer (provided).

5.2.7 Microscopy

This methodology is detailed in section 3.2.7. The final primary Ab dilutions ppRLC (#3674, Cell Signaling) was 1:50. A secondary Ab conjugated to DyLight 488: goat-anti-rabbit-IgG (Cell Signaling) was used at 1:200. Rhodamine-phalloidin (50 nM, Cytoskeleton, Denver, CO, USA) was used to stain F-actin fibers. DAPI was used to detect nuclei.

5.2.8 Physiological Tension Measurements in Human Uterine Muscle Strips Using Myography

These experiments were performed as described in 245, except using human muscle strips prepared from biopsies obtained from a transverse lower uterine incision at the time of caesarean section. Briefly, longitudinal muscle strips approximately 8 mm in length and 3 mm in width were excised and mounted vertically onto separate transducers in separated and jacketed 10 ml organ baths filled with physiological saline solution (PSS) of the following composition (mM): 140 NaCl2, 4 KCl, 1.0 KH2PO4, 2.0 $MgSO_4.7H_2O$, 1.0 HEPES, 5.0 $CaCl_2.2H_2O$, 5.5 glucose at pH 7.5 at 37^0C with 95% O_2–5% CO_2. One end of the tissue was tied to a fixed hook using a silk suture and the other end was attached to a Bridge 8 force-displacement transducer connected to a Biopac Systems MP100 unit with AcqKnowledge software, version 3.7.2 (World Precision Instruments, Sarasota, FL, USA).

The muscle strips were incubated for 60 – 90 min to establish a stable baseline. Cumulative concentration– response curves were established for OT (0.1 – 320 nM) added at 10 min intervals. The EC_{50} concentration (concentration at which half-maximal tension

occurred) was calculated as a measure of sensitivity for OT in the presence or absence of g-H using nonlinear regression for a sigmoid curve (Prism version 4.0 software, GraphPad Software, San Diego, CA, USA). The maximal tension measured at 320 nM of OT was set to 100% and all other values were plotted relative to this. The maximal response to OT in the presence or absence of g-H was calculated by measuring and summing the area under the curve for the total experimental period for OT and OT + g-H treated strips (n = 3 in each).

5.2.9 Statistical Analysis

Statistical analyses were performed using Prism version 5.0 software (GraphPad Software, San Diego, CA) or SPSS (PASW) version 19 (IBM, Armonk, New York, USA). The biochemical data are expressed as means ± S.E.M. Statistical analysis of concentration-response curves for stimulants and inhibitors was performed using one-way ANOVA. The EC_{50} and IC_{50} values were calculated using non-linear curve fitting. Comparison between two curves was performed using two-way ANOVA with the factors being concentration of stimulant and treatment (enzyme inhibitor(s) at a single concentration). If statistical significance was achieved, a post-hoc Tukey's test was conducted to determine which means were significantly different from one another. Two-tailed independent t-tests were used to analyze rhoA activation, WB, and phospho-RLC proportion data in Tables 5 and 6. $p < 0.05$ was used to establish statistical significance in all tests. Vascular myocyte data were considered as technical replicates and no statistical tests were performed.

5.3 Results

5.3.1 MLCK and ROK Contribute to OT- and Calp-Induced Changes in the Phospho-State Distribution of RLC

We evaluated the changes in phosphorylation that occur upon stimulation with OT and Calp treatments in the presence of specific and cell-permeable inhibitors of ROK and MLCK (g-H and ML7,(232-234) respectively). These data are compiled in Tables 5 and 6, respectively. The data in Table 5 suggest that MLCK inhibition with ML7 results in a reduced ability of OT and Calp to cause phosphorylation of RLC, evidenced by reduced levels of $1pRLC^T$ and $2pRLC^T$ relative to OT alone, and reduced $2pRLC^T$ synthesis relative to Calp alone. Interestingly, ROK inhibition with g-H appears to completely abolish the ability of either stimulant to induce $2pRLC^T$. In the case of OT + g-H, the reduced $2pRLC^T$ is accompanied by an accumulation of $1pRLC^T$ relative to OT alone. In contrast, the effect of g-H on Calp has little to no effect on $1pRLC^T$, but results in an accumulation of $0pRLC^T$ relative to Calp alone. These data suggest that the mechanisms utilized by OT and Calp to enhance phospho-RLC concentrations are different. However, both stimulants utilize ROK to induce $2pRLC^T$. The data in Table 6 suggest that ML7 does not affect the relative proportion of phospho-S19-RLC isotypes stimulable by OT or Calp, However, in agreement with Table 5, g-H causes a loss of $2pRLC^{19}$ relative to $1pRLC^{19}$.

Table 5. Changes in Phosphorylated RLC Proportions in hUSMC

		% of total RLC		
	N	0pRLC	1pRLC	2pRLC
Untreated	12	47 ± 4	36 ± 2	16 ± 3
g-H (1 μM)	5	86 ± 2*	7 ± 2**	6 ± 2***
OT (100 nM)	7	10 ± 2*	54 ± 11	36 ± 10***
OT + g-H	4	19 ± 7*	80 ± 8**	1 ± 1***
OT + ML7 (25 μM)	4	20 ± 8*	66 ± 4**	14 ± 6
OT + ML7 + g-H	4	40 ± 4	51 ± 6**	9 ± 2
Calp (0.5 mU/mL)	8	29 ± 6*	34 ± 4	38 ± 8***
Calp + g-H	3	76 ± 12*	33 ± 15	0 ± 0***
Calp + ML7	3	37 ± 3	37 ± 3	26 ± 0
Calp + ML7 + g-H	2	40 ± 0	34 ± 2	26 ± 1

All data are shown as mean ± SEM. *, **, and * indicate significant differences ($p < 0.05$) compared to 0pRLC, 1pRLC and 2pRLC in the untreated group, respectively.**

Table 6. Changes in Relative Proportions of Phospho-S19-RLC Isotypes in hUSMC

		% of phospho-S19-RLC	
	N	1pRLC	2pRLC
Untreated	12	60 ± 3	40 ± 3
g-H (1 μM)	5	91 ± 7**	9 ± 4***
OT (100 nM)	10	54 ± 4	46 ± 5
OT + g-H	4	62 ± 10	39 ± 15
OT + ML7 (25 μM)	6	62 ± 33	39 ± 22
OT + ML7 + g-H	6	71 ± 3**	29 ± 4
Calp (0.5 mU/mL)	10	43 ± 6**	57 ± 5
Calp + g-H	2	77 ± 1	23 ± 1
Calp + ML7	4	55 ± 4	45 ± 4
Calp + ML7 + g-H	3	57 ± 5	43 ± 5

All data are shown as mean ± SEM. ** and * indicate significant differences ($p < 0.05$) compared to 1pRLC and 2pRLC in the untreated group, respectively.**

These two tables show two interesting findings. The first is that, OT stimulation of hUSMC causes a parallel increase in pRLC and ppRLC, equivalent to an enhancement of approximately 20% in the proportion of total RLC made up by each of them. Secondly, in the face of g-H, neither OT nor Calp induced a ppRLC response, and in the case of OT, we observed an enhancement in pRLC in the presence of g-H (Table 5). To further evaluate the interactions of ROK and other key enzymes in hUSMC, and to facilitate comparisons between hUSMC and hVSMC, we used the ICW assay in subsequent experiments.

5.3.2 Resting Concentrations of Phospho-RLC Are Affected by ROK Inhibition in hUSMC and hVSMC

Primary cultures of hUSMC and hVSMC were treated with increasing concentrations of g-H. In hUSMC, g-H (Figure 5-1A) caused a concentration-dependent reduction in both pRLC and ppRLC to 56 ± 8% and 51 ± 6%, respectively. These pRLC and ppRLC data were consistent with reductions in p19RLC (Figure 5-1A and Figure 5-2). Note that the concentration range for g-H is much narrower in Figure 5-2A compared to Figure 5-1. In resting hVSMC, g-H (Figure 5-1B) resulted in a concentration-dependent reduction in pRLC to 28% of control, whereas ppRLC was reduced to 77%, again consistent with reductions measured using the p19RLC Ab.

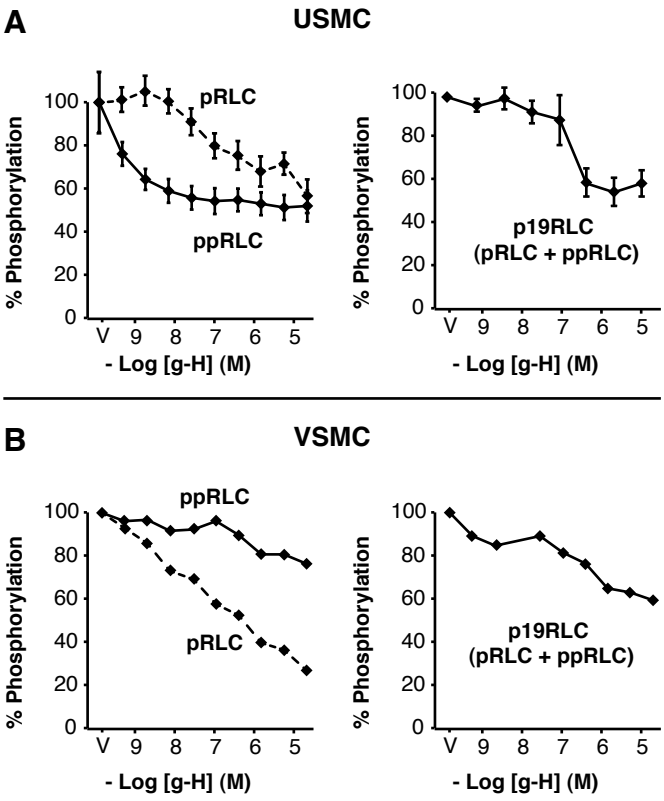

Figure 5-1. Comparison of Mono- and Diphosphorylated RLC Concentrations in Resting hUSMC and hVSMC Treated with a ROK Inhibitor.

The data presented in all panels were produced by ICW analyses. Data are reported by Abs directed toward monophospho-S19-RLC (pRLC, dashed lines), diphospho-T18/S19-RLC (ppRLC, solid lines) or toward total-phospho-S19-RLC (p19RLC (pRLC + ppRLC)). The first data point in all graphs corresponds to the vehicle control (V, 100%). **A.** Concentration-response curves to treatment of hUSMC (n=4) with g-H. Data are reported as means ± SEM. **B.** Equivalent hVSMC data to panel A, and corresponding to 3 independent experiments in hVSMC of different passages. In all panels, the x-axis corresponds to the negative log of the molar concentration of g-H. g-H (glycyl-H-1152); ROK inhibitor. hUSMC; uterine myocytes. hVSMC; vascular myocytes. In USMC, the effect of g-H on pRLC was significantly different ($p < 0.01$) from that on ppRLC, determined by two-way ANOVA.

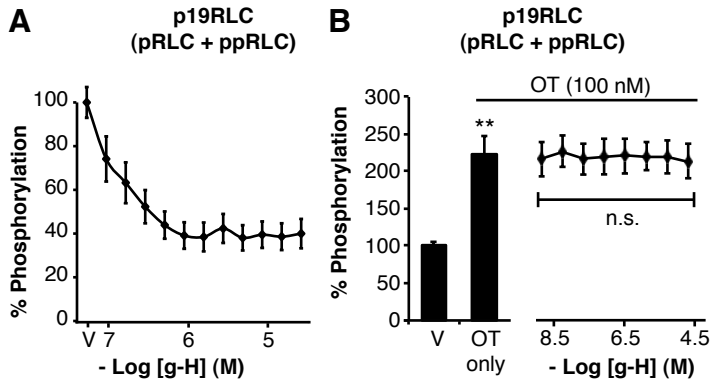

Figure 5-2. ICW Concentration-Response Data Measuring Total-Phospho-S19-RLC (p19RLC) in hUSMC.

A. Concentration-response curve to treatment with a ROK inhibitor. **B.** Concentration-response curve to ROK inhibitor in the presence of a constant 100 nM OT. In both panels, the x-axis corresponds to the negative log of the molar concentration of g-H. n=4-8. All data are reported as means ± SEM. g-H (glycyl-H-1152); ROK inhibitor. hUSMC; uterine myocytes. ** indicates a significant difference ($p < 0.05$) compared to vehicle (one-way ANOVA, followed by Tukey test). n.s.; not significant.

Based on these *in vitro* studies, we estimated calculated the concentrations of g-H at which the concentrations of phosphorylated RLC were decreased by half of the maximal effect (IC_{50}). For hUSMC, the IC_{50} for ROK effects on pRLC, ppRLC, and p19RLC were 76 ± 63 nM, 0.2 ± 0.2 nM, and 6.0 ± 15 nM, respectively. For hVSMC the IC_{50} for g-H on pRLC was 31 ± 23 nM. These data demonstrate that ppRLC content in hUSMC is approximately 100-fold more sensitive to g-H than pRLC content in either hVSMC or hUSMC.

5.3.3 Differential Effects of ROK Inhibition On Stimulant-Induced Phosphorylation of RLC in hUSMC and hVSMC

We have previously demonstrated the optimal time point (20 sec) for hUSMC stimulation of p19RLC with OT.(184 and chapter 3) Under these conditions, stimulation with OT (10 fM to 1 μM) resulted in a concentration-dependent increase in pRLC and ppRLC to 194 ± 9% and 156 ± 9%, in agreement with the p19RLC data in Figure 5-3A and with the data in chapter 3. The responses to ET-1 in hUSMC were similar to responses with OT (Figure 5-4). A time- and concentration-response study was conducted to determine the optimal conditions for stimulation of hVSMC with OT or endothelin-1 (ET-1) (Figure 5-5). hVSMC did not respond with phosphorylation of RLC when challenged with

OT, but responded with a concentration-dependent increase in pRLC to ET-1, maximal at 1 min. Stimulation of hVSMC with ET-1 (10 fM to 1 μM) for 1 min resulted in a concentration-dependent increase in pRLC 167% (Figure 5-3B), which accounted for all of p19RLC. Notably, hVSMC treated with ET-1 did not respond with increased ppRLC (Figure 5-3B and Figure 5-5B).

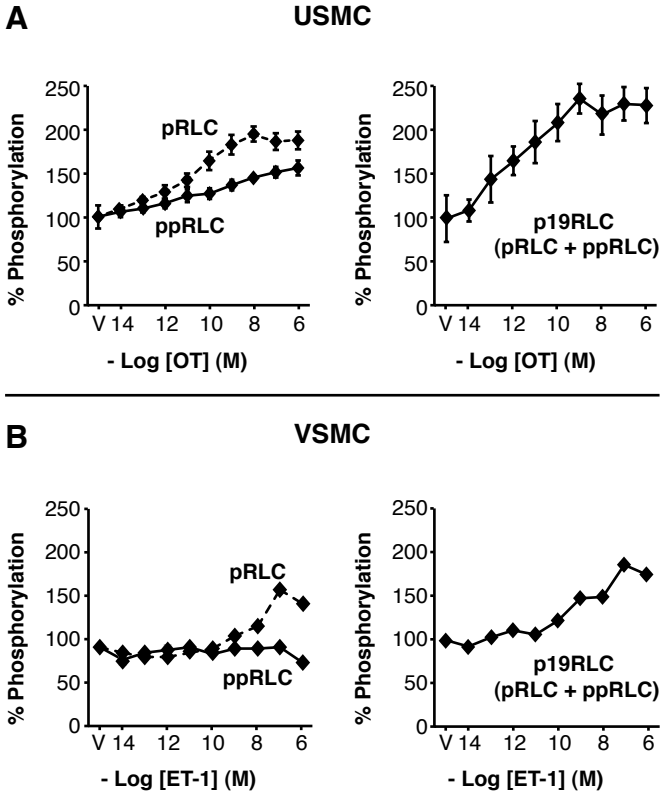

Figure 5-3. Comparison of Phosphorylation of RLC in hUSMC and hVSMC Stimulated With Physiological Agonists.

A. Concentration-response curves to treatment of hUSMC (n=4) with OT. Data are reported as means ± SEM. **B.** Equivalent hVSMC data in response to ET-1, and corresponding to 3 independent experiments in hVSMC of different passages. In all panels, the x-axis corresponds to the negative log of the molar concentration of OT or ET-1. OT; oxytocin. ET-1; endothelin-1. hUSMC; uterine myocytes. hVSMC; vascular myocytes.

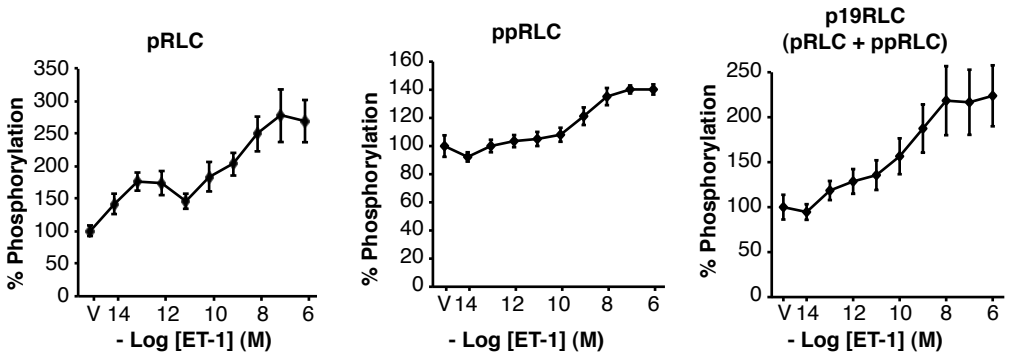

Figure 5-4. Concentration-Response to ET-1 in hUSMC.

A. Concentration-responses in pRLC, ppRLC, and p19RLC to ET-1 in hUSMC. In all panels the first data point corresponds to the vehicle (V, 100%). In all panels, the x-axis corresponds to the negative log of the molar concentration of ET-1. All data are reported as means ± SEM. ET-1, endothelin-1. There was a significant effect of ET-1 ($p < 0.01$), determined by one-way ANOVA in all panels.

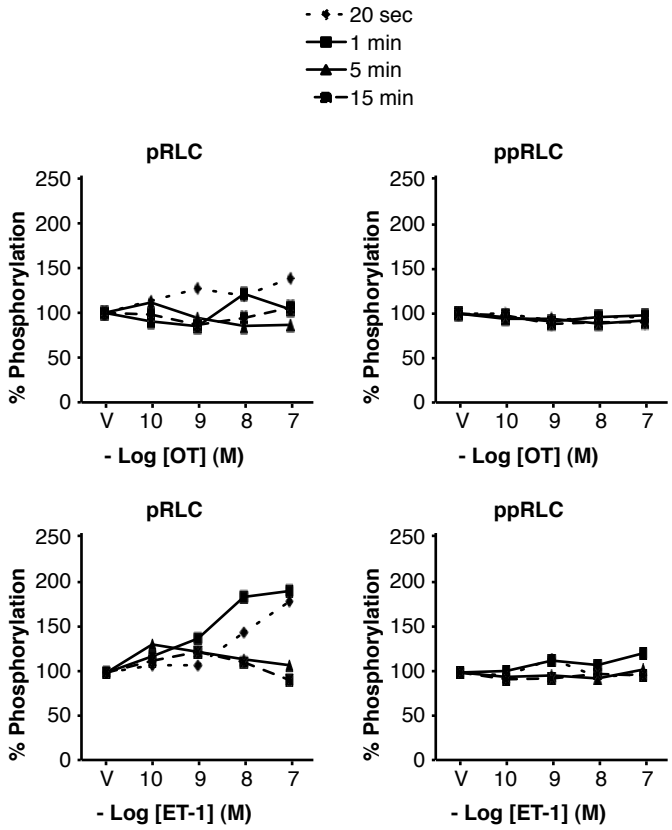

Figure 5-5. Optimization of hVSMC Phospho-RLC Responses.

Concentration- and time-response in vascular myocytes (hVSMC) treated with OT, or ET-1. hVSMC were stimulated with OT or ET-1 for 20 sec, 1 min, 5 min, or 15 min. In all panels the first data point corresponds to the vehicle (V, 100%). In all panels, the x-axis corresponds to the negative log of the molar concentration of OT or ET-1. All data correspond to 2-4 independent experiments in hVSMC of different passages. OT; oxytocin. ET-1, endothelin-1.

In the presence of g-H, the OT-induced enhancement in pRLC was not affected (Figure 5-6A). However, the OT-induced increase in ppRLC was abolished by g-H. The p19RLC response to OT was fully retained in the presence of g-H. Note the retention of OT-induced p19RLC occurs at concentrations of g-H greater than 1 μM (Figure 5-2B). These findings suggest that the suppression of ppRLC solely resulted from reduced phosphorylation of T18-RLC. In contrast to these OT-response data in hUSMC, hVSMC responded very differently to ET-1. Both the pRLC and p19RLC responses to ET-1 were abolished by g-H in hVSMC and ET-1 does not stimulate ppRLC in hVSMC (Figure 5-6B).

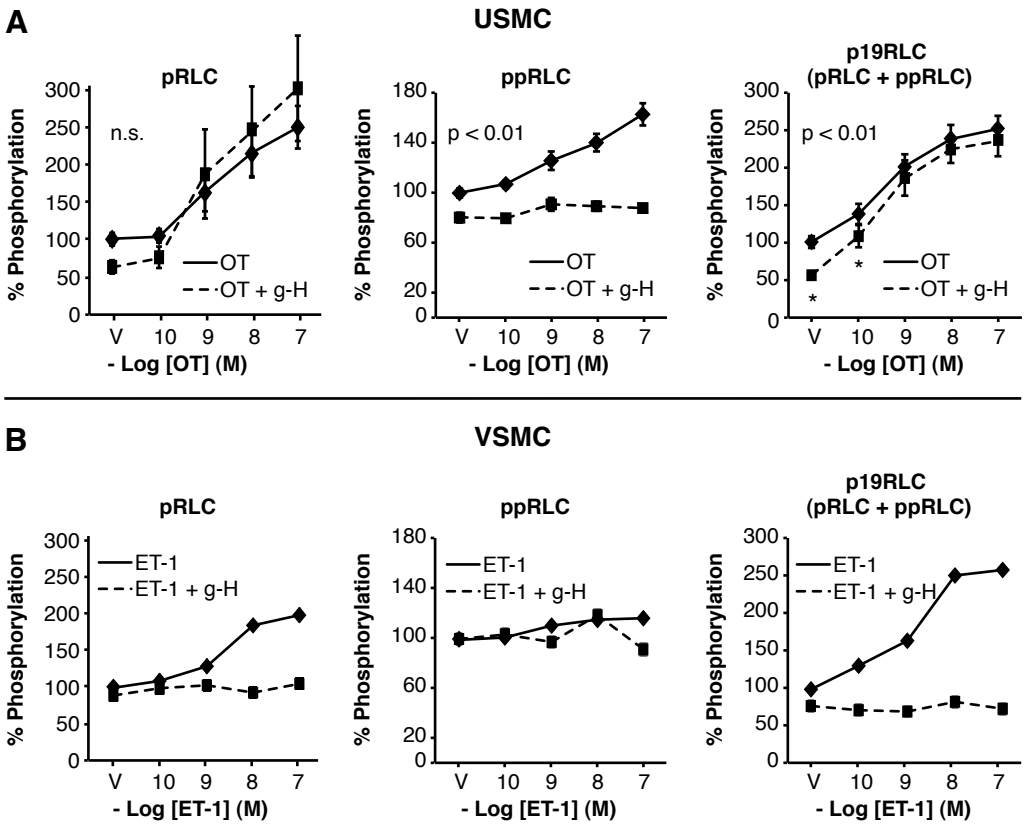

Figure 5-6. Comparison of Effect of ROK Inhibition On Phosphorylation of RLC in Stimulated hUSMC and hVSMC.

A. Concentration-responses in hUSMC (n=4) to OT ± g-H (1 μM). **B.** Equivalent data from hVSMC treated with ET-1 ± g-H (1 μM), and corresponding to 3 independent experiments in hVSMC of different passages. In all panels, the x-axis corresponds to the negative log of the molar concentration of OT or ET-1. g-H (glycyl-H-1152); ROK inhibitor. OT; oxytocin. ET-1; endothelin-1. hUSMC; uterine myocytes. hVSMC; vascular myocytes. In panel A, there was no statistically significant effect of g-H on the OT response in pRLC, but g-H significantly attenuated both ppRLC and p19RLC ($p < 0.01$), determined by two-way ANOVA. For the latter, these differences (*) only occurred without OT, and with 10^{-10} M OT as determined by a post-hoc Tukey test. n.s.; not significant.

To further explore the effects of ROK inhibition in hUSMC, we used two isoform-specific ROK inhibitors (Rho-15 (ROKI) and SR3677 (ROKII), (246, 247)) to evaluate resting and OT-stimulated concentrations of pRLC and ppRLC (Figure 5-7). Both of these agents caused concentration-dependent reductions in pRLC and ppRLC in resting myocytes, and inhibited OT-induced ppRLC but not pRLC. These data are in agreement with Figure 5-6 and suggested that either ROK isoenzyme can mediate these effects.

Figure 5-7. Effects of Isoform-Selective ROK Inhibitors On Resting and OT-Stimulated Phosphorylation of RLC in hUSMC.

A and **B.** Concentration-responses to ROKI-selective and ROKII-selective inhibitors, respectively. **C** and **D.** Concentration-responses to OT ± Rho-15 (25 μM) or SR3677 (25 μM). The x-axes correspond to the negative log of the molar concentration of the drug indicated. n=4. All data are reported as means ± SEM. OT; oxytocin. Rho-15; ROKI inhibitor. SR3677; ROKII inhibitor. In panels A and B, there was a significant effect of Rho-15 or SR3677 ($p < 0.01$) determined by one-way ANOVA. In panels C and D, there was a significant effect of treatment (Rho-15 or SR3677, $p < 0.01$) on OT-induced ppRLC, but not pRLC, determined by two-way ANOVA.

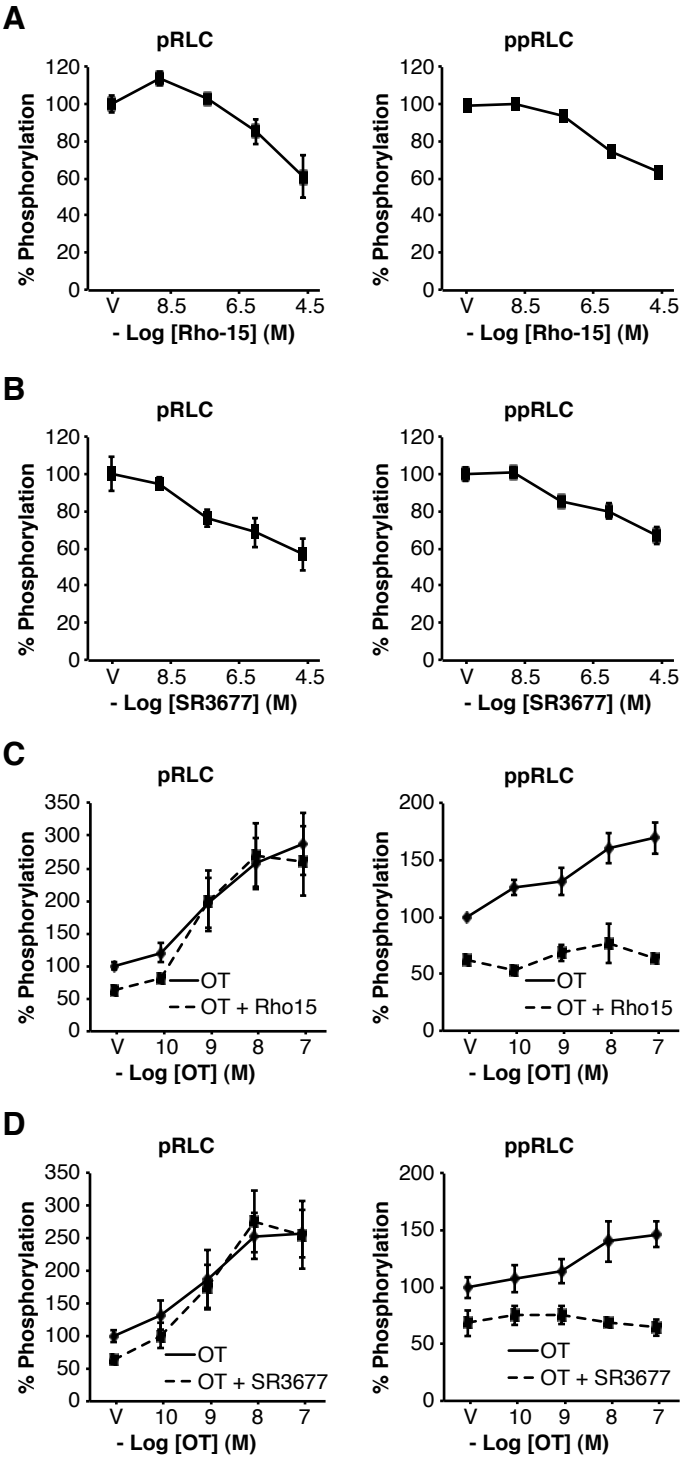

We verified that g-H treatment caused reduced OT-induced tension development in human uterine strips *ex vivo*. Pretreatment with g-H (1 μM) caused a right shift in the concentration response curve for OT with an increase in the EC_{50} from 1.3 to 27.1 nM (Figure 5-8). The total tension generated by muscle strips treated with g-H was significantly reduced (to 0.46 ± 0.15 compared to vehicle-treated controls), as assessed by calculating the total area under each OT-response curve. These data are in excellent agreement with g-H-mediated reduction in ppRLC measured in Figure 5-6 and Table 5 and suggested that hUSMC depend specifically on ppRLC for tension development. Therefore, we designed experiments to clarify the mechanism of ROK-mediated ppRLC stimulation downstream of OT in hUSMC.

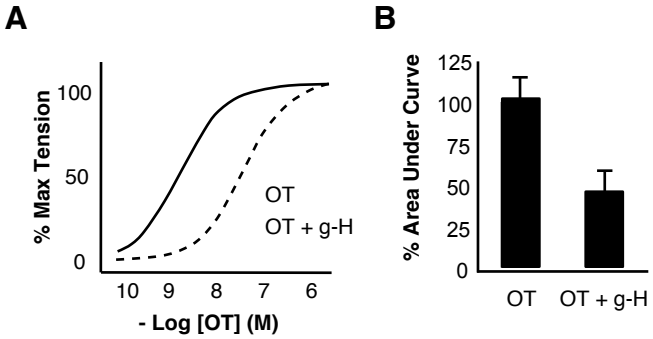

Figure 5-8. ROK Inhibition Attenuated OT-Induced Tension Development in Human Uterine Muscle Strips.

A. Normalized tension measurements in human uterine muscle strips (n=2) treated with increasing concentrations of OT ± g-H (1 μM). **B.** The baseline-subtracted total area under the curve (AUC) was expressed as a percentage of the AUC for OT (100%). The data are reported as means ± SD. The x-axis corresponds to the negative log of the molar concentration of OT. OT; oxytocin. g-H (glycyl-H-1152); ROK inhibitor.

5.3.4 Comparison of the Contribution of MLCK and ROK to Phosphorylation of RLC in hUSMC

To clarify the mechanisms governing phosphorylation of RLC in hUSMC, we evaluated the relative contribution of MLCK and ROK. Figure 5-9A demonstrates a concentration-dependent reduction in pRLC (to 71 ± 8%) and ppRLC (to 65 ± 6%) in resting hUSMC. Figure 5-9B shows that increasing concentrations of g-H in the presence of a constant 25 μM ML7 resulted in further reductions in both pRLC and ppRLC (to 64 ± 11% and 71 ± 4%) compared to the reduction achieved by ML7 alone (25 μM ML7 alone is

designated as 100% in Figure 5-9B). Next we determined the effect of ML7 ± g-H on the OT concentration-response profile for pRLC, and ppRLC. Figure 5-10A shows that ML7 (25 μM) significantly attenuated the OT-induced enhancement in pRLC and ppRLC, completely abolishing the latter. Combining g-H and ML7 further reduced basal pRLC, ppRLC, and the OT-stimulated response in pRLC (Figure 5-10B).

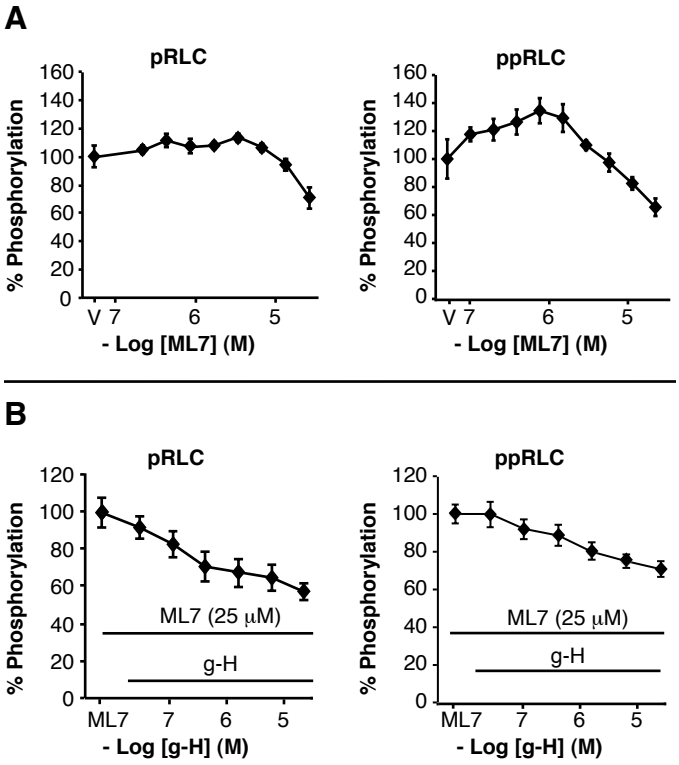

Figure 5-9. MLCK Is Required for Resting Concentrations of ppRLC in hUSMC.

A and **B**. Concentration-responses to ML7, or to g-H in the presence of a constant 25 μM of ML7, respectively. In panel **A** the first data point corresponds to the vehicle (V, 100%), and in panel **B** it corresponds to treatment with ML7 only (ML7 alone is set to 100%). In all panels, the x-axis corresponds to the negative log of the molar concentration of the drug tested. n=4-8. All data are reported as means ± SEM. ML7; MLCK inhibitor. g-H (glycyl-H-1152); ROK inhibitor. In all panels, there was a statistically significant effect of ML7 (panel A) or g-H (panel B) ($p < 0.01$), determined by one-way ANOVA.

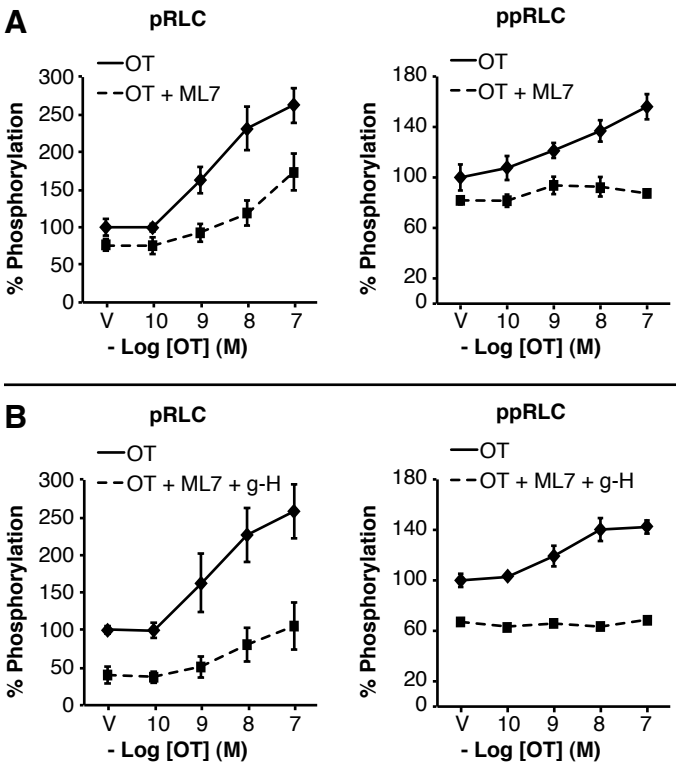

Figure 5-10. MLCK Is Required for OT-Stimulated ppRLC in hUSMC.

A. Concentration-responses in hUSMC treated with OT ± ML7. **B**. Concentration-responses to OT ± g-H and ML7 simultaneously. In all panels, the x-axis corresponds to the negative log of the molar concentration of OT. n=4-8. All data are reported as means ± SEM. OT; oxytocin. ML7; MLCK inhibitor (25 μM). g-H (glycyl-H-1152); ROK inhibitor (1 μM). In all panels, there was a significant effect of treatment (ML7, or ML7 + g-H, $p < 0.01$) on OT responses, determined by two-way ANOVA.

The effects ML7 in resting and stimulated myocytes were confirmed by measuring p19RLC (Figure 5-11). These data suggested that MLCK activity is required for synthesis of pRLC and ppRLC. The partial retention of the OT-stimulated response in pRLC in the presence of ML7 suggests incomplete inhibition of MLCK by 25 μM ML7. Note that the retention of pRLC and attenuation of ppRLC with g-H, and the attenuation of both pRLC and ppRLC responses with ML7, were also evident when ET-1 was used as the stimulus instead of OT (Figure 5-12), indicating that the responses are characteristic of the myocyte rather than the agonist.

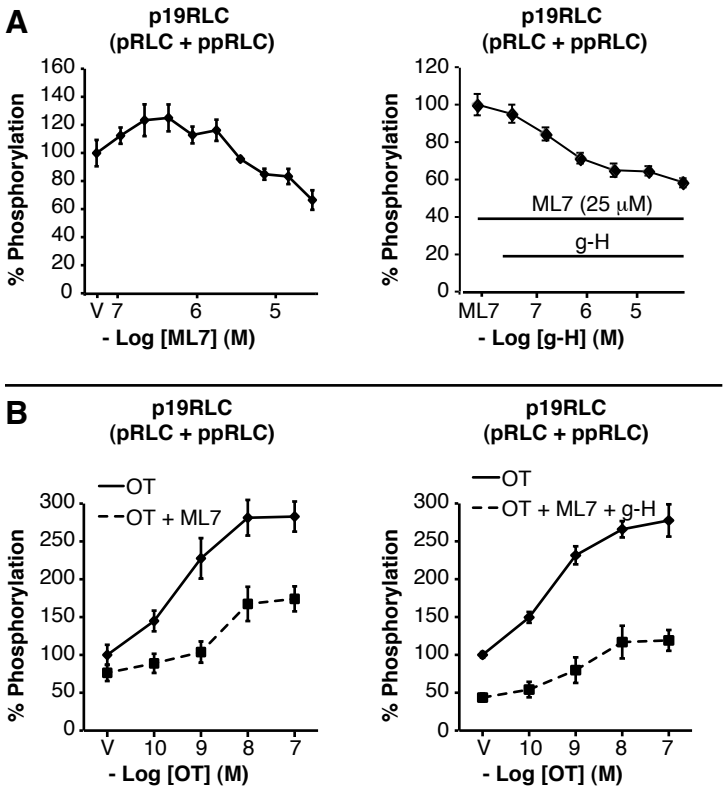

Figure 5-11. ICW Concentration-Response Data Measuring p19RLC in hUSMC.

A. Concentration-responses to treatment with ML7, or to g-H in the presence of a constant 25 μM of ML7 (ML7 alone is set to 100%). **B.** Concentration-responses to OT ± ML7 (25 μM), or g-H (1 μM) and ML7 simultaneously. In all panels, the x-axis corresponds to the negative log of the molar concentration of the drug indicated. n=4-8. All data are reported as means ± SEM. ML7; MLCK inhibitor. g-H (glycyl-H-1152); ROK inhibitor. In panels A, there was a significant effect of ML7 or g-H ($p < 0.01$) determined by one-way ANOVA. In panel B, there was a significant effect of treatment (ML7 or ML7 + g-H, $p < 0.01$) on OT responses, determined by two-way ANOVA.

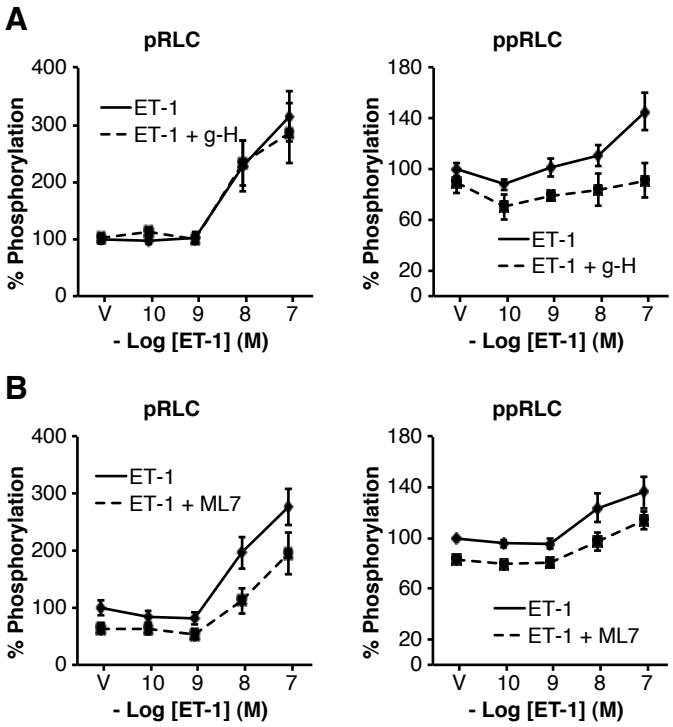

Figure 5-12. Effects of ROK and MLCK Inhibition on ET-1 Phosphorylated-RLC Concentration-Responses in hUSMC.

A. Concentration-responses to ET-1 ± g-H. **B**. Concentration-responses to ET-1 ± ML7. In all panels, the x-axis corresponds to the negative log of the molar concentration of ET-1. n=4-8. All data are reported as means ± SEM. ET-1; endothelin-1. ML7; MLCK inhibitor (25 μM). g-H (glycyl-H-1152); ROK inhibitor (1 μM). In all panels, there was a significant effect of treatment (g-H or ML7, $p < 0.01$) on ET-1 responses, except in panel A, where there was no effect of g-H on pRLC.

5.3.5 ROK-Mediated Inhibition of Protein Phosphatase 1 Contributes to OT-Induced Diphosphorylation of RLC

The attenuation of pRLC and ppRLC with ML7 in resting cells with an additive effect of g-H could be explained by direct phosphorylation of RLC at S19 as well as T18 by ROK,(147) or to rhoA-ROK inhibition of MLCP through phosphorylation of its targeting subunit (MYPT1).(136, 143) Therefore we evaluated the relative effects of MLCP inhibition alongside ROK inhibition on phosphorylated RLC in hUSMC. Figure 5-13A demonstrates that, OT (100 nM, 20 sec) induced rhoA activation. Figure 5-13B and C show that OT enhanced phosphorylation of T853, but that neither OT nor g-H affected MYPT1 phosphorylation at T696. Treatment with g-H reduced resting and OT-stimulated concentrations of phospho-T853-MYPT1.

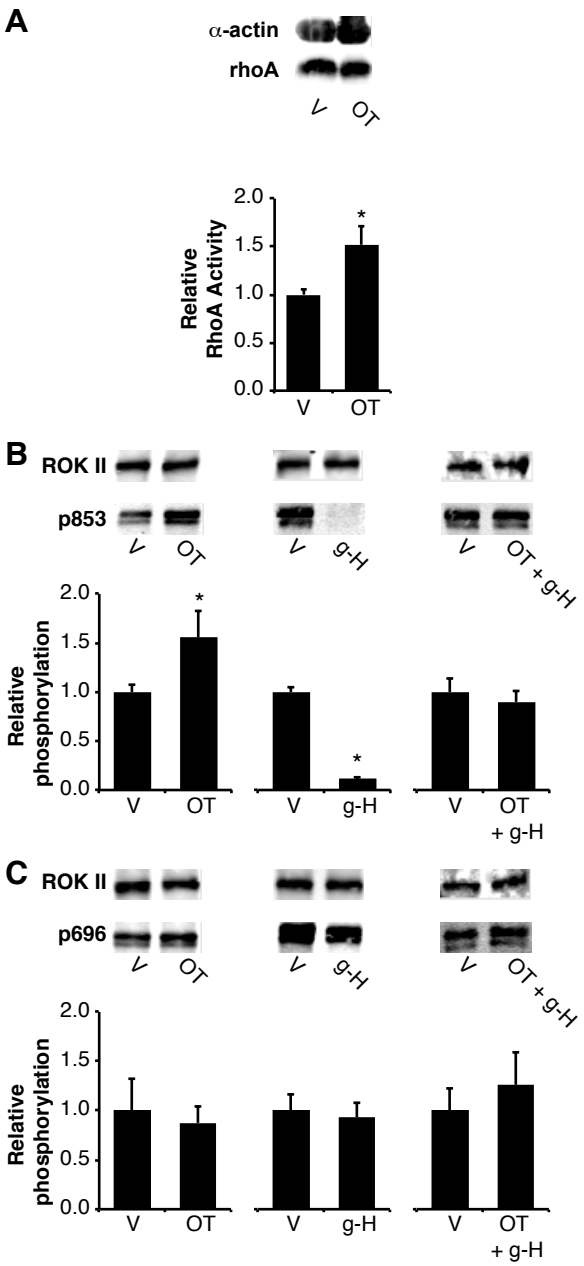

Figure 5-13. OT and ROK Inhibitor Cause Changes in Phosphorylation of the MYPT1 Subunit of MLCP in hUSMC.

A. Demonstration of OT-induced rhoA activation in hUSMC. Cells were treated with OT, and GTP-bound rhoA was quantified by an absorbance assay. Absorbance data were corrected for rhoA content by WB. **B** and **C.** Representative WB demonstrating phosphorylation of MYPT1 at T853 (p853) or T696 (p696). hUSMC were treated with OT, g-H, or both. ROKII content was used as a loading control. The histograms in each panel represent fold-changes relative to vehicle control, and are reported as means ± SEM (n = 4-6). OT; oxytocin (100 nM). g-H (glycyl-H-1152); ROK inhibitor (1 μM). * indicates $p < 0.05$ relative to vehicle.

To determine whether these events were associated with OT-induced inhibition of MLCP by ROK as a contributory mechanism to the resting and OT-stimulated concentrations of pRLC and ppRLC in hUSMC, we utilized the protein phosphatase inhibitor CalA, which inhibits phosphoprotein phosphatase 1 (PP1, MLCP) and 2A (PP2A) phosphatases.(241) Figure 5-14A shows the concentration-response curve for pRLC and ppRLC to CalA with or without g-H in resting hUSMC. These data demonstrate that the resting concentration of ppRLC is particularly sensitive to CalA such that at 25 nM (highest concentration used), there is a significant enhancement in ppRLC with relatively little effect on pRLC.

In the presence of g-H, the basal concentrations of pRLC and ppRLC were reduced but the responses to CalA were largely unaltered. In contrast, when the reverse experiment was performed to determine the concentration-response to g-H in the presence of constant CalA (25 nM), we observed a markedly different pattern (Figure 5-14B). In agreement with Figure 5-1A, pRLC was reduced by g-H. However, in the presence of CalA, this g-H-induced reduction in pRLC was eliminated and the concentration of pRLC was increased. The effects on ppRLC were much more pronounced, with a massive increase in resting ppRLC that was maintained throughout the concentration-response curve for g-H.

The effects of CalA on OT-induced pRLC and ppRLC responses are shown in Figure 5-14C. CalA had the unexpected effect of reducing the OT-induced response in pRLC. In contrast, CalA appears to maximize the cellular capacity to generate ppRLC such that OT-stimulation cannot elevate ppRLC beyond the level of CalA alone. This is compatible with the CalA-induced effects noted in Figure 5-14B. Interestingly, the loss of pRLC with CalA treatment upon OT-stimulation is reversed by co-incubation with CalA and g-H simultaneously (Figure 5-14D), whereas the ppRLC response to OT stimulation in the presence of CalA was not affected by the addition of g-H.

Figure 5-14. MLCP Exhibits Preferential Activity Toward ppRLC in hUSMC.

A Concentration-response in hUSMC to CalA ± g-H. **B.** Concentration-response to g-H ± CalA. **C**. Concentration-responses to OT ± CalA. **D**. Concentration-responses to OT ± g-H and CalA simultaneously. In all panels, the x-axis corresponds to the negative log of the molar concentration. n=4-8. All data are reported as means ± SEM. OT; oxytocin. g-H (glycyl-H-1152); ROK inhibitor (1 μM). CalA (calyculin A); MLCP inhibitor (25 nM). In all panels, there was a significant effect of treatment (g-H, CalA, or CalA + g-H, $p < 0.01$) determined by two-way ANOVA, except panel D, where there was no effect on pRLC.

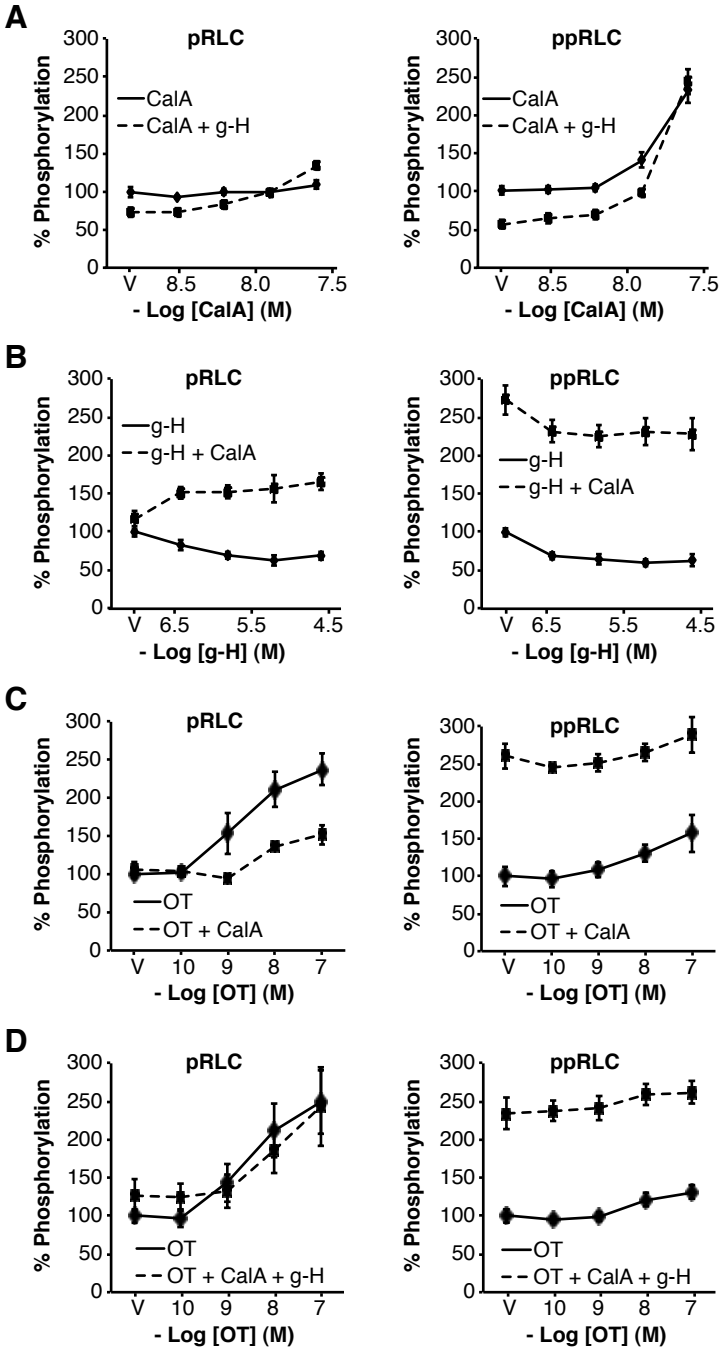

To confirm that these CalA effects are attributable to protein phosphatase 1 (PP1), and therefore to MLCP activity, rather than to PP2, we tested two PP2-specific inhibitors (endothall, and cantharidic acid, (248)), and determined that neither of these agents reproduced the changes in phosphorylated RLC observed with CalA (Figure 5-15).

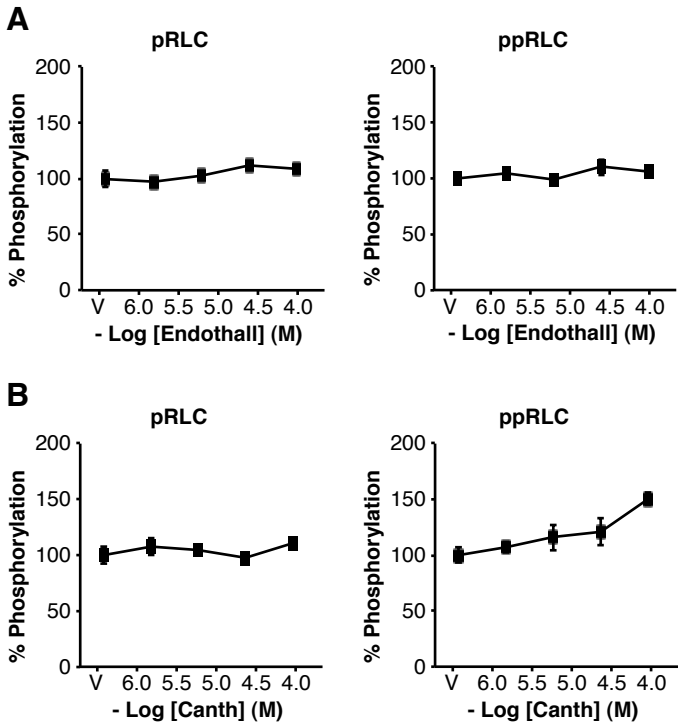

Figure 5-15. Effects of PP2 Inhibitors On Resting Concentrations of Phosphorylated RLC in hUSMC.

A and **B**. Concentration-responses to endothall or cantharidic acid (Canth), respectively. In all panels, the x-axis corresponds to the negative log of the molar concentration of endothall or cantharidic acid. n=4. All data are reported as means ± SEM.

5.3.6 RhoA Activation Is Associated With Diphosphorylation of RLC

As mentioned, ROK is one of the main signal transduction effectors of rhoA, which is activated alongside rhoA recruitment to the plasma membrane of responsive cells.(131, 132, 138-140) To complement the above g-H data, we activated rhoA activity in hUSMC using Calp. In chapter 3 and Table 5, we showed that cultured hUSMC respond to Calp stimulation with an increase in rhoA activity that resulted in specific enhancement of ppRLC. Figure 5-16 demonstrates that hUSMC stimulation with Calp caused an enhancement in phosphorylation of MYPT1 at T853, but not T696. Together with Figure

5-13, these data point toward T853 as the primary target of ROK in hUSMC. The data in Figure 5-17 demonstrate that both pRLC and ppRLC are stimulated by Calp treatment in a concentration-dependent manner. Figure 5-17A shows that ML7 significantly reduced ppRLC stimulation by Calp, and but does not appear to shift the pRLC response-curve. Similarly, g-H attenuated ppRLC stimulation, but exhibits no effect on pRLC (Figure 5-17B). There appear to be no additive or synergistic effects of combining g-H and ML7 (Figure 5-17C).

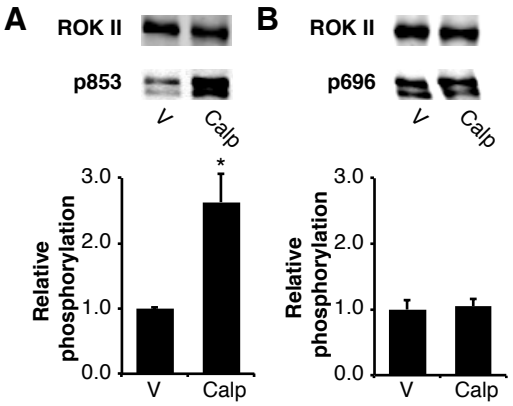

Figure 5-16. RhoA Activation Causes Phosphorylation of the MYPT1 Subunit of MLCP in hUSMC.

A and **B.** Representative WB demonstrating phosphorylation of MYPT1 at T853 (p853) or T696 (p696), respectively. hUSMC (n=4) were treated with Calp. ROKII content was used as a loading control. Histograns represent fold-changes relative to vehicle control, and are reported as means ± SEM. Calp; calpeptin (rhoA activator, 0.5 mU/mL). * indicates $p < 0.05$ relative to vehicle.

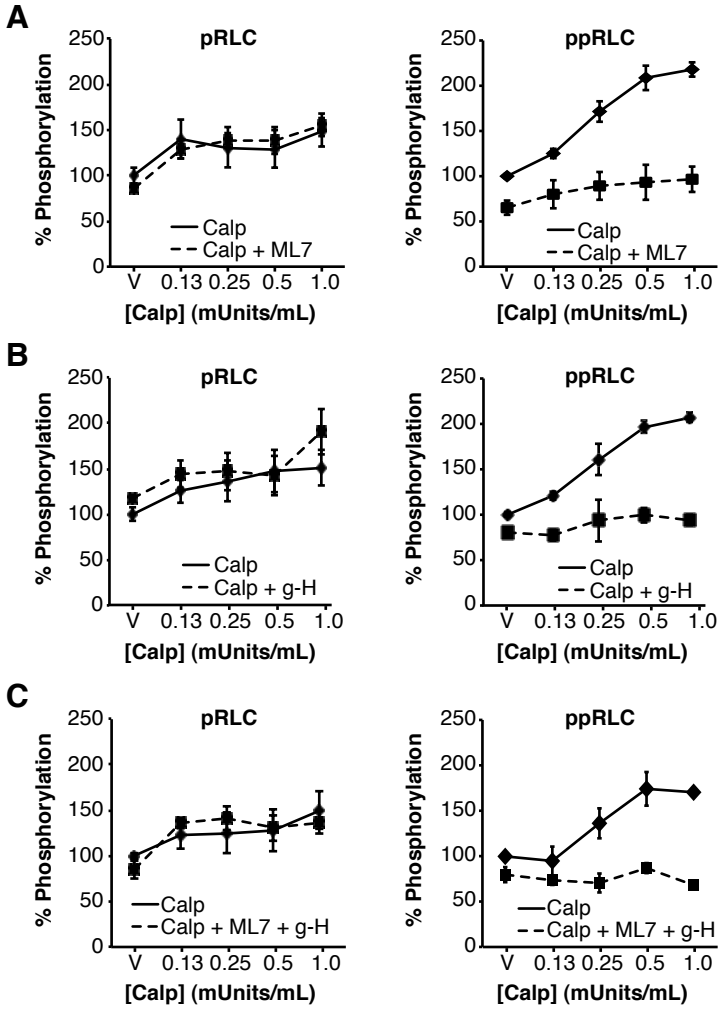

Figure 5-17. Activation of RhoA Induces ROK-Dependent Synthesis of ppRLC in hUSMC.

A, **B** and **C.** Concentration-response curves for hUSMC with Calp ± ML7, g-H, or both drugs. In all graphs, the x-axis corresponds to the concentration of Calp (mU/mL). n=4-8. All data are reported as means ± SEM. Calp; calpeptin (rhoA activator). ML7; MLCK inhibitor (25 μM). g-H (glycyl-H-1152); ROK inhibitor (1 μM). In all panels, there was a significant effect of treatment (ML7, g-H, or ML7 + g-H, $p < 0.01$) on the Calp response in ppRLC, but not for pRLC (not significant), determined by two-way ANOVA.

5.3.7 Sub-Cellular Distribution of Diphosphorylated RLC in hUSMC

The above data strongly suggested that ppRLC is an important and rapidly inducible endpoint downstream of OT in hUSMC. In chapter 3 we showed that, in OT-stimulated hUSMC, the distribution of p19RLC mirrors that of 'total' (bulk) RLC and is co-localized with filamentous actin (F-actin), signifying proximity to the contractile machinery. Figure 5-18 demonstrates that OT stimulation enhances ppRLC in a fibrillar distribution that is associated with F-actin.

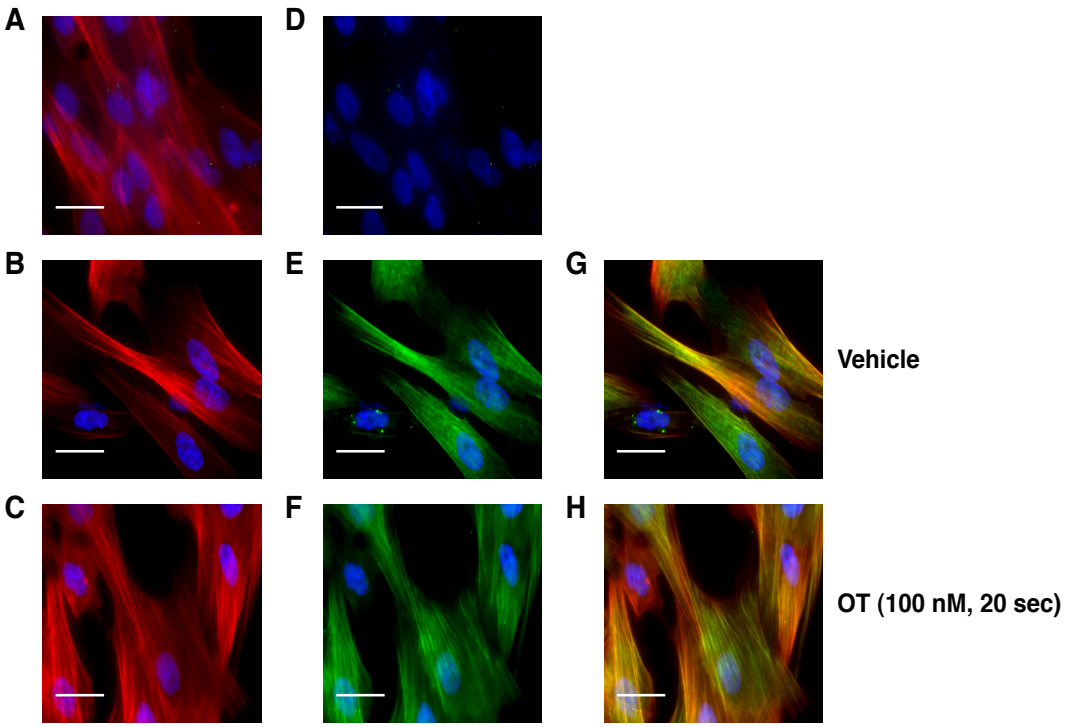

Figure 5-18. Sub-Cellular Localization of ppRLC in hUSMC.

Immunofluorescent staining of hUSMC. **A - C**. Filamentous actin (F-actin) stained with rhodamine-phalloidin (red). **D - F.** Identical fields corresponding to panels A-C showing staining with a secondary Ab conjugated to Alexa-Fluor 488 (green). In panel D, the primary Ab has been omitted (secondary Ab only). In panels E and F, the anti-ppRLC Ab was used. **G** and **H.** Merged images after combining panels B and E, or C and F, respectively. Panels B, E, and G correspond to vehicle treatment, and panels C, F, and H to cells stimulated with 100 nM OT. In all panels, nuclei are stained with DAPI (blue). Images are shown at 400X magnification. White bars represent 25 microns.

5.4 Discussion

5.4.1 hUSMC Require MLCK and ROK for Diphosphorylation of RLC

Our data suggested that ROK participates downstream of MLCK in the sequential phosphorylation of RLC during an OT stimulus. MLCK inhibition reduced the OT-inducible pRLC and ppRLC, whereas ROK inhibition only attenuated the latter, as determined by phos-tag WB and ICW analyses. These data agree that with previous evidence that MLCK is the primary enzyme mediating phosphorylation of RLC at S19,(249, 250) and support our hypothesis that phosphorylation at T18 is mediated by ROK. Further, they agree with the concept of OT signaling through Ca^{2+}-dependent and Ca^{2+}–independent pathways. Specifically, activation of G-protein coupled receptors (GPCRs) in hUSMC promotes activation of a trimeric G-proteins containing $G\alpha_q$ or $G\alpha_{11}$ subunit,(77) leading to stimulation of phospholipase $C\beta$ (78) to generate second messengers (79, 80) which enhance intracellular Ca^{2+} concentrations.(82, 83) The involvement of rhoA-ROK Ca^{2+}-independent pathways linked through $G\alpha_{12/13}$ (115) is demonstrated by our data showing rhoA activation with OT, which agrees with work from uterine and other SMs demonstrating activation of rhoA,(116-118) and with other evidence demonstrating that ROK inhibition reduces tension development without altering Ca^{2+} concentrations in myometrium.(134, 135, 145, 149, 177, 178) These data also agree with and explain the observation that ppRLC is lost in resting or OT-stimulated hUSMC that were treated with g-H, alongside an enhancement of pRLC (Table 5).

5.4.2 hUSMC and hVSMC Differ in the Primary Phospho-RLC Responses to Stimulation

Understanding the regulation of phosphorylation of RLC is critical for developing strategies to reduce SM contractility for numerous medical disorders. In the field of parturition research, ROK is implicated in the augmented force of contraction characteristic of the myometrium at the time of labor onset. Several studies have documented the expression of ROK and its upstream activator rhoA in the myometrium of various species (133, 144, 171-173) and demonstrated that this system is activated by physiologically relevant myometrial stimulants.(116, 176, 178, 181) Also, ROK inhibition has been shown

to reverse agonist-induced cell shortening in cultured hUSMC,(251) suggesting that the ROK-sensitive contractility mechanisms are preserved in culture.

In the present study, we demonstrate that ROK activity is required for the maintenance of resting concentrations of pRLC and ppRLC in hUSMC, and of pRLC in hVSMC. In hUSMC, ppRLC concentrations are more sensitive than pRLC to ROK inhibition. When challenged with physiologically relevant stimuli such as OT or ET-1, hUSMC responded with a concentration-dependent increase in pRLC and ppRLC, the latter of these being completely dependent on ROK activity. The similarity of responses to OT and ET-1 suggest that these mechanisms are fundamental properties of the hUSMC, and not phenomena attributable to a specific agonist. In support of this rationale, other OT and ET-1 stimulation data obtained from rat myometrium tension measurements demonstrated similar responses between these two agonists.(245)

In contrast, stimulation of hVSMC with ET-1 induced a concentration-dependent increase in pRLC, but not in ppRLC. The ET-1-induced pRLC response in pRLC was abolished by ROK inhibition. We interpret these data as demonstrating that, in hUSMC, ROK is the enzyme that phosphorylates pRLC at T18. In hVSMC, the loss of pRLC with g-H likely results from relative over-activity of RLC phosphatase (MLCP), which is inhibited by ROK.(143) The contrasting resting and stimulation data presented here for hUSMC compared to hVSMC signify potential fundamental differences in the mechanisms for tension development. This rationale agrees with other reports suggesting that ppRLC in hVSMC appears to be less important than pRLC,(252-254) since pRLC corresponds linearly with tension development in hVSMC.(255) In some SMs, ppRLC accounts for only a small proportion (5% - 11%) of phosphorylated RLC.(223, 256) In contrast, hUSMC have been noted to exhibit higher levels of ppRLC compared to arterial myocytes (23% vs. 9%, respectively).(228) We have previously shown that in the resting state, approximately 47% of the pool of RLC is represented by unphosphorylated RLC, 36% pRLC, and 16% by ppRLC, and that after OT stimulation, ppRLC reaches 35-45% in hUSMC.(214)

Our data for the hVSMC differ somewhat from data derived from cultured rabbit aortic myocytes where stimulation with $PGF_{2\alpha}$ resulted in moderate enhancement in ppRLC.(257) Importantly, in those experiments the stimulation of ppRLC occurred over

several minutes, and was sustained. In hUSMC, induction of ppRLC is immediate (assessed at 20 sec) and returns to basal levels by one minute. In addition, the ppRLC in rabbit aortic myocytes appeared at the cellular edges in contrast to our demonstration that ppRLC strongly co-localized with the F-actin that traverses the longitudinal axis of hUSMC. Other reports from vascular myocytes similarly demonstrate a different distribution of ppRLC than that shown here.(258, 259) Our data support the concept that ppRLC synthesis in hUSMC accompanies the triggering of cell shortening, whereas the rabbit aorta data may reflect cytoskeletal rearrangements necessary for cell migration.(260, 261) This is in keeping with phosphorylation of RLC being a generic molecular trigger for a variety of myosin II motor isoforms, which occur within each cell type to achieve a specific goal (see refs 58 and 262).

5.4.3 Inhibition of MLCP Contributes to ROK-Mediated Diphosphorylation of RLC

Concomitant activation of MLCK and inhibition of MLCP has been viewed as an attractive mechanism to explain the improved tension development of physiological agonists compared to depolarizing stimuli.(106, 107) Since MLCP is almost completely inhibited by ROK in hVSMC,(108) we also evaluated the effects of MLCP inhibition on phosphorylated RLC in hUSMC. These data suggest that in the resting state, ROK largely functions by regulating phosphatase activity toward RLC. The effects of MLCP inhibition on OT-stimulated phosphorylation of RLC were quite surprising. In particular, we noted that a right-shift in the OT-response curve for pRLC with MLCP inhibition, that was reversed by ROK inhibition. Also, MLCP inhibition maximized the cellular capacity to synthesize ppRLC, since OT stimulation could not enhance ppRLC further. These data demonstrate an unexpectedly strong ROK-dependent drive toward ppRLC in hUSMC that is held in balance by MLCP activity, and which is uncovered by pharmacological inhibition of MLCP. Our data suggest that these effects might result from the action of ROK at T853 of MYPT1. Importantly, these studies extend our understanding of the role of ROK by demonstrating that ROK is required ppRLC production during a contractile stimulus, as opposed to simply preventing the degradation of phosphorylated RLC by regulation of MLCP as is currently held.

Chapter 6

Final Conclusions and Implications

6 Final Conclusions and Implications

6.1 A Novel Mechanism for Phosphorylation of RLC in hUSMC

The most important novel contribution of this thesis emerges from the data in chapter 5, and represents our efforts to explore the possibility of ppRLC as a unique entity in hUSMC at the biochemical level. These data support the concept that, in hUSMC, pRLC is converted to ppRLC by ROK, in a mechanism that clearly distinguishes hUSMC from hVSMC. We therefore propose a new mechanism for myometrial contractility presented in Figure 6-1. The key aspect of this scheme is the ROK-dependent synthesis of ppRLC that is unique to hUSMC and might contribute significantly to tension development in the myometrium.

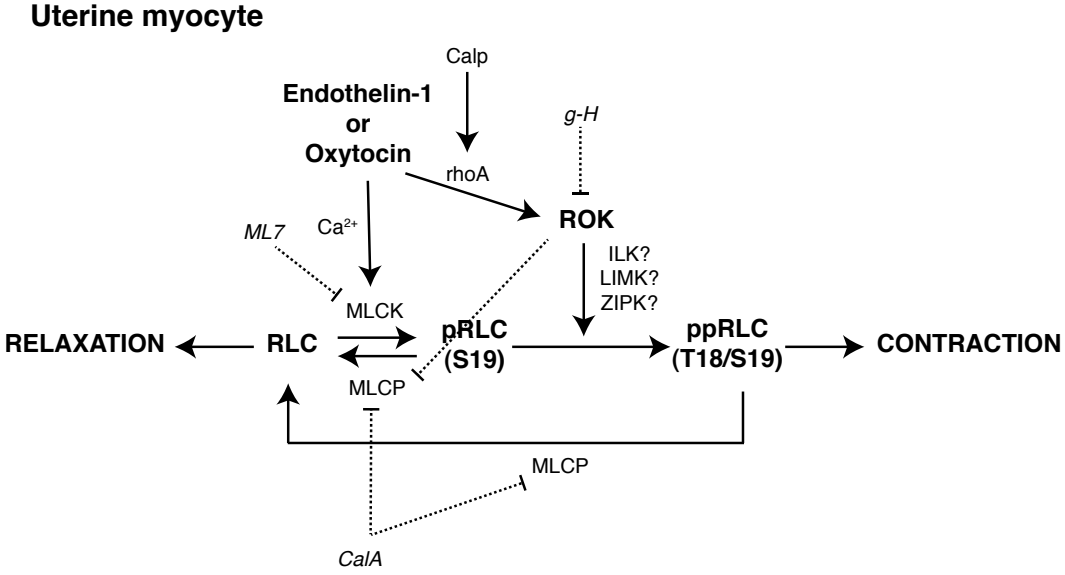

Figure 6-1. Proposed Mechanism for Phosphorylation of RLC in Stimulated hUSMC.

Stimulation of uterine myocytes induces Ca^{2+} entry from the extracellular space, which results in MLCK activation. MLCK converts RLC to pRLC by phosphorylating S19. Recruitment of ROK through activation of rhoA results in the conversion of pRLC to ppRLC by active phosphorylation of T18 and inhibition of MLCP. It is unclear whether ROK phosphorylates RLC directly, or whether phosphorylation of T18 is achieved by recruiting an intermediate enzyme such as ILK, LIMK or ZIPK. The resultant ppRLC contributes to tension development in uterine smooth muscle. Muscle relaxation occurs by dephosphorylation of pRLC and ppRLC by MLCP. Arrows indicate activation or enzymatic conversion. Dotted lines indicate inhibition. RLC; myosin regulatory light chain. pRLC; monophosphorylated RLC. ppRLC; diphosphorylated RLC. MLCK; RLC kinase. MLCP; RLC phosphatase. ROK; rho-kinase. ILK; integrin-linked kinase. LIMK; LIM kinase. ZIPK; zipper-interacting protein kinase. g-H (glycyl-H-1152); ROK inhibitor. ML7; MLCK inhibitor. CalA; MLCP inhibitor.

This key mechanistic difference between hUSMC and hVSMC might have functional implications. Specifically, as mentioned previously, the uterus has a phasic contractile pattern and, in relation to other types of SM, is required to generate substantial tension to deliver the products of conception at the time of parturition. This physiological feature might be the tissue-level correlate to the enhancement in the rate of ATP turnover of myosin ATPase caused by ppRLC relative to pRLC.(71, 72, 221) Thus, ROK-mediated phosphorylation of pRLC at T18 may be an adaptive mechanism to optimize tension generation in a phasic pattern. This concept would be compatible with several studies demonstrating expression of rhoA and ROK in the myometrium of various species that increase as parturition approaches, and with demonstrations that rhoA-ROK activity is inducible in myometrium (reviewed in 1). This scheme also provides a mechanistic explanation for the effects of other ROK inhibitors in attenuating spontaneous and stimulant-induced tension development in myometrium of various species.(121, 134, 135, 145, 177-179) Lastly, this proposed mechanism explains the increased sensitivity to loss of ppRLC in comparison to pRLC in hUSMC. Specifically, the schematic shows that in hUSMC, the formation of ppRLC is mediated by ROK through two mechanisms (inhibition of MLCP, and phosphorylation of pRLC at T18), whereas the formation of pRLC is only influenced by ROK through one mechanism (inhibition of MLCP). Thus, a given concentration of ROK inhibitor will yield a larger reduction in ppRLC in comparison to pRLC in hUSMC.

The reasons for the biochemical differences in ROK activity and sensitivity to ROK inhibition between hUSMC and hVSMC elucidated here are unclear. However, to explain these data we might consider the possibility of differences in the composition of the contractile apparatus of different SMs. First, phosphorylation of T18 in hUSMC might result from expression of different isoforms of RLC or ROK. In this case, differences in the amino acid sequence that alter the tertiary structure of the RLC substrate might enable presentation of pRLC in a favorable conformation to enable additional phosphorylation of T18 by ROK. Alternatively, a ROK variant with an active site that accommodates pRLC as a substrate might explain these data. The possibility of protein variants in uterine vs. vascular SM could be extended to other proteins facilitating the interaction between ROK and RLC, such as the MHCs or components of the actin cables. As mentioned in section

1.5, various isoforms of these proteins are expressed in SM. In light of our data, it might be useful to purify and sequence some of these proteins from myometrium to attempt to determine whether different isoforms of RLC or ROK are expressed in hUSMC as an explanation for the propensity toward diphosphorylation of RLC in these cells. Such differences in the amino acid sequences, if they exist, are likely to be small, since in our experiments we have detected these proteins of interest by WB at the correct molecular weight and with commercially available Abs. In the likely event that the main players are found to be identical between uterine and vascular SMs, an alternative explanation could involve differential recruitment of scaffolding proteins or intermediary kinases that enable diphosphorylation of RLC. For example, the scheme in Figure 6-1 presents the possibility that an intermediate enzyme acts on T18 of pRLC downstream of ROK, since our data do not clarify whether ROK causes direct or indirect (through an intermediary kinase) phosphorylation of RLC. Specifically, integrin linked kinase,(263) LIM kinase,(264) and zipper-interacting protein kinase (265) have been shown to phosphorylate RLC and interact with ROK, and therefore any of these might be involved in ROK-mediated ppRLC production. Still, our work helped to confirm and differentiate the role of ROK in hUSMC and hVSMC.

6.2 Other Features of Phosphorylation of RLC in hUSMC

The data presented in the preceding chapters revealed several additional features of phosphorylation of RLC in hUSMC. In addition to demonstrating the use and validation of the ICW technique, the data in chapter 3 indicate that hUSMC respond to an OT-challenge with a concentration-dependent increase in p19RLC as early as 20 seconds post-stimulus, and a return to basal levels by 60 sec. This rapid induction of p19RLC agrees with other OT-response data in the literature,(56, 202) and we suspect that the accompanying and similarly rapid decay of p19RLC in hUSMC might represent the biochemical underpinnings of the phasic nature of tension development in the intact myometrium. The work in chapter 3 also enabled us to optimize and standardize the protocol for performing experiments in cultured hUSMC for both subsequent chapters. This helped us to minimize inter-experiment variability arising from differences in cell seeding density and length of culture after seeding.

One limitation of the ICW approach used was that only a single phosphorylation endpoint could be measured at one time in the same sample. Therefore, to complement this technology, we used the phos-tag based separation of phospho-proteins described in chapter 4. This work showed that when pRLC and ppRLC are quantified simultaneously, hUSMC respond to OT by producing equal amounts of pRLC and ppRLC, suggesting that ppRLC plays an important role in the uterine SM response to OT. In addition, induction of rhoA activity using calpeptin, or inhibition of ROK using g-H, demonstrated strong effects on ppRLC in contrast to pRLC. The most striking finding revealed by this method occurred when OT stimulation was attempted in the presence of ROK inhibition. OT was unable to stimulate ppRLC, and instead there was an accumulation of pRLC. This particular experiment strongly suggested a key mechanistic feature of phosphorylation of RLC in hUSMC, which is that ROK is required to produce ppRLC, but not pRLC. Therefore, this finding also supports the idea that ppRLC contributes significantly to the ability of the myometrium to generate tension.

6.3 Clinical Relevance

Over the past three decades, there has been essentially no progress in developing pharmacological or other methods to prevent or successfully treat PTL. The ineffectiveness of uterine SM relaxants such as β-adrenergic agonists and calcium channel blockers is due largely to the prohibitive incidence of cardiovascular side effects. Several national and international organizations, including the Institute of Medicine, have noted the need for enhancement of research in this area.(266, 267) The overall conclusion of this work is that targeting the synthesis of ppRLC might permit the management of uterine SM disorders such as PTL while avoiding significant side effects in other vascular SM beds. Our data show that ROK might be a suitable target for this purpose, on the basis of higher sensitivity to ROK inhibition in the reduction of ppRLC in hUSMC as compared to that of pRLC in hVSMC. Clarifying the possibility of an intermediate kinase acting to create ppRLC downstream of ROK might further improve the therapeutic selectivity for uterine SM.

Chapter 7

Study Limitations and Future Directions

7 Study Limitations and Future Directions

The experiments described in the above study shed light on the fundamental biochemical response of the contractile machinery in hUSMC to stimulation. The strength of our approach was the use of a high-throughput and precise primary assay (ICW) that enabled a focusing of our efforts with complementary low-throughput techniques (WB and myography). However, the principle flaws of the above experimental design are the reliance on *in vitro* cell culture model and on inhibition studies dependent on pharmacological agents for most of the data presented. This section discusses the limitations of the experimental approach and proposes alternative avenues of investigation to complement the above experiments.

7.1 Cell Culture Model

One primary problem with culture models is that cellular dedifferentiation might occur. This results from loss or altered expression of proteins that might be critical to function and cell phenotype. For SMCs, these alterations might result in conversion from 'contractile' phenotype to a 'synthetic' one.(268) This phenomenon that was observed in vascular SMCs, in which there was a loss of contractile capability as resources are diverted toward cell proliferation (DNA synthesis, cell division, secretion of extracellular matrix components etc.).(269) A recent microarray analysis comparing gene expression in myometrial tissue and cultured hUSMC demonstrated significant alteration in the expression of mRNAs for a variety of genes with wide-ranging functions; these changes occurred as early as passage 3 of subculture.(270) Another recent report demonstrated a decline in mRNA levels for OT receptors over the first 10 culture passages.(271)

In our studies, we used primary hUSMC from passages 3-12 and demonstrated that rapid intracellular signaling systems are stimulable by several different physiologically relevant contractile agonists (see preceding chapters, and appendix 8.3). Similarly, two immortalized hUSMC lines have been shown to retain key SM markers, primarily at the mRNA level, and to retain OT-binding capability in addition to their biochemical responsiveness to OT.(272, 273) These positive OT-response data suggest that the membrane receptors remain coupled to intracellular signaling systems, though it is unknown whether the receptor coupling has itself undergone change by subculturing.

These data also complicate the interpretation of altered mRNA expression between SM tissues and dispersed cells, since retention of key signaling pathways might also indicate at least partial retention of the differentiated contractile phenotype in culture. Moreover, several reports using primary hUSMC (passages 3-8) seeded into collagen matrices have shown that agonist stimulation causes a significant reduction in collagen disc area.(251, 274, 275) These data demonstrate retention of the hallmark ability of SMCs to shorten upon stimulation in cultured myocytes, and therefore suggest at least partial retention of their contractile phenotype.(269) Interestingly, the retention or loss of the contractile phenotype has been shown to be a cell-density-dependent phenomenon in experiments using cultured porcine aortic SMCs.(276) In those studies, cells seeded near full confluence were more likely to retain the contractile phenotype. This finding might suggest that when SMCs are seeded sufficiently densely, they do not require synthetic or proliferative capabilities and can focus resources on their primary contractile role. These data shed new light on the data presented in chapter 3, which demonstrated that seeding density is a parameter that affects the responsiveness of hUSMC to OT. Specifically, the explanation for our finding that the largest amplitude OT-response occurred in hUSMC seeded at 600 cells/mm^2 might involve the retention of key 'contractile' phenotype characteristics that are selected against at lower cell densities.

A second problem with the cell culture model is that cultures are of variable purity, since the muscle biopsies are heterogenous. This problem is unavoidable when preparing primary cultures, but can be circumvented by using any of the several immortalized human myometrial cell lines, which have been produced from either pregnant (PHM-1) or non-pregnant (ULTR, hTERT-ULTR, hTERTmyo) women.(272, 273, 277, 278) These uterine cell lines also have the added advantage of increasing the number of passages over which cells remain viable. However, it is difficult to know the extent to which the transformation methods have altered the contractile phenotype beyond the effects of dispersion and culturing, and therefore we avoided use of these cell lines in our studies.

Due to relative ease of accessibility for research purposes, our studies have focused on hUSMC derived from the lower uterine segment collected from women at the time of elective caesarean section. However, since the fetus must be expelled through a

downward movement out of the uterus and into the vaginal canal, there might be some aspect of directed propagation of force in the myometrium from the uterine fundus toward the cervix. In addition, the lower pole of the uterus must relax, or at least distend as the fundus contracts to deliver the fetus, but it remains unclear what mechanisms control these events. Evidence suggests that these physiological aspects of uterine function might be achieved by topographical or regional differences in biochemical responses, protein (membrane receptors, enzymes, channels etc.) expression, or local hormone milieu for uterine myocytes residing within the uterine wall. (279-287) With respect to the present studies, it is possible that any such topographical differences intrinsic to the myocyte might be carried over into cell culture, and might impact the interpretation of results if cells derived from the lower segment do not adequately reflect the behaviour of the uterus as a whole. To further complicate matters, it is impossible to know the extent to which any of these differences have been retained or altered by dispersion and culturing, as described earlier in this section. Still, to validate the primary biochemical responses under study in the main data chapter (chapter 5) with respect to topographical differences in myocyte responsiveness, we obtained paired samples of myocytes isolated from the uterine fundus and lower segments. These data are shown in appendix 8.3. In our hands, both fundal and lower segment hUSMC responded to OT and ET-1 stimulation with p19RLC and ppRLC responses, and in each case these responses were attenuated by ROK or MLCK inhibition. Thus, with respect to the primary mechanisms of interest in this work, we did not detect any significant differences between in responsiveness between fundal and lower segment hUSMC, which agree with other biochemical and physiological data.(56, 282, 288)

Lastly, all experiments presented were performed on cultures derived from pregnant myometrial tissues at the end of a full term gestation. Due to this narrow focus, we cannot assess the possibility that the signaling mechanisms under study have undergone change as the uterus progresses from the quiescent non-pregnant state toward activation at full term, as has been shown for a variety of genes with diverse cellular roles.(289-295) For this reason, future experiments should be expanded to include non-pregnant tissues and tissues from women in preterm labour. In addition, since the comparison between uterine and vascular SMs revealed some surprising differences in

behaviour, it would be interesting to perform similar *in vitro* studies on a larger number of independent vascular myocyte cultures, including myocytes derived from proper resistance vessels as opposed to coronary arteries, and on myocytes derived from other SMs such as those of gastrointestinal, esophageal, sphincteric, or bronchial origin.

7.2 Biochemical Endpoints

A second limitation in scope arises from the focus on a small number of phosphorylation events. A significant amount of mechanistic information could be clarified by expanding the complement of phospho-proteins being assessed. For example, evidence suggests that endogenous peptide inhibitors play a role in regulating protein phosphatases such as MLCP.(156) A subgroup of these peptide inhibitors are the phosphatase holoenzyme inhibitors (PHIs), of which CPI-17 (17-kDa-protein kinase C--potentiated inhibitor of PP1c) has been implicated in inhibition of MLCP in the myometrium.(296-301) The inhibitory effect of CPI-17 for the catalytic subunit of MLCP is enhanced by several orders of magnitude through phosphorylation of T38 by PKC and also by ROK,(302) suggesting that phosphorylation of CPI-17 is necessary to 'activate' this inhibitor. Similarly, rhoA, ROK, and even the MHCs and various related proteins have been shown to be kinase targets.(1, 279) Extending the current studies to include these relevant phospho-proteins might be useful to clarify the mechanistic details of the effects of ROK inhibition observed here, and might present novel therapeutic opportunities for intervention.

Similarly, the biochemical techniques used here could be greatly complemented by use of an expanded set of additional assays. These might include assessments of ROK activity, Ca^{2+} measurements with cell permeant dyes such as Fura-2 to assess Ca^{2+}-sensitization, or collagen disc assays to confirm that ROK inhibitors antagonize cell shortening in culture. However, the most fruitful technical approach might be one involving physiological tissue-bath myographic experiments coupled with biochemical analyses in tissues that are flash-frozen at different stages of tension development. Specifically, the present experiments could be supported by an analysis of pRLC and ppRLC in actively contracting myometrial strips to assess whether there is a positive correlation between tension generation and ppRLC content, in the absence or presence of a ROK inhibitor. These experiments will yield data about the ROK-dependent synthesis of ppRLC in intact

muscle. Such an *ex vivo* approach would provide important information in a setting that more closely approximates the *in vivo* situation, and would provide a strong validation of the primary conclusions drawn from the present experiments. The *ex vivo* approach would also be useful to confirm differences in sensitivity to ROK inhibition between uterine and vascular tissues by measuring tension development in paired patient samples of myometrium and resistance vessels.

7.3 Pharmacological Approach

The work described here relied heavily on pharmacological enzyme inhibitors. Where possible, these drugs were selected on the basis that they offer the best combination of potency and selectivity for the enzyme target. The experiments performed with these agents have produced several internally consistent and reconcilable data sets, which agree with other published evidence. However, it is impossible to guarantee that these agents have not acted on unintended targets during the course of our experiments. Therefore to improve upon these experiments, the most direct loss-of-function approach amenable for use with cell cultures is that of small interfering RNA (siRNA). With appropriately validated siRNA oligonucleotides, we could address a number of additional questions. For example, using siRNAs aimed at the mRNAs for each of the ROK isoforms or toward ILK, we can more clearly discern which enzymes are required for ppRLC synthesis in hUSMC. This information would help to direct development of inhibitors to achieve therapeutic specificity. siRNAs could also be used to explore the apparent enhanced activity of MLCP in hUSMC toward ppRLC over pRLC that was observed in Figure 5-14. We speculate that other members of the MYPT family, which arise from other genes, can replace MYPT1 as the substrate targeting subunit of MLCP to yield an alternate configuration for this enzyme. Specifically, MBS85 (myosin binding subunit of 85-kDa), is ubiquitously expressed, exhibits high homology to MYPT1, and is specifically associated with pRLC as a substrate as well as with PP1.(303) Thus, use of siRNAs aimed at MYPT1 or MBS85, or toward their potential protein phosphatase binding partners might yield important information regarding ppRLC degradation. To this end, we have begun optimizing siRNA knockdowns in hUSMC (see appendix 8.4). Alternatively, future loss-of-function studies might employ gene knockout animals. Mice with genetic deletions for ROK-1 (-/-), ROK-2 (-/-), and a heterozygous ROK-1 (+/-) ROK-2 (+/-) have already been

produced,(304-306) but have not yet been studied with regards to alterations in SM contractility.

To complement these inhibition studies, a gain-of-function approach would also be beneficial. In addition to stimulation with physiological agonists, cellular responses could be augmented by protein over-expression. Specifically, future studies might employ the use of transient or stable transfection approaches, or alternatively, the protein transduction technology, which utilizes a short viral peptide ('TAT') to introduce proteins into the cell interior.(307, 308) In contrast to transfection technologies, the TAT-fusion approach enables more control over the degree of overexpression since one can adjust the concentration of purified protein present in each experiment, and any off target effects at the genetic or mRNA levels are avoided. The primary drawback of this approach is the requirement for time-consuming DNA sub-cloning and protein purification protocols necessary to produce functional TAT-fusion constructs. However, we have successfully produced TAT-RhoA and transduced hUSMC with this construct (appendix 8.5). In addition to overexpression of wild-type proteins, this overexpression approach could be particularly useful to introduce dominant negative or dominant positive mutants for any protein of interest. Thus, for example, the use of TAT-RhoA (wild type) alongside TAT-RhoA(G14V) (dominant positive)(309), or TAT-RhoA(T19N) (dominant negative)(310) could help to clarify several issues, such as the pharmacological specificity of Calp for rhoA in hUSMC, and the extent to which hUSMC rely on rhoA for ROK-mediated ppRLC synthesis. This approach could also be used to augment or interrupt the coupling of receptors to G-proteins to attempt to discern the highest level at which rhoA-ROK become activated by receptor stimulation, and thereby present an additional opportunity for therapeutic intervention.

7.4 Physiological Implications of ppRLC

Our general approach differs from other work aimed at studying rhoA-ROK in that we chose to limit ourselves to an analysis of phosphorylation of RLC without monitoring intracellular Ca^{2+}. As was discussed in section 1.7, one of the principal features that sparked wide interest in rhoA-ROK and related signaling systems was the idea that activation of GPCRs achieves higher levels of tension development in comparison to

purely depolarizing stimuli, such as KCl.(104-106) As such, this signaling cascade was deemed a 'Ca^{2+} sensitization' (CS) mechanism for force development in SM. Unfortunately, without direct Ca^{2+} measurements, our data do not address the concept of CS in hUSMC. However, if the above-mentioned enhancement in the ATPase activity of myosin occurs upon formation of ppRLC in hUSMC, this might explain the observation of CS in myometrium.

The emphasis throughout on the phosphorylation state of RLC emerged from the rationale that, irrespective of its origin, any triggering of the uterine SM contractile response must act by causing phosphorylation of RLC. This rationale is therefore grounded in the assumption that the activation mechanism cannot be circumvented by any stimulus whether it occurs at the correct time, or prematurely. However, we acknowledge that, while to our knowledge there is no evidence suggesting that this assumption is intrinsically flawed, we cannot independently confirm that it is true. Specifically, there is evidence that pregnant human uterine SM is capable of producing larger forces per unit of phosphorylated RLC when compared to non-pregnant myometrium.(56) Thus, it might be possible that pregnant hUSMCs *in vivo* are sensitized to phosphorylated RLC. This raises the possibility that a pathological process might induce myocyte activation by activating these phospho-RLC-sensitizing mechanisms, instead of those that serve to increase phosphorylated RLC. It is possible then that a strategy aimed at reducing ppRLC in hUSMC might still be ineffective at preventing or arresting PTL even if complete specificity for uterine SM is attained.

Still, the present work strongly suggests that exactly such a therapeutic strategy might be effective. Therefore, of all of the possible future directions to explore, the most logical extension of this project involves *in vivo* work in animal models aimed at demonstrating efficacy of ROK inhibitors in arresting or preventing PTL. Particularly in rodents, robust methods for inducing PTL have been widely used, enabling expedient development and execution of experimental protocols to assess exactly this endpoint.(52, 311) For example, an experimental protocol using control animals and animals treated with different doses of g-H could be evaluated for pregnancy prolongation after pharmacological precipitation of parturition with a progesterone receptor antagonist (RU486). The

expectation would be that ROK inhibitors should enable the pregnancy to be carried until normal term. In these animal experiments, blood pressure monitoring would also be beneficial to evaluate whether ROK inhibition enables selectivity between uterine and vascular SM. Along these lines, the initial report describing the first high-specificity inhibitor for ROK, Y-27632, successfully reduced blood pressure in three different hypertensive rat models, but did not significantly affect blood pressure in the control group.(312) As has been discussed throughout this thesis, ROK inhibitors have been repeatedly used to reduce uterine contractility in normal animals of various species. Thus, that Y-27632 does not affect normal blood pressure in rats supports our hypothesis that uterine and vascular SM utilize ROK for different physiological purposes. Successful experiments using the rodent models of parturition could be succeeded by similar trials in higher species such as dogs, and eventually in women.

One additionally intriguing aspect of our work that requires further exploration is the reason for the different phosphorylation responses in uterine SM in contrast to vascular SM. In section 6.1, we speculated that these differences might have functional implications relating to the phasic contractile pattern of the uterus that contrasts the tonic contractile patterns typical of vascular SM. To determine if ppRLC is a biochemical determinant of these distinct physiological behaviors, the SMs from various organs could be harvested from animals in the above therapeutic efficacy studies, and many of the same experiments shown in the preceding chapters could be performed on these tissues. These studies would help to establish the true uniqueness of the uterine myocyte with respect to ppRLC synthesis, and will clarify whether there is any relationship between stoichiometry of phosphorylation of RLC to SM function. Considering that phosphorylation of RLC triggers cell shortening in all SMs studied thus far, it seems reasonable that at least some of the subtle differences in SM function across different organs might emerge from distinct peculiarities of their corresponding contractile apparati.

Appendices

Appendix 8.1

Physiological Pathways and Molecular Mechanisms Governing Uterine Contractility

Human Reproduction Update Advance Access published June 14, 2010
Human Reproduction Update, Vol.00, No.0 pp. 1–20, 2010
doi:10.1093/humupd/dmq016

human reproduction update

Physiological pathways and molecular mechanisms regulating uterine contractility

Hector N. Aguilar[1] and B.F. Mitchell[1,2,*]

[1]Department of Physiology, University of Alberta, Edmonton, Alberta, Canada [2]Department of Obstetrics and Gynaecology, 220 HMRC, University of Alberta, Edmonton, AB, Canada T6G 2S2

*Correspondence address. Tel: +1-780-492-8561; Fax: +1-780-492-1308; E-mail: brymitch@ualberta.ca

Submitted on October 31, 2009; resubmitted on April 29, 2010; accepted on May 7, 2010

TABLE OF CONTENTS

BACKGROUND: Uterine contractile activity plays an important role in many and varied reproductive functions including sperm and embryo transport, implantation, menstruation, gestation and parturition. Abnormal contractility might underlie common and important disorders such as infertility, implantation failure, dysmenorrhea, endometriosis, spontaneous miscarriage or preterm birth.

METHODS: A systematic review of the US National Library of Medicine was performed linking 'uterus' or 'uterine myocyte' with 'calcium ion' (Ca^{2+}), 'myosin light chain kinase' and 'myosin light chain phosphatase'. This led to many cross-references involving non-uterine myocytes and, where relevant, these data have been incorporated into the following synthesis.

RESULTS: We have grouped the data according to three main components that determine uterine contractility: the contractile apparatus; electrophysiology of the myocyte including excitation-contraction coupling; and regulation of the sensitivity of the contractile apparatus to Ca^{2+}. We also have included information regarding potential therapeutic methods for regulating uterine contractility.

CONCLUSIONS: More research is necessary to understand the mechanisms that generate the frequency, amplitude, duration and direction of propagation of uterine contractile activity. On the basis of current knowledge of the molecular control of uterine myocyte function,

there are opportunities for systematic testing of the efficacy of a variety of available potential pharmacological agents and for the development of new agents. Taking advantage of these opportunities could result in an overall improvement in reproductive health.

Key words: calcium signaling / myosin light chain kinase / RhoA-associated kinase / myosin phosphatase / calcium sensitization

Introduction

The uterus is a hollow organ with a well-differentiated lining layer (endometrium), a thick muscular coat (myometrium) and a serosal outer layer. There has been remarkable progress towards understanding the physiology and clinical pathophysiology of the endometrium and this has resulted in many important interventions to affect conception and contraception as well as menstrual function. In contrast, although there is growing awareness of the potential importance of abnormal function of the uterine muscle layer, there has been relatively little research concerning the role of the myometrium in common disorders of reproduction. Myometrial function may be of vital importance in physiological processes such as sperm and embryo transport and implantation, and in disorders such as dysmenorrhea and endometriosis. At present there is limited understanding of regulation of uterine contractility in the non-pregnant state. Yet, better understanding of this physiology is essential to design and test interventions that can prevent or treat the important clinical problems noted above. To fill in the gaps in our knowledge of uterine physiology in the non-pregnant state, we shall borrow liberally from knowledge gained from experiments using both human and animal models, whether pregnant or not. The goal of this review is to provide an overview of the molecular mechanisms that might regulate uterine contractility, particularly emphasizing recent findings with potential clinical applicability to improvement of reproductive health.

Methods

The initial search strategy involved searching the United States National Library of Medicine (http://www.ncbi.nlm.nih.gov/sites/entrez?db=pubmed) and matching 'uterus' or 'uterine myocyte' with 'calcium signaling', 'myosin light chain kinase (MLCK)', ' myosin light chain phosphatase (MLCP)' or 'calcium sensitization'. Papers were selected based on the relevance to our objectives as determined by review of the titles and abstracts. After synthesizing a review of this information, key references obtained from these papers were individually reviewed and selected based on their potential relevance to uterine smooth muscle (SM). This information was used to expand the discussion of the regulation of uterine SM. The term 'uterine contractility' then was entered and articles were selected based on their clinical relevance to disorders of reproduction in non-pregnant women. Finally, the review was edited and shortened to focus on molecular mechanisms regulating contractility of the non-pregnant uterus with emphasis on information that could be clinically applicable for the improvement of reproductive health.

The contractile apparatus

Anatomical considerations and uterine contractile activity

Uterine contractions occur throughout the menstrual cycle in the non-pregnant state and throughout gestation. There are four important parameters that change under various physiological or pathophysiological conditions: frequency, amplitude, duration and direction of propagation. Over the past two decades, considerable information regarding myometrial function in non-pregnant women has been obtained from the use of open-tipped pressure catheter recordings or from three-dimensional ultrasound or magnetic resonance imaging (MRI). Several reviews have described these changes and their potential clinical significance (Brosens *et al.*, 1998; van Gestel *et al.*, 2003; Bulletti *et al.*, 2004; Bulletti and de Ziegler, 2006). Contractile activity in the non-pregnant uterus appears to be fundamentally different than in the pregnant organ. The contractions observed during the menstrual cycle have been termed 'endometrial waves' (Ijland *et al.*, 1996). Using a variety of imaging techniques, these contractions appear to involve only the sub-endometrial layer of the myometrium. These observations have led to a new concept of uterine anatomy that encompasses two distinct zones of the myometrium (Fig. 1).

In the early follicular phase following menstruation, contractile waves occur once or twice per minute and last 10–15 s with low-amplitude (usually <30 mmHg). As ovulation approaches, the frequency increases to 3–4 per minute. During the luteal phase, the frequency and amplitude decrease perhaps to facilitate implantation. In the absence of implantation of a blastocyst, the contraction frequency remains low but the amplitude increases dramatically (50–200 mmHg) producing labor-like contractions at the time of menstruation. The most fascinating aspect of endometrial waves is the integrated directionality of the SM activity and the changes that occur through the

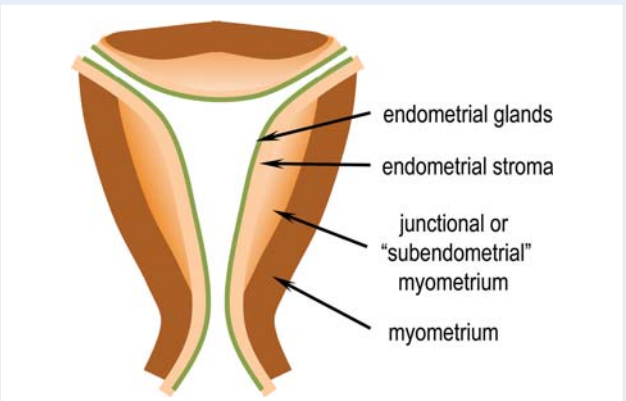

Figure 1 Concept of the sub-endometrial layer of myometrium. This thinner, innermost layer of muscle fibers, which are arranged predominantly in a circular configuration around the uterine cavity, is suggested to be of different embryological origin with physiological properties distinct from the more prominent outer layer. The circular sub-endometrial layer may facilitate the changing vectors of 'endometrial waves' that might play important roles in common reproductive disorders. The outer layer is likely to be more important in more intense uterine activity including abortion or parturition.

reproductive cycle. These have been classified and are described in greater detail by others (Ijland *et al.*, 1996; van Gestel *et al.*, 2003).

In non-primate species, the myometrium consists of two distinct layers—an outer longitudinal layer and an inner circular layer. However, in the human, the myometrial substructure is not so well defined (Huszar and Naftolin, 1984). The outer longitudinal layer is much less distinct and the major thickness of the myometrium is composed of intertwined muscle bundles that frequently surround abundant vascular channels. This histological arrangement may be of vital hemostatic importance following delivery of the hemochorial placenta that is characteristic of primates. Perhaps of particular interest to the physiology of the myometrium in the non-pregnant state, the inner (sub-endometrial) portion of the myometrium has been the focus of compelling research over the past three decades (reviewed in Brosens *et al.*, 1998).

In 1983, Hricak used MRI to demonstrate a distinct tissue layer occupying the inner one-third of the myometrium, which appeared as a low intensity signal area that blended into the endometrial stroma (Hricak *et al.*, 1983). During the reproductive years, this 'junctional' or 'sub-endometrial' layer appears anatomically distinct from the outer, denser myometrium but this distinctiveness is blurred in pre-pubertal and post-menopausal years. Noe *et al.* (1999) have proposed and provided some evidence to support the view that this junctional layer is also embryologically and functionally distinct from the outer myometrium. They suggest that the inner, junctional myometrium, which is composed of short muscle bundles arranged in a predominantly circular pattern, is derived from the paramesonephric (Mullerian) ducts of the female embryo but the outer, more predominant myometrium originates from non-Mullerian tissue. The junctional myometrium is rich in estrogen and progesterone receptors that are regulated throughout the menstrual cycle (Noe *et al.*, 1999). In contrast, there appears to be no such cyclic changes in sex steroid receptor expression in the thick outer layer of the myometrium, which contains predominantly long muscle fibers arranged longitudinally and is the major contractile tissue during parturition and abortion. More recent and sophisticated MRI studies using diffusion tensor imaging to provide a three-dimensional view confirmed the overall presence of anisotropy, indicating a lack of organization of fibers, but also provided more evidence to support the presence of a distinct inner, sub-endometrial circular layer of fibers throughout the uterine corpus and tubes (Weiss *et al.*, 2006).

The proposed junctional zone rationalizes the types of contractile activity observed in the video images from ultrasound or MRI studies. These waves have been described by most investigators as having peristalsis-like character. This is reminiscent of small intestinal peristaltic motility, which is mediated by the actions of distinct inner circular and outer longitudinal muscle layers, although the exact mechanism of coordination for these impulses remains unclear. Interestingly, regarding gastro-intestinal motility, the phenomenon of reverse peristalsis is well described (Andrews and Blackshaw, 2006). Thus, the presence of a functional inner circular layer of muscle fibers could represent a mechanism for this peristaltic and anti-peristaltic activity that is well-documented through the menstrual cycle. The circular arrangement of the muscle fibers may underlie the ability of the contractile activity to travel from fundus to cervix or in the opposite direction, depending on the local hormonal milieu and, undoubtedly, many other factors.

Regardless of the presence or absence of physiologically distinct myometrial zones, uterine contractions are dependent on the individual contractile activity of the cellular elements, the uterine myocytes. The remainder of this review will describe the molecular mechanisms that are likely to be involved in this activity. Most myometrial research has focused on changes that occur during pregnancy and in particular, those that might be related to the occurrence of preterm labor (for review see Mitchell and Taggart, 2009). In addition, much of what we know about SM contractility has been derived from studies of vascular SM, from either human or animal sources, or from other SM tissues such as rodent ileum or frog stomach. In this review, we will present findings that are specific to the myometrium as well as information derived from other types of SM. Because of the paucity of information regarding the uterine tissues from non-pregnant women, it is impossible to present a picture of uterine physiology specific to the non-pregnant state. We have attempted to identify studies that have focused specifically on human uterine myocytes, but we have not exhaustively named the species and SM types for findings that are highly likely to be applicable to the human uterine myocyte.

SM cells (SMCs) are relatively small and densely packed with myofilaments and associated dense bodies that occupy 80–90% of the cell volume and constitute the contractile machinery (see Fig. 2A and excellent reviews: Gabella, 1984; Morgan and Gangopadhyay, 2001; Gunst and Zhang, 2008). As in all muscle tissue, the predominant proteins expressed in uterine SM are myosin and actin. In skeletal or striated muscle, there is ~3-fold more myosin than actin. Conversely, SM has more actin than myosin by a factor ranging from 2 to 10 (Gabella, 1984). In uterine SM, there is ~6-fold more actin than myosin (Word *et al.*, 1993).

The myofilaments are classified according to their diameter. Thin filaments (6–8 nm diameter) are polymers of globular monomeric actin. Thick filaments (15–18 nm diameter) are made up of myosin. In general, the actin and myosin filaments run in parallel and in the longitudinal dimension of the cell. In contrast, intermediate filaments (10 nm diameter) may be composed of a large number of proteins, although desmin and vimentin are the predominant constituents.

Actin thin filaments

Monomeric actin is a soluble globular protein. In cells at rest, ~80% of the actin is polymerized into actin filaments. There are six isoforms of actin, each expressed from a separate gene. In SMCs, there are two major pools of filamentous actin. The thin filaments that form part of the contractile machinery are predominantly composed of α- and γ-actin (Draeger *et al.*, 1990). These filaments ultimately slide along the myosin thick filaments to shorten the cell during a contraction (Fig. 2B). Another pool of actin (mainly β-actin) constitutes an important structural protein of the cytoskeleton just below the plasma membrane (PM). Although not a part of the classical contractile machinery, this actin polymerizes in the presence of a contractile stimulant and, by strengthening the PM, might play an integral role in development of the mechanical tension generated (Gunst and Zhang, 2008).

According to the current concept of uterine SM contractile activity, muscle shortening occurs when the thin filaments exert tension along the longitudinal direction of the cell. This process has three basic requirements: (i) a force is required to move the actin filaments; (ii) the force must be transmitted along the actin thin filaments from

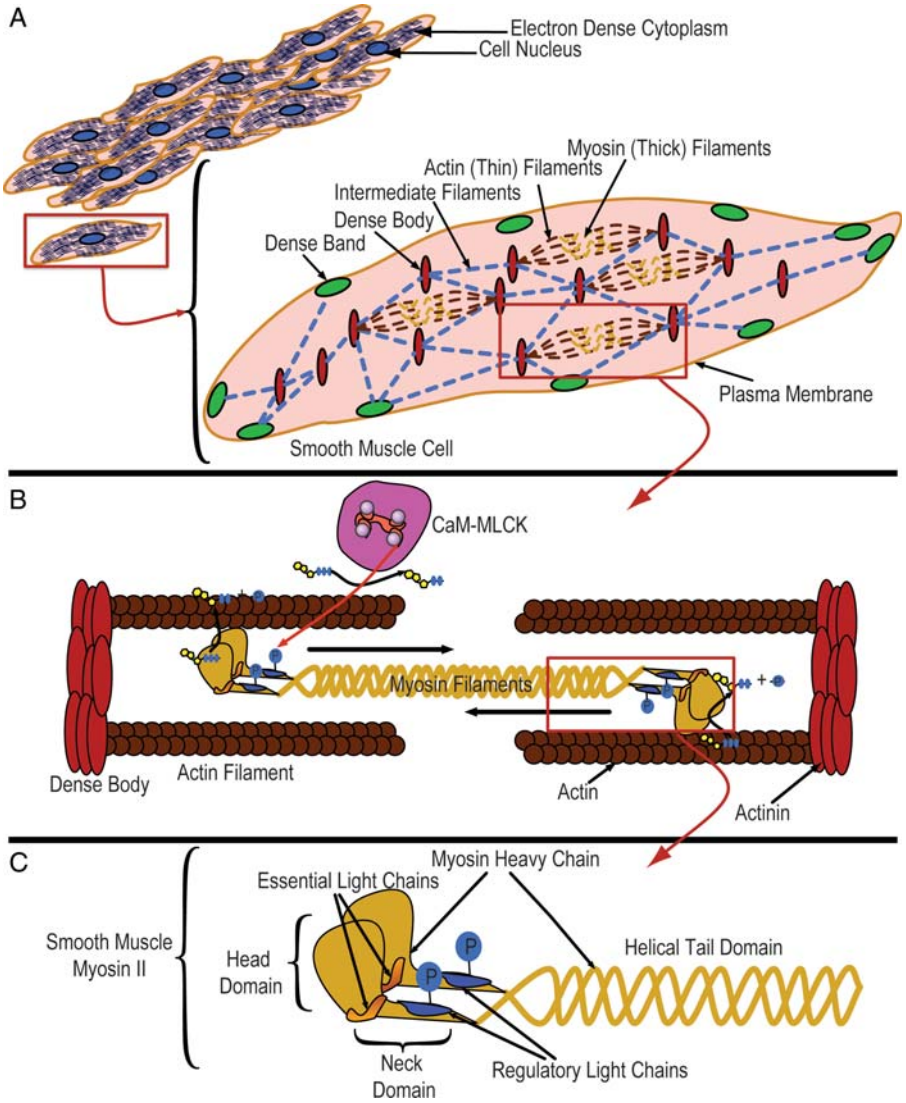

Figure 2 Smooth muscle (SM) contractile machinery. (**A**) The smooth muscle cell cytoplasm is densely packed with elements of the contractile machinery (thick and thin filaments), and other structural components (dense bodies, dense bands, intermediate filaments). The network formed by the combination of these elements results in force transduction along the longitudinal axis of the cell and cell shortening. (**B**) The contractile elements are composed of myosin thick filaments and actin thin filaments anchored to dense bodies. The movement of thin filaments caused by phosphorylation of myosin light chains and subsequent ATP hydrolysis by the myosin II ATPase decreases the distance between anchor points. (**C**) Myosin II is a hexamer composed of two heavy chains, two essential light chains and two regulatory light chains. Phosphorylation of the two regulatory light chains causes formation of a cross bridge between actin and myosin filaments and also creates a change in the angle of the neck region of myosin II, which causes motion of the actin thin filaments resulting in shortening of the cell.

the longitudinal poles of the cell towards the cell center; and (iii) the actin filaments must be firmly attached to the cytoskeleton of the myocyte. The myosin motor described in the next section fulfills the first of these functions. The other two functions are filled by specialized structures called dense bodies and dense bands, respectively (Fig. 2A). These electron-dense structures, as viewed by electron microscopy, are found commonly in all SMCs. The dense bodies appear in the cytosol and act to bridge thin filaments together along the contractile plane of the cell. A major protein component is α-actinin. It appears that dense bodies serve as anchors from which the thin filaments can exert force to bring the polar cell membranes towards each other resulting in cell shortening. Interestingly, dense bodies also are associated with β-actin, which is the type found in the cytoskeleton, suggesting that dense bodies may integrate the functions of the contractile machinery and the cytoskeleton during contraction. In comparison, dense bands are associated with the PM. They are composed of a large number of proteins including α-actinin, vinculin and cytoskeletal actin. The actin filaments of the contractile machinery become tethered to the cytoskeleton by virtue of these dense bands, which thus play an important role in transmitting the forces from the contractile units toward the PM to bring about cell shortening. The dense bands form rib-like structures

around the circumference of the cell and, towards the pole of the cell, may occupy essentially the entire surface. In the central regions of the cell, the dense bands alternate with bands of caveolae. Dense bands also contain intermediate filaments and bind integrins from the extracellular space. This suggests that they mediate interactions between the contractile machinery and the extracellular matrix.

Myosin thick filaments

The term 'myosin' encompasses a large superfamily of genes that share the ability to bind to actin and possess ATPase enzyme activity. The 'myosin motor' of human muscle tissue (Fig. 2B and C) is predominantly of the class myosin II (MII, for review, see Eddinger and Meer, 2007). In SM, MII is a hexamer molecule composed of two heavy chains (MHC) and two pairs of myosin light chains (MLC). The MII hexamer consists of three regions. The 'tail' domain is made up of the C-terminal ends of the MHCs, which are intertwined in an α-helical rod and form the major constituents of the thick filaments of SMCs. The 'head' domain is composed of the globular N-terminal end of the MHCs that protrudes laterally from the filament. The head constitutes the 'motor domain' that contains the actin-binding region as well as the ATP hydrolysis site that provides the energy required for force production. The intermediate 'neck' domain is the region creating the angle between the head and tail. This hinge-like lever arm is the site of non-covalent binding of the MLCs—one from each pair binds to each MHC. The two MLCs have molecular masses of 20 (MLC_{20}) and 17 (MLC_{17}) kDa. In vascular and uterine SM, MLC_{20}, also known as 'regulatory light chain', has a pivotal role in regulating muscle contraction (Gorecka *et al.*, 1976; Arner and Pfitzer, 1999). Its role will be discussed extensively in the following sections. The MLC_{17} is called the 'essential light chain' and its exact function is unclear. However, MLC_{17} may contribute to the structural stability of the myosin head along with MLC_{20} and may also play a role in the regulation of contraction through physical interactions with actin that are dependent on the particular MLC_{17} isoform expressed in a given tissue (Hernandez *et al.*, 2007). The head and neck domains, along with the MLCs, that lean outward from the thick filaments are called cross-bridges to reflect their function as the parts of the myosin macromolecule that interact with the actin filaments during contractile activity.

In SM, there is a single gene that codes for the dominant MHC. However, there are splice variants of this gene that result in four distinct SM MHC isoforms (Hamada *et al.*, 1990; Dauvois *et al.*, 1993; Eddinger and Meer, 2007). In addition, SM may contain non-muscle (NM) MHC that can arise from multiple genes (Gaylinn *et al.*, 1989; Eddinger and Meer, 2007). To add further complexity, two variants of MLC_{17} ($MLC_{17a/b}$) also exist, as a result of alternate splicing at the MLC_{17} gene. In contrast, different genes encode the two MLC_{20} isoforms, one coding for MLC_{20} that will associate with SM MHC and the other codes for a distinct protein that associates only with NM MHC (Taubman *et al.*, 1987; Gaylinn *et al.*, 1989; Kumar *et al.*, 1989; Eddinger and Meer, 2007). Literally hundreds of permutations of four light and two heavy chains are possible if we allow complete promiscuity amongst all splicing possibilities and combinations of NM and SM MHCs, although it is unlikely that more than a few such combinations are actually used or permitted within a specific SM bed. Despite varying expression ratios of the multiple $MHC/MLC_{20}/MLC_{17}$ splice variants, a high level of functional specificity can be achieved (Morano 2003; Eddinger and Meer, 2007). Thus, the possibility for fine-tuning of the contractile machinery exists. In this regard, differences in expression of various MII isoforms have been demonstrated to occur in different regions of the same organ (Parisi and Eddinger, 2002). Thus, regional differences in isoform expression could produce slightly different contractility profiles, which may influence the vector of propagation of forces. In the uterus, this could underlie the changes in uterine motility vectors observed during different phases of the menstrual cycle as noted earlier. Clearly, much more research is required to clarify the physiological roles that may be fulfilled for each SM tissue by this heterogeneity of expression and isoform association amongst MII constituents.

Once the contraction has occurred, the cross bridge attachments need to be released in order that the muscle can relax. Although less is known about this phenomenon, it appears to be related to dephosphorylation of MLC_{20}. In some situations, the dephosphorylated MLC_{20} is very slow to allow detachment of the actin from the myosin cross bridge, resulting in a prolonged contraction. This has been referred to as a 'latch-bridge' (Hai and Murphy, 1988). This phenomenon may be of great value especially for tonically active SM beds as it would allow them to maintain basal tone through holding in an isometric state without a great energy cost.

Phosphorylation of Ser^{19} on MLC_{20} causes a conformational change that increases the angle in the neck domain of the MHC, thus mobilizing the cross-bridges and causing the actin thin filament to slide along the myosin thick filament. Upon MII activation, the myosin and actin filaments move by ~10 nm relative to each other in what is referred to as the power stroke. Through an unknown mechanism, phosphorylation of Ser^{19} on MLC_{20} also activates the ATPase activity of the myosin head region to provide the energy to fuel the contraction. Phosphorylation of Thr^{18} on MLC_{20} is also possible and may further increase the ATPase activity of MII (Ikebe *et al.*, 1986, 1987, 1988). However, phosphorylation of Ser^{19} has been the primary interest in studies of regulation of SM contractile activity. This phosphorylation reaction is mediated by the enzyme MLC_{20} kinase (MLCK), which is predominantly regulated by the intracellular concentration of free calcium ion ($[Ca^{2+}]_i$). These mechanisms are the focus of a subsequent section.

Intermediate filaments

Intermediate filaments form the structural network of the cytoskeleton and are largely responsible for the shape and spatio-temporal organization within the cell (Fig. 2A). These filaments may play important roles in signal transduction, contractile activity and other important processes (for review see Taggart and Morgan, 2007; Tang, 2008). Unfortunately, there has been very little research into the intermediate filaments of uterine SMCs. In other tissues, more than 65 separate proteins have been found in intermediate filaments (Hesse *et al.*, 2001). The proportion of vimentin, desmin and the many other constituents of intermediate filaments may vary greatly, both in concentration and distribution, from one cell type to another. Although long considered as part of the cytoskeleton of the cell, there is increasing acceptance that these filaments play a role in force development during contraction of SM tissue. As noted in Fig. 2A, vimentin filaments insert into cytoplasmic dense bodies or dense bands, which also serve

as anchors for actin thin filaments. They also insert into PM desmosomes, which are complex intercellular junctions. Thus, when the actin and myosin filaments are activated during a contraction, the intermediate filaments may facilitate the spatial reorganization of the contractile machinery to optimize force development (Wang *et al.*, 2006). In response to uterine contractile activation, vimentin is phosphorylated at Ser^{56} by p21-activated kinase (Li *et al.*, 2006). This results in some disassembly of vimentin polymers and this may facilitate the spatial reorganization that optimizes force generation.

Other proteins of the contractile apparatus

In addition to the constituents of the filamentous structures discussed above, other proteins accessory to the contractile machinery may play important roles in contractile regulation. These proteins are primarily associated with the thin filaments and include tropomyosin, calponin and caldesmon. Tropomyosin is an actin-associated protein that spans seven actin monomers and is laid out end to end over the entire length of the thin filaments. In striated muscle, tropomyosin serves to enhance actin–myosin interactions. However, it has an uncertain role in SM. Calponin may be expressed at levels reaching stoichiometric equivalence with actin, and has been proposed to be a load-bearing protein. Caldesmon may be involved in tethering actin, myosin and tropomyosin, and in so doing may enhance the ability of SM to maintain tension. In addition, caldesmon may be directly involved as a molecular switch for MII ATPase activity dependant on its phosphorylation state. All three of these proteins may have a role in inhibiting MII ATPase activity. For a more thorough discussion regarding these and other important regulatory proteins, the reader is referred to other reviews (Morgan and Gangopadhyay, 2001; Szymanski 2004; Kordowska *et al.*, 2006).

Electrophysiology of uterine myocytes (excitation-contraction coupling)

Uterine SM has a phasic pattern of contractile activity—maintenance of a resting tone with discrete, intermittent contractions of varying frequency, amplitude and duration. As noted earlier, the state of contractility is regulated predominantly by $[Ca^{2+}]_i$. From a functional, physiological point of view, the regulation of $[Ca^{2+}]_i$ can be considered in three phases: maintenance of basal concentrations, which play a role in resting tone of the SM; the marked increase in $[Ca^{2+}]_i$ that occurs with contractile agonist stimulation (Fig. 3A); and the restoration of $[Ca^{2+}]_i$ to resting state following stimulation (Fig. 3B). In general, these processes are controlled by inter-related ion channel and pump mechanisms. In this section, we will discuss the electrophysiological events underlying this phasic activity.

Maintenance of the resting state (resting membrane potential)

The resting membrane potential (V_{rest}) of uterine myocytes has been recorded between −35 and −80 mV (reviewed in Sanborn, 2000). The ionic currents that maintain this potential and the changes that occur in response to pharmacologic and signaling molecules constitute the complex electrophysiologic network that controls the contractile activity of the uterus. V_{rest} undergoes rhythmic oscillations, which have been termed 'slow waves'. These waves reflect the distribution of Ca^{2+}, Na^+, K^+ and Cl^- ions between the intracellular and extracellular spaces and this, in turn, reflects the permeability of the PM to each of those ions (Sanborn, 2000; Khan *et al.*, 2001a, b). Of these relevant ions, the largest electrochemical gradient in the resting state exists for Ca^{2+}, which has 10^4 greater concentration in the extracellular space as compared with the cytosolic compartment ($[Ca^{2+}]_i = 0.15$ μM compared with 1.5 mM outside the cell). This ensures that the opening of membrane Ca^{2+} channels stimulated by uterotonins is followed by a rapid and significant rise in $[Ca^{2+}]_i$.

Uterine myocyte excitability, as with most other excitable cell types, depends on the movement of Na^+, Ca^{2+} and Cl^- ions into the cytosolic compartment from the extracellular space, and of K^+ ions in the opposite direction. The former three are concentrated in the extracellular space, whereas the latter is concentrated in the intracellular milieu of SMCs (Sanborn, 1995). The major factors in the establishment of V_{rest} are the various K^+ channels present in the SMCs. A variety of K^+ channels with different pharmacologic, kinetic and voltage dependence properties have been identified in human uterine myocytes (Khan *et al.*, 2001a, b). These channels conduct an outward current during periods where the muscle is not active, and thereby maintain V_{rest}. Further, this outward conductance of K^+ repolarizes the membrane post-stimulation, thus decreasing excitability in the absence of a stimulus. Ca^{2+}, voltage and metabolites such as ATP can gate various types of membrane-localized K^+ channels, denoted as K_{Ca}, K_V and K_{ATP}, respectively. All of these types of K^+ channels have been detected in human myometrium but debate continues as to which channels play predominant roles and how they interact among each other (Anwer *et al.*, 1993; Khan *et al.*, 1997; Khan *et al.*, 2001a, b; Brainard *et al.*, 2005; Aaronson, 2006; Bursztyn *et al.*, 2007; Smith, 2007).

Ca^{2+}-sensitive K^+ channels may play a key role in regulation of V_{rest}. These channels, denoted as BK_{Ca} (also referred to as maxi-K), are made up of four α and four β subunits, have a large conductance capacity and respond to increased $[Ca^{2+}]_i$ as well as changes in PM voltage (Ledoux *et al.*, 2006). The mechanism by which these channels sense the presence of elevated $[Ca^{2+}]_i$ is not known. These channels limit cellular excitability by conducting K^+ out of the cell when $[Ca^{2+}]_i$ rises, thus antagonizing the depolarizing stimulus. Other K^+ channels have been studied in myometrium from various species (Inoue *et al.*, 1990; Sanborn 1995; Miyoshi *et al.*, 2004). In particular, several members of the KCNQ family of K^+ channels have been observed in non-pregnant murine uterine SM and some appear to have increased expression at the time of progesterone dominance (McCallum *et al.*, 2009). Although their roles are less clearly defined, they could play subtle but important roles in uterine contractility.

Certainly, K^+ channels are not the sole charge carriers in the myometrium. Many surface proteins have electrogenic properties. For example, currents mediated by Cl_{Ca} (Ca^{2+}-activated Cl^- channels) may play a role in pacemaking, as inhibition of these channels showed alteration in spontaneous and agonist-stimulated contractions in rat myometrium (Jones *et al.*, 2004). Additionally, the expression of Na^+ channels and of connexin-43, a main constituent of myometrial gap junctions, has been demonstrated to increase with gestation in

human tissues as well as those of rodents (Garfield *et al.*, 1978; Inoue and Sperelakis, 1991; Garfield *et al.*, 1995). Gap junctions serve to interconnect adjacent myocytes both electrically and metabolically (Young, 2007). As may be expected, a mutation in connexin-43 leading to decreased intercellular connectivity reduced the force of myometrial contractions in addition to impairing responsiveness to oxytocin (OT) (Tong *et al.*, 2009). For completeness, it should be noted that Na^+ channels which conduct fast depolarizing currents may be involved in enhanced responsiveness to contractile stimuli and in ensuring the rapid and complete electrical propagation of action potentials (APs) in myometrial SM (Sperelakis *et al.*, 1992a, b; Sanborn, 1995). The mRNAs encoding Na^+ channel subunits have been found in pregnant rat and human myometrium (George *et al.*, 1992; Boyle and Heslip, 1994), although this type of channel is normally absent from SM.

Agonist stimulation (generation of APs)

In all excitable tissues, the AP embodied by membrane depolarization is the trigger for many intracellular events. This is also the case in SM where PM depolarization leads to the entry of extracellular Ca^{2+} which in turn causes $[Ca^{2+}]_i$ to rise and contraction to occur (Wray, 1993). Two types of APs have been recorded in myometrial SM from various species—simple APs involving depolarization followed by rapid repolarization, and complex APs, which entail an initial depolarization with a sustained plateau. Different combinations of ionic currents may be at play during these two different patterns of electrical activity (Khan *et al.*, 2001a, b; Bursztyn *et al.*, 2007). Although a single AP is sufficient to induce the propagation of an electrical wave of activity in the myometrium, multiple coordinated depolarizations are necessary for forceful and sustained contractions (Garfield and Maner, 2007). The number of cells involved in the coordinated effort of these clusters encodes the frequency, amplitude and duration of the contraction (Maul *et al.*, 2003). Estrogen treatment has been noted to cause slight depolarization and alter both inward and outward currents in uterine muscle cells from late pregnant rats (Inoue *et al.*, 1999).

The concept of a pacemaker in the myometrium has been considered and investigated for many years. Clearly, the uterus is 'myogenic' in that it contracts *in vivo* and *in vitro* without the need for external stimuli. Decades of research employing a variety of histological techniques have yielded no evidence for the presence of cells with the histological and electrophysiological properties of a functional pacemaker (Gherghiceanu and Popescu, 2005, Hinescu and Hinescu, 2005; Popescu *et al.*, 2005; Radu *et al.*, 2005; Cretoiu *et al.*, 2006; Hinescu *et al.*, 2006, 2007, 2008; Popescu *et al.*, 2006; Mandache *et al.*, 2007; Popescu *et al.*, 2007; Suciu *et al.*, 2007) such as has been described in other tissues including the gut and urethra (Sergeant *et al.*, 2000; Huizinga and Lammers, 2009). The essential issues of the origin of the electrical impulse initiating a myometrial contraction and the regulation of its direction of propagation remain unclear in either the pregnant or non-pregnant uterus. Clearly, much more research is required to understand the regulation, and therefore dysregulation of uterine contractility that causes such a broad and important variety of reproductive disorders noted earlier.

Regardless of the origin of the contraction, the individual uterine myocyte contractile activity is mediated by subsequent changes in $[Ca^{2+}]_i$. Thus, regulation of Ca^{2+} flux across the PM is of ultimate importance to determine the state of contractile activity. Ca^{2+} is one of the most ubiquitously used second messenger signaling molecules in biological systems. Ca^{2+} transients regulate a wide range of cellular processes, including fertilization, secretion, proliferation, learning, cytoskeletal rearrangements, gene expression, in addition to SM contraction. In SM, the liberation of Ca^{2+} from intracellular stores along with the influx of Ca^{2+} from the extracellular space serve to activate the biochemical pathways which lead to actin–myosin cross-bridging and force development in the presence of ATP.

The predominant Ca^{2+} channels in the uterine myocyte are the L-type Ca^{2+} channels, which are ubiquitous, large conductance, voltage-operated channels (VOC; Sperelakis *et al.*, 1992a, b). Since Ca^{2+} is a divalent cation, it contributes to both the chemical and electrical environments of the cell and is itself influenced by electrochemical forces. When the uterine myocyte membrane potential is depolarized to approximately −40 mV, the L-type VOC open to allow a massive influx of Ca^{2+} (Sanborn, 2000). The resulting rise in $[Ca^{2+}]_i$ initiates a chain of events (see below) resulting in a contraction.

The myometrium contains other types of Ca^{2+} channels including isoforms and splice variants of T-type Ca^{2+} channels (Ohkubo *et al.*, 2005). These channels exhibit faster kinetics than the L-type Ca^{2+} channel (Sperelakis *et al.*, 1992a, b). Interestingly, myometrial T-type Ca^{2+} channels have a greater conductance capacity than the L-type Ca^{2+} channel (Young *et al.*, 1993) and thus were suggested to play a prominent role in AP propagation. In comparison, the L-type Ca^{2+} channel may be more suited to allow bulk Ca^{2+} entry over a longer period of time to mediate the signaling effects of Ca^{2+} as a second messenger. As they become activated at lower (more negative) voltages than L-type Ca^{2+}channels, T-type Ca^{2+} channels may aid in elevating the PM potential to the threshold necessary for L-type Ca^{2+} channel activation, which then may lead to firing of myometrial APs. Selective blockage of T-type Ca^{2+} channels significantly slowed the rate of spontaneous uterine contractions in myometrial strips from late pregnancy (Blanks *et al.*, 2007) supporting a role for these channels in myometrial regulation.

In general, uterine agonists interact with a specific G-protein coupled receptor (GPCR) in the myocyte PM resulting in activation of a trimeric G-protein containing a $G_{\alpha q}$ or $G_{\alpha 11}$ subunit (Fig. 3; Phaneuf *et al.*, 1993). Activation of this subunit in the uterine myocyte stimulates membrane phospholipase C_β (PLC_β) (Taylor *et al.*, 1991) to hydrolyze phosphatidylinositol bisphosphate (PIP_2) into inositol-trisphosphate (IP_3) and diacylglycerol (DAG), which serve as second messengers (Berridge, 1993; Exton, 1996). IP_3 interacts with a specific receptor (IP_3R) (Furuichi *et al.*, 1989) at the level of the sarcoplasmic reticulum (SR) causing release of Ca^{2+} from its intracellular storage site (Streb *et al.*, 1983; Gill, 1989) and a subsequent rise in $[Ca^{2+}]_i$. This pathway will be discussed further below. The other product of the reaction, DAG, activates classical and novel protein kinase C (PKC) isoforms. The precise role of the PKC pathway remains unclear although evidence suggests it may play a negative feedback role in uterine myocytes by stimulating internalization and degradation of receptors as well as decreasing transcription of mRNA for new receptor synthesis (Lajat *et al.*, 1998; Ball *et al.*, 2006; Devost *et al.*, 2008).

The IP_3–IP_3R mediated Ca^{2+} release from the SR is a major contributor to the increase in PM voltage from V_{rest} to the point where VOC

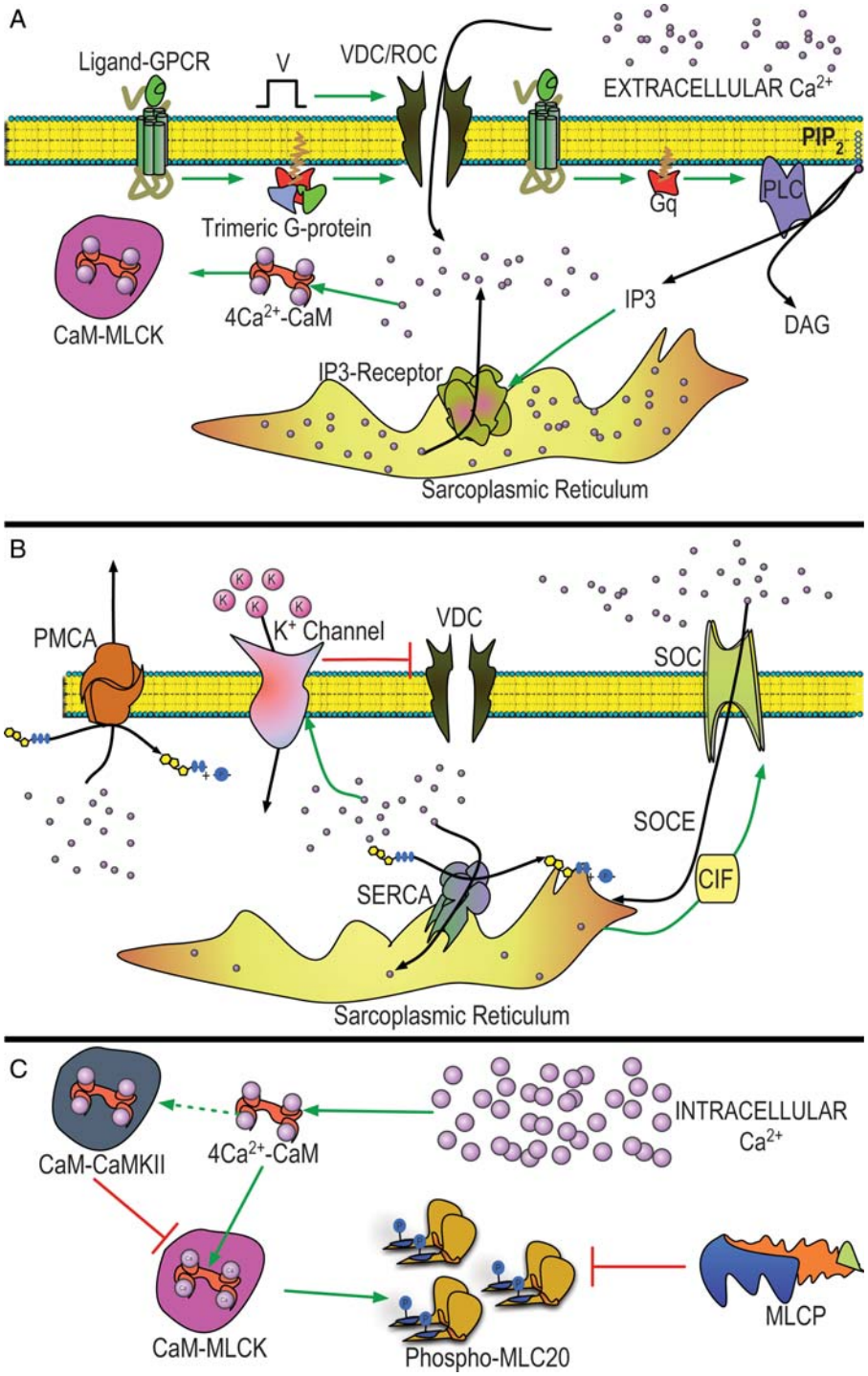

Figure 3 Excitation-contraction coupling in SM. (**A**) Agonist activation of GPCRs results in opening of receptor-operated (ROC) and voltage-dependent (VDC) PM Ca^{2+} channels. In parallel, the G-protein $G_{\alpha q}$ stimulates PLC to cleave PIP_2 into DAG and IP_3, the latter of which activates a receptor at the level of the SR to induce Ca^{2+} release from internal stores. These events result in a rise in the internal level of Ca^{2+} and ultimately activation of MLCK through the intermediary activation of CaM. (**B**) Ca^{2+} signals are terminated by extrusion of Ca^{2+} from the cytosolic compartment or sequestration into internal stores via PM Ca^{2+} ATPases (PMCA) and SR Ca^{2+} ATPases (SERCA), respectively. Activation of Ca^{2+}-sensitive K^+ channels serves to repolarize the myocyte membrane and induces closure of VDCs, limiting further Ca^{2+} entry. Internal stores may also be refilled by opening of store-operated channels (SOCE) upon reception of a signal (calcium influx factor, CIF) indicating store-depletion. (**C**) Ca^{2+}–CaM stimulated phosphorylation of MLC_{20} is self-limiting through parallel activation of CaMKII by CaM, resulting in inhibitory phosphorylation of MLCK. Dephosphorylation of MLC_{20} by MLC_{20} phosphatase (MLCP) results in resetting of the contractile system and relaxation at the level of the tissue. Green, red and black lines depict activation, inhibition and ion movement or ATP consumption, respectively.

for Ca^{2+} are opened to trigger an AP. ROCs for Ca^{2+} or K^+ may also contribute to this. Another mechanism, as yet poorly understood, is known as Ca^{2+}-induced Ca^{2+} release (CICR) whereby the increasing $[Ca^{2+}]_i$ sensitizes other Ca^{2+} channels to open, thus creating a feed-forward loop. This mechanism may involve ryanodine receptors in the SR. The IP_3Rs are themselves sensitive to Ca^{2+} and can mediate CICR (Wray *et al.*, 2003). This activity can give rise to sudden increases in $[Ca^{2+}]_i$ that can be observed as spontaneous Ca^{2+} 'sparks' and subsequent Ca^{2+} 'waves' using ion-imaging techniques. Although these phenomena were not detected in uterine SM from pregnant rats (Burdyga *et al.*, 2007), their presence in non-pregnant human myometrium could allow for localized and directional increases in Ca^{2+} release separated in space from other areas of the cell (McCarron *et al.*, 2004). Such mechanisms could play a role in mediating the variety of patterns of directional myometrial activity seen particularly in the non-gravid uterus. However, despite the fact that the necessary components of CICR are expressed in the non-pregnant and pregnant human uterus (Awad *et al.*, 1997; Taggart and Wray, 1998; Martin *et al.*, 1999; Kupittayanant *et al.*, 2002), the importance of CICR is questionable under physiological conditions (Kupittayanant *et al.*, 2002).

A final potential method of regulating Ca^{2+} release is referred to as store-operated Ca^{2+} entry (SOCE). Through pathways that are not yet understood, when the intracellular stores of Ca^{2+} in the SR are emptied, an unknown signal [denoted as 'calcium influx factor' (CIF), Fig. 3] is sent to the PM to allow entry of extracellular Ca^{2+} into the cytosol (Venkatachalam *et al.*, 2002). The channels through which Ca^{2+} entry occurs in this mechanism are referred to as 'store-operated channels' (SOCs). SOCE is likely responsible for the prolonged phase of influx of Ca^{2+} through the PM, which has been observed following the drug-induced emptying of Ca^{2+} from the SR. It is likely that this mechanism is more important for longer-term Ca^{2+} homeostasis rather than for the regulation of the AP activity that occurs on a millisecond time-scale in uterine myocytes. The molecular identity and characterization of the SOC remains unknown. The current carried by some SOCs is termed I_{CRAC} (CRAC: Ca^{2+} Release-Activated Current). This current is small, reflecting the lower conductance of SOCs, and is non-voltage-dependent but very sensitive to feedback inhibition by Ca^{2+} (Zweifach and Lewis, 1995). It has been proposed that members of the transient receptor potential (TRP) channel family may be candidates for mediating this current in myometrial SM from pregnant women (Dalrymple *et al.*, 2002). Most known isoforms of the TRP family are expressed in pregnant human myometrium (Yang *et al.*, 2002). SOCE and other aspects of Ca^{2+} handling in the myometrium have been thoroughly reviewed recently (Noble *et al.*, 2009) and interested readers are referred there for a more complete discussion.

As noted above, agonist treatment of uterine myocytes from non-pregnant or pregnant women elevates IP_3 concentrations and this causes release of Ca^{2+} from the SR into the cytoplasm (Luckas *et al.*, 1999). Pharmacological emptying of the SR Ca^{2+} stores increases tone in human myometrium from late gestation (Kupittayanant *et al.*, 2002). Emptying of the SR Ca^{2+} store in these same experiments had little if any effect on the cytosolic Ca^{2+} concentrations achieved or the force generated following OT stimulation. These data suggest that the agonist-stimulated, IP_3-mediated release of Ca^{2+} is a much less important determinant of cyosolic Ca^{2+} or force generation than the massive influx of Ca^{2+} from the extracellular space through PM Ca^{2+} channels. It is suggested that the role of the SR may be primarily that of a sink for Ca^{2+} clearance from the cytosol after an AP. Thus, the precise role of the SR and the IP_3 pathway of agonist signal transduction remain unclear in uterine myocytes obtained from late human pregnancy.

Another interesting aspect of myocyte stimulation and subsequent Ca^{2+} signal generation involves the role of specialized PM microdomains in signal transduction. In general, 'lipid rafts' are areas of the lipid bilayer that are rich in cholesterol and therefore move less fluidly in the PM. One type of lipid raft relevant to uterine myocyte biology is termed 'caveolae'. These structures are associated with and stabilized by a scaffolding protein called 'caveolin' that is present at the PM of uterine myocytes (Hagiwara *et al.*, 2002; Ku *et al.*, 2005). Caveolae are enriched in key proteins mediating myocyte excitability, such as BK_{Ca} channels (Brainard *et al.*, 2005), that have already been discussed here. The expression of caveolins may be important to regulation of labor in rodent species but may be less significant in humans (Taggart *et al.*, 2000; Riley *et al.*, 2005a, b; Riley *et al.*, 2005a, b). For a more thorough discussion on the topic of caveolae, readers are referred elsewhere (Noble *et al.*, 2006).

Myosin light chain kinase

The events discussed above ultimately yield a marked increase in $[Ca^{2+}]_i$, which is the necessary trigger for activation of calmodulin (CaM), a Ca^{2+}-dependent cytosolic protein which binds four Ca^{2+} ions (Fig. 3C; Johnson *et al.*, 1996). The $4Ca^{2+}$-CaM complex activates the key enzyme MLCK and causes an immediate and marked increase in phosphorylation of MLC_{20}, which activates the contractile machinery (Shojo and Kaneko, 2001). There are three isoforms of MLCK [smooth muscle (smMLCK), skeletal muscle (skMLCK) and cardiac (cMLCK)] (Takashima, 2009). The remainder of this review will deal only with smMLCK. The $4Ca^{2+}$–CaM complex assumes a conformation that allows activation of smMLCK and markedly enhances the enzyme activity in phosphorylation of MLC_{20} (Shojo and Kaneko, 2001). As mentioned previously, smMLCK catalyzes the phosphorylation of the MLC_{20} on the N-terminus at Ser^{19} (Kamm and Stull, 2001) to generate phospho-MLC_{20} ($PMLC_{20}$). This phosphorylation event is permissive on actin–myosin cross-bridging since it results in both a conformational change in MII from the folded to extended state (Onishi and Wakabayashi, 1982; Craig *et al.*, 1983; Onishi *et al.*, 1983), which may facilitate myofilament formation and further enhance the ATPase activity of MII *in vitro* (Ikebe *et al.*, 1985). Furthermore, in SM almost the entire pool of MLC_{20} may be phosphorylated within a few seconds during a maximal stimulus by virtue of the rapid kinetics of smMLCK (Dillon *et al.*, 1981; Hai and Murphy, 1989; Takashima, 2009).

The smMLCK isoform is a ubiquitously expressed enzyme encoded by a single gene. There are two isoforms (220 and 130 kDa) arising through use of alternate promoters (Stull *et al.*, 1998). The larger of these two smMLCK isoforms is differentially expressed in embryonic tissues as compared with adult tissues and is also called 'NM' or 'endothelial' MLCK. This may indicate a different functional role for MLCK activity in the embryo as compared with adult tissues. The 130 kDa smMLCK achieves its highest levels of expression in SM. In both rat and human myometrium, smMLCK inhibition using the

inhibitors wortmannin and ML-9 entirely abolished contractions that were induced using OT or depolarization with KCl (Longbottom *et al.*, 2000). These findings indicate that there is no alternative pathway for contraction in uterine SM, and that that MLC_{20} phosphorylation by smMLCK is both necessary and sufficient for contraction to occur. This is in contrast to the contractile mechanism of skeletal muscle, which depends on Ca^{2+} availability and requires proteins such as troponin C to undergo a conformational change so as to permit actomyosin complex formation (Gordon *et al.*, 2000). smMLCK contains several phosphorylation target-sites for PKA, PKC and other kinases. PKA-mediated phosphorylation of a site on the CaM-binding region of smMLCK, which impairs the ability of CaM to activate the enzyme, has been shown to decrease uterine contractile activity (Stull *et al.*, 1993).

The role of CaM is not limited to the activation of smMLCK. In fact there is evidence that CaM may be involved in regulating membrane channels and Ca^{2+}-ATPases (see next section) that serve to limit the transient rise in $[Ca^{2+}]_i$ and therefore aid in resetting the system for the next contraction. Note that the events of Ca^{2+} influx and contraction are separated temporally. The activation of smMLCK by CaM and movement from the cytosol toward the contractile apparatus may be the rate-limiting steps of contraction (Wray *et al.*, 2003) in terms of the speed of response of the SMC.

Restoration of the resting state

Ca^{2+} removal post-contraction is essential to induce relaxation of the SM and to replenish the SR for the next contractile stimulus (Fig. 3B). This is achieved by a variety of mechanisms, including the closure of PM Ca^{2+} channels and simultaneous extrusion of Ca^{2+} from the cytosolic compartment into the extracellular space and into intracellular stores via PM Ca^{2+}-ATPase (PMCA) and the SR/ER Ca^{2+}-ATPase (SERCA), respectively. PMCA and SERCA are multi-spanning transmembrane proteins of the P-type Ca^{2+}-ATPases family, which move one Ca^{2+} ion out of the intracellular compartment and one H^+ ion in the opposite direction during each enzymatic cycle, with the aid of ATP hydrolysis (Moller *et al.*, 1996). The unbalanced movement of ionic charge across the membrane helps to maintain V_{rest} in a hyperpolarized state. In addition, the movement of protons by these enzymes may have implications for pH differences between the intra- and extracellular spaces. One of the main structural differences between PMCA and SERCA is the presence of a large carboxy-terminal tail in PMCA which allows the enzyme to be activated by Ca^{2+}–CaM (Floyd and Wray, 2007).

PMCA isoforms 1 and 4 are ubiquitously expressed; whereas there is evidence that isoform 2b may be uniquely expressed in the uterus (Penniston and Enyedi, 1998). Expression of PMCA and SERCA is increased during labor, indicating a possible functional role in parturition for these enzymes (Paul 1998; Taggart and Wray, 1998; Shmigol *et al.*, 1999; Tribe *et al.*, 2000). There are few studies in myometrium from non-pregnant women, but it is possible that regulation of Ca^{2+} extrusion might alter frequency, amplitude, duration and even direction of uterine contractions.

Another important Ca^{2+}-extruding protein is the Na^+/Ca^{2+} exchanger (NCX). This membrane-spanning antiporter harnesses the power of the electrochemical gradient of Na^+ established by the Na^+/K^+ ATPase, for which specific isoforms are expressed in the uterus (Floyd *et al.*, 2003). This Na^+ gradient is used to extrude Ca^{2+} through the PM (Floyd and Wray, 2007). Several experimental approaches have shown that PMCA, SERCA and NCX mechanisms are all important in clearance of the Ca^{2+} following the peak of the AP regardless of whether the Ca^{2+} originated from the intracellular stores or from the extracellular space (Taggart and Wray, 1997; Shmigol *et al.*, 1998, 1999).

An additional mechanism of Ca^{2+} clearance from the cytosol involves Ca^{2+}-dependent feedback. This process is voltage and time-dependent and serves to counterbalance excitatory signals (McDonald *et al.*, 1994). Two distinct mechanisms have been demonstrated in uterine SM. First, Ca^{2+} itself can feed back to inhibit L-type Ca^{2+} channel function as demonstrated through decreased rates of channel inactivation following the removal of Ca^{2+} from the experimental medium (Jmari *et al.*, 1986; Sanborn 2000; Wray *et al.*, 2003). Second, Ca^{2+}-dependent feedback may be mediated by CaM. In addition to activating smMLCK, $4Ca^{2+}$–CaM can activate a variety of cellular proteins, including CaM-Kinase II (CaMKII) and the protein phosphatase (PP) calcineurin. It has been suggested that CaMKII mediates the facilitatory effects of Ca^{2+} on the L-type channel (Wu *et al.*, 1999; Dzhura *et al.*, 2000) although the inhibitory effects are mediated through dephosphorylation of an activity-enhancing site on the channel by calcineurin (Schuhmann *et al.*, 1997). Thus, there exists a balance between events facilitating SM contraction and those that serve to dampen the response to Ca^{2+}. In recent years, there has been a significant increase in understanding specific mechanisms that can alter the sensitivity of the myocyte to Ca^{2+}. This will be the focus of the next section.

Mechanisms of calcium sensitization

As mentioned previously, SM contraction is dependent on the state of phosphorylation of MLC_{20}, which is primarily regulated by Ca^{2+}–CaM. However, the concentration of $[Ca^{2+}]_i$ does not always parallel the intracellular concentration of phosphorylated MLC_{20} and/or the degree of contractile activation. In some situations, particularly after stimulation with an endogenous agonist such as OT, a given rise in $[Ca^{2+}]_i$ will cause a larger-than-expected force of contraction. This phenomenon is known as 'Ca^{2+} sensitization' (CS) (Somlyo and Somlyo, 1998). The advent of Ca^{2+}-responsive fluorophores enabled the demonstration that the ratio of force output to Ca^{2+}-entry induced by SM agonists was not always constant (Bradley and Morgan, 1987). Further, these agonists were capable of inducing larger amplitude forces compared with depolarizing stimuli such as high K^+ solutions (Bradley and Morgan, 1987; Somlyo and Somlyo, 1994). At the biochemical level, $PMLC_{20}$ concentrations reflect an enzymatic balance between the activities of smMLCK and MLC_{20} phosphatase (MLCP). Thus, either elevation in smMLCK activity or inhibition of MLCP activity could produce the observed force enhancement. Subsequent experiments demonstrated that inhibition of MLCP is the major mechanism controlling CS (Kitazawa *et al.*, 1989; Noda *et al.*, 1995). Abundant evidence is accumulating to demonstrate that a pathway is activated following stimulation of GPCRs to inhibit MLCP and thus potentiate the $PMLC_{20}$ generated from the simultaneous activation of MLCK. This pathway involves

the small GTPase rhoA and its effector, rhoA-associated kinase (ROK) (Fig. 4). In SMCs, rhoA–ROK activation may be mediated by trimeric G-proteins (Kozasa *et al.*, 1998; Klages *et al.*, 1999). ROK phosphorylation of the subcellular targeting subunit (MYPT1) of MLCP interferes with the ability of the catalytic subunit (PP1c) to act on $PMLC_{20}$, thereby preventing desphosphorylation. This major pathway of CS is the focus of this section.

RhoA and its associated kinase

RhoA is a small monomeric G-protein and a member of the rho subfamily of the ras superfamily of monomeric GTPases. For activation, rhoA translocates to the PM by virtue of a C-terminal post-translational modification in the form of a prenyl (lipid) moiety (Hori *et al.*, 1991; Fujihara *et al.*, 1997; Lee *et al.*, 2001). The prenyl group confers the ability to interact with the PM and also with guanine nucleotide exchange factors (GEFs). GEFs mediate the exchange of guanosine diphosphate (GDP) for guanosine triphosphate (GTP) on G-proteins such as rhoA, a necessary step resulting in protein activation, which allows interaction with its downstream effectors. Completion of the G-protein signal is achieved by GTPase Activating Proteins (GAPs) that enhance the rate of hydrolysis of the γ-phosphate of the bound GTP.

In its inactive state, rhoA is sequestered in the cytosol by rho-guanine nucleotide dissociation inhibitor (rhoGDI). RhoGDI contains a hydrophobic pocket that surrounds the prenyl moiety on the C-terminus of rhoA and prevents its association with the PM and with the activating GEFs (Fukumoto *et al.*, 1990; Bourmeyster *et al.*, 1992; Hancock and Hall, 1993). RhoGDI also diminishes the intrinsic GTPase activity of rhoA (Read *et al.*, 2000) as well as the activating capacity of GAPs (Hancock and Hall, 1993). RhoA can be inhibited by cyclic adenosine monophosphate (cAMP)- or cyclic guanosine monophosphate (cGMP)-induced phosphorylation at Ser^{188} mainly by enhancing sequestration by rhoGDI (Lang *et al.*, 1996; Sawada *et al.*, 2001; Ellerbroek *et al.*, 2003). RhoA was implicated as a mediator in the process of CS by experiments demonstrating that this phenomenon was diminished using a specific inhibitor of rhoA (Hirata *et al.*, 1992) and that the molecular mechanism downstream of rhoA involved MLCP inhibition (Kitazawa *et al.*, 1991; Noda *et al.*, 1995).

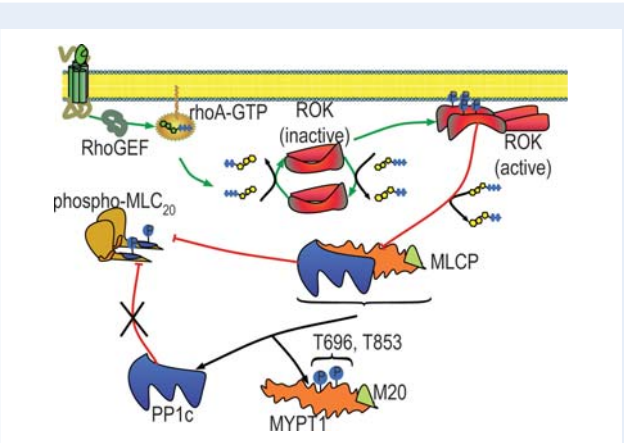

Figure 4 RhoA and Rho-kinase signaling pathway. Activation of G-protein coupled receptors (GPCRs) leads to recruitment of rhoA to the PM after exchange of GDP for GTP facilitated by a specific rho guanine nucleotide exchange factor (GEF). Rho-associated kinase (ROK) is activated by rhoA in a mechanism proposed to involve trans-autophosphorylation and oligomerization. ROK phosphorylates the myosin targeting subunit (MYPT1) of MLCP at two potential sites (T696, T853) thus promoting dissociation of the holoenzyme and preventing the dephosphorylation of MLC_{20} by the phosphatase subunit (PP1c) through interrupted targeting. Green, red and black lines depict activation, inhibition and ATP consumption, respectively.

ROK, a serine/threonine kinase (Leung *et al.*, 1996; Matsui *et al.*, 1996), is one of the main signal transduction effectors of rhoA. There are two isoforms (ROK-1 and ROK-2) arising from separate genes and both are expressed in human and rat myometrium (Niiro *et al.*, 1997; Moore *et al.*, 2000; Moran *et al.*, 2002; Somlyo and Somlyo, 2003). ROK is recruited to the PM of responsive cells upon rhoA translocation (Matsui *et al.*, 1996; Sin *et al.*, 1998; Amano *et al.*, 2000; Miyazaki *et al.*, 2006). The activation of ROK appears to involve trans-autophosphorylation and dimerization (Ishizaki *et al.*, 1996; Chen *et al.*, 2002). As mentioned, ROK can inactivate MLCP by phosphorylation of MYPT1 (see the following section) (Noda *et al.*, 1995; Kimura *et al.*, 1996). An ATP-competitive cell-permeable inhibitor of ROK (Y-27632) diminishes spontaneous and agonist-stimulated myometrial contractility *in vitro* (Fu *et al.*, 1998; Kupittayanant *et al.*, 2001; Tahara *et al.*, 2002). Further, agonist stimulation of uterine myocytes in culture promotes rhoA and ROK recruitment to the PM (Fig. 4) suggesting that these proteins play a role in agonist-induced contractions (Taggart *et al.*, 1999; Lee *et al.*, 2001). However, ongoing experiments in our laboratory indicate that the time course for $PMLC_{20}$ formation and rhoA activation in agonist-stimulated human uterine SMCs may differ significantly (unpublished data). In addition to its effects on MLCP, ROK can also directly phosphorylate MLC_{20} on Ser^{19} *in vitro* leading to enhancement in myosin ATPase activity (Amano *et al.*, 1996; Somlyo and Somlyo, 2003). The physiological relevance of this event has been questioned given that GTP-γ-S induced activation of rhoA did not increase the level of $PMLC_{20}$ nor contraction to any significant extent *in vivo*, in the absence of Ca^{2+} (Somlyo and Somlyo, 2000), suggesting that smMLCK remains a compulsory element in $PMLC_{20}$ formation.

Myosin light chain phosphatase

This key enzyme has been the subject of many recent reviews (Hartshorne *et al.*, 1998; Ceulemans and Bollen, 2004; Hartshorne *et al.*, 2004; Ito *et al.*, 2004; Matsumura and Hartshorne, 2007). The MLCP holoenzyme is a serine/threonine phosphatase that consists of three subunits. The catalytic subunit of 38 kDa is a member of the type 1 protein phosphatase family (PP1c) (Shirazi *et al.*, 1994). As with other members of this phosphatase family, it has broad substrate specificity and therefore the activity of the holoenzyme is determined mainly by the substrate targeting subunit (see below). There are many endogenous peptide inhibitors of the PP1c catalytic subunit but the physiological significance of these with respect to the holoenzyme is unclear (Cohen, 2002). Some evidence suggests that one such endogenous inhibitor may be relevant in myometrial SM. This inhibitor is termed CPI-17 (17-kDa-protein kinase C-potentiated inhibitor of PP1c) and is highly expressed in SM, including human myometrium (Ozaki *et al.*, 2003; Lartey *et al.*, 2007). The inhibitory effect of CPI-17 for the catalytic subunit of MLCP is

enhanced by several orders of magnitude through phosphorylation of Thr^{38} by PKC and also by ROK (Eto *et al*., 1995), suggesting that phosphorylation of CPI-17 is necessary to 'activate' this inhibitor.

MYPT1 (also known as the 'myosin-binding subunit' Gosser *et al*., 1997) is highly expressed in SM and has several isoforms resulting from splice variants of a single gene (Okubo *et al*., 1994; Shimizu *et al*., 1994; Dirksen *et al*., 2000; Ogut and Brozovich, 2000, Matsumura and Hartshorne, 2007). This subunit associates with PP1c through a PP-binding motif in its N-terminal region (Terrak *et al*., 2004). Its major function is to bind $PMLC_{20}$ and provide access to the catalytic subunit for removal of the phosphate moiety. Phosphorylation of MYPT1 is an important mechanism of regulation of MLCP activity. MYPT1 has two major phosphorylation sites (Thr^{696}, Thr^{853} in human sequence) that are targets for ROK (Kawano *et al*., 1999). Phosphorylation of Thr^{696} causes marked inhibition of PP1c activity, either by interacting with the catalytic site or by causing a conformational change (Hartshorne *et al*., 1998; Ito *et al*., 2004). Phosphorylation of Thr^{853} disrupts the $PMLC_{20}$ binding motif and thus reduces the ability of MLCP to associate with its target. Phosphorylation of either of these sites has also been shown to disrupt the ability of MYPT1 to target PP1c to a particular subcellular location (Noda *et al*., 1995; Ichikawa *et al*., 1996; Kimura *et al*., 1996; Hartshorne *et al*., 1998; Wu *et al*., 2005). It is not clear which of these sites is the predominant mediator of ROK-induced inhibition in uterine myocytes.

If they are physiologically relevant, the biochemical determinants mediating CS are likely opposed by mechanisms working to decrease the sensitivity of SM to Ca^{2+}. This concept is termed 'Ca^{2+}-desensitization' (CD). Some evidence suggests that CD can be achieved by inhibition of smMLCK through phosphorylation of an inhibitory site leading to a decreased affinity for CaM (Tansey *et al*., 1994); the candidate kinases in such a mechanism may be dependent on cyclic nucleotides (Murphy and Walker, 1998; Nakamura *et al*., 2007) and may depend on the expression of a specific isoform of MYPT1 (Payne *et al*., 2006). Further, these kinases may also target MYPT1 and potentially increase MLCP activity as part of CD and SM relaxation. For example, protein kinase G phosphorylates Ser^{695} of MYPT1 which causes relaxation, probably by interfering with basal phosphorylation of Thr^{696} (Nakamura *et al*., 2007). Further, phosphorylation by PKC of an undetermined residue in the N-terminal portion of MYPT1 reduced its affinity for PP1c and hence the activity of MLCP (Toth *et al*., 2000). The physiological relevance of CD remains elusive. However, implementation of such a mechanism in tissues such as the human myometrium would aid in ensuring a long period of dormancy during gestation. MYPT1 also can be phosphorylated by a host of other kinases but their physiological roles are uncertain. The variety of phosphorylation targets available on MYPT1 indicates that this protein may be a key convergence point for many signaling pathways involved in contractility modulation, which may be important in both the pregnant and non-pregnant uterus.

The third subunit of MLCP is a small peptide of approximately 20 kDa termed sm-M20. Although it may bind MLC_{20}, this does not affect the rate of phosphatase activity (Hartshorne *et al*., 1998). Its role is unknown.

Calcium sensitization in uterine SM

CS is becoming increasingly recognized as a potential functional mechanism for the regulation of uterine contractility. Most of the studies have been focused on the uterus during gestation but these same mechanisms may be equally applicable in the non-pregnant state. The mRNAs for rhoA, ROK-1 and ROK-2 are present in the non-gravid uterus and increase during pregnancy (Moore *et al*., 2000; Tahara *et al*., 2002; Kim *et al*., 2003; Riley *et al*., 2005a, b).

Further evidence supporting a physiological role for CS is provided by the presence of antagonism to this system during the quiescent phase of pregnancy. The rnd family of proteins (rnd1-3) consists of monomeric G-proteins with preferential affinity for GTP compared with GDP and with low GTPase activity. By diminishing the availability of GTP, they can interfere with rhoA–ROK interactions resulting in CD (Riento and Ridley, 2003). Protein levels of rnd2 and rnd3 are increased in human myometrium during pregnancy compared with tissues from non-pregnant women (Lartey *et al*., 2006). Conversely, when assessing mRNA levels using semi-quantitative techniques, pregnant rats had increased concentrations of all three rnd isoforms whereas, in human myometrium, the only increase in mRNA was for rnd1 (Kim *et al*., 2003). Although this area requires further study, the data are compatible with a role for rnd proteins regulating myometrial activity in pregnancy. Thus, pharmacological modulation of this system in non-pregnant subjects may present a therapeutic opportunity.

Various uterotonins have been evaluated for their ability to induce CS. This mechanism appears to be an important component of the potent contractile effects of OT on the human myometrium (Shmygol *et al*., 2006). Further, OT-stimulated contractions of human myometrium obtained at term elective Caesarean section are inhibited by the ROK inhibitor Y-27632 independently of the change in $[Ca^{2+}]_i$ (Woodcock *et al*., 2004). In addition, ROK inhibition impedes tension development and promotes relaxation without altering the level of $[Ca^{2+}]_i$ in spontaneous and agonist-stimulated contractions (Niiro *et al*., 1997; Vedernikov *et al*., 2000; Kupittayanant *et al*., 2001; Moran *et al*., 2002; Woodcock *et al*., 2004; Woodcock *et al*., 2006). Similar observations were made in rat muscle strips stimulated with carbachol (Oh *et al*., 2003). Finally, rhoA and ROK are translocated to the PM in freshly isolated myometrial cells stimulated with uterine agonists, indicating rhoA–ROK activation (Taggart *et al*., 1999). Taken together, these data argue for rhoA–ROK as mediating CS in myometrium of different species and, importantly, rhoA–ROK activity as being inducible by physiologically relevant stimuli.

On the other hand, there are some data that question the role of ROK in OT-induced contractions in human myometrium obtained at term elective Caesarean section. Y-27632 caused no significant attenuation of force in spontaneous contractions induced by a physiological dose (10 nM) of OT. However, when the muscle strips were pre-exposed to KCl, then treated with a higher dose of OT (100 nM) that is more likely to produce a tetanic contraction, there was a significant suppressive effect of the ROK inhibitor (Kupittayanant *et al*., 2001). This might suggest that the ROK pathway is more important in promoting force enhancement during tonic rather than phasic contractions. Clearly, more study is necessary to determine the importance of these pathways in basal or stimulated uterine myocyte contractile function.

$PGF_{2\alpha}$ has also been shown to induce CS in human myometrium (Woodcock *et al*., 2006) and in mouse tissues with the accompanying formation of GTP-rhoA (Tahara *et al*., 2005) again implicating rhoA–ROK as important mediators of CS. Upon $PGF_{2\alpha}$ stimulation of human

myometrial strips, peak $[Ca^{2+}]_i$ remains unchanged, but peak force of spontaneous contractions is significantly increased.

RhoA and ROK are not the only entities studied with regards to their potential involvement in myometrial CS. Activators or inhibitors of PKC might influence myometrial contractility in either the pregnant or non-pregnant states, perhaps through regulation of activity of CPI-17 (Ozaki *et al.*, 2003).

Interestingly, CS may not be the only mechanism for enhancing uterine contractility. The myometrium during late pregnancy is capable of producing larger forces per unit of $PMLC_{20}$ as compared with non-pregnant myometrium (Word *et al.*, 1993). Similar experiments in rats indicate that while pregnant tissues generate higher levels of absolute force, this was not due to a CS effect, but rather a sensitization of the system to $PMLC_{20}$ itself, although the mechanism of this phenomenon is not yet clear.

In summary, mechanisms of CS may be important therapeutic targets for regulation of uterine activity. However, despite the large volume of literature demonstrating the relationships between agonist stimulation and CS, there is little information regarding the physiological role of this mechanism in the uterus. This knowledge gap may be filled with the use of new research tools that are available to analyze the involvement of rhoA–ROK. Recently, mice with genetic deletions for ROK-1 (−/−), ROK-2 (−/−) and a heterozygous ROK-1 (+/−) ROK-2 (+/−) have been produced, although they have not yet been studied with regards to alterations in SM contractility or Ca^{2+} sensitivity (Thumkeo *et al.*, 2003; Shimizu *et al.*, 2005; Thumkeo *et al.*, 2005).

Therapeutic approaches to regulation of uterine contractility

Perhaps the most common gynecological problem associated with uterine motility is primary dysmenorrhea. There is reasonable evidence to support the efficacy of the usual treatments including the contraceptive pill (Wong *et al.*, 2009) or non-steroidal anti-inflammatory drugs (Marjoribanks *et al.*, 2003). The mechanisms of these therapies appear to be directed towards limiting the contractile stimuli to the uterus (through steroid hormonal effects of suppression of inflammatory stimuli) rather than directly interfering with the contractions themselves. Hence, the duration of the effects (and side-effects) of treatment may actually be longer than the duration of the increased uterine contractility resulting in the painful contractions. Furthermore, in view of the intense increases in intrauterine pressure that usually accompany dysmenorrhea, it is likely that it is the outer, predominant zone of the myometrium that is mediating the contractions rather than then inner junctional zone that may be the site of pathophysiology in the other important disorders including abnormal sperm transport, fertilization, implantation, endometriosis and ectopic pregnancy.

The recently developed concept that contractile activity in the non-pregnant uterus results from a distinct zone of the inner myometrium emphasizes our lack of understanding of this organ even at the level of its anatomy and histology. Understanding its physiology and pharmacology lags even further behind. Much additional research is necessary before therapeutic agents can be designed or attempted, to increase the clarity of the recommendation on the basis of strong evidence. Even with the greater volume of research information concerning uterine contractility in late gestation, most attempts to prevent or inhibit uterine contractions have had little, if any, beneficial effect and have resulted in common and serious side-effects (Mitchell and Olson, 2004). However, there are some considerations with fair supportive evidence as to where research into therapeutic manipulation of endometrial wave activity in the non-pregnant state could be undertaken immediately.

The strongest evidence regarding regulation of the junctional zone of the myometrium concerns the effects of ovarian steroids (Bulletti *et al.*, 1993; Kunz *et al.*, 1998; Fanchin *et al.*, 2000). Perhaps the research strategy with the greatest potential for success would be a systematic assessment of the effects of estradiol and/or progesterone (or their well-characterized antagonists) on endometrial waves at different stages of the reproductive cycle. There is almost a complete void of research data in this potentially fruitful area. Endpoints would include parameters that have both physiological as well as clinical relevance: effects on frequency, amplitude, duration and direction of wave propagations as well as measures of clinical effectiveness. Vaginal suppositories of progesterone will diminish uterine activity at the time of embryo transfer following *in vitro* fertilization (Fanchin *et al.*, 2001) but the effects on the rate of successful cycles has not been systematically evaluated.

An important pharmacological principle is to minimize potential toxicity by maximizing the specificity of the therapeutic agent for the target organ. OT is the most potent and specific contractile agonist and its receptor levels in non-pregnant rat uterine tissue are very high, similar to those at the time of parturition (Arthur *et al.*, 2008). More studies are required to determine the expression of the OT/OT receptor system specifically in the human and particularly in the junctional myometrium through the reproductive cycle. However, vaginally administered OT increases basal uterine tone as well as the frequency and amplitude of cervical–fundal contractions (Kunz *et al.*, 1998; Wildt *et al.*, 1998), but despite obvious potential use to aid sperm transport in normal or donor insemination cycles, it has never been assessed for therapeutic efficacy in this regard. This is an obvious area for increased clinical research. In addition, the possibility that new, orally active anti-oxytocic agents will have a role to play in treating these conditions involving the junctional myometrium or in alleviating dysmenorrhea needs to be appropriately investigated. In a recent case report, the anti-cholinergic hyoscine bromide (another antagonist of the pro-contractile pathway) was used to decrease the frequency of uterine peristalsis and appeared to be of benefit in three women with repeated failures with *in vitro* fertilization (Kido *et al.*, 2009).

At present, there are many well-characterized inhibitors and activators of many of the pathways described in this review. For example, Ca^{2+} channel blockers can effectively prevent the Ca^{2+} influx necessary to enable a contraction. Inhibitors of CaM and smMLCK have been thoroughly studied *in vitro* and have demonstrated the expected reduction in $PMLC_{20}$ levels. However, there currently are no antagonists of these proteins in use therapeutically. The energy supply could be disrupted using myosin ATPase inhibitors to reduce the rate of active cross bridge cycling. CS mechanisms can be manipulated using well-studied agents that are activators or inhibitors of rhoA, ROK or MLCP. As noted, stimulation of cAMP or cGMP can affect several key factors, particularly smMLCK and MYPT1, which can diminish uterine contractile activity. The concerns with all of these agents relate to their non-specificity and, as has been learned from their

use in pregnancy, the resulting potential for significant side-effects. Considering the centrality of many of these protein targets in mediating SM contractility in all muscle beds, it may be difficult to develop pharmacological tools with therapeutic efficacy for uterine disorders without significant advances in drug targeting technologies.

Conclusions and future perspectives

There have been major advances in the understanding of the molecular physiology of SM contractility over the past two decades. The vast majority of research has focused on vascular SM but there appear to be many commonalities with uterine SM. Over a similar time span there has been increasing evidence, using a variety of advanced technologies, describing changing patterns of uterine contractions through different phases of the menstrual cycle. A unique feature of uterine contractility in the non-pregnant state is the apparent change in direction of contractile waves depending on the stage of the reproductive cycle. Indirect evidence suggests this directionality may be important in a wide variety of diseases or dysfunctions of the reproductive system. Recent studies suggest the presence of a unique, subendometrial junctional zone of the myometrium that may generate and regulate these 'endometrial waves'.

There is a pressing need to more completely understand human myometrial contractile activity. This is particularly true concerning the important and unique aspects relating to the origin and direction of impulse of contractions. In addition, it will be necessary to design and validate delivery systems for therapeutic agents that will optimize effects on the uterine SM and minimize unwanted effects in other SM beds. These developments will hopefully lead to more successful approaches to diagnosis and management of enigmatic reproductive disorders including endometriosis, infertility and dysmenorrhea.

Funding

The authors gratefully acknowledge funding support from the Canadian Institutes of Health Research (MOP-81384: 2006-2011) and from the Alberta Heritage Foundation for Medical Research through a Major Equipment Grant (2007) and the Team Grant Program – Preterm Birth and Healthy Outcomes (#200700595).

References

Aaronson PI. TRPC Channel upregulation in chronically hypoxic pulmonary arteries: the HIF-1 bandwagon gathers steam. *Circ Res* 2006;**12**:1465–1467.

Abernethy DR, Soldatov NM. Structure-functional diversity of human L-type Ca2+ channel: perspectives for new pharmacological targets. *J Pharmacol Exp Ther* 2002;**3**:724–728.

Amano M, Ito M, Kimura K, Fukata Y, Chihara K, Nakano T, Matsuura Y, Kaibuchi K. Phosphorylation and activation of myosin by Rho-associated kinase (Rho-kinase). *J Biol Chem* 1996;**34**:20246–20249.

Amano M, Fukata Y, Kaibuchi K. Regulation and functions of Rho-associated kinase. *Exp Cell Res* 2000;**1**:44–51.

Andrews J, Blackshaw LA. Small intestinal motor and sensory function and dysfunction. In: Feldman M, Friedman LS, Brandt LJ (eds). *Sleisenger and Fordtran's Gastrointestinal and Liver Disease*. Saunders, 2006, 2093–2111.

Anwer K, Oberti C, Perez GJ, Perez-Reyes N, McDougall JK, Monga M, Sanborn BM, Stefani E, Toro L. Calcium-activated K+ channels as modulators of human myometrial contractile activity. *Am J Physiol* 1993;**265**(4 Pt 1):C976–C985.

Arner A, Pfitzer G. Regulation of cross-bridge cycling by Ca2+ in smooth muscle. *Rev Physiol Biochem Pharmacol* 1999;**134**:63–146.

Arthur P, Taggart MJ, Zielnik B, Wong S, Mitchell BF. Relationship between gene expression and function of utertonic systems in the rat during gestation, uterine activation and both term and preterm labour. *J Physiol* 2008;**Pt 24**:6063–6076.

Awad SS, Lamb HK, Morgan JM, Dunlop W, Gillespie JI. Differential expression of ryanodine receptor RyR2 mRNA in the non-pregnant and pregnant human myometrium. *Biochem J* 1997;**322**(Pt 3):777–783.

Ball A, Wang JW, Wong S, Zielnik B, Mitchell J, Wang N, Stemerman MB, Mitchell BF. Phorbol ester treatment of human myometrial cells suppresses expression of oxytocin receptor through a mechanism that does not involve activator protein-1. *Am J Physiol Endocrinol Metab* 2006;**5**:E922–E928.

Berridge MJ. Inositol trisphosphate and calcium signalling. *Nature* 1993;**6410**:315–325.

Blanks AM, Zhao ZH, Shmygol A, Bru-Mercier G, Astle S, Thornton S. Characterization of the molecular and electrophysiological properties of the T-type calcium channel in human myometrium. *J Physiol* 2007;**581**(Pt 3):915–926.

Bourmeyster N, Stasia MJ, Garin J, Gagnon J, Boquet P, Vignais PV. Copurification of rho protein and the rho-GDP dissociation inhibitor from bovine neutrophil cytosol. Effect of phosphoinositides on rho ADP-ribosylation by the C3 exoenzyme of Clostridium botulinum. *Biochemistry* 1992;**51**:12863–12869.

Boyle MB, Heslip LA. Voltage-dependent Na+ channel mRNA expression in pregnant myometrium. *Recept Channels* 1994;**3**:249–253.

Bradley AB, Morgan KG. Alterations in cytoplasmic calcium sensitivity during porcine coronary artery contractions as detected by aequorin. *J Physiol* 1987;**385**:437–448.

Brainard AM, Miller AJ, Martens JR, England SK. Maxi-K channels localize to caveolae in human myometrium: a role for an actin-channel-caveolin complex in the regulation of myometrial smooth muscle K+ current. *Am J Physiol Cell Physiol* 2005;**1**:C49–C57.

Brosens JJ, Barker FG, de Souza NM. Myometrial zonal differentiation and uterine junctional zone hyperplasia in the non-pregnant uterus. *Hum Reprod Update* 1998;**5**:496–502.

Bulletti C, de Ziegler D. Uterine contractility and embryo implantation. *Curr Opin Obstet Gynecol* 2006;**4**:473–484.

Bulletti C, Prefetto RA, Bazzocchi G, Romero R, Mimmi P, Polli V, Lanfranchi GA, Labate AM, Flamigni C. Electromechanical activities of human uteri during extra-corporeal perfusion with ovarian steroids. *Hum Reprod* 1993;**10**:1558–1563.

Bulletti C, D DEZ, Setti PL, Cicinelli E, Polli V, Flamigni C. The patterns of uterine contractility in normal menstruating women: from physiology to pathology. *Ann N Y Acad Sci* 2004;**1034**:64–83.

Burdyga T, Wray S, Noble K. In situ calcium signaling: no calcium sparks detected in rat myometrium. *Ann N Y Acad Sci* 2007;**1101**:85–96.

Bursztyn L, Eytan O, Jaffa AJ, Elad D. Modeling myometrial smooth muscle contraction. *Ann N Y Acad Sci* 2007;**1101**:110–138.

Ceulemans H, Bollen M. Functional diversity of protein phosphatase-1, a cellular economizer and reset button. *Physiol Rev* 2004;**1**:1–39.

Chen XQ, Tan I, Ng CH, Hall C, Lim L, Leung T. Characterization of RhoA-binding kinase ROKalpha implication of the pleckstrin homology domain in ROKalpha function using region-specific antibodies. *J Biol Chem* 2002;**15**:12680–12688.

Cohen PT. Protein phosphatase 1–targeted in many directions. *J Cell Sci* 2002;**Pt 2**:241–256.

Craig R, Smith R, Kendrick-Jones J. Light-chain phosphorylation controls the conformation of vertebrate non-muscle and smooth muscle myosin molecules. *Nature* 1983;**5907**:436–439.

Cretoiu D, Ciontea SM, Popescu LM, Ceafalan L, Ardeleanu C. Interstitial Cajal-like cells (ICLC) as steroid hormone sensors in human myometrium: immunocytochemical approach. *J Cell Mol Med* 2006; **3**:789–795.

Dalrymple A, Slater DM, Beech D, Poston L, Tribe RM. Molecular identification and localization of Trp homologues, putative calcium channels, in pregnant human uterus. *Mol Hum Reprod* 2002; **10**:946–951.

Dauvois S, White R, Parker MG. The antiestrogen ICI 182780 disrupts estrogen receptor nucleocytoplasmic shuttling. *J Cell Sci* 1993; **106**(Pt 4):1377–1388.

Devost D, Carrier ME, Zingg HH. Oxytocin-induced activation of eukaryotic elongation factor 2 in myometrial cells is mediated by protein kinase C. *Endocrinology* 2008;**1**:131–138.

Dillon PF, Aksoy MO, Driska SP, Murphy RA. Myosin phosphorylation and the cross-bridge cycle in arterial smooth muscle. *Science* 1981; **4481**:495–497.

Dirksen WP, Vladic F, Fisher SA. A myosin phosphatase targeting subunit isoform transition defines a smooth muscle developmental phenotypic switch. *Am J Physiol Cell Physiol* 2000;**3**:C589–C600.

Draeger A, Amos WB, Ikebe M, Small JV. The cytoskeletal and contractile apparatus of smooth muscle: contraction bands and segmentation of the contractile elements. *J Cell Biol* 1990;**6 Pt 1**:2463–2473.

Dzhura I, Wu Y, Colbran RJ, Balser JR, Anderson ME. Calmodulin kinase determines calcium-dependent facilitation of L-type calcium channels. *Nat Cell Biol* 2000;**3**:173–177.

Eddinger TJ, Meer DP. Myosin II isoforms in smooth muscle: heterogeneity and function. *Am J Physiol Cell Physiol* 2007;**2**:C493–C508.

Ellerbroek SM, Wennerberg K, Burridge K. Serine phosphorylation negatively regulates RhoA in vivo. *J Biol Chem* 2003;**21**:19023–19031.

Eto M, Ohmori T, Suzuki M, Furuya K, Morita F. A novel protein phosphatase-1 inhibitory protein potentiated by protein kinase C. Isolation from porcine aorta media and characterization. *J Biochem (Tokyo)* 1995;**6**:1104–1107.

Exton JH. Regulation of phosphoinositide phospholipases by hormones, neurotransmitters, and other agonists linked to G proteins. *Annu Rev Pharmacol Toxicol* 1996;**36**:481–509.

Fanchin R, Ayoubi JM, Olivennes F, Righini C, de Ziegler D, Frydman R. Hormonal influence on the uterine contractility during ovarian stimulation. *Hum Reprod* 2000;**15**(Suppl.1):90–100.

Fanchin R, Righini C, de Ziegler D, Olivennes F, Ledee N, Frydman R. Effects of vaginal progesterone administration on uterine contractility at the time of embryo transfer. *Fertil Steril* 2001;**6**:1136–1140.

Floyd R, Wray S. Calcium transporters and signalling in smooth muscles. *Cell Calcium* 2007;**4–5**:467–476.

Floyd R, Mobasheri A, Martin-Vasallo P, Wray S. Na,K-ATPase isoforms in pregnant and nonpregnant rat uterus. *Ann N Y Acad Sci* 2003; **986**:614–616.

Fu X, Gong MC, Jia T, Somlyo AV, Somlyo AP. The effects of the Rho-kinase inhibitor Y-27632 on arachidonic acid-, GTPgammaS-, and phorbol ester-induced Ca2+-sensitization of smooth muscle. *FEBS Lett* 1998;**1–2**:183–187.

Fujihara H, Walker LA, Gong MC, Lemichez E, Boquet P, Somlyo AV, Somlyo AP. Inhibition of RhoA translocation and calcium sensitization by in vivo ADP-ribosylation with the chimeric toxin DC3B. *Mol Biol Cell* 1997;**12**:2437–2447.

Fukumoto Y, Kaibuchi K, Hori Y, Fujioka H, Araki S, Ueda T, Kikuchi A, Takai Y. Molecular cloning and characterization of a novel type of regulatory protein (GDI) for the rho proteins, ras p21-like small GTP-binding proteins. *Oncogene* 1990;**9**:1321–1328.

Furuichi T, Yoshikawa S, Miyawaki A, Wada K, Maeda N, Mikoshiba K. Primary structure and functional expression of the inositol 1,4,5-trisphosphate-binding protein P400. *Nature* 1989;**6245**:32–38.

Gabella G. Structural apparatus for force transmission in smooth muscles. *Physiol Rev* 1984;**2**:455–477.

Garfield RE, Maner WL. Physiology and electrical activity of uterine contractions. *Semin Cell Dev Biol* 2007;**3**:289–295.

Garfield RE, Sims SM, Kannan MS, Daniel EE. Possible role of gap junctions in activation of myometrium during parturition. *Am J Physiol* 1978; **5**:C168–C179.

Garfield RE, Ali M, Yallampalli C, Izumi H. Role of gap junctions and nitric oxide in control of myometrial contractility. *Semin Perinatol* 1995; **1**:41–51.

Gaylinn BD, Eddinger TJ, Martino PA, Monical PL, Hunt DF, Murphy RA. Expression of nonmuscle myosin heavy and light chains in smooth muscle. *Am J Physiol* 1989;**257**(5 Pt 1):C997–C1004.

George AL Jr, Knittle TJ, Tamkun MM. Molecular cloning of an atypical voltage-gated sodium channel expressed in human heart and uterus: evidence for a distinct gene family. *Proc Natl Acad Sci USA* 1992; **11**:4893–4897.

Gherghiceanu M, Popescu LM. Interstitial Cajal-like cells (ICLC) in human resting mammary gland stroma. Transmission electron microscope (TEM) identification. *J Cell Mol Med* 2005;**4**:893–910.

Gill DL. Calcium signalling: receptor kinships revealed. *Nature* 1989; **6245**:16–18.

Gordon AM, Homsher E, Regnier M. Regulation of contraction in striated muscle. *Physiol Rev* 2000;**2**:853–924.

Gorecka A, Aksoy MO, Hartshorne DJ. The effect of phosphorylation of gizzard myosin on actin activation. *Biochem Biophys Res Commun* 1976; **1**:325–331.

Gosser YQ, Nomanbhoy TK, Aghazadeh B, Manor D, Combs C, Cerione RA, Rosen MK. C-terminal binding domain of Rho GDP-dissociation inhibitor directs N-terminal inhibitory peptide to GTPases. *Nature* 1997;**6635**:814–819.

Gunst SJ, Zhang W. Actin cytoskeletal dynamics in smooth muscle: a new paradigm for the regulation of smooth muscle contraction. *Am J Physiol Cell Physiol* 2008;**3**:C576–C587.

Hagiwara Y, Nishina Y, Yorifuji H, Kikuchi T. Immunolocalization of caveolin-1 and caveolin-3 in monkey skeletal, cardiac and uterine smooth muscles. *Cell Struct Funct* 2002;**5**:375–382.

Hai CM, Murphy RA. Cross-bridge phosphorylation and regulation of latch state in smooth muscle. *Am J Physiol* 1988;**254**(1 Pt 1): C99–C106.

Hai CM, Murphy RA. Ca2+, crossbridge phosphorylation, and contraction. *Annu Rev Physiol* 1989;**51**:285–298.

Hamada Y, Yanagisawa M, Katsuragawa Y, Coleman JR, Nagata S, Matsuda G, Masaki T. Distinct vascular and intestinal smooth muscle myosin heavy chain mRNAs are encoded by a single-copy gene in the chicken. *Biochem Biophys Res Commun* 1990;**1**:53–58.

Hancock JF, Hall A. A novel role for RhoGDI as an inhibitor of GAP proteins. *EMBO J* 1993;**5**:1915–1921.

Hartshorne DJ, Ito M, Erdodi F. Myosin light chain phosphatase: subunit composition, interactions and regulation. *J Muscle Res Cell Motil* 1998; **4**:325–341.

Hartshorne DJ, Ito M, Erdodi F. Role of protein phosphatase type 1 in contractile functions: myosin phosphatase. *J Biol Chem* 2004; **36**:37211–37214.

Hernandez OM, Jones M, Guzman G, Szczesna-Cordary D. Myosin essential light chain in health and disease. *Am J Physiol Heart Circ Physiol* 2007;**4**:H1643–H1654.

Hesse M, Magin TM, Weber K. Genes for intermediate filament proteins and the draft sequence of the human genome: novel keratin genes and a surprisingly high number of pseudogenes related to keratin genes 8 and 18. *J Cell Sci* 2001;**Pt 14**:2569–2575.

Hinescu ME, Popescu LM. Interstitial Cajal-like cells (ICLC) in human atrial myocardium. *J Cell Mol Med* 2005;**4**:972–975.

Hinescu ME, Gherghiceanu M, Mandache E, Ciontea SM, Popescu LM. Interstitial Cajal-like cells (ICLC) in atrial myocardium: ultrastructural and immunohistochemical characterization. *J Cell Mol Med* 2006; **1**:243–257.

Hinescu ME, Ardeleanu C, Gherghiceanu M, Popescu LM. Interstitial Cajal-like cells in human gallbladder. *J Mol Histol* 2007; **4**:275–284.

Hinescu ME, Popescu LM, Gherghiceanu M, Faussone-Pellegrini MS. Interstitial Cajal-like cells in rat mesentery: an ultrastructural and immunohistochemical approach. *J Cell Mol Med* 2008;**1**:260–270.

Hirata K, Kikuchi A, Sasaki T, Kuroda S, Kaibuchi K, Matsuura Y, Seki H, Saida K, Takai Y. Involvement of rho p21 in the GTP-enhanced calcium ion sensitivity of smooth muscle contraction. *J Biol Chem* 1992;**13**:8719–8722.

Hori Y, Kikuchi A, Isomura M, Katayama M, Miura Y, Fujioka H, Kaibuchi K, Takai Y. Post-translational modifications of the C-terminal region of the rho protein are important for its interaction with membranes and the stimulatory and inhibitory GDP/GTP exchange proteins. *Oncogene* 1991;**4**:515–522.

Hricak H, Alpers C, Crooks LE, Sheldon PE. Magnetic resonance imaging of the female pelvis: initial experience. *AJR Am J Roentgenol* 1983; **6**:1119–1128.

Huizinga JD, Lammers WJ. Gut peristalsis is governed by a multitude of cooperating mechanisms. *Am J Physiol Gastrointest Liver Physiol* 2009; **1**:G1–G8.

Huszar G, Naftolin F. The myometrium and uterine cervix in normal and preterm labor. *N Engl J Med* 1984;**9**:571–581.

Ichikawa K, Ito M, Hartshorne DJ. Phosphorylation of the large subunit of myosin phosphatase and inhibition of phosphatase activity. *J Biol Chem* 1996;**9**:4733–4740.

Ijland MM, Evers JL, Dunselman GA, van Katwijk C, Lo CR, Hoogland HJ. Endometrial wavelike movements during the menstrual cycle. *Fertil Steril* 1996;**4**:746–749.

Ikebe M, Inagaki M, Kanamaru K, Hidaka H. Phosphorylation of smooth muscle myosin light chain kinase by Ca2 + -activated, phospholipid-dependent protein kinase. *J Biol Chem* 1985;**8**: 4547–4550.

Ikebe M, Hartshorne DJ, Elzinga M. Identification phosphorylation dephosphorylation of a second site for myosin light chain kinase on the 20000-dalton light chain of smooth muscle myosin. *J Biol Chem* 1986;**1**:36–39.

Ikebe M, Hartshorne DJ, Elzinga M. Phosphorylation of the 20,000-dalton light chain of smooth muscle myosin by the calcium-activated, phospholipid-dependent protein kinase. Phosphorylation sites and effects of phosphorylation. *J Biol Chem* 1987;**20**:9569–9573.

Ikebe M, Koretz J, Hartshorne DJ. Effects of phosphorylation of light chain residues threonine 18 and serine 19 on the properties and conformation of smooth muscle myosin. *J Biol Chem* 1988; **13**:6432–6437.

Inoue Y, Sperelakis N. Gestational change in Na+ and Ca2+ channel current densities in rat myometrial smooth muscle cells. *Am J Physiol* 1991;**3 Pt 1**:C658–C663.

Inoue Y, Nakao K, Okabe K, Izumi H, Kanda S, Kitamura K, Kuriyama H. Some electrical properties of human pregnant myometrium. *Am J Obstet Gynecol* 1990;**4**:1090–1098.

Inoue Y, Okabe K, Soeda H. Augmentation and suppression of action potentials by estradiol in the myometrium of pregnant rat. *Can J Physiol Pharmacol* 1999;**6**:447–453.

Ishizaki T, Maekawa M, Fujisawa K, Okawa K, Iwamatsu A, Fujita A, Watanabe N, Saito Y, Kakizuka A, Morii N *et al.* The small GTP-binding protein Rho binds to and activates a 160 kDa Ser/Thr protein kinase homologous to myotonic dystrophy kinase. *EMBO J* 1996;**8**:1885–1893.

Ito M, Nakano T, Erdodi F, Hartshorne DJ. Myosin phosphatase: structure, regulation and function. *Mol Cell Biochem* 2004;**1–2**:197–209.

Jmari K, Mironneau C, Mironneau J. Inactivation of calcium channel current in rat uterine smooth muscle: evidence for calcium- and voltage-mediated mechanisms. *J Physiol* 1986;**380**:111–126.

Johnson JD, Snyder C, Walsh M, Flynn M. Effects of myosin light chain kinase and peptides on Ca2+ exchange with the N- and C-terminal Ca2+ binding sites of calmodulin. *J Biol Chem* 1996;**2**:761–767.

Jones K, Shmygol A, Kupittayanant S, Wray S. Electrophysiological characterization and functional importance of calcium-activated chloride channel in rat uterine myocytes. *Pflugers Arch* 2004;**1**:36–43.

Kamm KE, Stull JT. Dedicated myosin light chain kinases with diverse cellular functions. *J Biol Chem* 2001;**7**:4527–4530.

Kawano Y, Fukata Y, Oshiro N, Amano M, Nakamura T, Ito M, Matsumura F, Inagaki M, Kaibuchi K. Phosphorylation of myosin-binding subunit (MBS) of myosin phosphatase by Rho-kinase in vivo. *J Cell Biol* 1999;**5**:1023–1038.

Khan RN, Smith SK, Morrison JJ, Ashford ML. Ca2+ dependence and pharmacology of large-conductance K+ channels in nonlabor and labor human uterine myocytes. *Am J Physiol* 1997;**273**(5 Pt 1):C1721–C1731.

Khan R, Matharoo-Ball B, Arulkumaran S, Ashford M. Potassium channels in the human myometrium. *Exp Physiol* 2001a;**2**:255–264.

Khan RN, Matharoo-Ball B, Arulkumaran S, Ashford ML. Potassium channels in the human myometrium. *Exp Physiol* 2001b;**2**:255–264.

Kido A, Togashi K, Hatayama H, Nakayama T, Yamamoto A, Kataoka M, Tulandi T. Uterine peristalsis in women with repeated IVF failures: possible therapeutic effect of hyoscine bromide. *J Obstet Gynaecol Can* 2009;**8**:732–735.

Kim YS, Kim B, Karaki H, Hori M, Ozaki H. Up-regulation of Rnd1 during pregnancy serves as a negative-feedback control for Ca2+ sensitization of contractile elements in rat myometrium. *Biochem Biophys Res Commun* 2003;**4**:972–978.

Kimura K, Ito M, Amano M, Chihara K, Fukata Y, Nakafuku M, Yamamori B, Feng J, Nakano T, Okawa K *et al.* Regulation of myosin phosphatase by Rho and Rho-associated kinase (Rho-kinase). *Science* 1996;**5272**:245–248.

Kitazawa T, Kobayashi S, Horiuti K, Somlyo AV, Somlyo AP. Receptor-coupled permeabilized smooth muscle. Role of the phosphatidylinositol cascade, G-proteins, and modulation of the contractile response to Ca2+. *J Biol Chem* 1989;**10**:5339–5342.

Kitazawa T, Masuo M, Somlyo AP. G protein-mediated inhibition of myosin light-chain phosphatase in vascular smooth muscle. *Proc Natl Acad Sci USA* 1991;**20**:9307–9310.

Klages B, Brandt U, Simon MI, Schultz G, Offermanns S. Activation of G12/G13 results in shape change and Rho/Rho-kinase-mediated myosin light chain phosphorylation in mouse platelets. *J Cell Biol* 1999; **4**:745–754.

Kordowska J, Huang R, Wang CL. Phosphorylation of caldesmon during smooth muscle contraction and cell migration or proliferation. *J Biomed Sci* 2006;**2**:159–172.

Kozasa T, Jiang X, Hart MJ, Sternweis PM, Singer WD, Gilman AG, Bollag G, Sternweis PC. p115 RhoGEF, a GTPase activating protein for Galpha12 and Galpha13. *Science* 1998;**5372**:2109–2111.

Ku CY, Word RA, Sanborn BM. Differential expression of protein kinase A, AKAP79, and PP2B in pregnant human myometrial membranes prior to and during labor. *J Soc Gynecol Investig* 2005;**6**:421–427.

Kumar CC, Mohan SR, Zavodny PJ, Narula SK, Leibowitz PJ. Characterization and differential expression of human vascular smooth muscle myosin light chain 2 isoform in nonmuscle cells. *Biochemistry* 1989;**9**:4027–4035.

Kunz G, Noe M, Herbertz M, Leyendecker G. Uterine peristalsis during the follicular phase of the menstrual cycle: effects of oestrogen, antioestrogen and oxytocin. *Hum Reprod Update* 1998;**5**:647–654.

Kupittayanant S, Burdyga T, Wray S. The effects of inhibiting Rho-associated kinase with Y-27632 on force and intracellular calcium in human myometrium. *Pflugers Arch* 2001;**1**:112–114.

Kupittayanant S, Luckas MJ, Wray S. Effect of inhibiting the sarcoplasmic reticulum on spontaneous and oxytocin-induced contractions of human myometrium. *BJOG* 2002;**3**:289–296.

Lajat S, Harbon S, Tanfin Z. Carbachol-induced desensitization of PLC-beta pathway in rat myometrium: downregulation of Gqalpha/G11alpha. *Am J Physiol* 1998;**275**(3 Pt 1):C636–C645.

Lang P, Gesbert F, Delespine-Carmagnat M, Stancou R, Pouchelet M, Bertoglio J. Protein kinase A phosphorylation of RhoA mediates the morphological and functional effects of cyclic AMP in cytotoxic lymphocytes. *EMBO J* 1996;**3**:510–519.

Lartey J, Gampel A, Pawade J, Mellor H, Bernal AL. Expression of RND proteins in human myometrium. *Biol Reprod* 2006;**3**:452–461.

Lartey J, Smith M, Pawade J, Strachan B, Mellor H, Lopez Bernal A. Up-regulation of myometrial RHO effector proteins (PKN1 and DIAPH1) and CPI-17 (PPP1R14A) phosphorylation in human pregnancy is associated with increased GTP-RHOA in spontaneous preterm labor. *Biol Reprod* 2007;**6**:971–982.

Ledoux J, Werner ME, Brayden JE, Nelson MT. Calcium-activated potassium channels and the regulation of vascular tone. *Physiology (Bethesda)* 2006;**21**:69–78.

Lee YH, Hwang MK, Morgan KG, Taggart MJ. Receptor-coupled contractility of uterine smooth muscle: from membrane to myofilaments. *Exp Physiol* 2001;**2**:283–288.

Leung T, Chen XQ, Manser E, Lim L. The p160 RhoA-binding kinase ROK alpha is a member of a kinase family and is involved in the reorganization of the cytoskeleton. *Mol Cell Biol* 1996;**10**:5313–5327.

Li QF, Spinelli AM, Wang R, Anfinogenova Y, Singer HA, Tang DD. Critical role of vimentin phosphorylation at Ser-56 by p21-activated kinase in vimentin cytoskeleton signaling. *J Biol Chem* 2006;**45**:34716–34724.

Longbottom ER, Luckas MJ, Kupittayanant S, Badrick E, Shmigol T, Wray S. The effects of inhibiting myosin light chain kinase on contraction and calcium signalling in human and rat myometrium. *Pflugers Arch* 2000;**2**:315–321.

Luckas MJ, Taggart MJ, Wray S. Intracellular calcium stores and agonist-induced contractions in isolated human myometrium. *Am J Obstet Gynecol* 1999;**2**:468–476.

Mandache E, Popescu LM, Gherghiceanu M. Myocardial interstitial Cajal-like cells (ICLC) and their nanostructural relationships with intercalated discs: shed vesicles as intermediates. *J Cell Mol Med* 2007;**5**:1175–1184.

Marjoribanks J, Proctor ML, Farquhar C. Nonsteroidal anti-inflammatory drugs for primary dysmenorrhoea. *Cochrane Database Syst Rev* 2003;**4**:CD001751.

Martin C, Chapman KE, Thornton S, Ashley RH. Changes in the expression of myometrial ryanodine receptor mRNAs during human pregnancy. *Biochim Biophys Acta* 1999;**2–3**:343–352.

Matsui T, Amano M, Yamamoto T, Chihara K, Nakafuku M, Ito M, Nakano T, Okawa K, Iwamatsu A, Kaibuchi K. Rho-associated kinase, a novel serine/threonine kinase, as a putative target for small GTP binding protein Rho. *EMBO J* 1996;**9**:2208–2216.

Matsumura F, Hartshorne DJ. Myosin phosphatase target subunit: Many roles in cell function. *Biochem Biophys Res Commun* 2008;**1**:149–156.

Maul H, Maner WL, Saade GR, Garfield RE. The physiology of uterine contractions. *Clin Perinatol* 2003;**4**:665–676. v.

McCallum LA, Greenwood IA, Tribe RM. Expression and function of K(v)7 channels in murine myometrium throughout oestrous cycle. *Pflugers Arch* 2009;**5**:1111–1120.

McCarron JG, MacMillan D, Bradley KN, Chalmers S, Muir TC. Origin and mechanisms of Ca2+ waves in smooth muscle as revealed by localized photolysis of caged inositol 1,4,5-trisphosphate. *J Biol Chem* 2004;**9**:8417–8427.

McDonald TF, Pelzer S, Trautwein W, Pelzer DJ. Regulation and modulation of calcium channels in cardiac, skeletal, and smooth muscle cells. *Physiol Rev* 1994;**2**:365–507.

Mitchell BF, Olson DM. Prostaglandin endoperoxide H synthase inhibitors and other tocolytics in preterm labour. *Prostaglandins Leukot Essent Fatty Acids* 2004;**2**:167–187.

Mitchell BF, Taggart MJ. Are animal models relevant to key aspects of human parturition? *Am J Physiol Regul Integr Comp Physiol* 2009;**3**:R525–R545.

Miyazaki K, Komatsu S, Ikebe M. Dynamics of RhoA and ROKalpha translocation in single living cells. *Cell Biochem Biophys* 2006;**3**:243–254.

Miyoshi H, Yamaoka K, Garfield RE, Ohama K. Identification of a non-selective cation channel current in myometrial cells isolated from pregnant rats. *Pflugers Arch* 2004;**4**:457–464.

Moller JV, Juul B, le Maire M. Structural organization, ion transport, and energy transduction of P-type ATPases. *Biochim Biophys Acta* 1996;**1**:1–51.

Moore F, Da Silva C, Wilde JI, Smarason A, Watson SP, Lopez Bernal A. Up-regulation of p21- and RhoA-activated protein kinases in human pregnant myometrium. *Biochem Biophys Res Commun* 2000;**2**:322–326.

Moran CJ, Friel AM, Smith TJ, Cairns M, Morrison JJ. Expression and modulation of Rho kinase in human pregnant myometrium. *Mol Hum Reprod* 2002;**2**:196–200.

Morano I. Tuning smooth muscle contraction by molecular motors. *J Mol Med* 2003;**8**:481–487.

Morgan KG, Gangopadhyay SS. Invited review: cross-bridge regulation by thin filament-associated proteins. *J Appl Physiol* 2001;**2**:953–962.

Murphy RA, Walker JS. Inhibitory mechanisms for cross-bridge cycling: the nitric oxide-cGMP signal transduction pathway in smooth muscle relaxation. *Acta Physiol Scand* 1998;**4**:373–380.

Nakamura K, Koga Y, Sakai H, Homma K, Ikebe M. cGMP-dependent relaxation of smooth muscle is coupled with the change in the phosphorylation of myosin phosphatase. *Circ Res* 2007;**7**:712–722.

Niiro N, Nishimura J, Sakihara C, Nakano H, Kanaide H. Up-regulation of rho A and rho-kinase mRNAs in the rat myometrium during pregnancy. *Biochem Biophys Res Commun* 1997;**2**:356–359.

Noble K, Zhang J, Wray S. Lipid rafts, the sarcoplasmic reticulum and uterine calcium signalling: and integrated approach. *J Physiol* 2006:**Pt 1**:29–35.

Noble K, Matthew A, Burdyga T, Wray S. A review of recent insights into the role of the sarcoplasmic reticulum and Ca entry in uterine smooth muscle. *Eur J Obstet Gynecol Reprod Biol* 2009;S11–S19.

Noda M, Yasuda-Fukazawa C, Moriishi K, Kato T, Okuda T, Kurokawa K, Takuwa Y. Involvement of rho in GTP gamma S-induced enhancement of phosphorylation of 20 kDa myosin light chain in vascular smooth muscle cells: inhibition of phosphatase activity. *FEBS Lett* 1995;**3**:246–250.

Noe M, Kunz G, Herbertz M, Mall G, Leyendecker G. The cyclic pattern of the immunocytochemical expression of oestrogen and progesterone receptors in human myometrial and endometrial layers: characterization of the endometrial-subendometrial unit. *Hum Reprod* 1999;**1**:190–197.

Ogut O, Brozovich FV. Determinants of the contractile properties in the embryonic chicken gizzard and aorta. *Am J Physiol Cell Physiol* 2000; **6**:C1722–C1732.

Oh JH, You SK, Hwang MK, Ahn DS, Kwon SC, Taggart MJ, Lee YH. Inhibition of rho-associated kinase reduces MLC20 phosphorylation and contractility of intact myometrium and attenuates agonist-induced Ca2+ sensitization of force of permeabilized rat myometrium. *J Vet Med Sci* 2003;**1**:43–50.

Ohkubo T, Inoue Y, Kawarabayashi T, Kitamura K. Identification and electrophysiological characteristics of isoforms of T-type calcium channel Ca(v)3.2 expressed in pregnant human uterus. *Cell Physiol Biochem* 2005;**4–6**:245–254.

Okubo S, Ito M, Takashiba Y, Ichikawa K, Miyahara M, Shimizu H, Konishi T, Shima H, Nagao M, Hartshorne DJ *et al.* A regulatory subunit of smooth muscle myosin bound phosphatase. *Biochem Biophys Res Commun* 1994;**1**:429–434.

Onishi H, Wakabayashi T. Electron microscopic studies of myosin molecules from chicken gizzard muscle I: the formation of the intramolecular loop in the myosin tail. *J Biochem* 1982;**3**: 871–879.

Onishi H, Wakabayashi T, Kamata T, Watanabe S. Electron microscopic studies of myosin molecules from chicken gizzard muscle II: The effect of thiophosphorylation of the 20K-dalton light chain on the ATP-induced change in the conformation of myosin monomers. *J Biochem* 1983;**4**:1147–1154.

Ozaki H, Yasuda K, Kim YS, Egawa M, Kanzaki H, Nakazawa H, Hori M, Seto M, Karaki H. Possible role of the protein kinase C/CPI-17 pathway in the augmented contraction of human myometrium after gestation. *Br J Pharmacol* 2003;**7**:1303–1312.

Parisi JA, Eddinger TJ. Smooth muscle myosin heavy chain isoform distribution in the swine stomach. *J Histochem Cytochem* 2002; **3**:385–393.

Paul RJ. The role of phospholamban and SERCA3 in regulation of smooth muscle-endothelial cell signalling mechanisms: evidence from gene-ablated mice. *Acta Physiol Scand* 1998;**4**:589–597.

Payne MC, Zhang HY, Prosdocimo T, Joyce KM, Koga Y, Ikebe M, Fisher SA. Myosin phosphatase isoform switching in vascular smooth muscle development. *J Mol Cell Cardiol* 2006;**2**:274–282.

Penniston JT, Enyedi A. Modulation of the plasma membrane Ca2+ pump. *J Membr Biol* 1998;**2**:101–109.

Phaneuf S, Europe-Finner GN, Varney M, MacKenzie IZ, Watson SP, Lopez Bernal A. Oxytocin-stimulated phosphoinsitide hydrolysis in human myometrial cells: involvement of pertussis toxin-sensitive and -insensitive G-proteins. *J Endocrinol* 1993;**136**:497–509.

Popescu LM, Gherghiceanu M, Cretoiu D, Radu E. The connective connection: interstitial cells of Cajal (ICC) and ICC-like cells establish synapses with immunoreactive cells. Electron microscope study in situ. *J Cell Mol Med* 2005;**3**:714–730.

Popescu LM, Gherghiceanu M, Hinescu ME, Cretoiu D, Ceafalan L, Regalia T, Popescu AC, Ardeleanu C, Mandache E. Insights into the interstitium of ventricular myocardium: interstitial Cajal-like cells (ICLC). *J Cell Mol Med* 2006;**2**:429–458.

Popescu LM, Ciontea SM, Cretoiu D. Interstitial Cajal-like cells in human uterus and fallopian tube. *Ann N Y Acad Sci* 2007;139–165.

Radu E, Regalia T, Ceafalan L, Andrei F, Cretoiu D, Popescu LM. Cajal-type cells from human mammary gland stroma: phenotype characteristics in cell culture. *J Cell Mol Med* 2005;**3**:748–752.

Read PW, Liu X, Longenecker K, Dipierro CG, Walker LA, Somlyo AV, Somlyo AP, Nakamoto RK. Human RhoA/RhoGDI complex expressed in yeast: GTP exchange is sufficient for translocation of RhoA to liposomes. *Protein Sci* 2000;**2**:376–386.

Riento K, Ridley AJ. Rocks: multifunctional kinases in cell behaviour. *Nat Rev Mol Cell Biol* 2003;**6**:446–456.

Riley M, Baker PN, Tribe RM, Taggart MJ. Expression of scaffolding, signalling and contractile-filament proteins in human myometria: effects of pregnancy and labour. *J Cell Mol Med* 2005a;**1**:122–134.

Riley M, Wu X, Baker PN, Taggart MJ. Gestational-dependent changes in the expression of signal transduction and contractile filament-associated proteins in mouse myometrium. *J Soc Gynecol Investig* 2005b;**5**:e33–e43.

Sanborn BM. Ion channels and the control of myometrial electrical activity. *Semin Perinatol* 1995;**1**:31–40.

Sanborn BM. Relationship of ion channel activity to control of myometrial calcium. *J Soc Gynecol Investig* 2000;**1**:4–11.

Sawada N, Itoh H, Yamashita J, Doi K, Inoue M, Masatsugu K, Fukunaga Y, Sakaguchi S, Sone M, Yamahara K *et al.* cGMP-dependent protein kinase phosphorylates and inactivates RhoA. *Biochem Biophys Res Commun* 2001;**3**:798–805.

Schuhmann K, Romanin C, Baumgartner W, Groschner K. Intracellular Ca2+ inhibits smooth muscle L-type Ca2+ channels by activation of protein phosphatase type 2B by direct interaction with the channel. *J Gen Physiol* 1997;**5**:503–513.

Sergeant GP, Hollywood MA, McCloskey KD, Thornbury KD, McHale NG. Specialised pacemaking cells in the rabbit urethra. *J Physiol* 2000;**526**(Pt 2):359–366.

Shimizu H, Ito M, Miyahara M, Ichikawa K, Okubo S, Konishi T, Naka M, Tanaka T, Hirano K, Hartshorne DJ *et al.* Characterization of the myosin-binding subunit of smooth muscle myosin phosphatase. *J Biol Chem* 1994;**48**:30407–30411.

Shimizu Y, Thumkeo D, Keel J, Ishizaki T, Oshima H, Oshima M, Noda Y, Matsumura F, Taketo MM, Narumiya S. ROCK-I regulates closure of the eyelids and ventral body wall by inducing assembly of actomyosin bundles. *J Cell Biol* 2005;**6**:941–953.

Shirazi A, Iizuka K, Fadden P, Mosse C, Somlyo AP, Somlyo AV, Haystead TA. Purification and characterization of the mammalian myosin light chain phosphatase holoenzyme. The differential effects of the holoenzyme and its subunits on smooth muscle. *J Biol Chem* 1994; **50**:31598–31606.

Shmigol A, Eisner DA, Wray S. Carboxyeosin decreases the rate of decay of the [Ca2+]*i* transient in uterine smooth muscle cells isolated from pregnant rats. *Pflugers Arch* 1998;**1**:158–160.

Shmigol AV, Eisner DA, Wray S. The role of the sarcoplasmic reticulum as a Ca2+ sink in rat uterine smooth muscle cells. *J Physiol* 1999; **520**(Pt 1):153–163.

Shmygol A, Gullam J, Blanks A, Thornton S. Multiple mechanisms involved in oxytocin-induced modulation of myometrial contractility. *Acta Pharmacol Sin* 2006;**7**:827–832.

Shojo H, Kaneko Y. Oxytocin-induced phosphorylation of myosin light chain is mediated by extracellular calcium influx in pregnant rat myometrium. *J Mol Recognit* 2001;**6**:401–405.

Sin WC, Chen XQ, Leung T, Lim L. RhoA-binding kinase alpha translocation is facilitated by the collapse of the vimentin intermediate filament network. *Mol Cell Biol* 1998;**11**:6325–6339.

Smith R. Parturition. *N Engl J Med* 2007;**3**:271–283.

Somlyo AP, Somlyo AV. Signal transduction and regulation in smooth muscle. *Nature* 1994;**6503**:231–236.

Somlyo AP, Somlyo AV. From pharmacomechanical coupling to G-proteins and myosin phosphatase. *Acta Physiol Scand* 1998; **4**:437–448.

Somlyo AP, Somlyo AV. Signal transduction by G-proteins, rho-kinase and protein phosphatase to smooth muscle and non-muscle myosin II. *J Physiol* 2000;**522**(Pt 2):177–185.

Somlyo AP, Somlyo AV. Ca2+ sensitivity of smooth muscle nonmuscle myosin II: modulated by G proteins kinases myosin phosphatase. *Physiol Rev* 2003;**4**:1325–1358.

Sperelakis N, Inoue Y, Ohya Y. Fast Na+ channels in smooth muscle from pregnant rat uterus. *Can J Physiol Pharmacol* 1992a;**4**:491–500.

Sperelakis N, Inoue Y, Ohya Y. Fast Na+ channels and slow Ca2+ current in smooth muscle from pregnant rat uterus. *Jpn J Pharmacol* 1992b;**114**:96P–106P.

Streb H, Irvine RF, Berridge MJ, Schulz I. Release of Ca2+ from a nonmitochondrial intracellular store in pancreatic acinar cells by inositol-1,4,5-trisphosphate. *Nature* 1983;**5938**:67–69.

Stull JT, Tansey MG, Tang DC, Word RA, Kamm KE. Phosphorylation of myosin light chain kinase: a cellular mechanism for Ca2+ desensitization. *Mol Cell Biochem* 1993;**127–128**:229–237.

Stull JT, Lin PJ, Krueger JK, Trewhella J, Zhi G. Myosin light chain kinase: functional domains and structural motifs. *Acta Physiol Scand* 1998; **4**:471–482.

Suciu L, Popescu LM, Gherghiceanu M. Human placenta: de visu demonstration of interstitial Cajal-like cells. *J Cell Mol Med* 2007; **3**:590–597.

Szymanski PT. Calponin (CaP) as a latch-bridge protein–a new concept in regulation of contractility in smooth muscles. *J Muscle Res Cell Motil* 2004;**1**:7–19.

Taggart MJ, Morgan KG. Regulation of the uterine contractile apparatus and cytoskeleton. *Semin Cell Dev Biol* 2007;**3**:296–304.

Taggart MJ, Wray S. Agonist mobilization of sarcoplasmic reticular calcium in smooth muscle: functional coupling to the plasmalemmal Na+/ Ca2+ exchanger? *Cell Calcium* 1997;**5**:333–341.

Taggart MJ, Wray S. Contribution of sarcoplasmic reticular calcium to smooth muscle contractile activation: gestational dependence in isolated rat uterus. *J Physiol* 1998;**511**(Pt 1):133–144.

Taggart MJ, Lee YH, Morgan KG. Cellular redistribution of PKCalpha, rhoA, and ROKalpha following smooth muscle agonist stimulation. *Exp Cell Res* 1999;**1**:92–101.

Taggart MJ, Leavis P, Feron O, Morgan KG. Inhibition of PKCalpha and rhoA translocation in differentiated smooth muscle by a caveolin scaffolding domain peptide. *Exp Cell Res* 2000;**1**:72–81.

Tahara M, Morishige K, Sawada K, Ikebuchi Y, Kawagishi R, Tasaka K, Murata Y. RhoA/Rho-kinase cascade is involved in oxytocin-induced rat uterine contraction. *Endocrinology* 2002;**3**:920–929.

Tahara M, Kawagishi R, Sawada K, Morishige K, Sakata M, Tasaka K, Murata Y. Tocolytic effect of a Rho-kinase inhibitor in a mouse model of lipopolysaccharide-induced preterm delivery. *Am J Obstet Gynecol* 2005;**3**:903–908.

Takashima S. Phosphorylation of myosin regulatory light chain by myosin light chain kinase, and muscle contraction. *Circ J* 2009;**2**:208–213.

Tang DD. Intermediate filaments in smooth muscle. *Am J Physiol Cell Physiol* 2008;**4**:C869–C878.

Tansey MG, Luby-Phelps K, Kamm KE, Stull JT. Ca(2+)-dependent phosphorylation of myosin light chain kinase decreases the Ca2+ sensitivity of light chain phosphorylation within smooth muscle cells. *J Biol Chem* 1994;**13**:9912–9920.

Taubman MB, Grant JW, Nadal-Ginard B. Cloning and characterization of mammalian myosin regulatory light chain (RLC) cDNA: the RLC gene is expressed in smooth, sarcomeric, and nonmuscle tissues. *J Cell Biol* 1987;**6**:1505–1513.

Taylor SJ, Chae HZ, Rhee SG, Exton JH. Activation of the beta 1 isozyme of phospholipase C by alpha subunits of the Gq class of G proteins. *Nature* 1991;**6318**:516–518.

Terrak M, Kerff F, Langsetmo K, Tao T, Dominguez R. Structural basis of protein phosphatase 1 regulation. *Nature* 2004;**6993**:780–784.

Thumkeo D, Keel J, Ishizaki T, Hirose M, Nonomura K, Oshima H, Oshima M, Taketo MM, Narumiya S. Targeted disruption of the mouse rho-associated kinase 2 gene results in intrauterine growth retardation and fetal death. *Mol Cell Biol* 2003;**14**:5043–5055.

Thumkeo D, Shimizu Y, Sakamoto S, Yamada S, Narumiya S. ROCK-I and ROCK-II cooperatively regulate closure of eyelid and ventral body wall in mouse embryo. *Genes Cells* 2005;**8**:825–834.

Tong D, Lu X, Wang HX, Plante I, Lui E, Laird DW, Bai D, Kidder GM. A dominant loss-of-function GJA1 (Cx43) mutant impairs parturition in the mouse. *Biol Reprod* 2009;**6**:1099–1106.

Toth A, Kiss E, Gergely P, Walsh MP, Hartshorne DJ, Erdodi F. Phosphorylation of MYPT1 by protein kinase C attenuates interaction with PP1 catalytic subunit and the 20 kDa light chain of myosin. *FEBS Lett* 2000;**2**:113–117.

Tribe RM, Moriarty P, Poston L. Calcium homeostatic pathways change with gestation in human myometrium. *Biol Reprod* 2000; **3**:748–755.

van Gestel I, MM IJ, Hoogland HJ, Evers JL. Endometrial wave-like activity in the non-pregnant uterus. *Hum Reprod Update* 2003; **2**:131–138.

Vedernikov YP, Mayes M, Moore E, Gei A, Saade GR, Garfield RE. The effects of pregnancy and smooth muscle contractility on cervical distensibility in the rat. *Am J Obstet Gynecol* 2000;**4**:905–908.

Venkatachalam K, van Rossum DB, Patterson RL, Ma HT, Gill DL. The cellular and molecular basis of store-operated calcium entry. *Nat Cell Biol* 2002;**11**:E263–E272.

Wang R, Li Q, Tang DD. Role of vimentin in smooth muscle force development. *Am J Physiol Cell Physiol* 2006;**3**:C483–C489.

Weiss S, Jaermann T, Schmid P, Staempfli P, Boesiger P, Niederer P, Caduff R, Bajka M. Three-dimensional fiber architecture of the nonpregnant human uterus determined ex vivo using magnetic resonance diffusion tensor imaging. *Anat Rec A Discov Mol Cell Evol Biol* 2006;**1**:84–90.

Wildt L, Kissler S, Licht P, Becker W. Sperm transport in the human female genital tract and its modulation by oxytocin as assessed by hysterosalpingoscintigraphy, hysterotonography, electrohysterography and Doppler sonography. *Hum Reprod Update* 1998;**5**:655–666.

Wong CL, Farquhar C, Roberts H, Proctor M. Oral contraceptive pill as treatment for primary dysmenorrhoea. *Cochrane Database Syst Rev* 2009;**2**:CD002120.

Woodcock NA, Taylor CW, Thornton S. Effect of an oxytocin receptor antagonist and rho kinase inhibitor on the [Ca++]i sensitivity of human myometrium. *Am J Obstet Gynecol* 2004;**1**:222–228.

Woodcock NA, Taylor CW, Thornton S. Prostaglandin F2alpha increases the sensitivity of the contractile proteins to Ca2+ in human myometrium. *Am J Obstet Gynecol* 2006;**5**:1404–1406.

Word RA, Stull JT, Casey ML, Kamm KE. Contractile elements and myosin light chain phosphorylation in myometrial tissue from nonpregnant and pregnant women. *J Clin Invest* 1993;**1**:29–37.

Wray S. Uterine contraction and physiological mechanisms of modulation. *Am J Physiol* 1993;**1 Pt 1**:C1–C18.

Wray S, Jones K, Kupittayanant S, Li Y, Matthew A, Monir-Bishty E, Noble K, Pierce SJ, Quenby S, Shmygol AV. Calcium signaling and uterine contractility. *J Soc Gynecol Investig* 2003;**5**:252–264.

Wu Y, MacMillan LB, McNeill RB, Colbran RJ, Anderson ME. CaM kinase augments cardiac L-type Ca2+ current: a cellular mechanism for long Q-T arrhythmias. *Am J Physiol* 1999;**276**(6 Pt 2):H2168–H2178.

Wu Y, Muranyi A, Erdodi F, Hartshorne DJ. Localization of myosin phosphatase target subunit and its mutants. *J Muscle Res Cell Motil* 2005;**2–3**:123–134.

Yang M, Gupta A, Shlykov SG, Corrigan R, Tsujimoto S, Sanborn BM. Multiple Trp isoforms implicated in capacitative calcium entry are expressed in human pregnant myometrium and myometrial cells. *Biol Reprod* 2002;**3**:988–994.

Young RC. Myocytes, myometrium, and uterine contractions. *Ann N Y Acad Sci* 2007;**1101**:72–84.

Young RC, Smith LH, McLaren MD. T-type and L-type calcium currents in freshly dispersed human uterine smooth muscle cells. *Am J Obstet Gynecol* 1993;**4**:785–792.

Zweifach A, Lewis RS. Rapid inactivation of depletion-activated calcium current (ICRAC) due to local calcium feedback. *J Gen Physiol* 1995; **2**:209–222.

Appendix 8.2

Detailed In-Cell Western Protocol

8.2 Detailed In-Cell-Western (ICW) Protocol Using Odyssey Scanner

This protocol has been optimized for to assess phosphorylation responses in human uterine myocytes, and the validation of the in-cell western method and culture optimization data are published in reference 184 and chapter 3. However, this approach is amenable for use with other cell culture systems. In principle, this assay can be used to measure any biochemical endpoint for which a suitable antibody (Ab) is available (i.e. it is not restricted to measuring protein phosphorylation). See the above reference for the general approach to Ab validation.

8.2.1 Materials

- Calibrated, multi-channel pipette and sterile tips
- Sterile solution trays (can be reusable) with multiple slots (12 slots ideal)
- Black-walled 96 well plates with bottom surface suitable for microscopy
- e.g. μClear Bottom Optical Imaging Plates (Cat # 675090, VWR (Greiner Bio-One)). These plates are also 'half-area' (15 mm^2/well instead of 30 - 35 mm^2/well), effectively doubling the number of assays that can be performed with the same cellular material, and minimizing Ab consumption.
- DMEM
- DMEM + Antibiotic/Antimycotic (A/A)
- DMEM + FBS (10%)
- PBS + 11.1% Formaldehyde ('3X Fixing Solution')
- PBS + 0.1% TritonX100 ('Permeabilizing Solution')
- Odyssey Blocking Buffer (OBB, LiCOR) (http://www.licor.com/bio/reagents/blocking_buffers/index.jsp)
- PBS (pH 7.4)
- PBS + 0.1% Tween20 (PBS-T)
- Suitable 800 channel secondary Ab (LiCOR) (http://www.licor.com/bio/reagents/irdye_secondary_antibodies.jsp)
- DRAQ5
- Available from two sources: 1) Biostatus Limited - 5 mM solution, or 2) LiCOR – 1 mM solution, as part of the ICW Kit. (http://www.licor.com/bio/reagents/in-cell_western.jsp))
- Sapphire700 (LiCOR, Cat# 928-40022)

8.2.2 Day 1: Cell Plating

1. To maximize data yield, prepare cultures in T75 flasks from 4-6 different patients at the same time, such that you can plate cells from at least 4 of these at one time.
2. Start by sterilizing at least 4 solution trays with EtOH or UV or both.
3. When cultures are confluent, wash 1X with DMEM + A/A without FBS, then add 4 mL 0.05% Trypsin. Allow dispersion for 3-5 min.
4. When the cells are free from the substrate, collect all cells from one patient into a 50 mL tube and use 5 mL of DMEM + A/A to wash and collect remaining cells from each flask.
5. Mix the cell suspension thoroughly by vigorously pipetting up and down with a 10 mL pipette 5-10 times.
6. Transfer a small volume (~100 μL) from each 50 mL tube into a microtube for cell counting.
7. Place the 50 mL tube in a centrifuge and spin for 10 min at low speed to pellet the cells, and proceed with counting the cells in the microtube with a hemocytometer.
8. After counting, remove the DMEM + A/A, and resuspend the cell pellet in an appropriate volume of DMEM + FBS to a concentration of 1,000,000 cells/mL. Make sure to resuspend by vigorously pipetting as in step 4.
9. Dilute this solution in DMEM + FBS (10%) to 100,000 cells/mL in one of the sterilized solution trays from step 2. You will need 90 μL/well (9000 cells/well), and 24 wells per plate for each patient sample (see plate layout in 8.2.2.1) to achieve a density of 600 cells/mm^2 (15 mm^2/well). See reference 184 for cell density optimization. Prepare as much of this cell mixture as needed for the number of assays you wish to perform the next day.
10. Using a calibrated multichannel pipette, dispense 90 μL/well of the cell suspension into each well of the microplates.
11. Allow the newly plated cells to settle for 15-30 minutes at room temperature (R/T).
12. Gently move the seeded plates into the incubator (37^0C).

8.2.2.1 General Plate Layout for Cell Seeding

This layout will allow you to measure four patient samples (n=4, in duplicate) in every column of every plate you prepared.

Row/column	1	2	3	4	5	6	7	8	9	10	11	12
A	PATIENT 1											
B												
C	PATIENT 2											
D												
E	PATIENT 3											
F												
G	PATIENT 4											
H												

8.2.3 Day 2: Cell Treatment

Based on the plate layout above, you can perform three general types of experiments (see 8.2.3.1 through 8.2.3.3), which can be adjusted to suit your needs.

General notes and tips before continuing:

- Each well is broken down into 3 equal volumes of 30 μL:
    - Volume 1: DMEM only, or DMEM containing a drug (normally an enzyme inhibitor) **at the desired final concentration**
    - Volume 2: DMEM containing a second drug (normally a cell stimulant) **at double the desired final concentration**
    - Volume 3: Fixing Solution containing formaldehyde **at triple the desired final concentration** (3X Fixing Solution, 11.1% Formaldehyde)
- The first column of each plate is reserved for a background assay control – treat this column with the vehicle control(s).
- Use a calibrated 12-channel repeating pipette in combination with 12-slot solution tray to prepare and dispense treatment solutions to minimize assay variability (particularly crucial for short time course experiments)
- If you are using drugs requiring variable treatment exposures, start with the longest treatment first, then add subsequent treatments at the correct time such that the entire plate can be quenched with 3X fixing solution at the same time
- Avoid pipetting any solutions directly onto the cells – pipette onto the walls of the wells instead

1. Wash the cells once with DMEM (without any additives).
2. Replace 30 μL of DMEM and incubate for 2-4 hrs at 37^0C. If a long period of cell starvation is required, perform that step now.
    a. If you are pre-treating cells with one drug (e.g. inhibitor of enzyme X) before a second drug (e.g. cell stimulant that acts by stimulating enzyme X), dilute the first drug in DMEM to the desired final concentration and replace the 30 μL of DMEM with 30 μL/well of DMEM containing the drug to the correct wells before the next step.
3. Prepare all of your cell treatments at **double the final concentration** you desire, taking into account the total volume necessary to treat all plates requiring the treatment with 30 μL/well.

4. At the desired time point, stop the reactions by adding formalin to a final concentration of 3.7% formaldehyde (Note: 'formalin' is an aqueous solution of formaldehyde. **100% Formalin contains 37% Formaldehyde**).

5. Allow fixation for 15 min at R/T. Proceed to next section (8.2.4) immediately to avoid loss of post-translational modifications. If you are interested in measuring total protein levels, it might be possible to store microplates at 4^0C in PBS for some time, but we have not attempted that in our studies.

8.2.3.1 Concentration-Response (Single Drug)

9 point concentration response curve to a stimulant or inhibitor. See example result in 8.2.3.4.1.

Row or Column	1	2	3	4	5	6	7	8	9	10	11	12
A	Vehicle	Vehicle		Conc. 1	Conc. 2	Conc. 3	Conc. 4	Conc. 5	Conc. 6	Conc. 7	Conc. 8	Conc. 9
B												
C												
D												
E												
F												
G												
H												
Volume 1	30 μL of DMEM without additives (incubate 2-4 hrs with this only)											
Volume 2	30 μL Vehicle control (contains drug diluent equivalent to highest concentration used)			30 μL/well of 9 different dilutions of drug (one dilution per column). Each dilution should be at twice the desired final concentration.								
Volume 3 (FIXING)	30 μL/well of 3X Fixing solution (11.1% Formaldehyde in PBS)											

8.2.3.2 Concentration-Response to First Drug in Presence or Absence of a Second Drug

4 point concentration-response to a stimulant in the presence or absence of an enzyme inhibitor. See example result in 8.2.3.4.2.

Row or Column	1	2	3	4	5	6	7	8	9	10	11	12
A B C D E F G H	Vehicle + Vehicle for Drug 2	Vehicle + Vehicle for Drug 2	Conc. 1 + Vehicle for Drug 2	Conc. 2 + Vehicle for Drug 2	Conc. 3 + Vehicle for Drug 2	Conc. 4 + Vehicle for Drug 2	Vehicle + Drug 2		Conc. 1 + Drug 2	Conc. 2 + Drug 2	Conc. 3 + Drug 2	Conc. 4 + Drug 2
Volume 1	30 µL/well vehicle control corresponding to Drug 2 Replace the 30 µL/well of DMEM without additives that was added in Step 2 under section 8.2.3, after the equilibration period of 2-4 hrs.						30 µL/well of Drug 2 Replace the 30 µL/well of DMEM without additives that was added in Step 2 under section 8.2.3, after the equilibration period of 2-4 hrs.					
Volume 2	30 µL/well Vehicle control (contains drug diluent (DMSO, DMF etc.) equivalent to highest concentration used.		30 µL/well of 4 different dilutions of drug (one dilution per column). Each dilution should be at twice the desired final concentration.				30 µL/well Vehicle control (contains drug diluent (DMSO, DMF etc.) equivalent to highest concentration used.		30 µL/well of 4 different dilutions of drug (one dilution per column). Each dilution should be at twice the desired final concentration.			
Volume 3 (FIXING)	30 µL/well of 3X Fixing solution (11.1% Formaldehyde in PBS)											

8.2.3.3 Concentration-Response of Second Drug in Presence of Constant Concentration of First Drug

This approach might be useful to test interactions between two drugs that are likely to antagonize each other. For example, use this approach to test the concentration responsiveness of an enzyme inhibitor in the presence of maximal stimulation. See example result in 8.2.3.4.3.

Row or Column	1 2 3	4	5	6	7	8	9	10	11	12
A B C D E F G H	Vehicle + Vehicle for Drug 2	Drug 1 only	Drug 1 + Conc. 1 for Drug 2	Drug 1 + Conc. 2 for Drug 2	Drug 1 + Conc. 3 for Drug 2	Drug 1 + Conc. 4 for Drug 2	Drug 1 + Conc. 5 for Drug 2	Drug 1 + Conc. 6 for Drug 2	Drug 1 + Conc. 7 for Drug 2	Drug 1 + Conc. 8 for Drug 2
Volume 1	30 μL/well vehicle control corresponding to highest concentration of Drug 2. Replace the 30 μL/well of DMEM without additives that was added in Step 2 under section 8.2.3, after the equilibration period of 2-4 hrs.		30 μL/well Conc. 1 for Drug 2	30 μL/well Conc. 2 for Drug 2	30 μL/well Conc. 3 for Drug 2	30 μL/well Conc. 4 for Drug 2	30 μL/well Conc. 5 for Drug 2	30 μL/well Conc. 6 for Drug 2	30 μL/well Conc. 7 for Drug 2	30 μL/well Conc. 8 for Drug 2
Volume 2	30 μL/well Vehicle control for Drug 1	30 μL/well Drug 1 at twice the desired final concentration.								
Volume 3 (FIXING)	30 μL/well of 3X Fixing solution (11.1% Formaldehyde in PBS)									

8.2.3.4 Example Results

8.2.3.4.1 OT Response Curve:

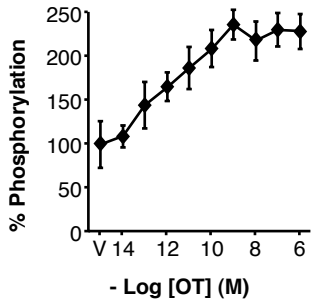

8.2.3.4.2 OT Response Curve With and Without ROK Inhibitor (g-H):

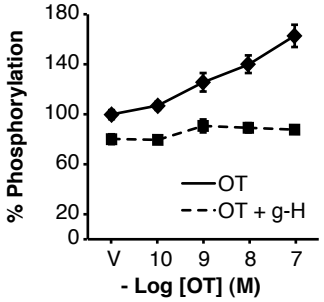

8.2.3.4.3 Constant 100 nM OT and Concentration-Response to ROK Inhibitor (g-H):

In this example, the ROK inhibitor did not affect OT-induced phosphorylation.

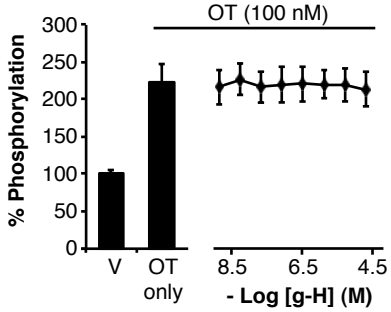

8.2.4 Day 2 Continued: Application of Primary Abs

1. Wash the cells 3x10 min in PBS + 0.1% Triton X-100 at R/T to permeabilize the cells. Use 60-75 μL/well of permeabilization solution/well. Use a rocker/shaker.
2. Rinse with 1X with PBS to remove detergent.
3. Block with OBB, 20 μL/well for 60 minutes at R/T on a rocker/shaker. During this incubation, prepare primary Abs to be used.
4. Incubate with primary Ab diluted in OBB + 0.1% Tween20 overnight at 4^0C (i.e. in the fridge or cold room; no need for agitation or parafilm) according to the plate layout below. **Omit primary Ab from the background control wells** – column 1.

Row/column	1	2	3	4	5	6	7	8	9	10	11	12
A	NO PRIMARY AB (use OBB + 0.1% Tween20 only)	Primary Ab at desired dilution in OBB + 0.1% Tween20										
B												
C												
D												
E												
F												
G												
H												

8.2.5 Day 3: Development of Plates and Preparation for Scanning

General notes and tips before continuing:

- a maximum of 6 plates at once
- the focus offset to be used is 4.0 mm for the Greiner-Bio-One plates
    - if you have chosen to use different plates for these assays, the scan images might be misaligned (i.e. the 700 ('red') and 800 ('green') channel scans might not sit evenly on top of each other). In this situation adjust the offset up or down to try to eliminate that problem. Alternatively, simply align the images after each scan by selecting 'File' → 'Align images in the Odyssey software.

1. The next day, wash 3x10 min with PBS-T with about 60-75 μL/well.
2. Prepare secondary Ab: select appropriate 800 channel (green) secondary Ab (mouse, rabbit, chicken etc.) diluted in OBB + 0.1% Tween20 + 0.01% SDS. Secondary Abs should be used at 1:1000. Prepare 2.5 mL of this solution for every plate you have. Place 10% of this solution in a tube labeled 'Ab only'.
3. To the remaining 90%, add DRAQ5 (if 5 mM then use 1:10,000) and Sapphire700 (1:1,000). Note if you bought the DRAQ5 from LiCOR (1 mM stock) and not Biostatus Ltd., then the dilution is 1:2000, NOT 1:10,000. These cell dyes are used to normalize for the number of cells in a well. They are detected in the 700 (red) channel.
4. Follow the plate layout below, using 20 μL/well.

Row/column	1	2 3 4 5 6 7 8 9 10 11 12
A B C D E F G H	SECONDARY Ab (1:1000) ONLY (solution from step 2 above)	Secondary Ab at 1:1000, with DRAQ5 (1:10,000) and Sapphire700 (1:1000) in OBB + 0.1% Tween20 + 0.01% SDS

1. Incubate for 90 min on a rocker/shaker and cover with tin foil.
2. Wash 3x10 min in PBS-T with about 60-75 μL/well, on a rocker/shaker.
3. Add 20 μL/well of PBS to each well to eliminate any surface disturbance during scanning.
4. Open the Odyssey software, and select 'ICW' from the first dialog box.
5. Scan the plate(s) at intensity 5 for the 700 channel and 7 for the 800 channel, with 4.0 mm offset.
6. Save the data when scanning is completed.

8.2.6 Data Analysis

See the Licor Odyssey manual.

In general, follow these steps:

- Under the 'in-cell western' menu in the Odyssey software, select 'add a grid' with the appropriate well size (if you followed this protocol, you're using **HALF AREA** 96 well plates). Modify the well size if you have to such that the well outlines correspond to the well sizes on the scan.

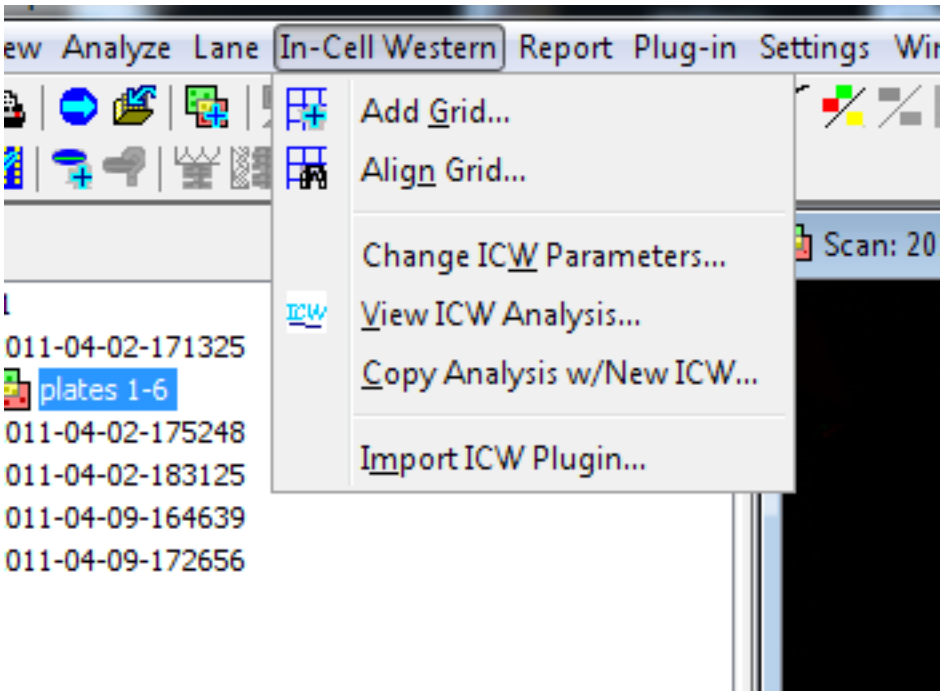

- Select ‘Change ICW Parameters’, then link appropriate rows together – for example, A/B, C/D, E/F, G/H, since these pairs belong to one patient. If more than two wells correspond to the same treatment, use the ‘independent link’ option to link all wells together to obtain an average reading for all replicates simultaneously.

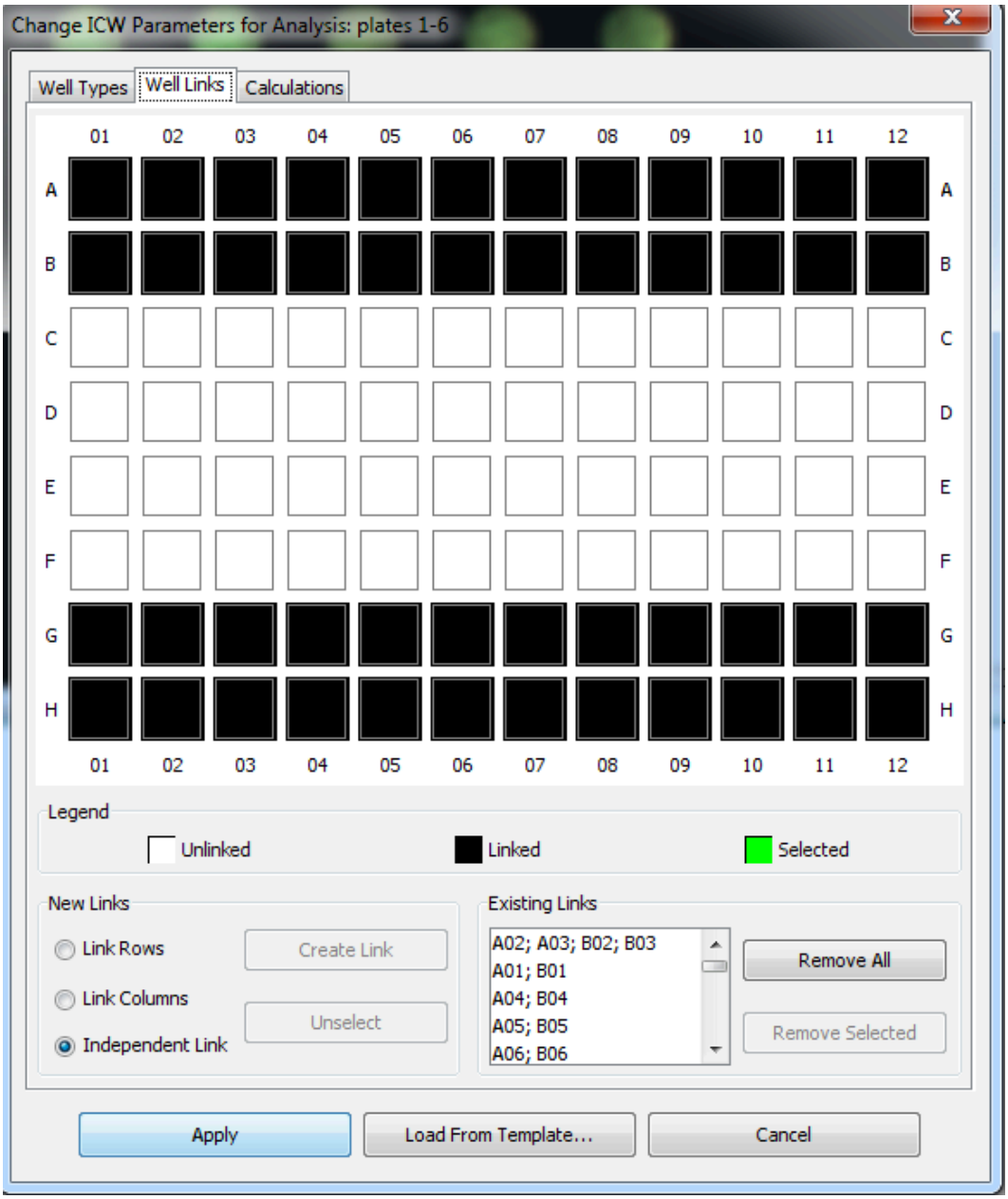

- Analyze data from 1 patient at a time, since each one has its own vehicle control. Assign the background controls to column 1, and the '100% control' to the vehicle control lanes according to your experimental layout. Everything else is a 'sample'. Move the grid around the image from patient to patient to avoid having to reassign well identities.

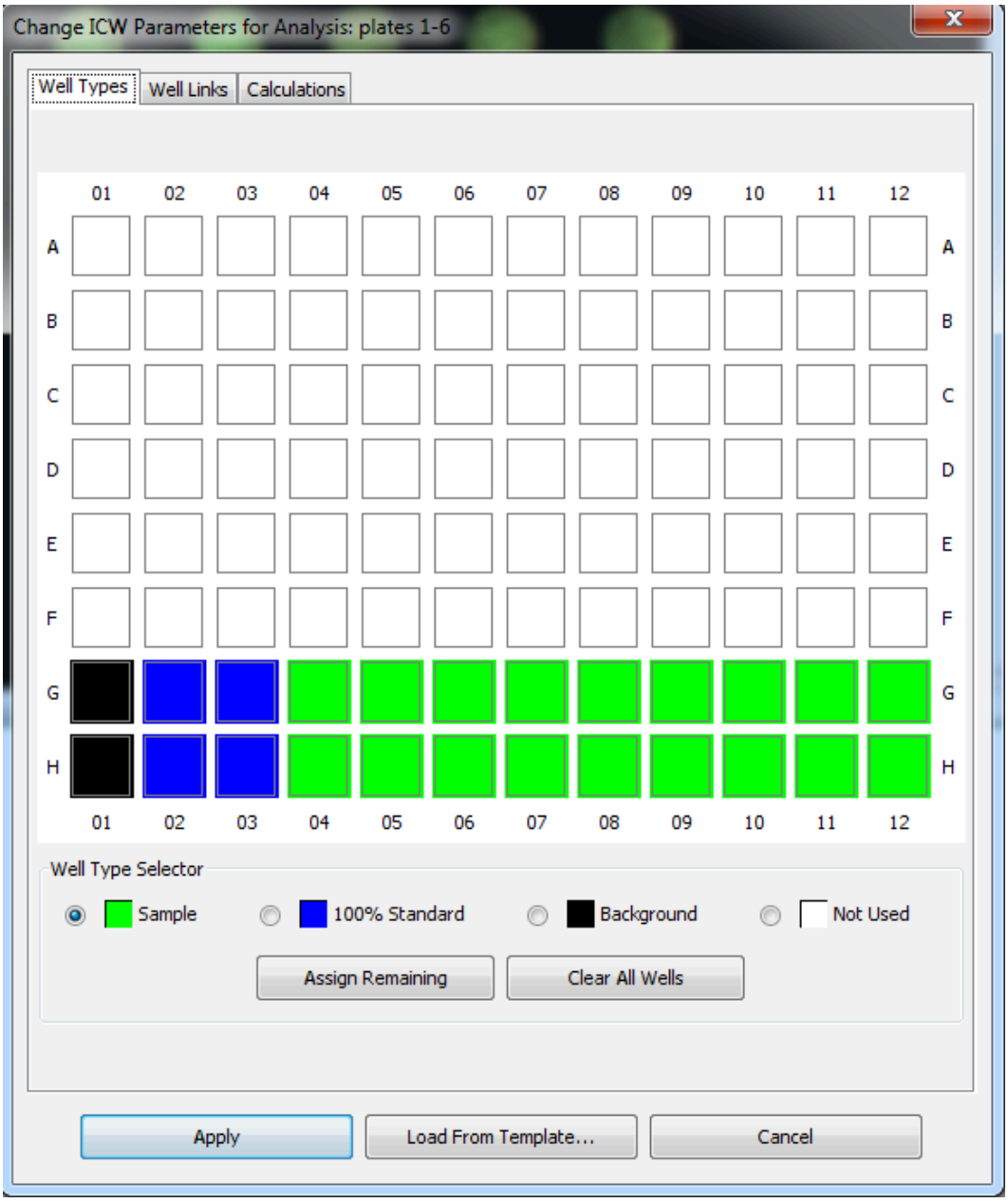

- Calculate the percent response in the 800 channel (secondary Ab) relative to the 700 channel (cell dyes) as indicated in the image below.

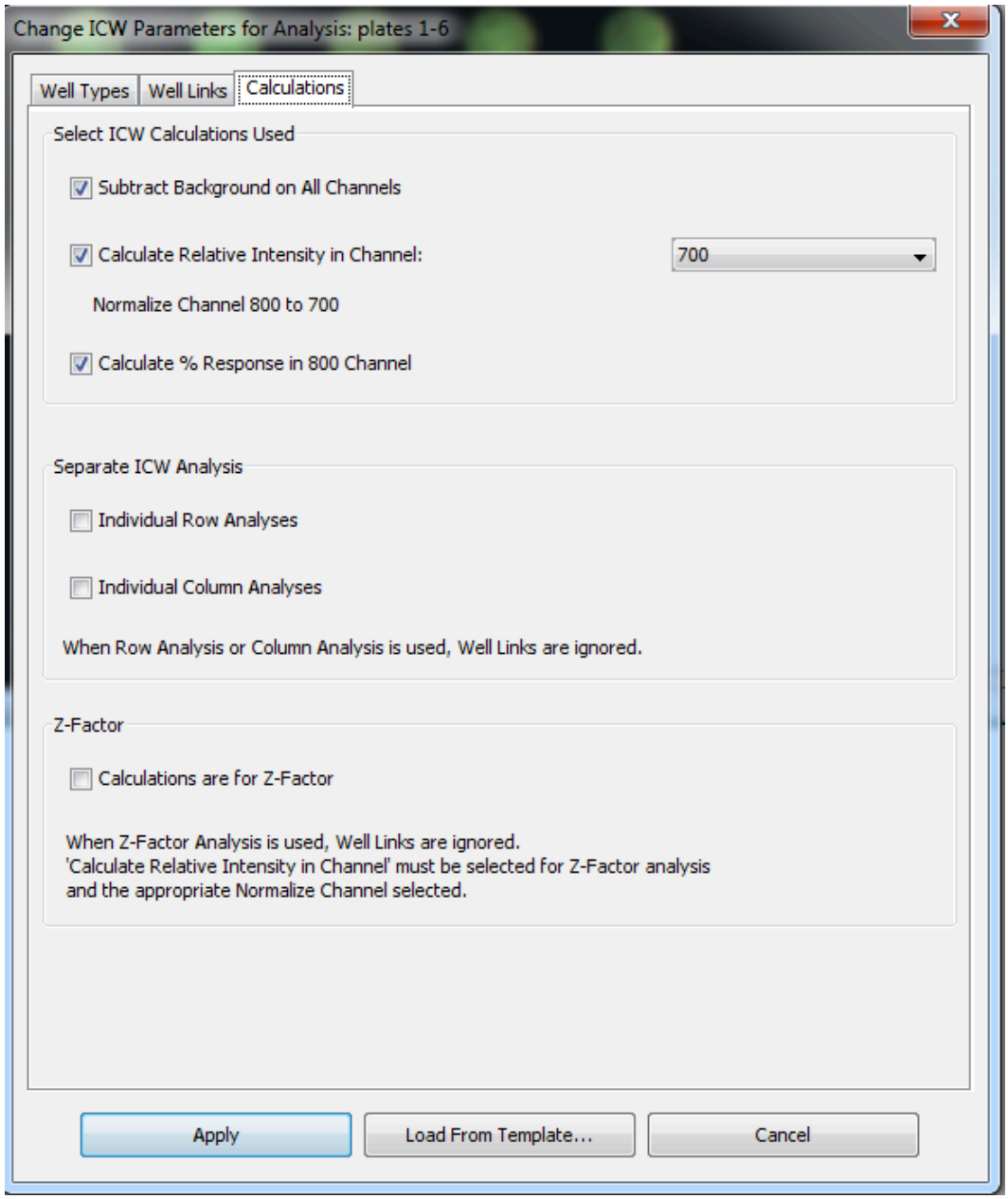

- Select ‘View ICW Analysis’ from the In-Cell Western menu, and click ‘copy’.
- Paste the data into excel to organize, average patient data, and plot it.

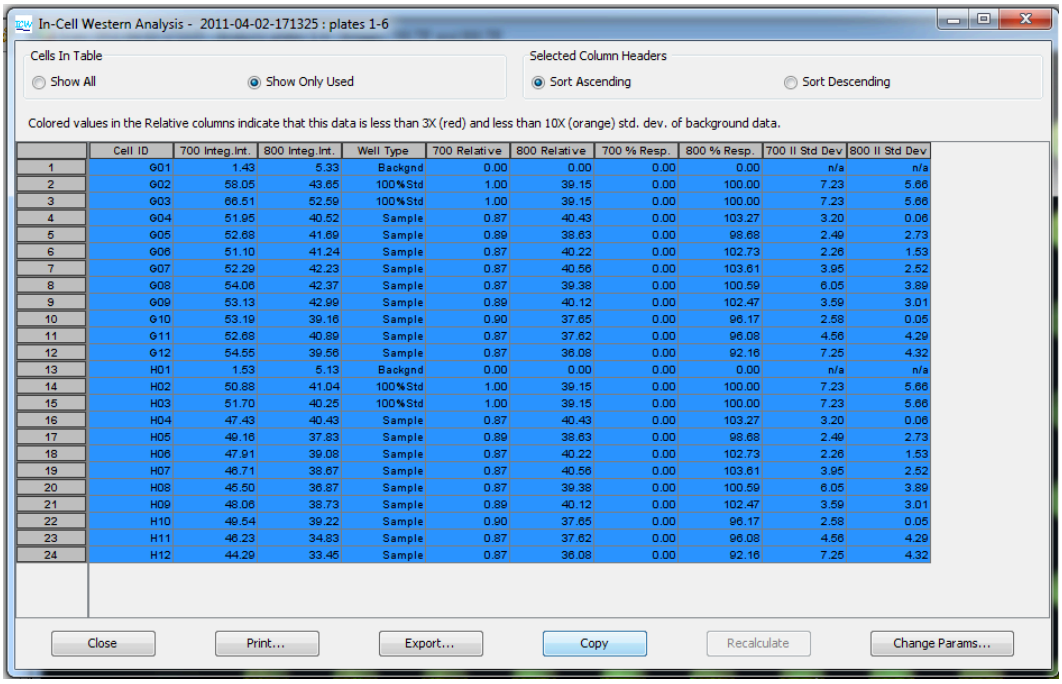

	Cell ID	700 Integ.Int.	800 Integ.Int.	Well Type	700 Relative	800 Relative	700 % Resp.	800 % Resp.	700 II Std Dev	800 II Std Dev
1	G01	1.43	5.33	Backgnd	0.00	0.00	0.00	0.00	n/a	n/a
2	G02	58.05	43.65	100%Std	1.00	39.15	0.00	100.00	7.23	5.66
3	G03	66.51	52.59	100%Std	1.00	39.15	0.00	100.00	7.23	5.66
4	G04	51.95	40.52	Sample	0.87	40.43	0.00	103.27	3.20	0.06
5	G05	52.68	41.69	Sample	0.89	38.63	0.00	98.68	2.49	2.73
6	G06	51.10	41.24	Sample	0.87	40.22	0.00	102.73	2.26	1.53
7	G07	52.29	42.23	Sample	0.87	40.56	0.00	103.61	3.95	2.52
8	G08	54.06	42.37	Sample	0.87	39.38	0.00	100.59	6.05	3.89
9	G09	53.13	42.99	Sample	0.89	40.12	0.00	102.47	3.59	3.01
10	G10	53.19	39.16	Sample	0.90	37.65	0.00	96.17	2.58	0.05
11	G11	52.68	40.89	Sample	0.87	37.62	0.00	96.08	4.56	4.29
12	G12	54.55	39.56	Sample	0.87	36.08	0.00	92.16	7.25	4.32
13	H01	1.53	5.13	Backgnd	0.00	0.00	0.00	0.00	n/a	n/a
14	H02	50.88	41.04	100%Std	1.00	39.15	0.00	100.00	7.23	5.66
15	H03	51.70	40.25	100%Std	1.00	39.15	0.00	100.00	7.23	5.66
16	H04	47.43	40.43	Sample	0.87	40.43	0.00	103.27	3.20	0.06
17	H05	49.16	37.83	Sample	0.89	38.63	0.00	98.68	2.49	2.73
18	H06	47.91	39.08	Sample	0.87	40.22	0.00	102.73	2.26	1.53
19	H07	46.71	38.67	Sample	0.87	40.56	0.00	103.61	3.95	2.52
20	H08	45.50	36.87	Sample	0.87	39.38	0.00	100.59	6.05	3.89
21	H09	48.06	38.73	Sample	0.89	40.12	0.00	102.47	3.59	3.01
22	H10	49.54	39.22	Sample	0.90	37.65	0.00	96.17	2.58	0.05
23	H11	46.23	34.83	Sample	0.87	37.62	0.00	96.08	4.56	4.29
24	H12	44.29	33.45	Sample	0.87	36.08	0.00	92.16	7.25	4.32

Appendix 8.3

Comparison of Primary hUSMC Derived From Fundal and Lower Uterine Segments

8.3 Comparison of Primary hUSMC Derived From Fundal and Lower Uterine Segments

8.3.1 Introduction

In order to validate the use of cultured hUSMC derived from the lower segment of the uterus, we compared the responses in p19RLC and ppRLC to stimulation with OT and ET-1 in paired samples of cultured myocytes derived from 5 patients. We evaluated the effect of ROK inhibition (g-H, 1 μM) and MLCK inhibition (ML7, 25 μM) on each of these responses.

8.3.2 Materials and Methods

The research group of Dr. DM Slater and Dr. S Wood (University of Calgary, Calgary, Alberta) collected the tissues and isolated the cells used for this project. Their methods are briefly described here for completeness.

8.3.2.1 Tissue Collection

Paired (fundal and lower segment) myometrial and decidual biopsies were collected from pregnant women undergoing Caesarean section. Samples were processed for hUSMC isolation. Institutional ethical committee approval was obtained and patients completed informed consent forms (Office of Medical Bioethics, University of Calgary).

8.3.2.2 Isolation and Culture of hUSMC

hUSMC were isolated from myometrial biopsies as described in 313 and 314.

8.3.2.3 Pharmacological Agents

ROK and MLCK inhibitors (g-H and ML7) are described in section 5.2.1.

8.3.2.4 In-Cell Westerns

This assay and the primary Abs used are described in sections 3.2.6 and 4.2.5, respectively.

8.3.3 Results

Figure 8-1 demonstrates that hUSMC derived from fundus or lower segment of the uterus respond with concentration-dependent enhancements in p19RLC when challenged

with OT and ET-1. The maximal responses to both of these agonists were similar in both fundus and lower segment groups, and the agonist responses were attenuated by inhibition of ROK (g-H) or MLCK (ML7) in both groups. Similarly, Figure 8-2 shows that hUSMC from both groups respond to OT and ET-1 with ppRLC synthesis that is sensitive to treatment with g-H or ML7.

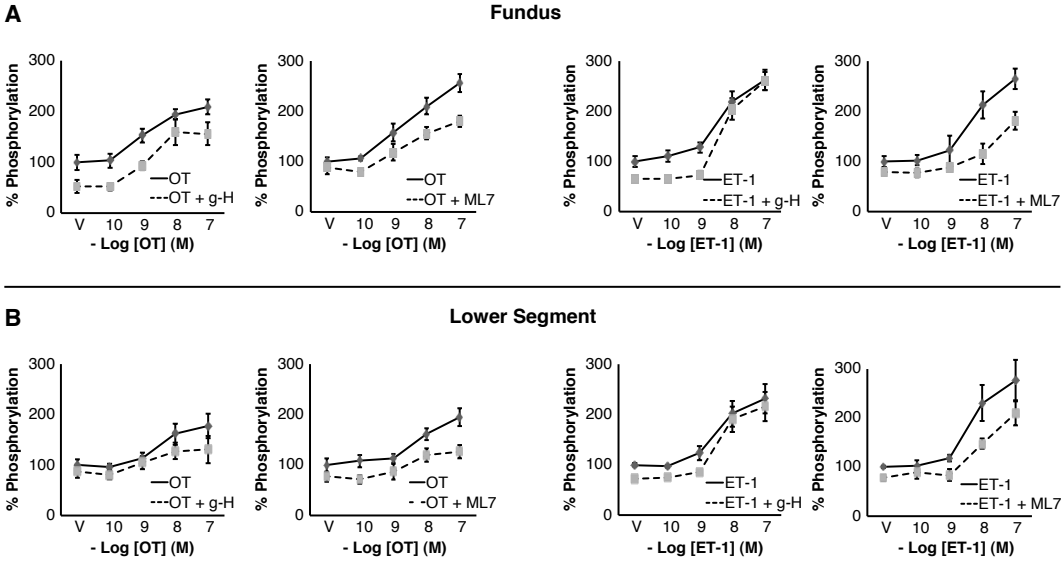

Figure 8-1. Comparison of p19RLC Responses to Stimulation in hUSMC Derived From Fundus or Lower Segment of the Uterus.

A. Concentration-responses in hUSMC (n=5, paired samples) derived from the uterine fundus to OT or ET-1 in the presence or absence of g-H (1 μM) or ML7 (25 μM). **B.** Equivalent data from hUSMC derived from the lower segment of the uterus. In all panels, the x-axis corresponds to the negative log of the molar concentration of OT or ET-1. g-H (glycyl-H-1152); ROK inhibitor. ML7; MLCK inhibitor. OT; oxytocin. ET-1; endothelin-1. hUSMC; uterine myocytes.

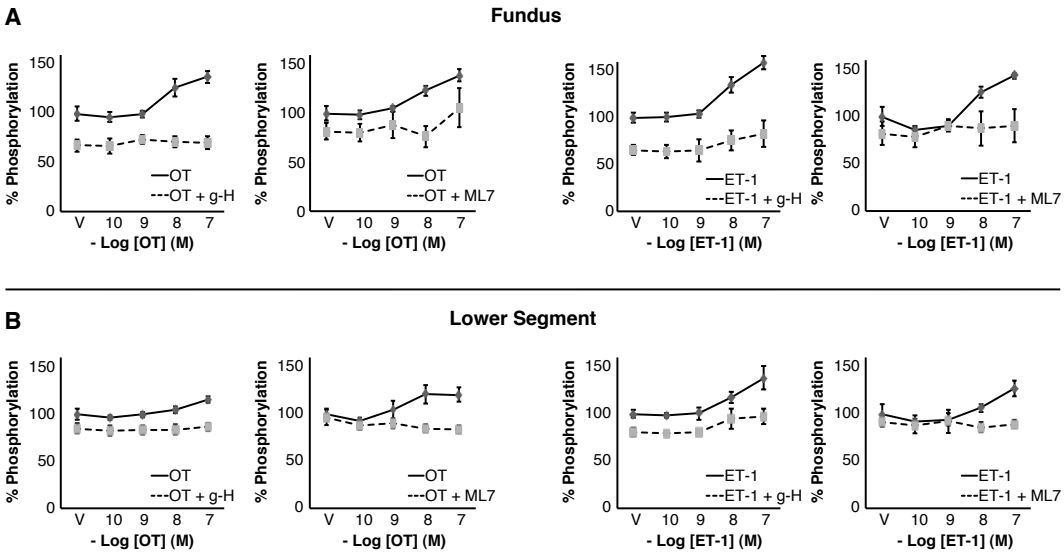

Figure 8-2. Comparison of ppRLC Responses to Stimulation in hUSMC Derived From Fundus or Lower Segment of the Uterus.

A. Concentration-responses in hUSMC (n=5, paired samples) derived from the uterine fundus to OT or ET-1 in the presence or absence of g-H (1 μM) or ML7 (25 μM). **B.** Equivalent data from hUSMC derived from the lower segment of the uterus. In all panels, the x-axis corresponds to the negative log of the molar concentration of OT or ET-1. g-H (glycyl-H-1152); ROK inhibitor. ML7; MLCK inhibitor. OT; oxytocin. ET-1; endothelin-1. hUSMC; uterine myocytes.

8.3.4 Conclusion

These data suggest that the mechanisms regulating phosphorylation of RLC in hUSMC derived from the fundus or lower segment of the uterus respond similarly to OT and ET-1, and are sensitive to ROK and MLCK inhibition. Thus, it is unlikely that we would have reached different conclusions from our primary studies if we had used hUSMC derived from a distinct region of the uterus instead of lower segment hUSMC.

Appendix 8.4

siRNA Transfection in Primary hUSMC

8.4 siRNA Transfection in hUSMC

8.4.1 Introduction

In order to provide further support for the pharmacological studies relying on enzyme inhibition and to explore new hypotheses as described in section 7.3, we have begun optimization of siRNA transfection assays in hUSMC.

8.4.2 Materials and Methods

8.4.2.1 Primary Cultures of hUSMC

hUSMC were cultured as described in 3.2.1.

8.4.2.2 Western Immunoblotting

WB were performed as described in 3.2.5. The final dilutions of anti-MYPT1 (MMAb, # 612164, BD Biosciences), anti-rhoA (BD Biosciences) were 1:500 and 1:200.

8.4.2.3 In-Cell Westerns

ICWs were performed as described in 3.2.6. The final dilutions of anti-MYPT1, anti-rhoA were 1:500 and 1:200, respectively.

8.4.2.4 Microscopy

Microscopy was performed as described in 3.2.7. The final dilutions of anti-MYPT1, anti-rhoA were both 1:100.

8.4.2.5 siRNA Transfection

Two different protocols were attempted for siRNA transfection. **Protocol 1:** cells were seeded at cell densities ranging from 400-600 cells/mm^2 into 96 well plates (same used for ICW) containing DMEM with 10% FBS. At the time of plating, 0.2 - 0.5 μL/well of Lipofectamine RNAiMAX transfection reagent (Invitrogen, Carlsbad, CA, USA) and a final concentration of 0 - 50 nM of validated siRNA oligonucleotides were added. The siRNAs used were against rhoA (ID: 758) and MYPT1 (IDs: 9235 and 9237). Two control siRNAs were also used: Silencer® Select GAPDH Positive Control (Cat#: 4390849) and Negative Control No. 1 (Cat#: 4390843). All siRNAs were purchased from Ambion, Inc (Invitrogen). siRNAs and transfection reagents were combined in Opti-MEM (Invitrogen), and cells were exposed to the lipofectamine/siRNA mixture in DMEM with 10% FBS for 1 - 6 days as indicated in the figure legends. **Protocol 2:** cells were seeded in DMEM with 10% FBS at

600 cells/mm^2 in the absence of lipofectamine/siRNAs. The following day, the cells were washed with DMEM without additives, and the cells were exposed to the desired lipofectamine/siRNA concentrations diluted in Opti-MEM for 6 - 8 hrs. After this exposure, the plates were washed again, and DMEM with 10% FBS was replaced into each well. Cells were then prepared for ICW or WST-8 assays at day 1 and day 3 post-exposure.

8.4.2.6 WST-8 Viability Assay

hUSMC viability was assessed by the WST-8 Cell Proliferation Assay Kit (Cayman Chemical Company, Ann Arbor, MI, USA) according to the manufacturer's specifications, with a few modifications. Since the ICW assay requires half-area 96 well plates, the total volume used for the assay is reduced from the indicated 110 μL to 55 μL. hUSMC were seeded at 600 cells/mm^2 as for ICWs. The next day, the cells were washed, treated with siRNAs and transfection reagents as described above, and after the 6 – 8 hr exposure, the cells were washed again and 35 μL of DMEM containing 10% FBS was replaced into each well. For day 1 viability assessment, 20 μL of DMEM containing 2 μL of reconstituted WST-8 reagent were added to each well and the plates were processed as indicated. This reduced level of WST-8 produced assay readings within the linear range of detection. For day 3 viability assessment, cells were washed on day and 35 μL of DMEM containing 10% FBS was replaced into each well. The following day, 20 μL of DMEM containing 2 μL of reconstituted WST-8 reagent were added to each well and the plates were processed as indicated. In each experiment, a negative control (DEAD) was created by permeabilizing a group of cells with 0.1% Triton X-100 for 15 min at 37^{0}C. In these negative control wells, 35 μL of DMEM was replaced immediately prior to adding the 20 μL of DMEM containing WST-8 to the whole plate.

8.4.3 Results

To monitor the efficiency of siRNA knockdown, we quantified protein levels by ICW. Figure 8-3 demonstrates the specificity of Abs toward MYPT1 and rhoA by microscopy and WB as was discussed in chapter 3. Abs toward MYPT1 or rhoA stain the cytosolic compartment of hUSMC in a fibrillar pattern, and recognize a single primary band of interest at running at 130 kDa and 21 kDa by WB, respectively.

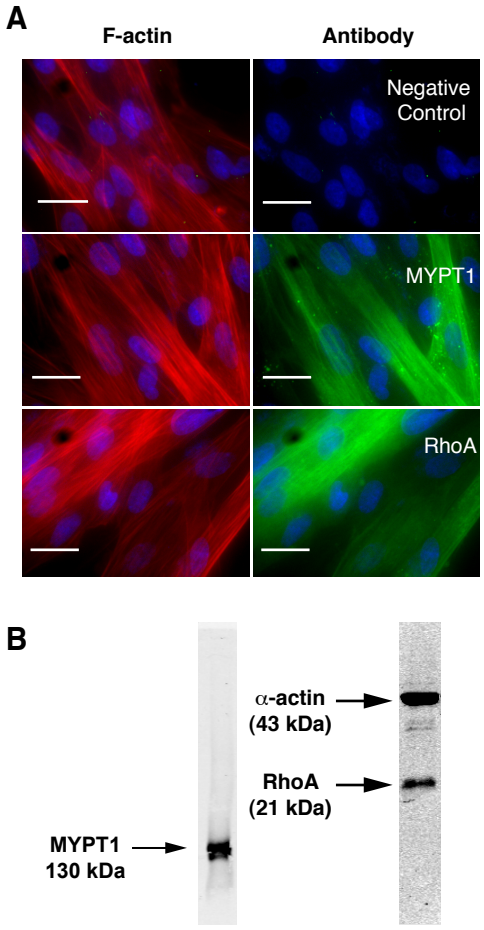

Figure 8-3. Demonstration of MYPT1 and rhoA Ab Specificity.

A. Immunofluorescent staining of hUSMC and demonstration of anti-MYPT1 Ab specificity. In the left micrographs, filamentous actin (F-actin) is stained with rhodamine-phalloidin (red). In the right micrographs the same fields of view corresponding to negative control (secondary only), or to staining of MYPT1 and rhoA are shown. The green signal is derived from a secondary Ab conjugated to Alexa-Fluor 488. In all panels, nuclei are stained with DAPI (blue). Images are shown at 400X magnification. White bars represent 25 microns. **B.** WB produced by probing with the primary Abs used to stain MYPT1 and rhoA in panel A. The membranes was probed after SDS-PAGE separation and transfer of 25 μg of protein from hUSMC. The rhoA membrane was additionally probed with an Ab toward α-actin. The acrylamide content was 5% and 15% for the WB shown.

The first optimization experiments we performed were aimed at evaluating the time course, siRNA concentrations, and transfection reagent content per well (see 'protocol 1' in 8.4.2.5). We measured GAPDH, rhoA and MYPT1 content in hUSMC in parallel experiments. The data in Figure 8-4 indicated that a 48 hr incubation period appeared to reduce protein levels for each of those monitored further than that achievable after 24 hrs of exposure. It was unclear as to whether there was a benefit to 0.2 or 0.3 μL/well transfection reagent, but a third group exposed to 0.5 μL/well exhibited significant toxicity (cell death).

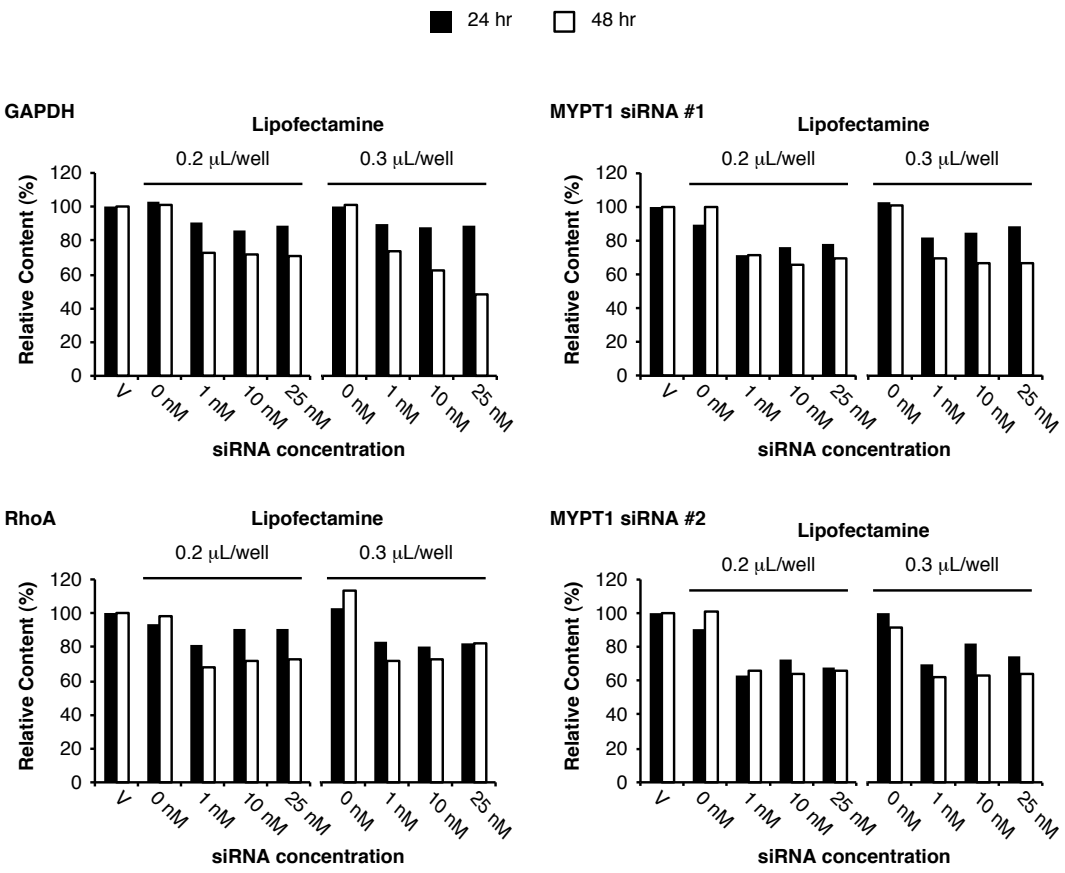

Figure 8-4. Optimization of siRNA Protein Knockdown Parameters in hUSMC Using Protocol 1.

Quantification of GAPDH, rhoA and MYPT1 protein levels in hUSMC (n=2) by ICW using the anti-GAPDH Ab shown in Figure 3-2 and anti-rhoA and anti-MYPT1 Abs from Figure 8-3. hUSMC were treated with vehicle (no siRNA or transfection reagent), or specific siRNAs toward GAPDH, rhoA or either of two specific siRNAs toward MYPT1 (MYPT1 #1 and #2). The concentration of transfection reagent (Lipofectamine) was either 0.2 or 0.3 μL/well in each experiment, and the duration of exposure was either 24 (black histograms) or 48 (white histograms) hrs.

In the next optimization, we restricted our measurements to MYPT1 protein levels. We used a constant 0.3 μL/well transfection reagent and varied the concentration of siRNAs toward MYPT1. We also extended the exposure length to include 72 hrs, and also further evaluated the effect of the density of cell plating on MYPT1 protein knockdown. The data in Figure 8-5 indicated that that 72 hrs of exposure was better at achieving MYPT1 knockdown than 24 or 48 hrs of exposure. There appeared to be no benefit of increasing siRNA concentration from 10 nM to 50 nM, and cell density did not appear to be a factor in knockdown efficiency. The trends were similar both of the siRNAs toward MYPT1 tested. Therefore, in subsequent experiments we used an intermediate concentration of 25 nM for siRNAs, and on the basis of an optimal cell density for myocyte responsiveness established in chapter 3, we also selected 600 cells/mm^2 as the cell density.

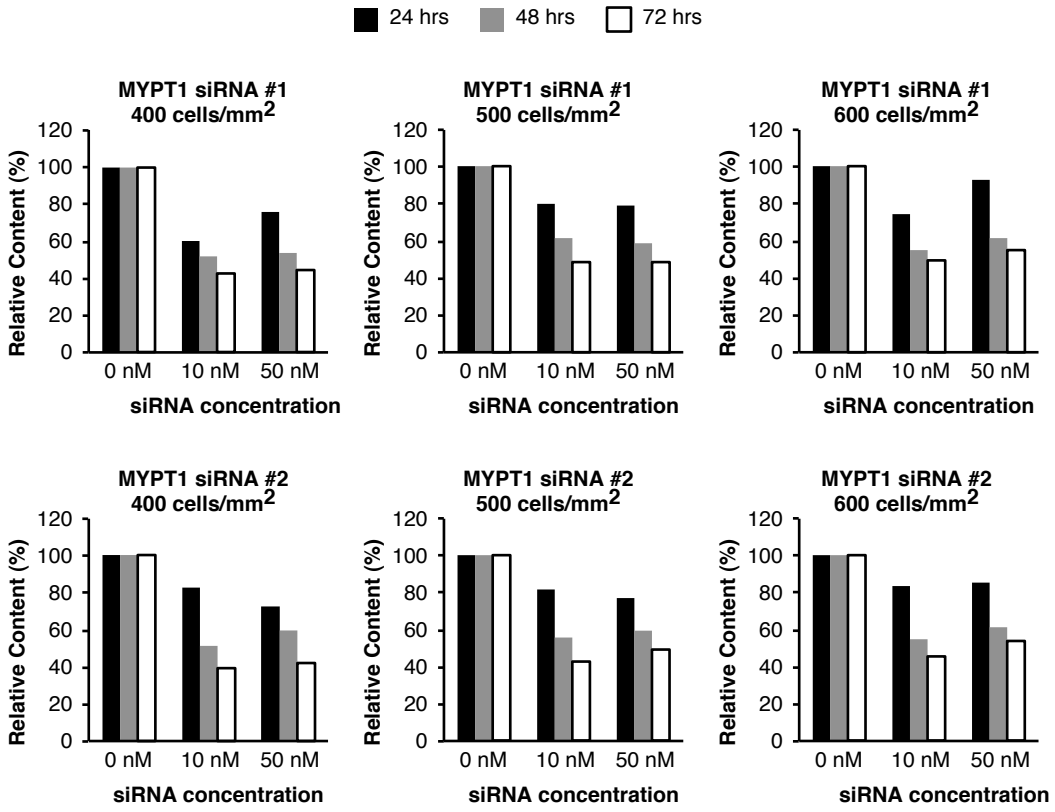

Figure 8-5. Optimization of Cell Density for MYPT1 Knockdown by siRNA in hUSMC Using Protocol 1.

Quantification of MYPT1 protein levels in hUSMC (n=2) by ICW. hUSMC were treated with 0.3 μL/well of lipofectamine transfection reagent in all experiments with either 0, 10, or 50 nM of specific siRNAs toward MYPT1 (MYPT1 #1 and #2). The duration of exposure was 24, 48, or 72 hrs (black, grey, and white histograms, respectively). In addition, the density of cells was varied from 400 – 600 cells/mm^2.

To further decrease MYPT1 knockdown we extended the time course to 6 days of exposure with 0.3 μL/well lipofectamine with 25 nM siRNAs, including a wash and replacement of transfection reagents and siRNAs at day 3. Figure 8-6A shows that under these revised conditions, two specific siRNAs to MYPT1 achived knockdown of MYPT1 protein to 25-30% of control levels, whereas the siRNA toward GAPDH and an siRNA without known specificity did not affect MYPT1 levels. Unfortunately, Figure 8-6B shows that cells treated in this manner did not reliably respond to OT with p19RLC or ppRLC synthesis as was demonstrated in chapters 3 through 5. The reasons for this failure to respond are unclear, but it is possible that the cells were damaged or not viable due to extended exposure to transfection reagents or to prolonged culturing at full cell density.

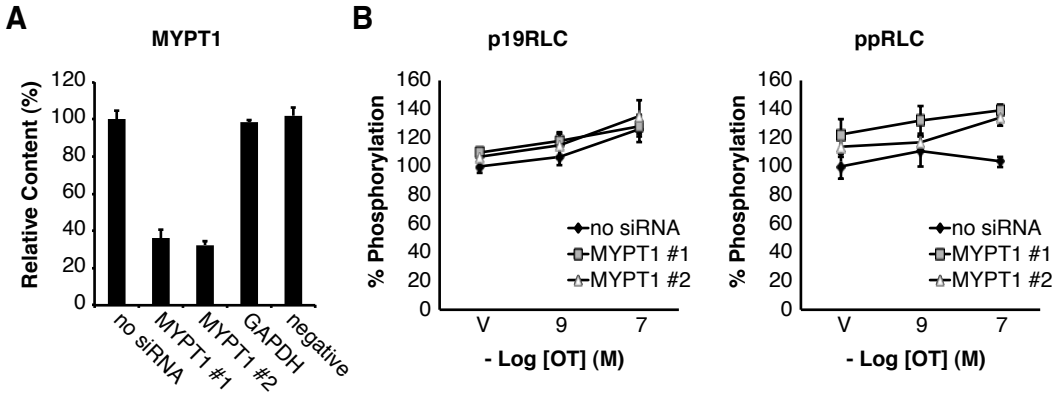

Figure 8-6. Demonstration of MYPT1 Protein Levels and Phospho-RLC Responses in hUSMC Treated With siRNAs Toward MYPT1 Using Protocol 1.

A. Quantification of MYPT1 protein in hUSMC (n=4) by ICW using the anti-MYPT1 Ab from Figure 8-3. hUSMC were treated with vehicle (no siRNA), either of two specific siRNAs toward MYPT1 (MYPT1 #1 and #2), an siRNA toward GAPDH, or an siRNA without specificity (negative) for any human mRNA. **B.** ICW quantification of p19RLC and ppRLC in response to OT-stimulation in hUSMC (n=4) treated with no siRNA, or with either of two siRNAs toward MYPT1 (MYPT1 #1 and #2). The x-axes correspond to the negative log of the molar concentration of OT. Data are shown as means ± SEM.

In order to determine the extent to which the transfection protocols affect cell viability, we modified the transfection protocol (see 'protocol 2' in 8.4.2.5) and assessed cell viability using an absorbance assay that depends on cellular metabolic activity. Under this revised protocol, hUSMC appeared to tolerate higher concentrations of transfection reagent (up to 1 μL/well) at a constant 25 nM siRNA oligonucleotide (Figure 8-7).

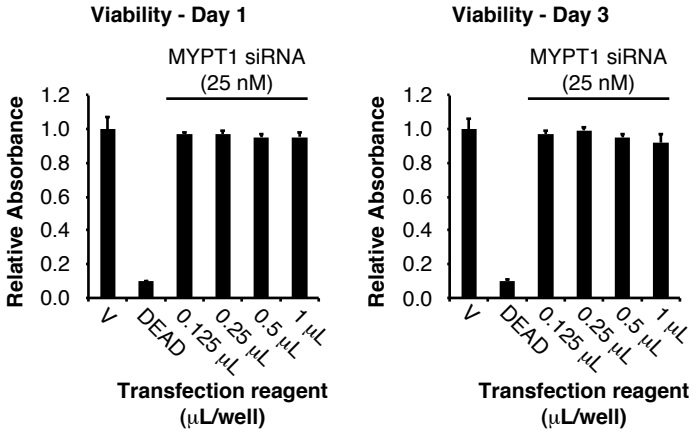

Figure 8-7. Demonstration of Cell Viability in hUSMC Treated With siRNA Toward MYPT1 Using Protocol 2.

Measurement of hUSMC (n=4) viability at Day 1 and Day 3 post-exposure to siRNA treatment as determined by WST-8 assay. hUSMC were treated with either no siRNA or transfection reagent (vehicle, V), or with a constant 25 nM of siRNA toward MYPT1 with 0.125, 0.25, 0.5, or 1 μL of transfection reagent per well. In each assay, one group of cells were killed by permeabilization with 0.1% Triton-X 100 to generated a negative control (DEAD). Data are shown as means ± SEM.

8.4.4 Future Directions

Future experiments should focus on optimizing MYPT1 protein knockdown by ICW in parallel with assessments of cell viability to minimize toxicities of the transfection protocol. Several of the parameters tested here should be revisited under the revised Protocol 2. Specifically, seeding at reduced cell densities should be attempted, since cells seeded at full confluence (600 cells/mm^2) might become senescent over extended culturing periods and such extended culturing might be necessary to achieve adequate knockdown. Once optimized, MYPT1 knockdown should be verified by WB. A determination of concentration-dependent responses in phosphorylation of RLC to OT in hUSMC with confirmed reduction of MYPT1 levels should then be performed before extending the protocol to other proteins of interest.

Appendix 8.5

Protein Transduction Using TAT-Fusions in Primary hUSMC

8.5 Protein Transduction Using TAT-Fusions in hUSMC

8.5.1 Introduction

In order to complement the pharmacological enzyme inhibition studies in chapter 5 and the siRNA protein knockdown approach in section 8.4, we have begun protein transduction experiments. This approach relies on subcloning the DNA sequence for a protein of interest into a vector that enables tagging with the human immunodeficiency virus (HIV) peptide called 'TAT'. The TAT peptide has the capability of causing the uptake of cargo fused to it into the intracellular space of mammalian cells. The general approach for production such TAT-fusions is outlined in 307.

Worthy of note, the specific methods for protein expression outlined below were low-yield, and will need to be improved before use with other TAT-fusions. It is unclear whether the suboptimal yield was due to poor reagent choice, or whether technical proficiency at the protein expression and purification steps was the primary problem. Still, the end product of this method produced a pure and functional TAT-rhoA fusion that is capable of enhancing rhoA protein and activity in hUSMC.

8.5.2 Materials and Methods

8.5.2.1 Primary Cultures of hUSMC

hUSMC were cultured as described in 3.2.1.

8.5.2.2 Western Immunoblotting

WB were performed as described in 3.2.5. The final dilution of anti-rhoA (BD Biosciences) was 1:200.

8.5.2.3 In-Cell Westerns

ICWs were performed as described in 3.2.6. The final dilution of anti-rhoA (BD Biosciences) was 1:200.

8.5.2.4 Nucleic Acid Electrophoresis

DNA samples prepared in ddH_2O were combined with loading buffer (final concentrations: 5% glycerol, 0.04% bromophenol blue (Sigma-Aldrich), 0.04% xylene cyanol (Sigma-Aldrich)) and loaded onto agarose (Invitrogen) gels between 0.75-1.5% (w/v) prepared in 1X Tris-acetate-EDTA (TAE, final concentrations: 40 mM Tris, 0.1% (v/v)

glacial acetic acid, 1.25 mM EDTA, pH 8.5) with or without 1 μg/mL EtBr for visualization under UV light, cast in an Owl horizontal electrophoresis apparatus (Owl (Thermo Fisher), Rochester, NY, USA). Electrophoresis was carried out in 1X TAE buffer of the same composition, at 100V for 30-60 min. Each gel also contained 2 μL of 1 Kb Plus DNA Track-It™ molecular weight standard (Invitrogen). Agarose gels were then visualized using a UV transilluminator or a Fluor-S-MAX™ imager (BioRad). For cloning purposes, exposure of DNA to UV light was avoided by omitting EtBr from the agarose gel and staining with 0.002% methylene blue (Sigma-Aldrich) in 0.1X TAE O/N, then destaining in 0.1X TAE until the bands were visible above background.

8.5.2.5 Subcloning into pTAT-HA Vector

The plasmid encoding wild type (WT) rhoA (Cat#: RHO0A00000) was purchased from The Missouri S&T cDNA Resource Center (Rolla, MO, USA). The pTAT-HA vector was obtained from Dr. S Dowdy (UC San Diego, CA, USA).(308) These plasmids were propagated in *E. coli* (Subcloning Efficiency™ DH5α™ Competent Cells, Invitrogen), and purified using a standard plasmid isolation (mini prep) kit (Qiagen, Toronto, ON, Canada) in LB media containing 50 μg/mL ampicillin. The WT rhoA insert was amplified by polymerase chain reaction (PCR) from the rhoA WT plasmid using a high-fidelity proofreading enzyme (PWO DNA Polymerase, Roche-Applied Sciences, Laval, QC, Canada) using primers containing Nco or EcoRI restriction sites to achieve directional insertion (see Figure 8-8). The amplified rhoA inserts were purified by a PCR product purification kit (Qiagen). The purified inserts and pTAT-HA plasmid were digested with NcoI and EcoRI (New England Biolabs, Ipswitch, MA, USA) according to the manufacturers instructions. The vector was dephosphorylated with CIAP (Invitrogen). After digestion, the inserts and opened plasmid were purified by an agarose gel purification kit (Qiagen), then ligated using T4 DNA ligase for 1 -2 hr, R/T (New England Biolabs). The ligation reaction was used to transform *E. coli* (MAX Efficiency® DH5α™ Competent Cells, Invitrogen) according to the manufacturer's instructions, which were grown O/N at 37^0C on agar plates containing ampicillin. The following day, colonies were screened by PCR with a pair of primers upstream and downstream of the insert sequence. Further screening was performed by plasmid amplification in *E. coli*, purification, then restriction digestion,

separation on agarose and visualization by UV. DNA sequences were confirmed by DNA sequencing (Eurofins MWG Operon, Huntsville, AL, USA). Bacterial stocks with confirmed in-frame fusions were amplified in selective (ampicillin) media, and frozen at -80^{0}C in LB containing 15% glycerol.

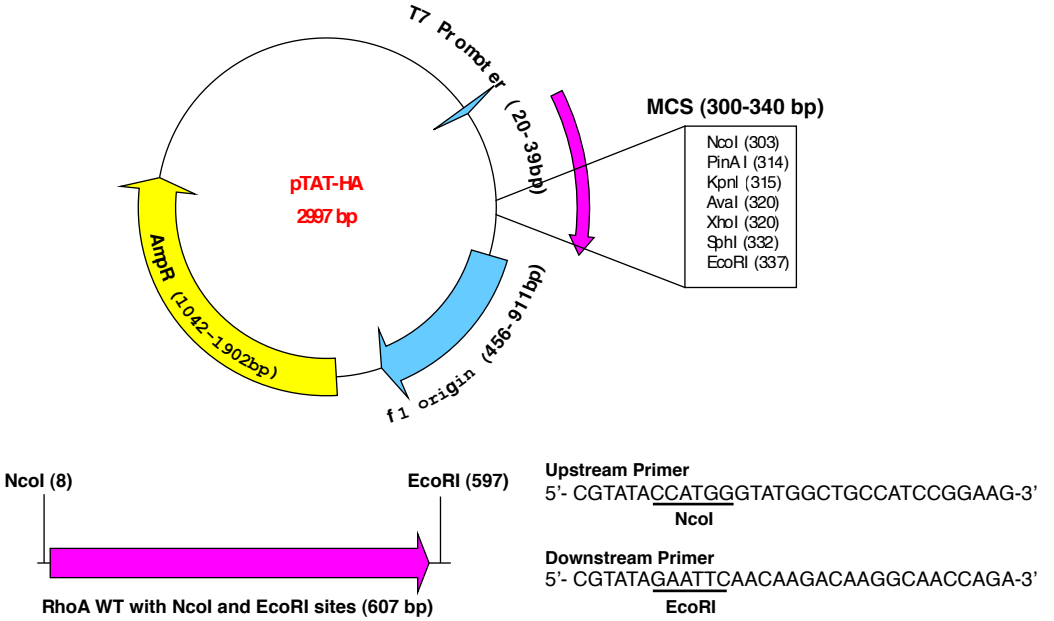

Figure 8-8. Structural Features of pTAT-HA Plasmid and of RhoA (Wild Type) Insert and Primers Used for Subcloning to Create TAT-RhoA Fusion.

Wild type (WT) RhoA was directionally subcloned into the multiple cloning site (MCS) of the pTAT-HA plasmid vector using NcoI and EcoRI restriction sites using the primers shown. This resulted in an in-frame fusion of rhoA with the hexahistidine (His6)-TAT- hemagluttinin (HA) leader, allowing for purification on a Ni^{2+}-column, protein transduction, and protein identification, respectively. Replication of this plasmid Expression of this construct is driven by an IPTG inducible promoter (T7 promoter). Successful transformants containing pTAT-HA are selected with ampicillin via AmpR resistance gene. Numbers indicate the boundaries or position of the feature or restriction site.

8.5.2.6 Expression and Purification of TAT-rhoA

After confirmation of an in-frame fusion by DNA sequencing (see Figure 8-9), pTAT-HA-rhoA plasmids were purified from *E. coli*, and then used to transform competent BL21 bacteria (R2, Rosetta^{TM}2(DE3)pLysS BL21 *E. coli* (Cam^{R}), Novagen (EMD Chemicals), Gibbstown, NJ, USA) which express an enhanced complement of tRNAs for human codons. Transformants were plated onto selective LB agar plates containing 50 μg/mL ampicillin and 10 μg/mL chloramphenicol, and grown O/N at 37^{0}C. 5 colonies were picked from the selective plates after O/N growth and used to inoculate 2 mL cultures of MagicMedia^{TM} (Invitrogen) expression medium containing 50 μg/mL ampicillin and 10 μg/mL chloramphenicol, and grown O/N at 37^{0}C. MagicMedia was selected because it allows for expression of proteins driven by the T7 promoter without the need to add IPTG manually. 1.5 mL of this culture was harvested by centrifugation (4000 x *g*), resuspended and lysed in 100 μL of 1X SDS-PAGE loading buffer via boiling for 10 min, then 5 μL of each was loaded onto SDS-PAGE minigels to evaluate protein expression by coomassie staining or WB. The remaining 0.5 mL of the culture was adjusted to 10% glycerol and frozen at -20^{0}C until needed. R2 transformants demonstrating the best yield of recombinant protein were selected for preparation of 15 mL starter cultures of LB with antibiotics. 5 mL of each 15 mL starter culture (O/N at 37^{0}C) of LB inoculated with transformed R2 was removed and used as a control for non-induced expression. The remaining 10 mL was transferred into 1-2L cultures of MM with the appropriate antibiotics and grown for 18-24 hrs. Cells were harvested by low speed centrifugation and the cell pellets were frozen -80^{0}C until ready for purification.

A **pTAT-HA Open Reading Frame:**

DNA sequence:

START

TTTGTTTAACTTTAAGAAGGAGATATACATATGCGGGGTTCTCATCATCATCATCATCATGGT
ATGGCTAGCATGACTGGTGGACAGCAAATGGGTCGGGATCTGTACGACGATGACGATAAGG
ATCGATGGGGATCCAAGCTTGGCTACGGCCGCAAGAAACGCCGCCAGCGCCGCCGCGGT
GGATCCACCATGTCCGGCTATCCATATGACGTCCCAGACTATGCTGGCTCCATGGCCGGTA
CCGGTCTCGAGGTGCATGCGGTGAATTCGAAGCTTGATCCGGCTGCTAACAAAGCCCGAA

EcoRI NcoI

Translation:

His6 TAT

MRGSHHHHHHGMASMTGGQQMGRDLYDDDDKDRWGSKLGYGRKKRRQRRRGGSTMSGYP
YDVPDYAGSMAGTGLEVHAVNSKLDPAANKAR*

HA

B **TAT-RhoA WT fusion:**

DNA sequence:

TTTGTTTAACTTTAAGAAGGAGATATACATATGCGGGGTTCTCATCATCATCATCATCATGGT
ATGGCTAGCATGACTGGTGGACAGCAAATGGGTCGGGATCTGTACGACGATGACGATAAGG
ATCGATGGGGATCCAAGCTTGGCTACGGCCGCAAGAAACGCCGCCAGCGCCGCCGCGGT
GGATCCACCATGTCCGGCTATCCATATGACGTCCCAGACTATGCTGGCTCCATGGGTATGG
CTGCCATCCGGAAGAAACTGGTGATTGTTGGTGATGGAGCCTGTGGAAAGACATGCTTGC
TCATAGTCTTCAGCAAGGACCAGTTCCCAGAGGTGTATGTGCCCACAGTGTTTGAGAACTA
TGTGGCAGATATCGAGGTGGATGGAAAGCAGGTAGAGTTGGCTTTGTGGGACACAGCTGG
GCAGGAAGATTATGATCGCCTGAGGCCCCTCTCCTACCCAGATACCGATGTTATACTGATG
TGTTTTTCCATCGACAGCCCTGATAGTTTAGAAAACATCCCAGAAAAGTGGACCCCAGAAG
TCAAGCATTTCTGTCCCAACGTGCCCATCATCCTGGTTGGGAATAAGAAGGATCTTCGGAA
TGATGAGCACACAAGGCGGGAGCTAGCCAAGATGAAGCAGGAGCCGGTGAAACCTGAAG
AAGGCAGAGATATGGCAAACAGGATTGGCGCTTTTGGGTACATGGAGTGTTCAGCAAAGA
CCAAAGATGGAGTGAGAGAGGTTTTTGAAATGGCTACGAGAGCTGCTCTGCAAGCTAGAC
GTGGGAAGAAAAAATCTGGTTGCCTTGTCTTGAATTCGAAGCTTGATCCGGCTGCTAACAA
AGCCCGAA

Translation:

MRGSHHHHHHGMASMTGGQQMGRDLYDDDDKDRWGSKLGYGRKKRRQRRR
GGSTMSGYPYDVPDYAGSMGMAAIRKKLVIVGDGACGKTCLLIVFSKDQFPEVYVPTVFE
NYVADIEVDGKQVELALWDTAGQEDYDRLRPLSYPDTDVILMCFSIDSPDSLENIPEKWT
PEVKHFCPNVPIILVGNKKDLRNDEHTRRELAKMKQEPVKPEEGRDMANRIGAFGYMECS
AKTKDGVREVFEMATRAALQARRGKKKSGCLVLNSKLDPAANKAR*

RhoA WT

Figure 8-9. DNA and Protein Sequences of pTAT-HA Plasmid Open Reading Frame and of TAT-RhoA (Wild Type) Fusion.

A. The DNA and translated protein sequences of the primary translated reading frame (open reading frame) of the pTAT-HA plasmid is shown without any insert. The start translation codon (ATG) and primary restriction sites used for synthesis of TAT-RhoA (EcoRI and NcoI) are highlighted by underline. **B.** The DNA and translated protein sequences of the TAT-RhoA (wild type, WT) fusion are shown. Orange text corresponds to the hexahistidine (His6) purification tag. Blue text corresponds to TAT peptide. Brown text corresponds to hemagluttinin (HA) tag. Red text corresponds to rhoA (WT) insert. Bold black text corresponds to restriction sites. * at the end of the peptide sequence indicates a stop codon (end of translation).

8.5.2.7 Protein Isolation Using Ni^{2+} Affinity Chromatography

The bacterial pellets were lysed in a buffer containing 8M Urea, 50 mM NaH_2PO_4, 300 mM NaCl, 10 mM imidazole, 1% (v/v) Triton-X-100, 1X bacterial protease inhibitors (Sigma-Aldrich), 1 mg/mL lysozyme (Sigma-Aldrich), 0.1 mg/mL DNAseI (Roche), and 1 mg/mL RNAseA, at pH 8.0, and incubating for 20 min on ice and then sonicating. The lysate was cleared of cell debris by centrifugation for 10 min at 4^0C). The lysate was loaded onto a 1mL Ni^{2+}-Sepharose column (GE Healthcare Bio-Sciences, Piscataway, NJ, USA) that was previously equilibrated with 5 column volumes of lysis buffer. The flowthrough was collected, and the column was washed and eluted sequentially with increasing concentrations of imidazole (20 mM to 200 mM) in buffers containing 50 mM NaH_2PO_4, 300 mM NaCl, pH 8.0. 2-4 fractions (1 mL each) were collected. WB and coomassie staining were used to determine which fractions contained TAT-rhoA. These fractions were pooled and desalted by equilibrating a PD-10 column (GE Healthcare) with 25 mL of DMEM, then adding 1.5 mL of the pool to the column. The purified proteins were eluted with 6 mL of DMEM and 1 mL fractions were collected. A small aliquot of each was analyzed via WB or coomassie staining. The desalted fractions containing purified proteins protein were pooled and adjusted to 10% glycerol, then stored at -80^0C until needed.

8.5.3 Results

The above methods produced a pure and concentrated form of TAT-rhoA that is was confirmed by both anti-hemagluttinin (HA) and anti-rhoA Abs, and which runs at a higher molecular weight (37 kDa) than rhoA alone (21 kDa, compare Figure 8-10A and B to Figure 8-3). Then hUSMC are treated overnight with the purified TAT-rhoA, both protein levels (Figure 8-10C) and rhoA activity (Figure 8-10D) are increased relative to vehicle. Interestingly, treatment with the rhoA activator calpeptin (Calp) did not appear to further enhance the measured rhoA activity (Figure 8-10D) in hUSMC that were also treated with TAT-rhoA. The reasons for this failure to enhance rhoA activity are unclear, but might indicate that other cellular factors, such as receptors or activating proteins are limiting.

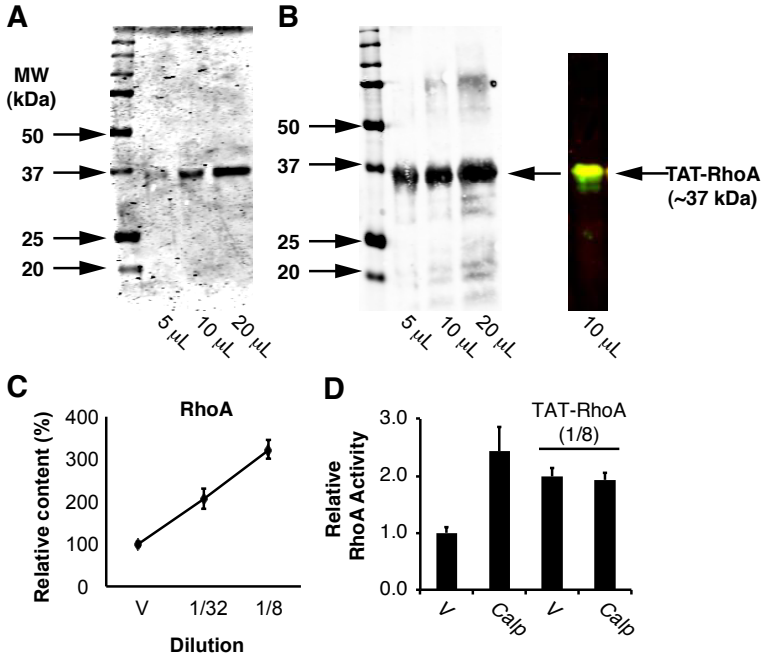

Figure 8-10. Demonstration of Purified TAT-RhoA (Wild Type) Fusion and of Transduction of TAT-RhoA Into hUSMC.

A. Coomassie stained tris-glycine gel after SDS-PAGE separation of purified TAT-RhoA protein. The sizes of molecular weight (MW) markers are indicated. Three lanes of a 12% acrylamide gel were loaded with 5, 10, and 20 µL of purified protein. **B.** The WB on the left was probed using anti-rhoA Ab demonstrating a band at the same position as in panel A. The adjacent colour WB was probed simultaneously with Abs toward rhoA (green) and toward the hemagluttinin (HA) tag (red) in the N-terminus of the fusion protein, as illustrated in Figure 8-9. The resultant overlap of red and green produces the yellow appearance of the band. **C.** Quantification of rhoA protein in hUSMC by ICW using the anti-rhoA Ab from Figure 8-3. hUSMC were treated with vehicle or with 1/32 and 1/8 dilutions of purified TAT-RhoA. **D.** Demonstration of rhoA activation in hUSMC treated with vehicle (DMF) or Calp (0.5 mU/mL, rhoA activator) in the presence or absence of 1/8 dilution of purified TAT-RhoA. GTP-bound rhoA was quantified by an absorbance assay, and absorbance data were corrected for rhoA content by WB.

8.5.4 Future Directions

Overall, though this is a potentially powerful technique, in the absence of sound technical guidance this project proved to be a high difficulty and low yield endeavor. This approach should be revisited only for important questions that cannot be addressed by other means. To complement the existing TAT-rhoA (WT) protein, parallel studies with TAT- rhoA dominant positive and dominant negative mutants (G14V and T19N, respectively) might be useful.(310, 315)

References

9 References

1. Aguilar, H.N., and Mitchell, B.F. 2010. Physiological pathways and molecular mechanisms regulating uterine contractility. *Hum Reprod Update* 16(6):725-44.
2. McCormick, M.C. 1985. The contribution of low birth weight to infant mortality and childhood morbidity. *N Engl J Med* 312:82-90.
3. Goldenberg, R.L., Culhane, J.F., Iams, J.D., and Romero, R. 2008. Epidemiology and causes of preterm birth. *Lancet* 371:75-84.
4. Arbuckle T, L.S., Rouleau J, Rusen ID, Turner L, Wen SW. 2000. Health Canada. Canadian Perinatal Health Report, 2000.: Ottawa: Minister of Public Works and Government Services Canada, 2000.
5. Effer, S.B., Moutquin, J.M., Farine, D., Saigal, S., Nimrod, C., Kelly, E., and Niyonsenga, T. 2002. Neonatal survival rates in 860 singleton live births at 24 and 25 weeks gestational age. A Canadian multicentre study. *BJOG* 109:740-745.
6. Joseph, K.S., Kramer, M.S., Marcoux, S., Ohlsson, A., Wen, S.W., Allen, A., and Platt, R. 1998. Determinants of preterm birth rates in Canada from 1981 through 1983 and from 1992 through 1994. *N Engl J Med* 339:1434-1439.
7. Joseph, K.S., Marcoux, S., Ohlsson, A., Kramer, M.S., Allen, A.C., Liu, S., Wu Wen, S., Demissie, K., Sauve, R., and Liston, R. 2002. Preterm birth, stillbirth and infant mortality among triplet births in Canada, 1985-96. *Paediatr Perinat Epidemiol* 16:141-148.
8. Ananth, C.V., Joseph, K.S., Oyelese, Y., Demissie, K., and Vintzileos, A.M. 2005. Trends in preterm birth and perinatal mortality among singletons: United States, 1989 through 2000. *Obstet Gynecol* 105:1084-1091.
9. Wood, N.S., Marlow, N., Costeloe, K., Gibson, A.T., and Wilkinson, A.R. 2000. Neurologic and developmental disability after extremely preterm birth. EPICure Study Group. *N Engl J Med* 343:378-384.
10. Wood, N.S., Costeloe, K., Gibson, A.T., Hennessy, E.M., Marlow, N., and Wilkinson, A.R. 2005. The EPICure study: associations and antecedents of neurological and developmental disability at 30 months of age following extremely preterm birth. *Arch Dis Child Fetal Neonatal Ed* 90:F134-140.

11. Wood, N.S., Costeloe, K., Gibson, A.T., Hennessy, E.M., Marlow, N., and Wilkinson, A.R. 2003. The EPICure study: growth and associated problems in children born at 25 weeks of gestational age or less. *Arch Dis Child Fetal Neonatal Ed* 88:F492-500.
12. Bracewell, M.A., Hennessy, E.M., Wolke, D., and Marlow, N. 2008. The EPICure study: growth and blood pressure at 6 years of age following extremely preterm birth. *Arch Dis Child Fetal Neonatal Ed* 93:F108-114.
13. Costeloe, K., Hennessy, E., Gibson, A.T., Marlow, N., and Wilkinson, A.R. 2000. The EPICure study: outcomes to discharge from hospital for infants born at the threshold of viability. *Pediatrics* 106:659-671.
14. Costeloe, K. 2006. EPICure: facts and figures: why preterm labour should be treated. *BJOG* 113 Suppl 3:10-12.
15. Marlow, N., Hennessy, E.M., Bracewell, M.A., and Wolke, D. 2007. Motor and executive function at 6 years of age after extremely preterm birth. *Pediatrics* 120:793-804.
16. Marlow, N., Wolke, D., Bracewell, M.A., and Samara, M. 2005. Neurologic and developmental disability at six years of age after extremely preterm birth. *N Engl J Med* 352:9-19.
17. Petrou, S., Henderson, J., Bracewell, M., Hockley, C., Wolke, D., and Marlow, N. 2006. Pushing the boundaries of viability: the economic impact of extreme preterm birth. *Early Hum Dev* 82:77-84.
18. Saigal, S., and Doyle, L.W. 2008. An overview of mortality and sequelae of preterm birth from infancy to adulthood. *Lancet* 371:261-269.
19. Slattery, M.M., and Morrison, J.J. 2002. Preterm delivery. *Lancet* 360:1489-1497.
20. Monga, M., and Creasy, R.K. 1995. Pharmacologic management of preterm labor. *Semin Perinatol* 19:84-96.
21. Tara, P.N., and Thornton, S. 2004. Current medical therapy in the prevention and treatment of preterm labour. *Semin Fetal Neonatal Med* 9:481-489.
22. Oei, S.G. 2006. Calcium channel blockers for tocolysis: a review of their role and safety following reports of serious adverse events. *Eur J Obstet Gynecol Reprod Biol* 126:137-145.

23. Anotayanonth, S., Subhedar, N.V., Garner, P., Neilson, J.P., and Harigopal, S. 2004. Betamimetics for inhibiting preterm labour. *Cochrane Database Syst Rev*:CD004352.

24. Conde-Agudelo, A., Romero, R., and Kusanovic, J.P. 2011. Nifedipine in the management of preterm labor: a systematic review and metaanalysis. *Am J Obstet Gynecol* 204:134 e131-120.

25. Crowther, C.A., Hiller, J.E., and Doyle, L.W. 2002. Magnesium sulphate for preventing preterm birth in threatened preterm labour. *Cochrane Database Syst Rev*:CD001060.

26. King, J., Flenady, V., Cole, S., and Thornton, S. 2005. Cyclo-oxygenase (COX) inhibitors for treating preterm labour. *Cochrane Database Syst Rev*:CD001992.

27. Duckitt, K., and Thornton, S. 2002. Nitric oxide donors for the treatment of preterm labour. *Cochrane Database Syst Rev*:CD002860.

28. Soloff, M.S., Alexandrova, M., and Fernstrom, M.J. 1979. Oxytocin receptors: triggers for parturition and lactation? *Science* 204:1313-1315.

29. Fuchs, A.R., Fuchs, F., Husslein, P., Soloff, M.S., and Fernstrom, M.J. 1982. Oxytocin receptors and human parturition: a dual role for oxytocin in the initiation of labor. *Science* 215:1396-1398.

30. Akerlund, M., Carlsson, A.M., Melin, P., and Trojnar, J. 1985. The effect on the human uterus of two newly developed competitive inhibitors of oxytocin and vasopressin. *Acta Obstet Gynecol Scand* 64:499-504.

31. Pierzynski, P., Lemancewicz, A., Reinheimer, T., Akerlund, M., and Laudanski, T. 2004. Inhibitory effect of barusiban and atosiban on oxytocin-induced contractions of myometrium from preterm and term pregnant women. *J Soc Gynecol Investig* 11:384-387.

32. Romero, R., Sibai, B.M., Sanchez-Ramos, L., Valenzuela, G.J., Veille, J.C., Tabor, B., Perry, K.G., Varner, M., Goodwin, T.M., Lane, R., et al. 2000. An oxytocin receptor antagonist (atosiban) in the treatment of preterm labor: a randomized, double-blind, placebo-controlled trial with tocolytic rescue. *Am J Obstet Gynecol* 182:1173-1183.

33. Papatsonis, D., Flenady, V., and Liley, H. 2009. Maintenance therapy with oxytocin antagonists for inhibiting preterm birth after threatened preterm labour. *Cochrane Database Syst Rev*:CD005938.
34. Sanborn, B.M., Ku, C.Y., Shlykov, S., and Babich, L. 2005. Molecular signaling through G-protein-coupled receptors and the control of intracellular calcium in myometrium. *J Soc Gynecol Investig* 12:479-487.
35. Thornton, S., Goodwin, T.M., Greisen, G., Hedegaard, M., and Arce, J.C. 2009. The effect of barusiban, a selective oxytocin antagonist, in threatened preterm labor at late gestational age: a randomized, double-blind, placebo-controlled trial. *Am J Obstet Gynecol* 200:627 e621-610.
36. Tan, T.C., Devendra, K., Tan, L.K., and Tan, H.K. 2006. Tocolytic treatment for the management of preterm labour: a systematic review. *Singapore Med J* 47:361-366.
37. Blumenfeld, Y.J., and Lyell, D.J. 2009. Prematurity prevention: the role of acute tocolysis. *Curr Opin Obstet Gynecol* 21:136-141.
38. Caritis, S.N. 2011. Metaanalysis and labor inhibition therapy. *Am J Obstet Gynecol* 204:95-96.
39. Roberts, D., and Dalziel, S. 2006. Antenatal corticosteroids for accelerating fetal lung maturation for women at risk of preterm birth. *Cochrane Database Syst Rev* 3:CD004454.
40. Neilson, J.P. 2007. Antenatal corticosteroids for accelerating fetal lung maturation for women at risk of preterm birth. *Obstet Gynecol* 109:189-190.
41. Panter, K.R., Hannah, M.E., Amankwah, K.S., Ohlsson, A., Jefferies, A.L., and Farine, D. 1999. The effect of indomethacin tocolysis in preterm labour on perinatal outcome: a randomised placebo-controlled trial. *Br J Obstet Gynaecol* 106:467-473.
42. 1992. Treatment of preterm labor with the beta-adrenergic agonist ritodrine. The Canadian Preterm Labor Investigators Group. *N Engl J Med* 327:308-312.
43. Mitchell, B.F., and Olson, D.M. 2004. Prostaglandin endoperoxide H synthase inhibitors and other tocolytics in preterm labour. *Prostaglandins Leukot Essent Fatty Acids* 70:167-187.

44. Bulletti, C., D, D.E.Z., Setti, P.L., Cicinelli, E., Polli, V., and Flamigni, C. 2004. The patterns of uterine contractility in normal menstruating women: from physiology to pathology. *Ann N Y Acad Sci* 1034:64-83.

45. Bulletti, C., and de Ziegler, D. 2006. Uterine contractility and embryo implantation. *Curr Opin Obstet Gynecol* 18:473-484.

46. van Gestel, I., MM, I.J., Hoogland, H.J., and Evers, J.L. 2003. Endometrial wave-like activity in the non-pregnant uterus. *Hum Reprod Update* 9:131-138.

47. Brosens, J.J., Barker, F.G., and de Souza, N.M. 1998. Myometrial zonal differentiation and uterine junctional zone hyperplasia in the non-pregnant uterus. *Hum Reprod Update* 4:496-502.

48. Ijland, M.M., Evers, J.L., Dunselman, G.A., van Katwijk, C., Lo, C.R., and Hoogland, H.J. 1996. Endometrial wavelike movements during the menstrual cycle. *Fertil Steril* 65:746-749.

49. Huszar, G., and Naftolin, F. 1984. The myometrium and uterine cervix in normal and preterm labor. *N Engl J Med* 311:571-581.

50. Hricak, H., Alpers, C., Crooks, L.E., and Sheldon, P.E. 1983. Magnetic resonance imaging of the female pelvis: initial experience. *AJR Am J Roentgenol* 141:1119-1128.

51. Noe, M., Kunz, G., Herbertz, M., Mall, G., and Leyendecker, G. 1999. The cyclic pattern of the immunocytochemical expression of oestrogen and progesterone receptors in human myometrial and endometrial layers: characterization of the endometrial-subendometrial unit. *Hum Reprod* 14:190-197.

52. Mitchell, B.F., and Taggart, M.J. 2009. Are animal models relevant to key aspects of human parturition? *Am J Physiol Regul Integr Comp Physiol* 297:R525-545.

53. Gabella, G. 1984. Structural apparatus for force transmission in smooth muscles. *Physiol Rev* 64:455-477.

54. Morgan, K.G., and Gangopadhyay, S.S. 2001. Invited review: cross-bridge regulation by thin filament-associated proteins. *J Appl Physiol* 91:953-962.

55. Gunst, S.J., and Zhang, W. 2008. Actin cytoskeletal dynamics in smooth muscle: a new paradigm for the regulation of smooth muscle contraction. *Am J Physiol Cell Physiol* 295:C576-587.

56. Word, R.A., Stull, J.T., Casey, M.L., and Kamm, K.E. 1993. Contractile elements and myosin light chain phosphorylation in myometrial tissue from nonpregnant and pregnant women. *J Clin Invest* 92:29-37.

57. Draeger, A., Amos, W.B., Ikebe, M., and Small, J.V. 1990. The cytoskeletal and contractile apparatus of smooth muscle: contraction bands and segmentation of the contractile elements. *J Cell Biol* 111:2463-2473.

58. Eddinger, T.J., and Meer, D.P. 2007. Myosin II isoforms in smooth muscle: heterogeneity and function. *Am J Physiol Cell Physiol* 293:C493-508.

59. Gorecka, A., Aksoy, M.O., and Hartshorne, D.J. 1976. The effect of phosphorylation of gizzard myosin on actin activation. *Biochem Biophys Res Commun* 71:325-331.

60. Arner, A., and Pfitzer, G. 1999. Regulation of cross-bridge cycling by Ca2+ in smooth muscle. *Rev Physiol Biochem Pharmacol* 134:63-146.

61. Hernandez, O.M., Jones, M., Guzman, G., and Szczesna-Cordary, D. 2007. Myosin essential light chain in health and disease. *Am J Physiol Heart Circ Physiol* 292:H1643-1654.

62. Hamada, Y., Yanagisawa, M., Katsuragawa, Y., Coleman, J.R., Nagata, S., Matsuda, G., and Masaki, T. 1990. Distinct vascular and intestinal smooth muscle myosin heavy chain mRNAs are encoded by a single-copy gene in the chicken. *Biochem Biophys Res Commun* 170:53-58.

63. Iizuka, K., Yoshii, A., Samizo, K., Tsukagoshi, H., Ishizuka, T., Dobashi, K., Nakazawa, T., and Mori, M. 1999. A major role for the rho-associated coiled coil forming protein kinase in G-protein-mediated Ca2+ sensitization through inhibition of myosin phosphatase in rabbit trachea. *British journal of pharmacology* 128:925-933.

64. Hewett, T.E., Martin, A.F., and Paul, R.J. 1993. Correlations between myosin heavy chain isoforms and mechanical parameters in rat myometrium. *The Journal of physiology* 460:351-364.

65. Gaylinn, B.D., Eddinger, T.J., Martino, P.A., Monical, P.L., Hunt, D.F., and Murphy, R.A. 1989. Expression of nonmuscle myosin heavy and light chains in smooth muscle. *Am J Physiol* 257:C997-1004.

66. Taubman, M.B., Grant, J.W., and Nadal-Ginard, B. 1987. Cloning and characterization of mammalian myosin regulatory light chain (RLC) cDNA: the RLC gene is expressed in smooth, sarcomeric, and nonmuscle tissues. *J Cell Biol* 104:1505-1513.

67. Kumar, C.C., Mohan, S.R., Zavodny, P.J., Narula, S.K., and Leibowitz, P.J. 1989. Characterization and differential expression of human vascular smooth muscle myosin light chain 2 isoform in nonmuscle cells. *Biochemistry* 28:4027-4035.

68. Morano, I. 2003. Tuning smooth muscle contraction by molecular motors. *J Mol Med* 81:481-487.

69. Parisi, J.A., and Eddinger, T.J. 2002. Smooth muscle myosin heavy chain isoform distribution in the swine stomach. *J Histochem Cytochem* 50:385-393.

70. Hai, C.M., and Murphy, R.A. 1988. Cross-bridge phosphorylation and regulation of latch state in smooth muscle. *Am J Physiol* 254:C99-106.

71. Ikebe, M., Koretz, J., and Hartshorne, D.J. 1988. Effects of phosphorylation of light chain residues threonine 18 and serine 19 on the properties and conformation of smooth muscle myosin. *J Biol Chem* 263:6432-6437.

72. Ikebe, M., Hartshorne, D.J., and Elzinga, M. 1986. Identification, phosphorylation, and dephosphorylation of a second site for myosin light chain kinase on the 20,000-dalton light chain of smooth muscle myosin. *J Biol Chem* 261:36-39.

73. Ikebe, M., Hartshorne, D.J., and Elzinga, M. 1987. Phosphorylation of the 20,000-dalton light chain of smooth muscle myosin by the calcium-activated, phospholipid-dependent protein kinase. Phosphorylation sites and effects of phosphorylation. *J Biol Chem* 262:9569-9573.

74. Wray, S. 1993. Uterine contraction and physiological mechanisms of modulation. *Am J Physiol* 264:C1-18.

75. Sperelakis, N., Inoue, Y., and Ohya, Y. 1992. Fast Na+ channels and slow Ca2+ current in smooth muscle from pregnant rat uterus. *Jpn J Pharmacol* 58 Suppl 2:96P-106P.

76. Sanborn, B.M. 2000. Relationship of ion channel activity to control of myometrial calcium. *J Soc Gynecol Investig* 7:4-11.

77. Phaneuf, S., Europe-Finner, G.N., Varney, M., MacKenzie, I.Z., Watson, S.P., and Lopez Bernal, A. 1993. Oxytocin-stimulated phosphoinositide hydrolysis in human myometrial cells: involvement of pertussis toxin-sensitive and -insensitive G-proteins. *J Endocrinol* 136:497-509.
78. Taylor, S.J., Chae, H.Z., Rhee, S.G., and Exton, J.H. 1991. Activation of the beta 1 isozyme of phospholipase C by alpha subunits of the Gq class of G proteins. *Nature* 350:516-518.
79. Berridge, M.J. 1993. Inositol trisphosphate and calcium signalling. *Nature* 361:315-325.
80. Exton, J.H. 1996. Regulation of phosphoinositide phospholipases by hormones, neurotransmitters, and other agonists linked to G proteins. *Annu Rev Pharmacol Toxicol* 36:481-509.
81. Furuichi, T., Yoshikawa, S., Miyawaki, A., Wada, K., Maeda, N., and Mikoshiba, K. 1989. Primary structure and functional expression of the inositol 1,4,5-trisphosphate-binding protein P400. *Nature* 342:32-38.
82. Streb, H., Irvine, R.F., Berridge, M.J., and Schulz, I. 1983. Release of Ca2+ from a nonmitochondrial intracellular store in pancreatic acinar cells by inositol-1,4,5-trisphosphate. *Nature* 306:67-69.
83. Gill, D.L. 1989. Calcium signalling: receptor kinships revealed. *Nature* 342:16-18.
84. Garfield, R.E., and Maner, W.L. 2007. Physiology and electrical activity of uterine contractions. *Semin Cell Dev Biol* 18:289-295.
85. Johnson, J.D., Snyder, C., Walsh, M., and Flynn, M. 1996. Effects of myosin light chain kinase and peptides on Ca2+ exchange with the N- and C-terminal Ca2+ binding sites of calmodulin. *J Biol Chem* 271:761-767.
86. Shojo, H., and Kaneko, Y. 2001. Oxytocin-induced phosphorylation of myosin light chain is mediated by extracellular calcium influx in pregnant rat myometrium. *J Mol Recognit* 14:401-405.
87. Takashima, S. 2009. Phosphorylation of myosin regulatory light chain by myosin light chain kinase, and muscle contraction. *Circ J* 73:208-213.
88. Kamm, K.E., and Stull, J.T. 2001. Dedicated myosin light chain kinases with diverse cellular functions. *J Biol Chem* 276:4527-4530.

89. Craig, R., Smith, R., and Kendrick-Jones, J. 1983. Light-chain phosphorylation controls the conformation of vertebrate non-muscle and smooth muscle myosin molecules. *Nature* 302:436-439.
90. Onishi, H., and Wakabayashi, T. 1982. Electron microscopic studies of myosin molecules from chicken gizzard muscle I: the formation of the intramolecular loop in the myosin tail. *J Biochem* 92:871-879.
91. Onishi, H., Wakabayashi, T., Kamata, T., and Watanabe, S. 1983. Electron microscopic studies of myosin molecules from chicken gizzard muscle II: The effect of thiophosphorylation of the 20K-dalton light chain on the ATP-induced change in the conformation of myosin monomers. *J Biochem* 94:1147-1154.
92. Ikebe, M., Inagaki, M., Kanamaru, K., and Hidaka, H. 1985. Phosphorylation of smooth muscle myosin light chain kinase by Ca2+-activated, phospholipid-dependent protein kinase. *J Biol Chem* 260:4547-4550.
93. Hai, C.M., and Murphy, R.A. 1989. Ca2+, crossbridge phosphorylation, and contraction. *Annu Rev Physiol* 51:285-298.
94. Dillon, P.F., Aksoy, M.O., Driska, S.P., and Murphy, R.A. 1981. Myosin phosphorylation and the cross-bridge cycle in arterial smooth muscle. *Science* 211:495-497.
95. Stull, J.T., Lin, P.J., Krueger, J.K., Trewhella, J., and Zhi, G. 1998. Myosin light chain kinase: functional domains and structural motifs. *Acta Physiol Scand* 164:471-482.
96. Longbottom, E.R., Luckas, M.J., Kupittayanant, S., Badrick, E., Shmigol, T., and Wray, S. 2000. The effects of inhibiting myosin light chain kinase on contraction and calcium signalling in human and rat myometrium. *Pflugers Arch* 440:315-321.
97. Gordon, A.M., Homsher, E., and Regnier, M. 2000. Regulation of contraction in striated muscle. *Physiol Rev* 80:853-924.
98. Stevenson, R.C., McCabe, C.J., Pharoah, P.O., and Cooke, R.W. 1996. Cost of care for a geographically determined population of low birthweight infants to age 8-9 years. I. Children without disability. *Arch Dis Child Fetal Neonatal Ed* 74:F114-117.

99. Lukas, T.J., Burgess, W.H., Prendergast, F.G., Lau, W., and Watterson, D.M. 1986. Calmodulin binding domains: characterization of a phosphorylation and calmodulin binding site from myosin light chain kinase. *Biochemistry* 25:1458-1464.

100. Ikebe, M., and Reardon, S. 1990. Phosphorylation of smooth myosin light chain kinase by smooth muscle Ca2+/calmodulin-dependent multifunctional protein kinase. *J Biol Chem* 265:8975-8978.

101. Stull, J.T., Tansey, M.G., Tang, D.C., Word, R.A., and Kamm, K.E. 1993. Phosphorylation of myosin light chain kinase: a cellular mechanism for Ca2+ desensitization. *Mol Cell Biochem* 127-128:229-237.

102. Hashimoto, Y., and Soderling, T.R. 1990. Phosphorylation of smooth muscle myosin light chain kinase by Ca2+/calmodulin-dependent protein kinase II: comparative study of the phosphorylation sites. *Arch Biochem Biophys* 278:41-45.

103. Wray, S., Jones, K., Kupittayanant, S., Li, Y., Matthew, A., Monir-Bishty, E., Noble, K., Pierce, S.J., Quenby, S., and Shmygol, A.V. 2003. Calcium signaling and uterine contractility. *J Soc Gynecol Investig* 10:252-264.

104. Morgan, J.P., and Morgan, K.G. 1984. Stimulus-specific patterns of intracellular calcium levels in smooth muscle of ferret portal vein. *J Physiol* 351:155-167.

105. Himpens, B., Kitazawa, T., and Somlyo, A.P. 1990. Agonist-dependent modulation of Ca2+ sensitivity in rabbit pulmonary artery smooth muscle. *Pflugers Arch* 417:21-28.

106. Somlyo, A.P., and Somlyo, A.V. 1994. Signal transduction and regulation in smooth muscle. *Nature* 372:231-236.

107. Bradley, A.B., and Morgan, K.G. 1987. Alterations in cytoplasmic calcium sensitivity during porcine coronary artery contractions as detected by aequorin. *J Physiol* 385:437-448.

108. Noda, M., Yasuda-Fukazawa, C., Moriishi, K., Kato, T., Okuda, T., Kurokawa, K., and Takuwa, Y. 1995. Involvement of rho in GTP gamma S-induced enhancement of phosphorylation of 20 kDa myosin light chain in vascular smooth muscle cells: inhibition of phosphatase activity. *FEBS Lett* 367:246-250.

109. Kitazawa, T., Kobayashi, S., Horiuti, K., Somlyo, A.V., and Somlyo, A.P. 1989. Receptor-coupled, permeabilized smooth muscle. Role of the phosphatidylinositol cascade, G-proteins, and modulation of the contractile response to Ca2+. *J Biol Chem* 264:5339-5342.

110. Kozasa, T., Jiang, X., Hart, M.J., Sternweis, P.M., Singer, W.D., Gilman, A.G., Bollag, G., and Sternweis, P.C. 1998. p115 RhoGEF, a GTPase activating protein for Galpha12 and Galpha13. *Science* 280:2109-2111.

111. Klages, B., Brandt, U., Simon, M.I., Schultz, G., and Offermanns, S. 1999. Activation of G12/G13 results in shape change and Rho/Rho-kinase-mediated myosin light chain phosphorylation in mouse platelets. *J Cell Biol* 144:745-754.

112. Yeramian, P., Chardin, P., Madaule, P., and Tavitian, A. 1987. Nucleotide sequence of human rho cDNA clone 12. *Nucleic Acids Res* 15:1869.

113. Bishop, A.L., and Hall, A. 2000. Rho GTPases and their effector proteins. *Biochem J* 348 Pt 2:241-255.

114. Self, A.J., and Hall, A. 1995. Measurement of intrinsic nucleotide exchange and GTP hydrolysis rates. *Methods Enzymol* 256:67-76.

115. Fukuhara, S., Chikumi, H., and Gutkind, J.S. 2001. RGS-containing RhoGEFs: the missing link between transforming G proteins and Rho? *Oncogene* 20:1661-1668.

116. Taggart, M.J., Lee, Y.H., and Morgan, K.G. 1999. Cellular redistribution of PKCalpha, rhoA, and ROKalpha following smooth muscle agonist stimulation. *Exp Cell Res* 251:92-101.

117. Hersch, E., Huang, J., Grider, J.R., and Murthy, K.S. 2004. Gq/G13 signaling by ET-1 in smooth muscle: MYPT1 phosphorylation via ETA and CPI-17 dephosphorylation via ETB. *Am J Physiol Cell Physiol* 287:C1209-1218.

118. Rattan, S., Puri, R.N., and Fan, Y.P. 2003. Involvement of rho and rho-associated kinase in sphincteric smooth muscle contraction by angiotensin II. *Exp Biol Med (Maywood)* 228:972-981.

119. Hori, Y., Kikuchi, A., Isomura, M., Katayama, M., Miura, Y., Fujioka, H., Kaibuchi, K., and Takai, Y. 1991. Post-translational modifications of the C-terminal region of the rho protein are important for its interaction with membranes and the stimulatory and inhibitory GDP/GTP exchange proteins. *Oncogene* 6:515-522.

120. Fujihara, H., Walker, L.A., Gong, M.C., Lemichez, E., Boquet, P., Somlyo, A.V., and Somlyo, A.P. 1997. Inhibition of RhoA translocation and calcium sensitization by in vivo ADP-ribosylation with the chimeric toxin DC3B. *Mol Biol Cell* 8:2437-2447.

121. Lee, Y.H., Hwang, M.K., Morgan, K.G., and Taggart, M.J. 2001. Receptor-coupled contractility of uterine smooth muscle: from membrane to myofilaments. *Exp Physiol* 86:283-288.

122. Fukumoto, Y., Kaibuchi, K., Hori, Y., Fujioka, H., Araki, S., Ueda, T., Kikuchi, A., and Takai, Y. 1990. Molecular cloning and characterization of a novel type of regulatory protein (GDI) for the rho proteins, ras p21-like small GTP-binding proteins. *Oncogene* 5:1321-1328.

123. Bourmeyster, N., Stasia, M.J., Garin, J., Gagnon, J., Boquet, P., and Vignais, P.V. 1992. Copurification of rho protein and the rho-GDP dissociation inhibitor from bovine neutrophil cytosol. Effect of phosphoinositides on rho ADP-ribosylation by the C3 exoenzyme of Clostridium botulinum. *Biochemistry* 31:12863-12869.

124. Hancock, J.F., and Hall, A. 1993. A novel role for RhoGDI as an inhibitor of GAP proteins. *EMBO J* 12:1915-1921.

125. Read, P.W., Liu, X., Longenecker, K., Dipierro, C.G., Walker, L.A., Somlyo, A.V., Somlyo, A.P., and Nakamoto, R.K. 2000. Human RhoA/RhoGDI complex expressed in yeast: GTP exchange is sufficient for translocation of RhoA to liposomes. *Protein Sci* 9:376-386.

126. Lang, P., Gesbert, F., Delespine-Carmagnat, M., Stancou, R., Pouchelet, M., and Bertoglio, J. 1996. Protein kinase A phosphorylation of RhoA mediates the morphological and functional effects of cyclic AMP in cytotoxic lymphocytes. *EMBO J* 15:510-519.

127. Sawada, N., Itoh, H., Yamashita, J., Doi, K., Inoue, M., Masatsugu, K., Fukunaga, Y., Sakaguchi, S., Sone, M., Yamahara, K., et al. 2001. cGMP-dependent protein kinase phosphorylates and inactivates RhoA. *Biochem Biophys Res Commun* 280:798-805.

128. Ellerbroek, S.M., Wennerberg, K., and Burridge, K. 2003. Serine phosphorylation negatively regulates RhoA in vivo. *J Biol Chem* 278:19023-19031.

129. Hirata, K., Kikuchi, A., Sasaki, T., Kuroda, S., Kaibuchi, K., Matsuura, Y., Seki, H., Saida, K., and Takai, Y. 1992. Involvement of rho p21 in the GTP-enhanced calcium ion sensitivity of smooth muscle contraction. *J Biol Chem* 267:8719-8722.

130. Kitazawa, T., Masuo, M., and Somlyo, A.P. 1991. G protein-mediated inhibition of myosin light-chain phosphatase in vascular smooth muscle. *Proc Natl Acad Sci U S A* 88:9307-9310.

131. Leung, T., Chen, X.Q., Manser, E., and Lim, L. 1996. The p160 RhoA-binding kinase ROK alpha is a member of a kinase family and is involved in the reorganization of the cytoskeleton. *Mol Cell Biol* 16:5313-5327.

132. Matsui, T., Amano, M., Yamamoto, T., Chihara, K., Nakafuku, M., Ito, M., Nakano, T., Okawa, K., Iwamatsu, A., and Kaibuchi, K. 1996. Rho-associated kinase, a novel serine/threonine kinase, as a putative target for small GTP binding protein Rho. *EMBO J* 15:2208-2216.

133. Moore, F., Da Silva, C., Wilde, J.I., Smarason, A., Watson, S.P., and Lopez Bernal, A. 2000. Up-regulation of p21- and RhoA-activated protein kinases in human pregnant myometrium. *Biochem Biophys Res Commun* 269:322-326.

134. Niiro, N., Nishimura, J., Sakihara, C., Nakano, H., and Kanaide, H. 1997. Up-regulation of rho A and rho-kinase mRNAs in the rat myometrium during pregnancy. *Biochem Biophys Res Commun* 230:356-359.

135. Moran, C.J., Friel, A.M., Smith, T.J., Cairns, M., and Morrison, J.J. 2002. Expression and modulation of Rho kinase in human pregnant myometrium. *Mol Hum Reprod* 8:196-200.

136. Somlyo, A.P., and Somlyo, A.V. 2003. Ca2+ sensitivity of smooth muscle and nonmuscle myosin II: modulated by G proteins, kinases, and myosin phosphatase. *Physiol Rev* 83:1325-1358.

137. Lartey, J., and Lopez Bernal, A. 2009. RHO protein regulation of contraction in the human uterus. *Reproduction* 138:407-424.

138. Miyazaki, K., Komatsu, S., and Ikebe, M. 2006. Dynamics of RhoA and ROKalpha translocation in single living cells. *Cell Biochem Biophys* 45:243-254.

139. Sin, W.C., Chen, X.Q., Leung, T., and Lim, L. 1998. RhoA-binding kinase alpha translocation is facilitated by the collapse of the vimentin intermediate filament network. *Mol Cell Biol* 18:6325-6339.

140. Amano, M., Fukata, Y., and Kaibuchi, K. 2000. Regulation and functions of Rho-associated kinase. *Exp Cell Res* 261:44-51.

141. Ishizaki, T., Maekawa, M., Fujisawa, K., Okawa, K., Iwamatsu, A., Fujita, A., Watanabe, N., Saito, Y., Kakizuka, A., Morii, N., et al. 1996. The small GTP-binding protein Rho binds to and activates a 160 kDa Ser/Thr protein kinase homologous to myotonic dystrophy kinase. *EMBO J* 15:1885-1893.

142. Chen, X.Q., Tan, I., Ng, C.H., Hall, C., Lim, L., and Leung, T. 2002. Characterization of RhoA-binding kinase ROKalpha implication of the pleckstrin homology domain in ROKalpha function using region-specific antibodies. *J Biol Chem* 277:12680-12688.

143. Kimura, K., Ito, M., Amano, M., Chihara, K., Fukata, Y., Nakafuku, M., Yamamori, B., Feng, J., Nakano, T., Okawa, K., et al. 1996. Regulation of myosin phosphatase by Rho and Rho-associated kinase (Rho-kinase). *Science* 273:245-248.

144. Tahara, M., Morishige, K., Sawada, K., Ikebuchi, Y., Kawagishi, R., Tasaka, K., and Murata, Y. 2002. RhoA/Rho-kinase cascade is involved in oxytocin-induced rat uterine contraction. *Endocrinology* 143:920-929.

145. Kupittayanant, S., Burdyga, T., and Wray, S. 2001. The effects of inhibiting Rho-associated kinase with Y-27632 on force and intracellular calcium in human myometrium. *Pflugers Arch* 443:112-114.

146. Fu, X., Gong, M.C., Jia, T., Somlyo, A.V., and Somlyo, A.P. 1998. The effects of the Rho-kinase inhibitor Y-27632 on arachidonic acid-, GTPgammaS-, and phorbol ester-induced Ca2+-sensitization of smooth muscle. *FEBS Lett* 440:183-187.

147. Amano, M., Ito, M., Kimura, K., Fukata, Y., Chihara, K., Nakano, T., Matsuura, Y., and Kaibuchi, K. 1996. Phosphorylation and activation of myosin by Rho-associated kinase (Rho-kinase). *J Biol Chem* 271:20246-20249.

148. Somlyo, A.P., and Somlyo, A.V. 2000. Signal transduction by G-proteins, rho-kinase and protein phosphatase to smooth muscle and non-muscle myosin II. *J Physiol* 522 Pt 2:177-185.

149. Sward, K., Dreja, K., Susnjar, M., Hellstrand, P., Hartshorne, D.J., and Walsh, M.P. 2000. Inhibition of Rho-associated kinase blocks agonist-induced Ca2+ sensitization of myosin phosphorylation and force in guinea-pig ileum. *The Journal of physiology* 522 Pt 1:33-49.

150. Ceulemans, H., and Bollen, M. 2004. Functional diversity of protein phosphatase-1, a cellular economizer and reset button. *Physiol Rev* 84:1-39.

151. Ito, M., Nakano, T., Erdodi, F., and Hartshorne, D.J. 2004. Myosin phosphatase: structure, regulation and function. *Mol Cell Biochem* 259:197-209.

152. Hartshorne, D.J., Ito, M., and Erdodi, F. 1998. Myosin light chain phosphatase: subunit composition, interactions and regulation. *J Muscle Res Cell Motil* 19:325-341.

153. Matsumura, F., and Hartshorne, D.J. 2007. Myosin phosphatase target subunit: Many roles in cell function. *Biochem Biophys Res Commun*.

154. Hartshorne, D.J., Ito, M., and Erdodi, F. 2004. Role of protein phosphatase type 1 in contractile functions: myosin phosphatase. *J Biol Chem* 279:37211-37214.

155. Shirazi, A., Iizuka, K., Fadden, P., Mosse, C., Somlyo, A.P., Somlyo, A.V., and Haystead, T.A. 1994. Purification and characterization of the mammalian myosin light chain phosphatase holoenzyme. The differential effects of the holoenzyme and its subunits on smooth muscle. *J Biol Chem* 269:31598-31606.

156. Cohen, P.T. 2002. Protein phosphatase 1--targeted in many directions. *J Cell Sci* 115:241-256.

157. Kawano, Y., Fukata, Y., Oshiro, N., Amano, M., Nakamura, T., Ito, M., Matsumura, F., Inagaki, M., and Kaibuchi, K. 1999. Phosphorylation of myosin-binding subunit (MBS) of myosin phosphatase by Rho-kinase in vivo. *J Cell Biol* 147:1023-1038.

158. Okubo, S., Ito, M., Takashiba, Y., Ichikawa, K., Miyahara, M., Shimizu, H., Konishi, T., Shima, H., Nagao, M., Hartshorne, D.J., et al. 1994. A regulatory subunit of smooth muscle myosin bound phosphatase. *Biochem Biophys Res Commun* 200:429-434.

159. Shimizu, H., Ito, M., Miyahara, M., Ichikawa, K., Okubo, S., Konishi, T., Naka, M., Tanaka, T., Hirano, K., Hartshorne, D.J., et al. 1994. Characterization of the myosin-binding subunit of smooth muscle myosin phosphatase. *J Biol Chem* 269:30407-30411.

160. Dirksen, W.P., Vladic, F., and Fisher, S.A. 2000. A myosin phosphatase targeting subunit isoform transition defines a smooth muscle developmental phenotypic switch. *Am J Physiol Cell Physiol* 278:C589-600.

161. Ogut, O., and Brozovich, F.V. 2000. Determinants of the contractile properties in the embryonic chicken gizzard and aorta. *Am J Physiol Cell Physiol* 279:C1722-1732.

162. Terrak, M., Kerff, F., Langsetmo, K., Tao, T., and Dominguez, R. 2004. Structural basis of protein phosphatase 1 regulation. *Nature* 429:780-784.

163. Ito, K., Hirooka, Y., Kishi, T., Kimura, Y., Kaibuchi, K., Shimokawa, H., and Takeshita, A. 2004. Rho/Rho-kinase pathway in the brainstem contributes to hypertension caused by chronic nitric oxide synthase inhibition. *Hypertension* 43:156-162.

164. Ichikawa, K., Ito, M., and Hartshorne, D.J. 1996. Phosphorylation of the large subunit of myosin phosphatase and inhibition of phosphatase activity. *J Biol Chem* 271:4733-4740.

165. Wu, Y., Muranyi, A., Erdodi, F., and Hartshorne, D.J. 2005. Localization of myosin phosphatase target subunit and its mutants. *J Muscle Res Cell Motil* 26:123-134.

166. Murphy, R.A., and Walker, J.S. 1998. Inhibitory mechanisms for cross-bridge cycling: the nitric oxide-cGMP signal transduction pathway in smooth muscle relaxation. *Acta Physiol Scand* 164:373-380.

167. Nakamura, K., Koga, Y., Sakai, H., Homma, K., and Ikebe, M. 2007. cGMP-dependent relaxation of smooth muscle is coupled with the change in the phosphorylation of myosin phosphatase. *Circ Res* 101:712-722.

168. Payne, M.C., Zhang, H.Y., Prosdocimo, T., Joyce, K.M., Koga, Y., Ikebe, M., and Fisher, S.A. 2006. Myosin phosphatase isoform switching in vascular smooth muscle development. *J Mol Cell Cardiol* 40:274-282.

169. Toth, A., Kiss, E., Gergely, P., Walsh, M.P., Hartshorne, D.J., and Erdodi, F. 2000. Phosphorylation of MYPT1 by protein kinase C attenuates interaction with PP1 catalytic subunit and the 20 kDa light chain of myosin. *FEBS Lett* 484:113-117.

170. Alessi, D., MacDougall, L.K., Sola, M.M., Ikebe, M., and Cohen, P. 1992. The control of protein phosphatase-1 by targetting subunits. The major myosin phosphatase in avian smooth muscle is a novel form of protein phosphatase-1. *Eur J Biochem* 210:1023-1035.

171. Kim, Y.S., Kim, B., Karaki, H., Hori, M., and Ozaki, H. 2003. Up-regulation of Rnd1 during pregnancy serves as a negative-feedback control for Ca2+ sensitization of contractile elements in rat myometrium. *Biochem Biophys Res Commun* 311:972-978.

172. Riley, M., Baker, P.N., Tribe, R.M., and Taggart, M.J. 2005. Expression of scaffolding, signalling and contractile-filament proteins in human myometria: effects of pregnancy and labour. *J Cell Mol Med* 9:122-134.

173. Riley, M., Wu, X., Baker, P.N., and Taggart, M.J. 2005. Gestational-dependent changes in the expression of signal transduction and contractile filament-associated proteins in mouse myometrium. *J Soc Gynecol Investig* 12:e33-43.

174. Riento, K., and Ridley, A.J. 2003. Rocks: multifunctional kinases in cell behaviour. *Nat Rev Mol Cell Biol* 4:446-456.

175. Lartey, J., Gampel, A., Pawade, J., Mellor, H., and Bernal, A.L. 2006. Expression of RND proteins in human myometrium. *Biol Reprod* 75:452-461.

176. Shmygol, A., Gullam, J., Blanks, A., and Thornton, S. 2006. Multiple mechanisms involved in oxytocin-induced modulation of myometrial contractility. *Acta Pharmacol Sin* 27:827-832.

177. Woodcock, N.A., Taylor, C.W., and Thornton, S. 2004. Effect of an oxytocin receptor antagonist and rho kinase inhibitor on the [Ca++]i sensitivity of human myometrium. *Am J Obstet Gynecol* 190:222-228.

178. Woodcock, N.A., Taylor, C.W., and Thornton, S. 2006. Prostaglandin F2alpha increases the sensitivity of the contractile proteins to Ca2+ in human myometrium. *Am J Obstet Gynecol* 195:1404-1406.

179. Oh, J.H., You, S.K., Hwang, M.K., Ahn, D.S., Kwon, S.C., Taggart, M.J., and Lee, Y.H. 2003. Inhibition of rho-associated kinase reduces MLC20 phosphorylation and contractility of intact myometrium and attenuates agonist-induced Ca2+ sensitization of force of permeabilized rat myometrium. *J Vet Med Sci* 65:43-50.

180. Kupittayanant, S., Kupittayanant, P., and Suwannachat, C. 2009. Mechanisms of uterine contractility in laying hens. *Anim Reprod Sci* 115:215-224.

181. Tahara, M., Kawagishi, R., Sawada, K., Morishige, K., Sakata, M., Tasaka, K., and Murata, Y. 2005. Tocolytic effect of a Rho-kinase inhibitor in a mouse model of lipopolysaccharide-induced preterm delivery. *Am J Obstet Gynecol* 192:903-908.

182. Somlyo, A.P., and Somlyo, A.V. 1998. From pharmacomechanical coupling to G-proteins and myosin phosphatase. *Acta Physiol Scand* 164:437-448.

183. Himpens, B., Matthijs, G., and Somlyo, A.P. 1989. Desensitization to cytoplasmic Ca2+ and Ca2+ sensitivities of guinea-pig ileum and rabbit pulmonary artery smooth muscle. *J Physiol* 413:489-503.

184. Aguilar, H.N., Zielnik, B., Tracey, C.N., and Mitchell, B.F. 2010. Quantification of rapid Myosin regulatory light chain phosphorylation using high-throughput in-cell Western assays: comparison to Western immunoblots. *PLoS ONE* 5:e9965.

185. Weldon, S., Ambroz, K., Schutz-Geschwender, A., and Olive, D.M. 2008. Near-infrared fluorescence detection permits accurate imaging of loading controls for Western blot analysis. *Anal Biochem* 375:156-158.

186. Wang, Y.V., Wade, M., Wong, E., Li, Y.C., Rodewald, L.W., and Wahl, G.M. 2007. Quantitative analyses reveal the importance of regulated Hdmx degradation for p53 activation. *Proc Natl Acad Sci U S A* 104:12365-12370.

187. Jungblut, P., Eckerskorn, C., Lottspeich, F., and Klose, J. 1990. Blotting efficiency investigated by using two-dimensional electrophoresis, hydrophobic membranes and proteins from different sources. *Electrophoresis* 11:581-588.

188. Tovey, E.R., and Baldo, B.A. 1987. Comparison of semi-dry and conventional tank-buffer electrotransfer of proteins from polyacrylamide gels to nitrocellulose membranes. *Electrophoresis* 8:384-387.

189. Selkirk, J.V., Nottebaum, L.M., Ford, I.C., Santos, M., Malany, S., Foster, A.C., and Lechner, S.M. 2006. A novel cell-based assay for G-protein-coupled receptor-

mediated cyclic adenosine monophosphate response element binding protein phosphorylation. *J Biomol Screen* 11:351-358.

190. Kumar, N., Afeyan, R., Kim, H.D., and Lauffenburger, D.A. 2008. Multipathway model enables prediction of kinase inhibitor cross-talk effects on migration of Her2-overexpressing mammary epithelial cells. *Mol Pharmacol* 73:1668-1678.
191. Coevoets, R., Arican, S., Hoogeveen-Westerveld, M., Simons, E., van den Ouweland, A., Halley, D., and Nellist, M. 2009. A reliable cell-based assay for testing unclassified TSC2 gene variants. *Eur J Hum Genet* 17:301-310.
192. Bond, D., Primrose, D.A., and Foley, E. 2008. Quantitative evaluation of signaling events in Drosophila s2 cells. *Biol Proced Online* 10:20-28.
193. Schroter, T., Griffin, E., Weiser, A., Feng, Y., and LoGrasso, P. 2008. Detection of myosin light chain phosphorylation--a cell-based assay for screening Rho-kinase inhibitors. *Biochem Biophys Res Commun* 374:356-360.
194. Kinoshita, E., Kinoshita-Kikuta, E., Takiyama, K., and Koike, T. 2006. Phosphate-binding tag, a new tool to visualize phosphorylated proteins. *Mol Cell Proteomics* 5:749-757.
195. Laemmli, U.K. 1970. Cleavage of structural proteins during the assembly of the head of bacteriophage T4. *Nature* 227:680-685.
196. Lundholt, B.K., Scudder, K.M., and Pagliaro, L. 2003. A simple technique for reducing edge effect in cell-based assays. *J Biomol Screen* 8:566-570.
197. Takeya, K., Loutzenhiser, K., Shiraishi, M., Loutzenhiser, R., and Walsh, M.P. 2008. A highly sensitive technique to measure myosin regulatory light chain phosphorylation: the first quantification in renal arterioles. *Am J Physiol Renal Physiol* 294:F1487-1492.
198. Smith, P.J., Wiltshire, M., Davies, S., Patterson, L.H., and Hoy, T. 1999. A novel cell permeant and far red-fluorescing DNA probe, DRAQ5, for blood cell discrimination by flow cytometry. *J Immunol Methods* 229:131-139.
199. Kim, H.R., Appel, S., Vetterkind, S., Gangopadhyay, S.S., and Morgan, K.G. 2008. Smooth muscle signalling pathways in health and disease. *J Cell Mol Med* 12:2165-2180.

200. Hunter, T. 1995. Protein kinases and phosphatases: the yin and yang of protein phosphorylation and signaling. *Cell* 80:225-236.

201. Bhadriraju, K., Elliott, J.T., Nguyen, M., and Plant, A.L. 2007. Quantifying myosin light chain phosphorylation in single adherent cells with automated fluorescence microscopy. *BMC Cell Biol* 8:43.

202. Zhou, X.B., Lutz, S., Steffens, F., Korth, M., and Wieland, T. 2007. Oxytocin receptors differentially signal via Gq and Gi proteins in pregnant and nonpregnant rat uterine myocytes: implications for myometrial contractility. *Mol Endocrinol* 21:740-752.

203. Sharma, S.K., and Carew, T.J. 2002. Inclusion of phosphatase inhibitors during Western blotting enhances signal detection with phospho-specific antibodies. *Anal Biochem* 307:187-189.

204. Abeyrathne, P.D., and Lam, J.S. 2007. Conditions that allow for effective transfer of membrane proteins onto nitrocellulose membrane in Western blots. *Can J Microbiol* 53:526-532.

205. Towbin, H., Staehelin, T., and Gordon, J. 1979. Electrophoretic transfer of proteins from polyacrylamide gels to nitrocellulose sheets: procedure and some applications. *Proc Natl Acad Sci U S A* 76:4350-4354.

206. Bolt, M.W., and Mahoney, P.A. 1997. High-efficiency blotting of proteins of diverse sizes following sodium dodecyl sulfate-polyacrylamide gel electrophoresis. *Anal Biochem* 247:185-192.

207. Egger, D., and Bienz, K. 1994. Protein (western) blotting. *Mol Biotechnol* 1:289-305.

208. DenHollander, N., and Befus, D. 1989. Loss of antigens from immunoblotting membranes. *J Immunol Methods* 122:129-135.

209. Tovey, E.R., and Baldo, B.A. 1989. Protein binding to nitrocellulose, nylon and PVDF membranes in immunoassays and electroblotting. *J Biochem Biophys Methods* 19:169-183.

210. Aldridge, G.M., Podrebarac, D.M., Greenough, W.T., and Weiler, I.J. 2008. The use of total protein stains as loading controls: an alternative to high-abundance

single-protein controls in semi-quantitative immunoblotting. *J Neurosci Methods* 172:250-254.

211. Mandell, J.W. 2003. Phosphorylation state-specific antibodies: applications in investigative and diagnostic pathology. *Am J Pathol* 163:1687-1698.
212. Arnon, R., and Van Regenmortel, M.H. 1992. Structural basis of antigenic specificity and design of new vaccines. *FASEB J* 6:3265-3274.
213. Weber, L.P., Van Lierop, J.E., and Walsh, M.P. 1999. Ca2+-independent phosphorylation of myosin in rat caudal artery and chicken gizzard myofilaments. *J Physiol* 516 (Pt 3):805-824.
214. Aguilar, H.N., Tracey, C.N., Zielnik, B., and Mitchell, B.F. 2011. Phos-tag-Based Analysis of Myosin Regulatory Light Chain Phosphorylation in Human Uterine Myocytes. *PLoS ONE* 6(6): e20903.
215. Hunter, T. 2000. Signaling--2000 and beyond. *Cell* 100:113-127.
216. Thingholm, T.E., Jensen, O.N., and Larsen, M.R. 2009. Analytical strategies for phosphoproteomics. *Proteomics* 9:1451-1468.
217. Kinoshita, E., Kinoshita-Kikuta, E., and Koike, T. 2009. Separation and detection of large phosphoproteins using Phos-tag SDS-PAGE. *Nat Protoc* 4:1513-1521.
218. Deswal, S., Beck-Garcia, K., Blumenthal, B., Dopfer, E.P., and Schamel, W.W. 2010. Detection of phosphorylated T and B cell antigen receptor species by Phos-tag SDS- and Blue Native-PAGE. *Immunol Lett* 130:51-56.
219. Yang, L., Xue, Z., He, Y., Sun, S., Chen, H., and Qi, L. 2010. A phos-tag-based approach reveals the extent of physiological endoplasmic reticulum stress. *PLoS ONE* 5:e11621.
220. Hosokawa, T., Saito, T., Asada, A., Fukunaga, K., and Hisanaga, S. 2010. Quantitative measurement of in vivo phosphorylation states of Cdk5 activator p35 by Phos-tag SDS-PAGE. *Mol Cell Proteomics* 9:1133-1143.
221. Ikebe, M., and Hartshorne, D.J. 1985. Phosphorylation of smooth muscle myosin at two distinct sites by myosin light chain kinase. *J Biol Chem* 260:10027-10031.
222. Tashiro, Y., Matsumura, S., Murakami, N., and Kumon, A. 1984. The phosphorylation site for casein kinase II on 20,000-Da light chain of gizzard myosin. *Arch Biochem Biophys* 233:540-546.

223. Colburn, J.C., Michnoff, C.H., Hsu, L.C., Slaughter, C.A., Kamm, K.E., and Stull, J.T. 1988. Sites phosphorylated in myosin light chain in contracting smooth muscle. *J Biol Chem* 263:19166-19173.

224. Kinoshita, E., and Kinoshita-Kikuta, E. 2010. Improved Phos-tag SDS-PAGE under neutral pH conditions for advanced protein phosphorylation profiling. *Proteomics*.

225. Haeberle, J.R., Sutton, T.A., and Trockman, B.A. 1988. Phosphorylation of two sites on smooth muscle myosin. Effects on contraction of glycerinated vascular smooth muscle. *J Biol Chem* 263:4424-4429.

226. Sutton, T.A., and Haeberle, J.R. 1990. Phosphorylation by protein kinase C of the 20,000-dalton light chain of myosin in intact and chemically skinned vascular smooth muscle. *J Biol Chem* 265:2749-2754.

227. Barany, K., Csabina, S., de Lanerolle, P., and Barany, M. 1987. Evidence for isoforms of the phosphorylatable myosin light chain in rat uterus. *Biochim Biophys Acta* 911:369-371.

228. Csabina, S., Barany, M., and Barany, K. 1987. Comparison of myosin light chain phosphorylation in uterine and arterial smooth muscles. *Comp Biochem Physiol B* 87:271-277.

229. Csabina, S., Mougios, V., Barany, M., and Barany, K. 1986. Characterization of the phosphorylatable myosin light chain in rat uterus. *Biochim Biophys Acta* 871:311-315.

230. Schoenwaelder, S.M., and Burridge, K. 1999. Evidence for a calpeptin-sensitive protein-tyrosine phosphatase upstream of the small GTPase Rho. A novel role for the calpain inhibitor calpeptin in the inhibition of protein-tyrosine phosphatases. *J Biol Chem* 274:14359-14367.

231. Schoenwaelder, S.M., Petch, L.A., Williamson, D., Shen, R., Feng, G.S., and Burridge, K. 2000. The protein tyrosine phosphatase Shp-2 regulates RhoA activity. *Curr Biol* 10:1523-1526.

232. Tamura, M., Nakao, H., Yoshizaki, H., Shiratsuchi, M., Shigyo, H., Yamada, H., Ozawa, T., Totsuka, J., and Hidaka, H. 2005. Development of specific Rho-kinase inhibitors and their clinical application. *Biochim Biophys Acta* 1754:245-252.

233. Ono-Saito, N., Niki, I., and Hidaka, H. 1999. H-series protein kinase inhibitors and potential clinical applications. *Pharmacol Ther* 82:123-131.

234. Sasaki, Y., Suzuki, M., and Hidaka, H. 2002. The novel and specific Rho-kinase inhibitor (S)-(+)-2-methyl-1-[(4-methyl-5-isoquinoline)sulfonyl]-homopiperazine as a probing molecule for Rho-kinase-involved pathway. *Pharmacol Ther* 93:225-232.

235. Erdodi, F., Rokolya, A., Barany, M., and Barany, K. 1988. Phosphorylation of the 20,000-Da myosin light chain isoforms of arterial smooth muscle by myosin light chain kinase and protein kinase C. *Arch Biochem Biophys* 266:583-591.

236. Wilson, D.P., Sutherland, C., Borman, M.A., Deng, J.T., Macdonald, J.A., and Walsh, M.P. 2005. Integrin-linked kinase is responsible for Ca2+-independent myosin diphosphorylation and contraction of vascular smooth muscle. *Biochem J* 392:641-648.

237. Bengur, A.R., Robinson, E.A., Appella, E., and Sellers, J.R. 1987. Sequence of the sites phosphorylated by protein kinase C in the smooth muscle myosin light chain. *J Biol Chem* 262:7613-7617.

238. Nishikawa, M., Sellers, J.R., Adelstein, R.S., and Hidaka, H. 1984. Protein kinase C modulates in vitro phosphorylation of the smooth muscle heavy meromyosin by myosin light chain kinase. *J Biol Chem* 259:8808-8814.

239. Nishikawa, M., Hidaka, H., and Adelstein, R.S. 1983. Phosphorylation of smooth muscle heavy meromyosin by calcium-activated, phospholipid-dependent protein kinase. The effect on actin-activated MgATPase activity. *J Biol Chem* 258:14069-14072.

240. Van Duuren, B.L., Tseng, S.S., Segal, A., Smith, A.C., Melchionne, S., and Seidman, I. 1979. Effects of structural changes on the tumor-promoting activity of phorbol myristate acetate on mouse skin. *Cancer Res* 39:2644-2646.

241. Ishihara, H., Martin, B.L., Brautigan, D.L., Karaki, H., Ozaki, H., Kato, Y., Fusetani, N., Watabe, S., Hashimoto, K., Uemura, D., et al. 1989. Calyculin A and okadaic acid: inhibitors of protein phosphatase activity. *Biochem Biophys Res Commun* 159:871-877.

242. Kinoshita, E., Kinoshita-Kikuta, E., Matsubara, M., Yamada, S., Nakamura, H., Shiro, Y., Aoki, Y., Okita, K., and Koike, T. 2008. Separation of phosphoprotein

isotypes having the same number of phosphate groups using phosphate-affinity SDS-PAGE. *Proteomics* 8:2994-3003.

243. Turbedsky, K., Pollard, T.D., and Bresnick, A.R. 1997. A subset of protein kinase C phosphorylation sites on the myosin II regulatory light chain inhibits phosphorylation by myosin light chain kinase. *Biochemistry* 36:2063-2067.

244. Umemoto, S., Bengur, A.R., and Sellers, J.R. 1989. Effect of multiple phosphorylations of smooth muscle and cytoplasmic myosins on movement in an in vitro motility assay. *J Biol Chem* 264:1431-1436.

245. Arthur, P., Taggart, M.J., Zielnik, B., Wong, S., and Mitchell, B.F. 2008. Relationship between gene expression and function of uterotonic systems in the rat during gestation, uterine activation and both term and preterm labour. *J Physiol* 586:6063-6076.

246. Feng, Y., Yin, Y., Weiser, A., Griffin, E., Cameron, M.D., Lin, L., Ruiz, C., Schurer, S.C., Inoue, T., Rao, P.V., et al. 2008. Discovery of substituted 4-(pyrazol-4-yl)-phenylbenzodioxane-2-carboxamides as potent and highly selective Rho kinase (ROCK-II) inhibitors. *J Med Chem* 51:6642-6645.

247. Goodman, K.B., Cui, H., Dowdell, S.E., Gaitanopoulos, D.E., Ivy, R.L., Sehon, C.A., Stavenger, R.A., Wang, G.Z., Viet, A.Q., Xu, W., et al. 2007. Development of dihydropyridone indazole amides as selective Rho-kinase inhibitors. *J Med Chem* 50:6-9.

248. Li, Y.M., and Casida, J.E. 1992. Cantharidin-binding protein: identification as protein phosphatase 2A. *Proc Natl Acad Sci U S A* 89:11867-11870.

249. Pearson, R.B., Jakes, R., John, M., Kendrick-Jones, J., and Kemp, B.E. 1984. Phosphorylation site sequence of smooth muscle myosin light chain (Mr = 20 000). *FEBS Lett* 168:108-112.

250. Lebowitz, E.A., and Cooke, R. 1979. Phosphorylation of uterine smooth muscle myosin permits actin-activation. *J Biochem* 85:1489-1494.

251. Fitzgibbon, J., Morrison, J.J., Smith, T.J., and O'Brien, M. 2009. Modulation of human uterine smooth muscle cell collagen contractility by thrombin, Y-27632, TNF alpha and indomethacin. *Reprod Biol Endocrinol* 7:2.

252. Harnett, K.M., and Biancani, P. 2003. Calcium-dependent and calcium-independent contractions in smooth muscles. *Am J Med* 115 Suppl 3A:24S-30S.

253. Ogut, O., and Brozovich, F.V. 2003. Regulation of force in vascular smooth muscle. *J Mol Cell Cardiol* 35:347-355.

254. Hirano, K., Hirano, M., and Kanaide, H. 2004. Regulation of myosin phosphorylation and myofilament Ca2+ sensitivity in vascular smooth muscle. *J Smooth Muscle Res* 40:219-236.

255. Suzuki, A., and Itoh, T. 1993. Effects of calyculin A on tension and myosin phosphorylation in skinned smooth muscle of the rabbit mesenteric artery. *Br J Pharmacol* 109:703-712.

256. Miller-Hance, W.C., Miller, J.R., Wells, J.N., Stull, J.T., and Kamm, K.E. 1988. Biochemical events associated with activation of smooth muscle contraction. *J Biol Chem* 263:13979-13982.

257. Sakurada, K., Seto, M., and Sasaki, Y. 1998. Dynamics of myosin light chain phosphorylation at Ser19 and Thr18/Ser19 in smooth muscle cells in culture. *Am J Physiol* 274:C1563-1572.

258. Kogata, N., Tribe, R.M., Fassler, R., Way, M., and Adams, R.H. 2009. Integrin-linked kinase controls vascular wall formation by negatively regulating Rho/ROCK-mediated vascular smooth muscle cell contraction. *Genes Dev* 23:2278-2283.

259. Montanez, E., Wickstrom, S.A., Altstatter, J., Chu, H., and Fassler, R. 2009. Alpha-parvin controls vascular mural cell recruitment to vessel wall by regulating RhoA/ROCK signalling. *EMBO J* 28:3132-3144.

260. Vicente-Manzanares, M., and Horwitz, A.R. 2010. Myosin light chain mono- and di-phosphorylation differentially regulate adhesion and polarity in migrating cells. *Biochem Biophys Res Commun* 402:537-542.

261. Uchimura, T., Fumoto, K., Yamamoto, Y., Ueda, K., and Hosoya, H. 2002. Spatial localization of mono-and diphosphorylated myosin II regulatory light chain at the leading edge of motile HeLa cells. *Cell Struct Funct* 27:479-486.

262. Vicente-Manzanares, M., Ma, X., Adelstein, R.S., and Horwitz, A.R. 2009. Non-muscle myosin II takes centre stage in cell adhesion and migration. *Nat Rev Mol Cell Biol* 10:778-790.

263. Deng, J.T., Van Lierop, J.E., Sutherland, C., and Walsh, M.P. 2001. Ca2+-independent smooth muscle contraction. a novel function for integrin-linked kinase. *J Biol Chem* 276:16365-16373.

264. Maekawa, M., Ishizaki, T., Boku, S., Watanabe, N., Fujita, A., Iwamatsu, A., Obinata, T., Ohashi, K., Mizuno, K., and Narumiya, S. 1999. Signaling from Rho to the actin cytoskeleton through protein kinases ROCK and LIM-kinase. *Science* 285:895-898.

265. Niiro, N., and Ikebe, M. 2001. Zipper-interacting protein kinase induces Ca(2+)-free smooth muscle contraction via myosin light chain phosphorylation. *J Biol Chem* 276:29567-29574.

266. McCormick, M.C., and Behrman, R.E. 2007. The quiet epidemic of premature birth: commentary on a recent Institute of Medicine report. *Ambul Pediatr* 7:8-9.

267. Rubens, C.E., Gravett, M.G., Victora, C.G., Nunes, T.M., and Group, G.R. 2010. Global report on preterm birth and stillbirth (7 of 7): mobilizing resources to accelerate innovative solutions (Global Action Agenda). *BMC Pregnancy Childbirth* 10 Suppl 1:S7.

268. Palmberg, L., and Thyberg, J. 1986. Uterine smooth muscle cells in primary culture. Alterations in fine structure, cytoskeletal organization and growth characteristics. *Cell Tissue Res* 246:253-262.

269. Chamley-Campbell, J., Campbell, G.R., and Ross, R. 1979. The smooth muscle cell in culture. *Physiol Rev* 59:1-61.

270. Zaitseva, M., Vollenhoven, B.J., and Rogers, P.A. 2006. In vitro culture significantly alters gene expression profiles and reduces differences between myometrial and fibroid smooth muscle cells. *Mol Hum Reprod* 12:187-207.

271. Busnelli, M., Rimoldi, V., Vigano, P., Persani, L., Di Blasio, A.M., and Chini, B. 2010. Oxytocin-induced cell growth proliferation in human myometrial cells and leiomyomas. *Fertil Steril*.

272. Chang, B., Myatt, L., and Cui, X.L. 2009. Loss of proliferative capacity in a retroviral immortalized human uterine smooth muscle cell line derived from leiomyoma is restored by hTERT overexpression. *Reprod Sci* 16:1062-1071.

273. Monga, M., Ku, C.Y., Dodge, K., and Sanborn, B.M. 1996. Oxytocin-stimulated responses in a pregnant human immortalized myometrial cell line. *Biol Reprod* 55:427-432.

274. Dallot, E., Pouchelet, M., Gouhier, N., Cabrol, D., Ferre, F., and Breuiller-Fouche, M. 2003. Contraction of cultured human uterine smooth muscle cells after stimulation with endothelin-1. *Biol Reprod* 68:937-942.

275. Chevillard, G., Derjuga, A., Devost, D., Zingg, H.H., and Blank, V. 2007. Identification of interleukin-1beta regulated genes in uterine smooth muscle cells. *Reproduction* 134:811-822.

276. Chamley-Campbell, J.H., and Campbell, G.R. 1981. What controls smooth muscle phenotype? *Atherosclerosis* 40:347-357.

277. Perez-Reyes, N., Halbert, C.L., Smith, P.P., Benditt, E.P., and McDougall, J.K. 1992. Immortalization of primary human smooth muscle cells. *Proc Natl Acad Sci U S A* 89:1224-1228.

278. Condon, J., Yin, S., Mayhew, B., Word, R.A., Wright, W.E., Shay, J.W., and Rainey, W.E. 2002. Telomerase immortalization of human myometrial cells. *Biol Reprod* 67:506-514.

279. Fukui, Y., and Morita, F. 1996. Two phosphorylations specific to the tail region of the 204-kDa heavy chain isoform of porcine aorta smooth muscle myosin. *Journal of biochemistry* 119:783-790.

280. Myatt, L., and Lye, S.J. 2004. Expression, localization and function of prostaglandin receptors in myometrium. *Prostaglandins Leukot Essent Fatty Acids* 70:137-148.

281. Nathanielsz, P.W., Smith, G., and Wu, W. 2004. Topographical specialization of prostaglandin function in late pregnancy and at parturition in the baboon. *Prostaglandins Leukot Essent Fatty Acids* 70:199-206.

282. Wikland, M., Lindblom, B., Hammarstrom, S., and Wiqvist, N. 1983. The effect of prostaglandin I on the contractility of the term pregnant human myometrium. *Prostaglandins* 26:905-916.

283. Gordon-Wright, A.P., and Elder, M.G. 1980. Effect of prostaglandin E2 and its metabolites on lower segment myometrium in vitro. *Eur J Obstet Gynecol Reprod Biol* 10:297-302.

284. Pinto, R.M., Lerner, U., and Pontelli, H. 1967. The effect of progesterone on oxytocin-induced contraction of the three separate layers of human gestational myometrium in the uterine body and lower segment. *Am J Obstet Gynecol* 98:547-554.

285. Fuchs, A.R., Fuchs, F., Husslein, P., and Soloff, M.S. 1984. Oxytocin receptors in the human uterus during pregnancy and parturition. *Am J Obstet Gynecol* 150:734-741.

286. Dyal, R., and Crankshaw, D.J. 1988. The effects of some synthetic prostanoids on the contractility of the human lower uterine segment in vitro. *Am J Obstet Gynecol* 158:281-285.

287. Senior, J., Marshall, K., Sangha, R., and Clayton, J.K. 1993. In vitro characterization of prostanoid receptors on human myometrium at term pregnancy. *Br J Pharmacol* 108:501-506.

288. Luckas, M.J., and Wray, S. 2000. A comparison of the contractile properties of human myometrium obtained from the upper and lower uterine segments. *BJOG* 107:1309-1311.

289. Charpigny, G., Leroy, M.J., Breuiller-Fouche, M., Tanfin, Z., Mhaouty-Kodja, S., Robin, P., Leiber, D., Cohen-Tannoudji, J., Cabrol, D., Barberis, C., et al. 2003. A functional genomic study to identify differential gene expression in the preterm and term human myometrium. *Biol Reprod* 68:2289-2296.

290. Bethin, K.E., Nagai, Y., Sladek, R., Asada, M., Sadovsky, Y., Hudson, T.J., and Muglia, L.J. 2003. Microarray analysis of uterine gene expression in mouse and human pregnancy. *Mol Endocrinol* 17:1454-1469.

291. Rehman, K.S., Yin, S., Mayhew, B.A., Word, R.A., and Rainey, W.E. 2003. Human myometrial adaptation to pregnancy: cDNA microarray gene expression profiling of myometrium from non-pregnant and pregnant women. *Mol Hum Reprod* 9:681-700.

292. Havelock, J.C., Keller, P., Muleba, N., Mayhew, B.A., Casey, B.M., Rainey, W.E., and Word, R.A. 2005. Human myometrial gene expression before and during parturition. *Biol Reprod* 72:707-719.

293. Esplin, M.S., Fausett, M.B., Peltier, M.R., Hamblin, S., Silver, R.M., Branch, D.W., Adashi, E.Y., and Whiting, D. 2005. The use of cDNA microarray to identify differentially expressed labor-associated genes within the human myometrium during labor. *Am J Obstet Gynecol* 193:404-413.

294. Breuiller-Fouche, M., Charpigny, G., and Germain, G. 2007. Functional genomics of the pregnant uterus: from expectations to reality, a compilation of studies in the myometrium. *BMC Pregnancy Childbirth* 7 Suppl 1:S4.

295. Olson, D.M., Zaragoza, D.B., Shallow, M.C., Cook, J.L., Mitchell, B.F., Grigsby, P., and Hirst, J. 2003. Myometrial activation and preterm labour: evidence supporting a role for the prostaglandin F receptor--a review. *Placenta* 24 Suppl A:S47-54.

296. Senba, S., Eto, M., and Yazawa, M. 1999. Identification of trimeric myosin phosphatase (PP1M) as a target for a novel PKC-potentiated protein phosphatase-1 inhibitory protein (CPI17) in porcine aorta smooth muscle. *J Biochem* 125:354-362.

297. Eto, M., Karginov, A., and Brautigan, D.L. 1999. A novel phosphoprotein inhibitor of protein type-1 phosphatase holoenzymes. *Biochemistry* 38:16952-16957.

298. Lartey, J., Smith, M., Pawade, J., Strachan, B., Mellor, H., and Lopez Bernal, A. 2007. Up-regulation of myometrial RHO effector proteins (PKN1 and DIAPH1) and CPI-17 (PPP1R14A) phosphorylation in human pregnancy is associated with increased GTP-RHOA in spontaneous preterm labor. *Biol Reprod* 76:971-982.

299. Ozaki, H., Yasuda, K., Kim, Y.S., Egawa, M., Kanzaki, H., Nakazawa, H., Hori, M., Seto, M., and Karaki, H. 2003. Possible role of the protein kinase C/CPI-17 pathway in the augmented contraction of human myometrium after gestation. *Br J Pharmacol* 140:1303-1312.

300. Li, L., Eto, M., Lee, M.R., Morita, F., Yazawa, M., and Kitazawa, T. 1998. Possible involvement of the novel CPI-17 protein in protein kinase C signal transduction of rabbit arterial smooth muscle. *J Physiol* 508 (Pt 3):871-881.

301. Eto, M., Senba, S., Morita, F., and Yazawa, M. 1997. Molecular cloning of a novel phosphorylation-dependent inhibitory protein of protein phosphatase-1 (CPI17) in smooth muscle: its specific localization in smooth muscle. *FEBS Lett* 410:356-360.

302. Eto, M., Ohmori, T., Suzuki, M., Furuya, K., and Morita, F. 1995. A novel protein phosphatase-1 inhibitory protein potentiated by protein kinase C. Isolation from porcine aorta media and characterization. *J Biochem* 118:1104-1107.

303. Tan, I., Ng, C.H., Lim, L., and Leung, T. 2001. Phosphorylation of a novel myosin binding subunit of protein phosphatase 1 reveals a conserved mechanism in the regulation of actin cytoskeleton. *J Biol Chem* 276:21209-21216.

304. Shimizu, Y., Thumkeo, D., Keel, J., Ishizaki, T., Oshima, H., Oshima, M., Noda, Y., Matsumura, F., Taketo, M.M., and Narumiya, S. 2005. ROCK-I regulates closure of the eyelids and ventral body wall by inducing assembly of actomyosin bundles. *J Cell Biol* 168:941-953.

305. Thumkeo, D., Keel, J., Ishizaki, T., Hirose, M., Nonomura, K., Oshima, H., Oshima, M., Taketo, M.M., and Narumiya, S. 2003. Targeted disruption of the mouse rho-associated kinase 2 gene results in intrauterine growth retardation and fetal death. *Mol Cell Biol* 23:5043-5055.

306. Thumkeo, D., Shimizu, Y., Sakamoto, S., Yamada, S., and Narumiya, S. 2005. ROCK-I and ROCK-II cooperatively regulate closure of eyelid and ventral body wall in mouse embryo. *Genes Cells* 10:825-834.

307. Becker-Hapak, M., McAllister, S.S., and Dowdy, S.F. 2001. TAT-mediated protein transduction into mammalian cells. *Methods* 24:247-256.

308. Nagahara, H., Vocero-Akbani, A.M., Snyder, E.L., Ho, A., Latham, D.G., Lissy, N.A., Becker-Hapak, M., Ezhevsky, S.A., and Dowdy, S.F. 1998. Transduction of full-length TAT fusion proteins into mammalian cells: TAT-p27Kip1 induces cell migration. *Nat Med* 4:1449-1452.

309. Aktories, K., Braun, U., Rosener, S., Just, I., and Hall, A. 1989. The rho gene product expressed in E. coli is a substrate of botulinum ADP-ribosyltransferase C3. *Biochem Biophys Res Commun* 158:209-213.

310. Khosravi-Far, R., Solski, P.A., Clark, G.J., Kinch, M.S., and Der, C.J. 1995. Activation of Rac1, RhoA, and mitogen-activated protein kinases is required for Ras transformation. *Mol Cell Biol* 15:6443-6453.

311. Zakar, T., and Hertelendy, F. 2007. Progesterone withdrawal: key to parturition. *Am J Obstet Gynecol* 196:289-296.

312. Uehata, M., Ishizaki, T., Satoh, H., Ono, T., Kawahara, T., Morishita, T., Tamakawa, H., Yamagami, K., Inui, J., Maekawa, M., et al. 1997. Calcium sensitization of smooth muscle mediated by a Rho-associated protein kinase in hypertension. *Nature* 389:990-994.

313. Tribe, R.M., Moriarty, P., and Poston, L. 2000. Calcium homeostatic pathways change with gestation in human myometrium. *Biol Reprod* 63:748-755.

314. Astle, S., Newton, R., Thornton, S., Vatish, M., and Slater, D.M. 2007. Expression and regulation of prostaglandin E synthase isoforms in human myometrium with labour. *Mol Hum Reprod* 13:69-75.

315. Avraham, H., and Weinberg, R.A. 1989. Characterization and expression of the human rhoH12 gene product. *Mol Cell Biol* 9:2058-2066.